PROFESSIONAL DOCTORATES

Investigating MRNIP, a novel regulator of replication fork stability

Antonopoulou, Effrosyni

Award date:
2023

Awarding institution:
Bangor University

Investigating MRNIP, a novel regulator of replication fork stability

Effrosyni Antonopoulou

School of Medical Sciences

University of Bangor

This dissertation is submitted for the degree of Doctor of Philosophy

February 2023

Declaration

‘Yr wyf drwy hyn yn datgan mai canlyniad fy ymchwil fy hun yw’r thesis hwn, ac eithrio lle nodir yn wahanol. Caiff ffynonellau eraill eu cydnabod gan droednodiadau yn rhoi cyfeiriadau eglur. Nid yw sylwedd y gwaith hwn wedi cael ei dderbyn o’r blaen ar gyfer unrhyw radd, ac nid yw’n cael ei gyflwyno ar yr un pryd mewn ymgeisiaeth am unrhyw radd oni bai ei fod, fel y cytunwyd gan y Brifysgol, am gymwysterau deuol cymeradwy.’

Rwy’n cadarnhau fy mod yn cyflwyno’r gwaith gyda chytundeb fy Ngrichwyliwr (Goruchwylwyr)’

‘I hereby declare that this thesis is the results of my own investigations, except where otherwise stated. All other sources are acknowledged by bibliographic references. This work has not previously been accepted in substance for any degree and is not being concurrently submitted in candidature for any degree unless, as agreed by the University, for approved dual awards.’

I confirm that I am submitting the work with the agreement of my Supervisor’.

Acknowledgements

This challenging journey comes to an end, and I have so many people to thank for being my fellow travellers. First and foremost, my supervisor Dr Christopher Staples for giving me the opportunity to do some cool science on this interesting yet complicated project. He has always been there for me; giving me food for thought, pushing me to be better and come up with new ideas and concepts, and mostly being patient and understandable during stressful and difficult times without losing his enthusiasm and unconditional love for science. I would also like to thank the charity Cancer Research Wales for funding this project. Many thanks to my lab family; Ellen, Laura, Nick, Natalia, Joe, Alec for their continuous academic and emotional support; without them I would not have survived even the first month. My dearest friends Amelia and Angharad who were always there for me when I needed, a shoulder to cry, a friend to celebrate some good findings or listen again and again my presentations; I am deeply grateful that I have met you! I would also like to thank Matt for the last minute help of formatting the thesis! My partner Cammy who was always encouraging me to persevere and reminding me that everything will be fine at the end. Last but not least, I would like to thank my family and particularly my beloved mother for her endless support and love and for believing in me when I was doubting! Being away from you is hard, but I hope I made you proud!

Abstract

Although DNA replication is a tightly regulated process, cells are vulnerable to replication stress-induced genome instability, which is an enabling characteristic of tumourigenesis. Many chemotherapies work by interfering with cancer cell DNA replication. In response to replication stress, the replication fork is frequently remodelled (or reversed) into a 4-way chicken-foot-like structure which is protected from uncontrolled nucleolytic resection by a network of protective factors including the canonical tumour suppressors BRCA1 and BRCA2. Among the nucleases capable of acting at reversed forks is MRE11, which possesses both endonuclease and exonuclease activities and is a component of the MRN (MRE11, RAD50, NBS1) complex, which initiates Double-Strand Break (DSB) resection during DNA Double-Strand Break (DSB) repair. Our lab identified C5ORF45/MRE11-RAD50-NBS1 Interacting Protein (MRNIP) as a novel MRE11-interacting factor that limits nascent DNA degradation at stalled, reversed replication forks. However, the mechanisms underpinning fork protection by MRNIP are still unclear, and the further elucidation of MRNIP function is among the core aims of this study. MRNIP KO cells exhibit reduced levels of replication stress-induced MRE11 phosphorylation on Ser676/678. We demonstrate that expression of a phospho-mimetic MRE11 mutant prevents DNA degradation in MRNIP KO cells, suggesting that MRNIP-mediated MRE11 phosphorylation is crucial in preventing nascent DNA resection at reversed forks. In addition, we aimed to determine the role of MRNIP in the response to different chemotherapeutic drugs. Our findings indicate that cells lacking MRNIP are sensitive to the topoisomerase inhibitor Camptothecin but exhibit resistance to the chain terminating nucleoside analogue (CTNA) Gemcitabine. MRNIP was recently identified as being phosphorylated on Ser217, which is a potential non-canonical cyclin-dependent kinase 1 (CDK1) site. We find that Gemcitabine resistance in MRNIP KO cells requires Ser217, suggesting that MRNIP phosphorylation might provide a means to elicit cell cycle-specific control of MRE11. The function of this phosphorylation site appears context-dependent since alanine substitution of Ser217 did not affect MRE11-mediated nascent DNA degradation at HU-stalled forks.

Attempts to investigate nascent DNA degradation in response to Gemcitabine led to some unexpected but interesting results. We observed DNA degradation even in MRNIP-proficient cells treated with Gemcitabine, a process that seems to be independent of the action of the major nucleases commonly implicated at these sites.

We also examined MRNIP expression in a series of ovarian cancer cell (OC) lines. Loss of MRNIP protein and reduced mRNA levels were observed in certain High-Grade Ovarian Serous Adenocarcinoma cell lines, and MRNIP depletion led to different survival outcomes in response to different chemotherapeutic agents. We also identified CDK4 as a novel MRNIP interactor and found that CDK4 is stabilised in the absence of MRNIP, leading to elevated CDK4 levels in MRNIP KO cells. We also identify the E3 ligase Carboxy-terminus of Hsc70-interacting protein (CHIP) as a potential functional interactor and hypothesise that MRNIP limits the ability of CHIP to target and degrade CDK4.

In summary, this work reveals several novel phenotypes associated with MRNIP loss of function and adds depth to our mechanistic understanding of the functionality of a series of post-translational modifications of both MRE11 and MRNIP.

List of Contents

List of figures

List of Tables

Abbreviations

aa	Amino acids
AFM	Atomic Force Microscopy
AKT	Ak strain Transforming.
ALT	Alternative Lengthening of Telomeres
AP	Apurinic/apyrimidinic
APLF	Aprataxin and PNKP Like Factor
ATAC	Assay for Transposase-Accessible Chromatin with high-throughput sequencing
ATLD	Ataxia-Telangiectasia (A-T)–like disorder
ATM	Ataxia-Telangiectasia-mutated
ATP	Adenosine Triphosphate
ATR	Ataxia Telangiectasia and Rad3-related protein
ATRIP	Ataxia Telangiectasia and Rad3-related (ATR)-interacting protein
BCA	Bicinchoninic acid assay
BER	Base Excision Repair
BIR	Break-Induced Replication
BLM	Bloom syndrome
BRAF	V-raf murine sarcoma viral oncogene homolog B1
BRCA1/2	Breast cancer type 1/2
BRCT	Breast Cancer Associated 1 C–Terminus
BSA	Bovine serum albumin
CAK	CDK-activating kinase
CDK	Cyclin-dependent kinase
C/EBPa	CCAAT/enhancer binding protein alpha
CHIP	Carboxy-terminus of Hsc70-interacting protein
CHX	Cycloheximide
CK2	Casein Kinase II
CLSPN	Claspin

CPT	Camptothecin
CRISPR	Clustered regularly interspaced short palindromic repeats
CS	Cockayne syndrome
CSR	Class switch recombination
DAPI	4',6-diamidino-2-phenylindole
DDK	Dbf4-dependent kinase
DDR	DNA Damage Response
DLS	Dynamic Light Scattering
DMEM	Dulbecco's Modified Eagle Medium
DMSO	Dimethyl Sulfoxide
DNA	Deoxyribonucleic acid
DPBS	Dulbecco's Phosphate Buffered Saline
DSBs	Double Strand Breaks
DSGs	Daughter Strand Gaps
ECM	Extracellular Matrix
EDTA	Ethylenediaminetetraacetic Acid
EGF	Epidermal Growth Factor
EGFR	Epidermal Growth Factor Receptor
EM	Electron Microscopy
EMT	Epithelial-Mesenchymal Transition
FACS	Fluorescence-activated Cell Sorting
FANC	Fanconi Anaemia
FAT	FRAP-ATM-TRRAP
FBS	Foetal Bovine Serum
FHA	Forkhead-associated
FP	Fork protection
GAPDH	Glyceraldehyde-3-phosphate dehydrogenase
GAR	Glycine-arginine-rich
GI	Genome Instability
GINS	Go-ichi-ni-san

GSK	Glycogen Synthase Kinase
HARP	HepA-related protein
HCL	Hydrochloric acid
hCNTs	human Concentrative Nucleoside Transporters
HEAT	Huntingtin, elongation factor 3 (EF3), protein phosphatase 2A (PP2A), TOR1
hENTs	human Equilibrative Nucleoside Transporters
HIF-1α	Hypoxia-inducible factor-1α
HLTF	Helicase-like Transcription Factor
HMCES	5-Hydroxymethylcytosine Binding protein
HNTs	human Nucleoside Transporters
HPV	Human Papillomavirus
HR	Homologous Recombination
HU	Hydroxyurea
ICL	Interstrand Crosslink
ICP-MS	Inductively Coupled Plasma Mass Spectrometry
IFN-γ	Interferon gamma
IL-1β/-6/-8/-10/-12	Interleukin-1β/-6/-8/-10/-12
IR	Ionising Radiation
KO	Knock-out
KRAS	Kirsten rat sarcoma viral oncogene homolog
LB	Lysogeny Broth
LC3	Microtubule-associated protein 1A/1B-light chain 3
LKB1	Liver Kinase B1
LLPS	Liquid-liquid Phase Separation
MAPK	Mitogen-activated Protein Kinase
MCM	Minichromosome Maintenance
MDC1	DNA Damage Checkpoint 1
MET	Mesenchymal-Epithelial Transition
MMC	Mitomycin C
MMEJ	Microhomology-Mediated End Joining

MMR	Mismatch Repair
MRN complex	MRE11-RAD50-NBS1 complex
MRNIP	MRE11 RAD50 NBS1 Interacting Protein
MRX	MRE11-RAD50-XRS2
MS	Mass Spectrometry
MSCI	Meiotic Sex Chromosome Inactivation
MTT	3-(4,5-dimethylthiazol-2-yl)-2,5-diphenyl tetrazolium bromide
NBS	Nijmegen Breakage Syndrome
NBS1	Nijmegen Breakage Syndrome 1 mutated gene also known as nibrin
NER	Nucleotide Excision Repair
NF2	Neurofibromatosis type 2
NF-κB	Nuclear Factor-κB
NHEJ	Non-Homologous End-Joining
NK	Natural Killer
NOXA	Latin for damage
OC	Ovarian Cancer
OIS	Oncogene-Induced replication Stress
ORC	Origin Recognition Complex
PARG	Poly (ADP-ribose) glycohydrolase
PARP1	Poly (ADP-ribose) polymerase 1
PBS	Phosphate Buffered Saline
PCNA	Proliferating-Cell Nuclear Antigen
PCR	Polymerase Chain Reaction
PDAC	Pancreatic Ductal Adenocarcinoma
PD-ECGF	Platelet-derived Endothelial Cell Growth Factor
PDGF	Platelet-derived Growth Factor
PF4	Platelet Factor 4
PI3K	Phosphatidylinositol-3 kinase
PIKKs	Phosphatidylinositol 3-kinase-related protein kinases

PNK	Polynucleotide kinase/phosphatase
PP1	Protein Phosphatase 1
PTIP	Pax transcription activation domain-interacting protein
PUMA	P53 upregulated modulator of apoptosis
PVDF	Polyvinylidene fluoride
RAS	Rat sarcoma
Rb	Retinoblastoma
RFs	Reversed forks
RFC	Replication Factor C
RHINO	Rad1 and Hus1 interacting nuclear orphan
RNA	Ribonucleic acid
RNR	Ribonucleotide reductase
RPA	Replication Protein A
RPE	Retinal pigment epithelium
RPMI	Roswell Park Memorial Institute Medium
RS	Replication Stress
SASP	Senescence-associated Secretory Phenotype
SAXS	Small-angle X-ray scattering
SDS-PAGE	Sodium Dodecyl-sulphate Polyacrylamide gel electrophoresis
SMARCAL1	SWI/SNF-related matrix-associated actin-dependent regulator of chromatin subfamily A-like protein 1
SNF	Sucrose nonfermenting 2
SOC	Super Optimal Catabolite
SS	Seckel syndrome
SSA	Single-strand annealing
SSB	Single-strand break
TAE	Tris-acetate-EDTA
TBS	Tris-buffered saline
TC-NER	Transcription-coupled nucleotide excision repair
TCA	Tricarboxylic acid

TET	Ten-eleven translocation
TGF	Transforming Growth Factor
TLS	Translesion DNA synthesis
TMEJ	Theta-mediated End-Joining
TNF	Tumour Necrosis Factor
TOPB1	Topoisomerase II binding protein 1
TS	Tumour Suppressor
UTR	Untranslated Region
UV	Ultra-violet
VEGF	Vascular Endothelial Growth Factor
WRN	Werner Syndrome Protein
WRNIP1	Werner helicase Interacting protein 1
WT	Wild type
XLF	XRCC4-like factor
XP	Xeroderma Pigmentosum
ZNF384	Zinc finger protein 384

CHAPTER I

1 INTRODUCTION

1.1 Overview of Cancer

Tumourigenesis refers to the multi-step process in which cells undergo metabolic and behavioural changes causing their uncontrollable proliferation. These changes arise from both genetic and epigenetic modifications [1,2]. At the genetic level, cancer develops due to mutations in tumour suppressor (TS) genes and/or oncogenes which cause loss or gain of function, or abnormal expression. The epigenetic path to cancer is more complicated, and involves differential DNA methylation, expression and modification of histone variants, extensive alterations to nucleosome remodelling, and alterations to small non-coding regulatory RNAs and their expression [3]. Cancer should not be considered as a single disease; the term refers to a broad spectrum of diseases, with more than 100 distinct types and subtypes documented to date, and the presentation, development and outcome of which vary from patient to patient [4]. This heterogeneity and complexity pose significant barriers to effective treatment, and indeed cancer morbidity and mortality represent an important economic burden [5]. In addition, global cancer incidence continues to increase; more than 20 million new cases and 10 million deaths were documented in 2020 alone, ranking cancer among the leading causes of death worldwide (WHO).

1.2 Hallmarks of cancer

In an attempt to document and summarise the diversity of neoplastic disease, six common traits to all cancers, known as ‘’hallmarks’’, were initially proposed by Hanahan and Weinberg in 2011. These include; self-sufficiency in growth signals, insensitivity to anti-growth signals, evasion of apoptosis, limitless replicative potential, sustained angiogenesis and tissue invasion/ metastasis (Figure 1.1) [6].

1.2.1 Self Sufficiency in growth signals

Untransformed cells require growth signals, known as growth factors, to proliferate, differentiate and survive. Those growth factors act in an autocrine and paracrine manner and the behaviour of the cells is dependent on the immediate surrounding environment, the microenvironment. On the other hand, cancer cells can alter this microenvironment; by a) synthesising and secreting their own growth factors, b) altering the growth factor itself or c) altering downstream signalling pathways. For example, glioblastomas secrete platelet-derived growth factor (PDGF), and overexpression or hyperactivity of PDGF ligands and receptors are commonly associated with human gliomas of all grades [7,8]. In addition, truncated epidermal growth factor receptor (EGFR) is associated with higher tumour stage in head and neck cancers [9] and mutations in the rat sarcoma (*ras*) oncogene, which drive downstream activation of the phosphatidylinositol-3 kinase (PI3K) and mitogen-activated protein kinase (MAPK) pathways, are present in about 50% of colon cancers [10].

1.2.2 Insensitivity to anti-growth signals

Other than growth signals, anti-growth signals also act within a normal cell to maintain tissue homeostasis. Non-cancerous cells have a normal cell cycle where cell division is tightly controlled and halted, if necessary, to prevent the progressive growth of damaged cells. Each step of the cell cycle is regulated through various checkpoints; G1 (restriction checkpoint); intra-S, G2; and Metaphase (spindle assembly) checkpoints. G1, intra-S and G2 checkpoints are regulated in their turn by cyclins, cyclin dependent kinases (CDKs), and TS genes [11]. A plethora of TS genes act in a cell- and damage-specific manner to negatively regulate growth. Two primary examples are the retinoblastoma (Rb) and TP53 proteins, which are mutated or downregulated in many cancers [12]. Although they have vital direct roles in regulating cell proliferation, various evidence demonstrates that they are part of a larger and more complex network including inhibition involving Neurofibromatosis type 2 (NF2) [13,14] and Liver Kinase B1 (LKB1) [15,16] proteins as well as the Transforming growth factor-β (TGF-β) pathway [17].

1.2.3 Limitless replicative potential

In addition to aberrant growth patterns, a malignant cell typically displays limitless replicative potential. Most untransformed cell types undergo only a limited number of divisions before they reach the Hayflick limit, following which they are unable to divide, and either die or senesce [18]. The Hayflick limit is determined by telomere length; telomeres are specific regions at the ends of the chromosome which protect the chromosome end, and which shorten with each successive cell division. Cancerous cells escape this limit, growing indefinitely and becoming immortal [19], mostly via the upregulation or reactivation of telomerase, an enzyme that maintains telomeric lengths [20] and to a lesser extent by the activation of the Alternative Lengthening of Telomeres (ALT) mechanism, potentially via homology directed telomere synthesis [21].

1.2.4 Evasion of apoptosis

To divide and grow uncontrollably, cancerous cells must also evade induction of apoptosis. Apoptosis is an important process for tissue homeostasis. In response to an apoptotic stimulus, activation of the ‘’initiator’’ caspases (i.e., Caspases-2, -8, -9, or -10) by death receptors (e.g., FAS) or cytochrome C causes activation of ‘’executioner” caspases (i.e., Caspases-3 and -7). This leads to the proteolytic cleavage of cellular substrates and therefore cell death [22]. The Bcl-2 family includes pro-apoptotic (Bax, Bak, Bid, Bim) and anti-apoptotic (Bcl-2, Bcl-XL, Bcl-W) proteins which ensure appropriate regulation of the pathway [23]. Activated p53 also controls apoptosis mostly by direct transcriptional activation of the pro-apoptotic BH3-only proteins including p53 upregulated modulator of apoptosis (PUMA) and NOXA (Latin for damage) [24]. Evasion of cell death can be achieved by alterations in the aforementioned proteins or the downstream signal itself. An example of the latter includes activation of the PI3 kinase–AKT (Ak strain transforming)/PKB pathway which regulates antiapoptotic signals, and which is dysregulated in many human cancers [25].

1.2.5 Sustained angiogenesis

A high-quality supply of oxygen and nutrients, as well as efficient removal of metabolic waste products by the vasculature is important for cell survival. Similarly, an expanding tumour has a high demand for nutrients, oxygen and waste removal, which is achieved by the formation of new blood and lymphatic vessels – a process called angiogenesis and lymphangiogenesis, respectively [26]. Cancer cells disturb the balance between angiogenesis inducers and inhibitors. A plethora of proteins have been identified in the promotion of angiogenesis, including vascular endothelial growth factor (VEGF), epidermal growth factor (EGF), transforming growth factor (TGF)-α, TGF-β, basic fibroblast growth factor (bFGF), angiogenin, tumour necrosis factor (TNF)-α and platelet-derived endothelial cell growth factor (PD-ECGF), as well as cytokines such as interleukin-1, 6, and 8. In the absence of an efficient vascular network, tumours may become necrotic or apoptotic [27,28]. Hypoxia (oxygen deficiency) induces the expression of VEGF and its receptor via hypoxia-inducible factor-1α (HIF-1α). VEGF is secreted by cancer and stromal cells to stimulate the proliferation and migration of endothelial cells [29], whereas the expression of angiogenesis inhibitors such as angiostatin, endostatin, interferon, platelet factor 4 (PF4) and thrombospondin are downregulated in many cancers [30].

1.2.6 Tissue invasion & metastasis

Another major hallmark of most tumours is the ability to detach from the extracellular matrix (ECM) and metastasise. Metastasis accounts for 90% of cancer deaths and it is a complex and multi-step process involving invasion of the tumour cells to adjacent tissue, followed by invasion into the blood vessels, survival in the circulatory system, egress from the circulation, attachment and proliferation at a new location where a second tumour is subsequently established [31]. A developmental program termed epithelial-mesenchymal transition (EMT) plays a significant role in metastasis. During this process, epithelial cells lose their cell polarity and cell-cell adhesion structures including adhesins and desmosomes, rearranging their cytoskeleton to develop migratory and invasive characteristics [32]. Cancer cells do not undergo complete EMT, but instead exist in multiple transitional states expressing mixed epithelial and mesenchymal genes. Such cells in

partial EMT can be more aggressive than cells with a complete EMT phenotype [33]. Once cancer cells reach a desirable metastatic niche to accommodate the secondary tumour, EMT can be reversed by mesenchymal-to-epithelial transition (MET) process [34].

A decade later, two emerging hallmarks were added in an updated review; deregulation of cellular metabolism and evasion of immune destruction, as well as two enabling traits; genome instability (GI) and tumour-promoting inflammation [35].

1.2.7 Deregulation of cellular metabolism

The aberrant characteristics of cancerous cells are also driven by extensive metabolic reprogramming. Under aerobic conditions, normal cells catabolize glucose to pyruvate through glycolysis. Pyruvate can then be converted to acetyl-CoA to fuel the tricarboxylic acid (TCA) which is completely oxidised to carbon dioxide during mitochondrial respiration. This is an efficient process as 36 adenosine triphosphate (ATP) molecules are produced from one molecule of glucose. Under anaerobic conditions, glycolysis mainly occurs, and relatively little pyruvate is used to the mitochondria [36]. However, glycolysis is favoured in cancer cells even when oxygen is abundant, a phenomenon firstly described by the German physiologist Otto Heinrich Warburg and hence known as the ‘’Warburg’’ effect. In order to compensate for the low efficiency of glycolysis, glucose is highly consumed, facilitating the synthesis of large biomolecules necessary for cell proliferation and by extent tumour formation [37,38]. This is partially achieved by upregulating glucose transporters, such as glucose transporter 1 (GLUT1), which causes enhanced glucose import into the cytoplasm [39–41]. Activated oncogenes such as RAS, the master regulator of cell cycle entry and proliferative metabolism (MYC) as well as mutations in TS genes such as TP53 have also been implicated in metabolic reprogramming [41,42]. Activated PI3K also stimulates glycolysis by increasing the expression and membrane translocation of glucose transporters, and by phosphorylating glycolytic enzymes [43,44]. In addition, activation of the mammalian target of rapamycin (mTOR) indirectly affects metabolic programming via activation of HIF-1, even during normoxia [43].

1.2.8 Evasion of immune destruction

The concept of cancer immunosurveillance was introduced over a century ago by Paul Ehrlich [45], who proposed that tumours are constantly identified and eradicated by the immune system even before clinical manifestations take place. However, the prevalence of cancer suggests that cancer cells can in some circumstances evade the immune system. This is achieved by the dynamic process of immunoediting, which not only protects cancerous cells from immune destruction but also shapes the characteristics of emerging tumours [46,47]. This process involves three phases: elimination, equilibrium and escape. During the first phase, cytotoxic cells such as natural killer (NK) and CD8+ T cells eliminate the more immunogenic cancer cells [48] . However, cancer cell variants that are less immunogenic may arise - these become invisible to immune detection, and they enter the equilibrium phase. Tumour fate is also determined by different subsets of inflammatory cells; T-cells, interleukin 12 (IL-12), and interferon gamma (IFN-γ) facilitate tumour cells to become dormant. The tumour cells then may enter the escape phase where they defeat, escape or tolerize the immune system [49].

1.2.9 Tumour-promoting inflammation

The discovery of the strong link between inflammation and cancer development dates back to 1863 when Virchow noted the presence of leucocytes in neoplastic tissues. It has been estimated that 10-20% of cancer mortalities can be attributed to chronic inflammation [50]. The crosstalk between cancerous cells, the tumour microenvironment and the cells of the immune system via direct contact or cytokine/chemokine production mediates tumour maintenance, progression, invasion and metastasis [51]. For example, increased levels of TNFα, IL-6, IL-10, and TGFβ have been implicated in the pathogenesis of a plethora of human cancers including colon, breast, and prostate [52]. In addition, HIF-1α directly contributes to inflammation by producing pro-inflammatory mediators responsible for the recruitment of a variety of immune cells at tumour sites. Activation of nuclear factor-κB (NF-κB) promotes tumorigenesis via activation of IL-6, matrix metalloproteinase (MMP9), cyclooxygenase 2 (COX2), as well as pro-survival genes, such as Bcl-2 [53]. Activated NF-κB also activates TNF-α which promotes invasive

and metastatic potential in oral squamous cell carcinoma [54]. Moreover, chemicals including reactive oxygen and nitrogenous species can directly or indirectly sustain chronic inflammation by causing DNA damage [55]. Neutrophils (a major source of reactive oxygen species) are thought to inhibit nucleotide excision repair [56]. In addition, tumour-associated macrophages (TAMs) promote tumour growth by facilitating angiogenesis, invasion, and metastasis [57]. In fact, activated macrophages promote EMT via secretion of IL-1β, IL-8, TNF-α, and TGF-β [58,59] as well as proteolytic enzymes, including cathepsins, matrix metalloproteinases (MMPs) and serine proteases, which mediate ECM degradation and cell-ECM interactions [60–62].

1.2.10 Genome instability

Genome instability (GI) is a key player in tumour initiation and progression, although it is present even in precancerous lesions [63] and thus associated with cancer predisposition [64]. GI can be described as a high frequency of genomic sequential and structural alterations, ranging from short sequence variations as observed in tumours exhibiting microsatellite instability, to major architectural and karyotypic alterations including changes in chromosome number or structure [65]. Factors contributing to GI can be *trans*-acting suppressors of replication or defective DNA repair and checkpoint pathways, as well as *cis*-acting chromosomal sites including fragile sites and highly transcribed DNA sequences. According to the Knudson hypothesis, biallelic inactivation of TS genes via the introduction of mutations or epigenetic alterations (‘’two-hits’’) is required to drive GI [66]. He postulated this hypothesis by studying the retinoblastoma disease; a disease associated with inactivation of the TS suppressor Rb gene. The TP53 gene (often described as the ‘guardian of the genome’) provides a further illustrative example, the inactivation of which causes GI. Mutations in TP53 are found in the majority of human cancers [67]. In particular, germline mutations in p53 cause Li-Fraumeni syndrome which is characterised by cancer predisposition [68]. Perturbations to DNA replication (replication stress, which will be widely discussed in section 1.4) can also cause GI [69]. Moreover, common fragile sites are specific regions in the genome which are susceptible to chromosomal breakage following mild replication stress. They are favourable targets for high GI even from the early stages of tumorigenesis, emphasising the importance of the replication stress response in tumour suppression [70]. Defects in DNA damage proteins

can also cause GI and cancer prone diseases [67]. For example defects in XPA-XPG repair proteins cause Xeroderma Pigmentosum (XP) which is characterised by extreme sensitivity to sunlight [71]. Loss of function of CSA, CSB, XPB, XPD, XPG repair proteins cause a premature ageing syndrome known as Cockayne syndrome (CS) [72] . Loss of mismatch repair proteins MutS homologs 2,3 and 6 (MSH2, MSH3, MSH6), and MutL homolog 1 (MLH1) results in Lynch syndrome, which predisposes the individual to colorectal [73], ovarian [74] and breast [75] cancers. Mutations in genes encoding the RECQ DNA helicases WRN and BLM cause Werner [76] and Bloom syndromes [77], respectively. Defects in Fanconi Anaemia genes (FANCA-FANCP) cause Fanconi anaemia which is characterised by progressive bone marrow failure and cancer susceptibility [78]. Finally, dysfunction of Ataxia-telangiectasia mutated (ATM) and ataxia telangiectasia and Rad3-related protein (ATR) (master regulators of the DNA damage response) cause Ataxia Telangiectasia (A-T) which is characterised by poor coordination and balance (ataxia), enlarged blood vessels (telangiectasia), and immunodeficiency [79] and Seckel syndrome (SS) which is characterised by dwarfism, microcephaly and intellectual disability [80], respectively. Although cancer predisposition is not associated with SS, mutations in ATR have been found in breast and ovarian cancers [81].

The last addition to the hallmarks of cancer was this year when Hanahan proposed four new characteristics including unlocking phenotypic plasticity, nonmutational epigenetic reprogramming, polymorphic microbiomes, and senescent cells, recognising the great progress in cancer research over the last decade and the need of conceptualizing new discoveries in order to refine our understanding for cancer biology [82] (Figure 1.1).

1.2.11 Unlocking Phenotypic plasticity

During terminal differentiation, progenitor cells stop growing upon their organisation to form tissues. However, this process is bypassed during cancer pathogenesis, unlocking the phenotypic plasticity of the cells which continue to grow [83]. This can happen in several ways; cells originating from a fully differentiated state may reverse their course by dedifferentiating back to progenitor-like cell state; cells originating from an undifferentiated progenitor cell can shorten the differentiation process and remain in that partially differentiated, progenitor-like state; and cells that were committed to a certain

differentiation phenotype can switch developmental programs, or transdifferentiate, acquiring traits that are not associated with their cell of origin. Examples of disrupted dedifferentiation are the transcription factors Homeobox protein (HOXA5) [84,85] and SMA- and MAD-related protein 4 (SMAD4) [86] which are highly expressed in colon epithelial cells but are absent in advanced colon carcinomas that express colon and progenitor markers. Expression of SRY-Box Transcription Factor 10 (SOX10) blocks differentiation of neural progenitor cells into melanocytes allowing v-raf murine sarcoma viral oncogene homolog B1 (BRAF)-induced melanomas [87], while the pancreas associated transcription factor 1α (PTF1a*)* compromises *KRAS*-induced transdifferentiation and proliferation, favouring redifferentiation of already neoplastic cells into a quiescent acinar cell phenotype [88]. Notably, cellular plasticity is not a new characteristic but rather a ‘’switch’’ of existing mechanisms of normal cells for repair and regeneration.

1.2.12 Non-mutational epigenetic reprogramming

It has been shown by multiple studies that the tumour microenvironment favours epigenetic changes beneficial for the growth and expansion of cancerous cells. A common example is hypoxia, which causes dysfunctional vascularisation and alters the methylome by reducing the activity of ten-eleven translocation (TET) demethylases that catalyse DNA de-methylation [89]. Interestingly, non-mutational epigenetic reprogramming drives phenotypic plasticity as mentioned above via EMT [90,91]. Advanced technologies for profiling genome DNA methylation [92,93], histone modification [94], chromatin accessibility [95], and posttranscriptional modification and translation of RNA [96,97] have enabled us to understand the reciprocal role of non-mutational and mutational epigenetic regulation of cancer biology.

1.2.13 Polymorphic microbiomes

The human body is colonised by a plethora of microorganisms collectively known as the microbiota, of which the profound contribution to health and disease is being progressively uncovered via next generation sequencing technology and bioinformatic advances. Multiple studies have shown that microorganisms can have either a protective

or detrimental role in determining the path of cancer pathogenesis and in turn, therapeutic outcome [98]. Microorganisms promote tumorigenesis via different mechanisms; for example by the production of butyrate, which activates senescent cells and fibroblasts [99], as well as by modulating the expression of chemokines and cytokines that facilitate the suppression of natural killer cells and immune evasion. According to a recent study, gut derived bacteria migrated to the liver of mice with cholangiocarcinoma, inducing the secretion of the C-X-C motif Chemokine Ligand (CXCL1) from hepatocytes through Toll-like receptor 4 (TLR4) pathway and subsequently causing the accumulation of Myeloid-derived suppressor cells [100].

1.2.14 Senescence

Cellular senescence has been viewed classically to protect against neoplasia [101] although multiple studies now support the opposing argument, that senescent cells favour tumour development and progression [102,103] via the senescence-associated secretory phenotype (SASP), wherein they secrete high levels of cytokines and growth factors [101,104]. Cancer-associated fibroblasts also senesce, modulating ECM remodelling and production of growth factors and affecting angiogenesis as well as the immune system [105].

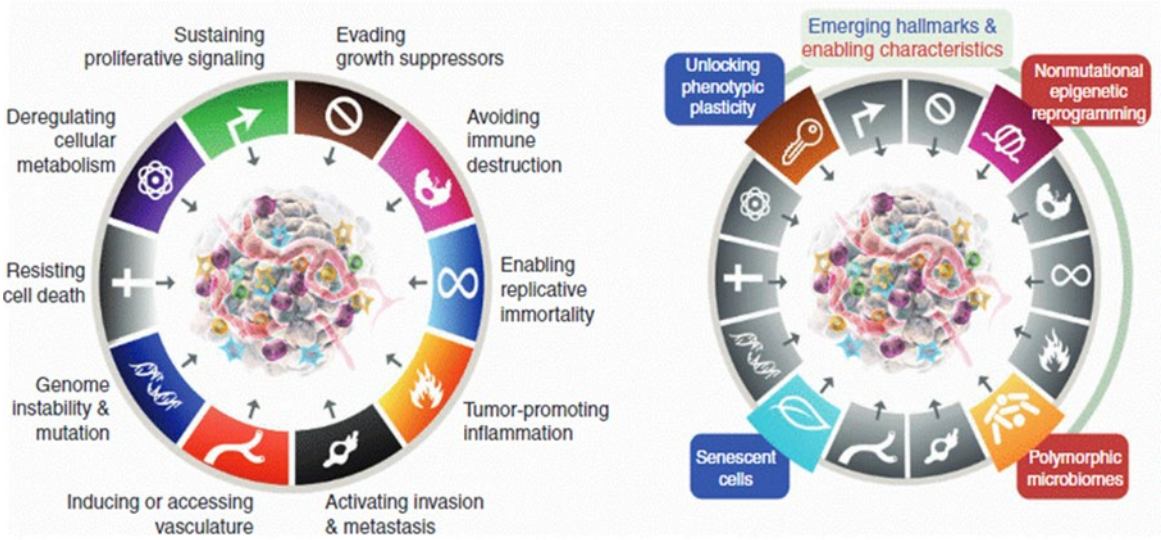

Figure 1.1 Hallmarks of cancer.

The figure displays ten common Hallmarks of cancer, as delineated by Hanahan and Weinberg (left). These include self-sufficiency in growth signals, insensitivity to anti-growth signals, evasion of apoptosis, limitless replicative potential, sustained angiogenesis, tissue invasion and metastasis, deregulation of cellular metabolism, evasion of immune destruction, genome instability and tumour promoting inflammation. Additional emerging hallmarks including unlocking phenotypic plasticity, non-mutational epigenetic reprogramming, senescent cells, and polymorphic microbiomes are also shown in the updated figure (right). Figure adapted from [6,35] .

1.3 DNA replication

Replication stress (which can cause genome instability) is an enabling factor in cancer pathogenesis and it is caused by a plethora of factors (which will be discussed in detail at section 1.4). DNA replication, wherein a double stranded DNA molecule is copied to produce two identical replicas from one original molecule and the two new daughter cells contain the same amount of genetic material as the parent cell, is essential for cellular life. It is also a universal process as it occurs in all living organisms, and is semi-conservative in nature, with each strand of DNA serving as a template for duplication; the resulting double helix includes one original strand and one newly-synthesised strand [106].

DNA replication begins at specific points called replication origins and it occurs via three main steps: initiation, elongation, and termination. Initiation of DNA replication is achieved by the Origin Recognition Complex (ORC), which is comprised of six subunits and recruits the Mini Chromosome Maintenance (MCM) complex to the replication origins. The MCM complex is a double hexamer, consisting of MCM2-7 proteins, that ensures that DNA replication occurs only once per cycle, and serves as a helicase by ATP hydrolysis [107,108]. Cell division control protein 6 homologue (CDC6) and chromatin licensing and DNA replication factor 1 (CDT1) also facilitate MCM origin loading to form the pre-replicative (pre-RC) complex [109]. CDKs, Dbf4-dependent kinase (DDK), the pre-RC complex, and other factors including RPA (Replication Protein A), CDC45 and GINS (go-ichi-ni-san) join the complex, whereupon the template DNA strand unwinds. This creates a ‘’Y’’ shape, also known as replication fork, where the two single strands act as templates for the new strands [110]. Topoisomerase 1 is recruited to sites ahead of the progressing replication fork, where it cuts the DNA in order to release torsional stress caused by supercoiling during replication [111]. Replication Factor C (RFC) then loads Proliferating-Cell Nuclear Antigen (PCNA) onto the DNA, thus supporting DNA polymerase efficiency. DNA replication occurs in a 5’→3’ direction. DNA polymerase ε scans the single strands and syntheses continuously complementary nucleotides in the leading strand. Due to the antiparallel nature of the DNA, the lagging strand requires the polymerase α-primase complex which assembles short single stranded nucleic acids followed by 15 to 20 deoxyribonucleotide primers, which are processed by DNA polymerase δ (pol δ) during the discontinuous synthesis of DNA [112]. Once DNA polymerase synthesises the new

nucleotides in both strands (elongation), the leading strand is complete, and the lagging strand contains Okazaki fragments. On the lagging strand, RNase H, Flap Endonuclease 1 (FEN1) and DNA2 remove the RNA primers in the beginning of each Okazaki fragment, followed by gap sealing by DNA ligase I [113] (Figure 1.2).

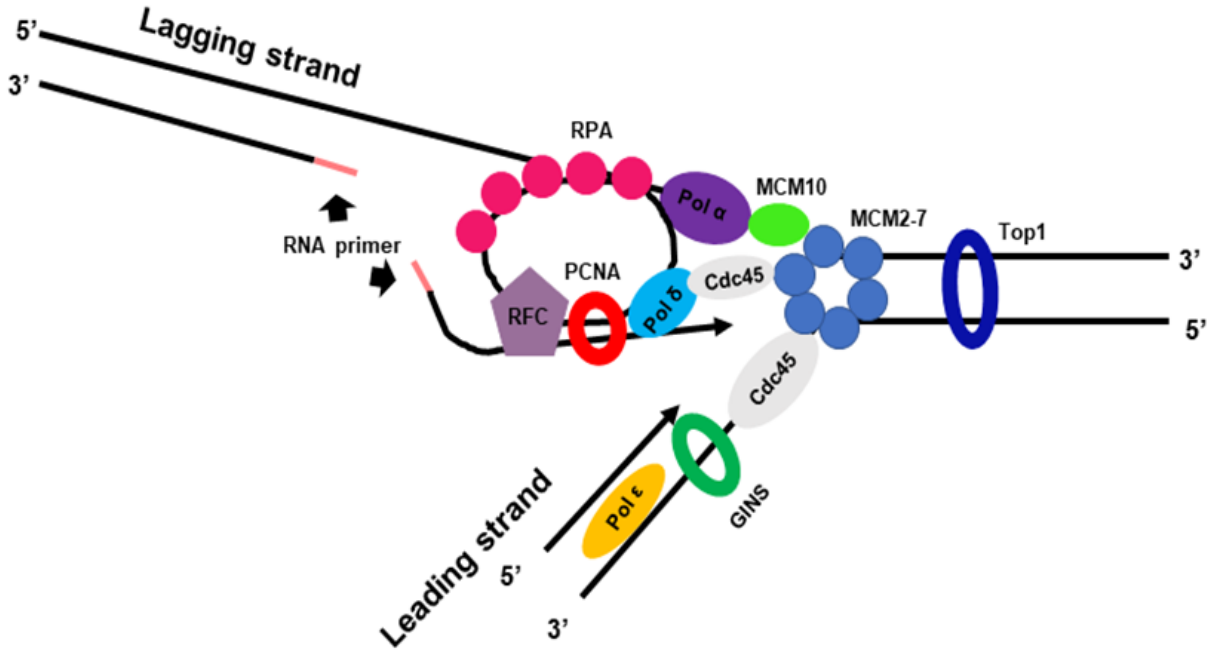

Figure 1.2. Mechanism of DNA replication.

DNA replication starts at specific sites called origins. The DNA is initially unwound by the MCM complex helicase activity, generating the replication fork. Topoisomerase activity ahead of the fork removes superhelical tension caused by strand separation. The leading strand is synthesized continuously in the 5′ to 3′ direction by polymerase ε whereas the lagging strand is synthesized discontinuously by polymerase δ creating short Okazaki fragments. PCNA secures polymerase interaction with the DNA strand. RPA also binds to single stranded DNA to stabilise the Okazaki fragments, which are further processed by RNase H, FEN1 and DNA2. DNA ligase then ligates the breaks in the Okazaki fragments.

DNA replication occurs during S phase of the cell cycle in a tightly regulated manner employing a plethora of proteins and a proof-reading system to ensure the faithful duplication of the genome. However, it is in some ways the most dangerous phase of the cell cycle, due to the probability of deleterious events. For example, DNA polymerases have an error rate of 1 out of 10^4-10^5 nucleotides which can lead to genomic alterations

and subsequent to GI [114,115]. Likewise, impediments to DNA replication can pose a significant threat to genome integrity, via a variety of mechanisms.

CDKs play a prominent role in regulating cell cycle transitions and DNA replication. CDKs are a family of serine/threonine protein kinases which phosphorylate a variety of target proteins and complex with specific cognate regulatory factors called cyclins, which direct kinase activity and substrate specificity [116]. CDKs can be considered as the engines that drive cell cycle progression, cyclins as the gears that change to facilitate cell cycle transition, and CDK inhibitors as the brakes which halt cell cycle progression. CDK/cyclin complexes were firstly discovered in yeast. Early experiments revealed the CDC2 gene in Saccharomyces pombe (CDC28 in Saccharomyces cerevisiae) as encoding a crucial CDK [117–119]. Since then, at least 20 mammalian CDKs and cyclins have been identified, and widespread compensation among CDKs and cyclins has been reported [120,121]. The major cyclins and CDKs acting at specific stages of the cell cycle are as follows; in G1 phase, cyclin D activates CDK4/CDK6 followed by activation of CDK2 by cyclin E; in S phase, cyclin A2 activates CDK2 promoting S phase progression; in G2 phase cyclin A2 activates CDK1 to facilitate the onset of M phase, and cyclin B/CDK1 drives the G2-M transition.

CDK4 is of particular relevance to this thesis. In G1, upon binding of cyclin D to CDK4/6, the cyclin-CDK complex enters the nucleus, where it is phosphorylated by the CDK-activating kinase (CAK) complex. This leads to the hypophosphorylation of the Rb tumour suppressor which in turn inhibits the transcription factor E2F, ultimately preventing the cell from entering G1 phase [122]. The INK4 family of proteins ($p16^{INK4A}$, $p15^{INK4B}$, $p18^{INK4C}$, and $p19^{INK4D}$, as well as the Cip and Kip family ($p21^{CIP1}$ and $p27^{KIP1}$) regulate the activity of CDK4/6 by directly binding to CDKs and acting as inhibitors [123]. Notably, dysregulation of the cyclin D-CDK4/6-INK4-Rb pathway causes cell cycle progression and is commonly found in many types of cancers [124]. Abnormal cyclin D-CDK4/6-INK4-Rb pathway can be caused via different mechanisms; direct mutation of the Rb gene, overexpression of D-type cyclins, mutation or amplification of CDK4/6 or inactivation of CDK inhibitors (i.e. $p16^{INK4}$) [124–126]. In addition, activation of another tumour suppressor gene, p53, induces the expression of the CDK inhibitor $p21^{CIP1}$ which appears to have an important tumour suppressive role [124], causing G1 arrest [127,128]. Conversely, tumour suppressor genes are inactivated during cancer pathogenesis, allowing cells to divide uncontrollably [129] (Figure 1.3) . Mutations in p53 are also present in the majority of human cancers, with mutant

p53 not only losing its tumour suppressive role but often obtaining additional oncogenic functions that afford cancer cells significant survival advantages [130].

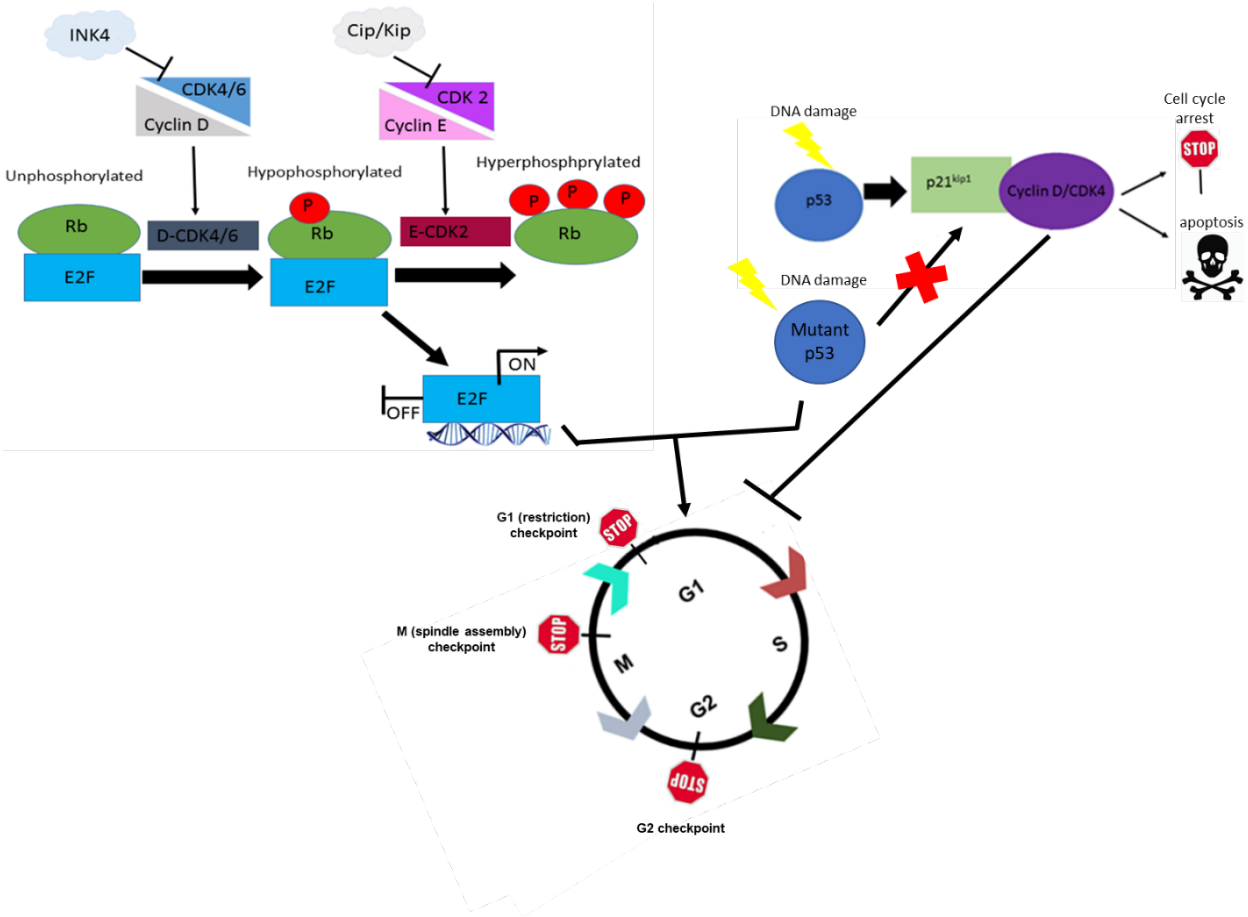

Figure 1.3 Function of Rb and p53 in cell cycle regulation.

Phosphorylation of Rb by both cyclin D-CDK4/6 and E-CDK2 leads to the dissociation and activation of E2F, allowing the transcription of the E2F target genes required for cell cycle progression and S phase entry. INK4 and CIP/KIP inhibitory families which target CDK4/6 and CDK2 respectively are also shown in the diagram. Upon DNA damage, p53 is activated which activates $p21^{KIP1}$. The latter binds to cyclin D/CDK4 and inhibits the progression of G1/S until the DNA is repaired. If DNA cannot be repaired, cells die by apoptosis. When p53 is mutated and DNA damage is induced, mutant p53 cannot bind to $p21^{KIP1}$ and cells proceed unchecked to G1/S which can cause GI. The cell cycle is constantly monitored by three main checkpoints; G1 (restriction) checkpoint which determines if the conditions are favourable for cell division, G2 checkpoint which ensures that all chromosomes have been accurately replicated and M (spindle assembly checkpoint) which determines whether all the sister chromatids are correctly attached to the spindle microtubules.

1.4 DNA replication stress

Although DNA replication is a tightly regulated process, many obstacles can disrupt replication fork progression. In the case of an impediment to replication, replication stress (RS) can occur. RS is characterised by slowing or stalling in replication fork (RF) progression which may lead to RF collapse and DNA damage [131]. However, if the stress is removed/repaired or bypassed/tolerated, RFs can restart (see 1.11.3 section). RS can be caused by a variety of sources; including intrinsic such as dormant replication origins, misincorporation of ribonucleotides, early replicating and common fragile sites, overexpression/activation of oncogenes, secondary DNA structures (G-quadruplexes, hairpins, cruciforms) as well as extrinsic such as ultra-violet, (UV) ionising radiation (IR) and chemotherapeutic agents (i.e., nucleoside analogues and topoisomerase inhibitors) [132] (Figure 1.4).

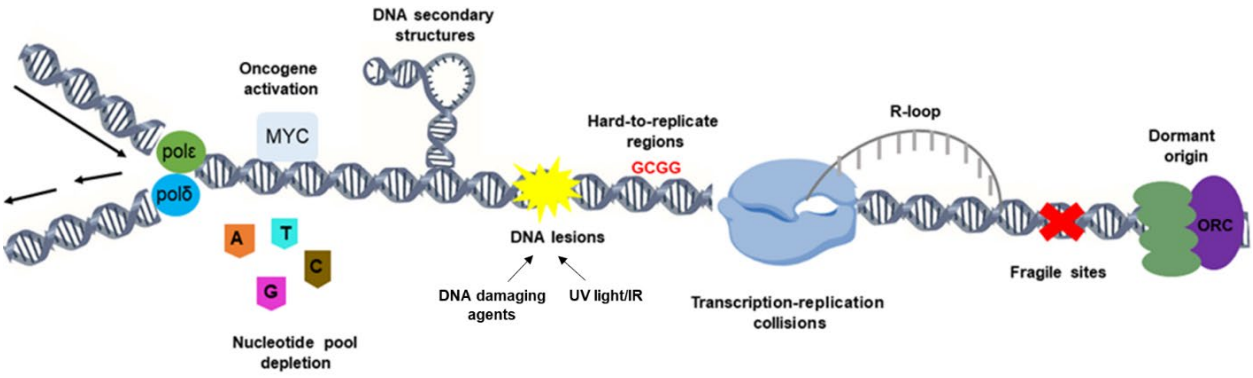

Figure 1.4 Causes of replication stress.

Obstacles in replication fork progression can arise both endogenously including activation of oncogenes, depletion of nucleotide pools, DNA secondary structures, difficult to replicate regions, collisions between replication and transcription and exogenously including UV, IR and genotoxic chemical compounds. Figure adapted from [132] .

Activation of oncogenes including cyclin E, HRas and MYC, are among the major sources of cancer-relevant RS [133]. Some mechanisms that drive oncogene-induced replication stress (OIS) include; reduced or increased origin firing, depletion of the nucleotide pool, shortage of replication factors, reduced fork elongation rates and increased transcription and replication-transcription conflicts [134,135].

The c-myc oncogene deregulates expression of CDKs and E2F transcription factors, both of which regulate cell cycle progression [136]. Likewise, overexpression of cyclin E in human cells causes GI and specifically inhibits MCM chromatin binding during G1 [137,138]. Moreover, cyclin E overexpression increases the number of active replication origins, impairing RF progression and activating the DNA damage pathway, leading to RAD51-mediated recombination [139,140]. Overexpression of cyclin D also decreases RF progression and is associated with the induction of double strand breaks (DSBs) mediated by MUS81 endonuclease in radioresistant cells [141]. Various oncogenes can compromise the licencing checkpoint; for example Human Papillomavirus E7 (HPV E7), which inactivates Rb and promotes G1 progression when MCM is depleted [142], while mutant KRAS sensitises cells to CDC6 depletion [143], and overexpression of c-myc sensitises cells to ORC1 depletion [144]. H-RAS drives RS through increased origin firing [145]. Expression of adenovirus transforming E1A oncogene also alters DNA replication, leading to increased replicon length, fork velocity, and inter-origin distance [146]. Recent work demonstrates that Cyclin E and MYC oncogenes reduce the length of G1 phase in U2OS human cell lines, allowing insufficient time for transcription to inactivate all intragenic origins, thereby leading to RS. However, it is important to note that different oncogenes induce RS via different mechanisms; for example, inhibition of origin firing does not abolish RAS-mediated RS [147], but rescues RS driven by cyclin E overexpression [140]. The number of stalled forks and the duration of arrest dictate how the cell will respond to RS [148–151].

1.4.1 Chemotherapeutic agents

Chemotherapeutic agents are one of the main extrinsic inducers of RS and can cause a broad spectrum of DNA lesions. As described earlier, GI and a high mutational rate, which can result from defective DNA damage surveillance, checkpoint, and repair mechanisms (see later sections), are key characteristics of cancerous cells. In some cases, such elevations in mutation rate are a consequence of impaired genome maintenance mechanisms. This inability of cancerous cells to repair their DNA efficiently can render them vulnerable to DNA damaging agents. Furthermore, cancer cells divide more rapidly than most untransformed cells. Hence, for over the last 60 years, DNA damaging agents have represented a mainstay for the treatment of both haematological and solid tumours [152,153].

Antimetabolites represent a group of anticancer drugs that structurally resemble natural nucleotides and hence interfere with DNA replication. Their incorporation into genomic DNA disrupts nucleic acid synthesis, causing DNA replication to halt. Examples of pyrimidine analogues include 5-fluorouracil (5-FU), Cytarabine, Floxuridine and Gemcitabine and examples of purine analogues include Fludarabine, Cladribine, 6-mercaptopurine and 8-azaguanine [154,155]. Some of their structures are shown below (Figure 1.5).

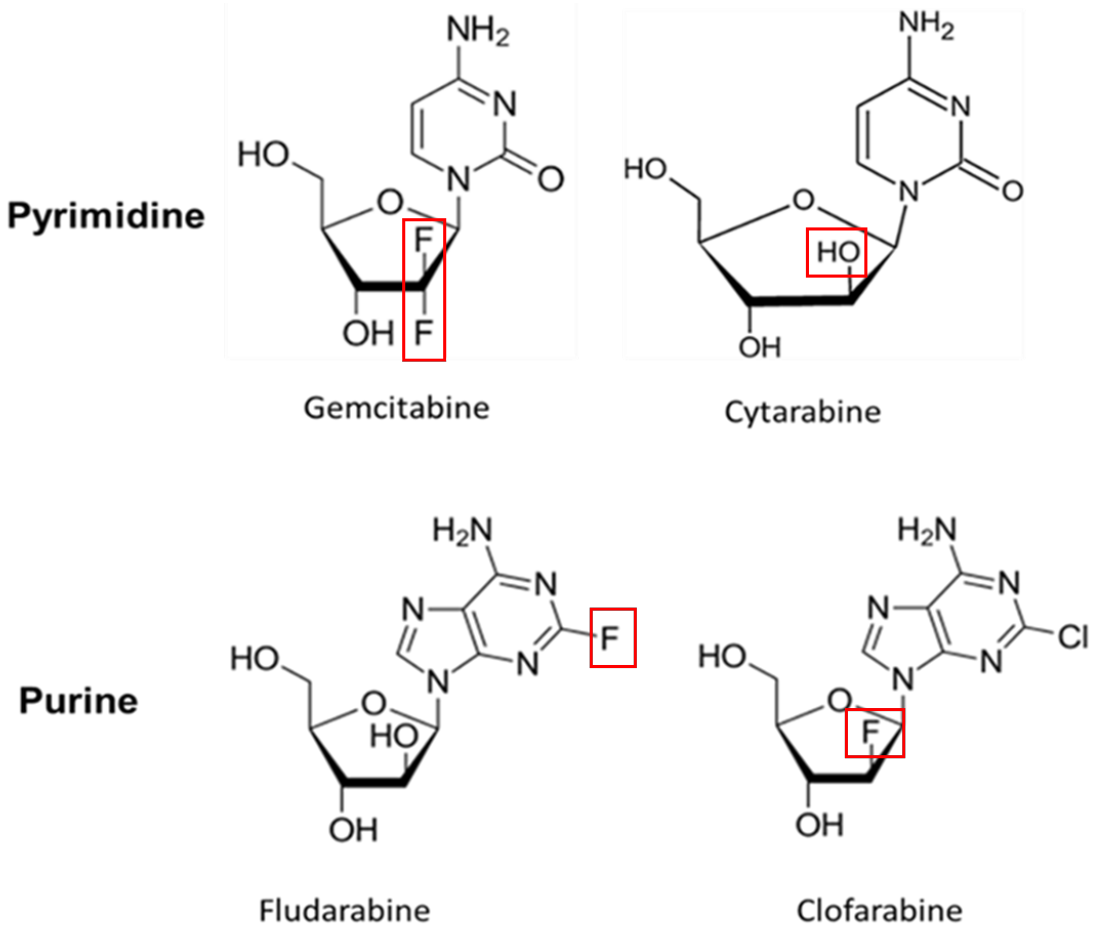

Figure 1.5 Chemical structures of Gemcitabine, Cytarabine, Fludarabine and Clofarabine.

Gemcitabine and Cytarabine are pyrimidine analogues while Fludarabine and Clofarabine are purine analogues. Gemcitabine differs structurally from cytosine due to its fluorine substituents on position 2' of the six member ring while cytarabine has an additional hydroxyl group on position 2'. Fludarabine is a derivative of Cytarabine having a halogen (fluorine) at the C2 position of the ring. Clofarabine is a hybrid of Fludarabine, and it is substituted with a fluorine at position 2 of the purine ring. Red boxes indicate the chemical groups of each nucleoside analogue that are different compared to the naturally occurring nucleosides. Figure taken from [154,155].

Gemcitabine is a cytidine analogue with two fluorine atoms in position 2' of the sugar ring and it is used as a chemotherapeutic against a variety of solid tumours such as lung and pancreas [156]. Due to its hydrophilic nature, passive diffusion into the cell is slow thus it is transported by human nucleoside transporters (hNTs), including both sodium-dependent human concentrative nucleoside transporters (hCNTs) and sodium-independent human equilibrative nucleoside transporters (hENTs). Following Gemcitabine intake into the

cells, it is rapidly phosphorylated by cellular kinases. Once triphosphorylated (dFdCTP), it is incorporated into the DNA during replication, a single deoxyribonucleotide is then added, preventing chain elongation [157]. DNA polymerases cannot add any further nucleotides, a mechanism known as masked chain termination which also prevents DNA repair enzymes to act upon [158]. In addition, the diphosphorylated form (dFdCDP) of Gemcitabine causes inhibition of ribonucleotide reductase (RNR) which lowers the pool of endogenous deoxynucleotides available for DNA synthesis [159]. dFdCTP is also incorporated into RNA [160] (Figure 1.6), the incorporation of which has been shown to be dependent on cell line and concentration of the drug leading to inhibition of RNA synthesis [161]. In addition, high levels of dFdCTP have shown to be inhibitory to CTP synthetase [162]. Although Gemcitabine is used for the treatment of several types of tumours, resistance commonly arises as tumours do not respond to the treatment or the duration of the response is short [163].

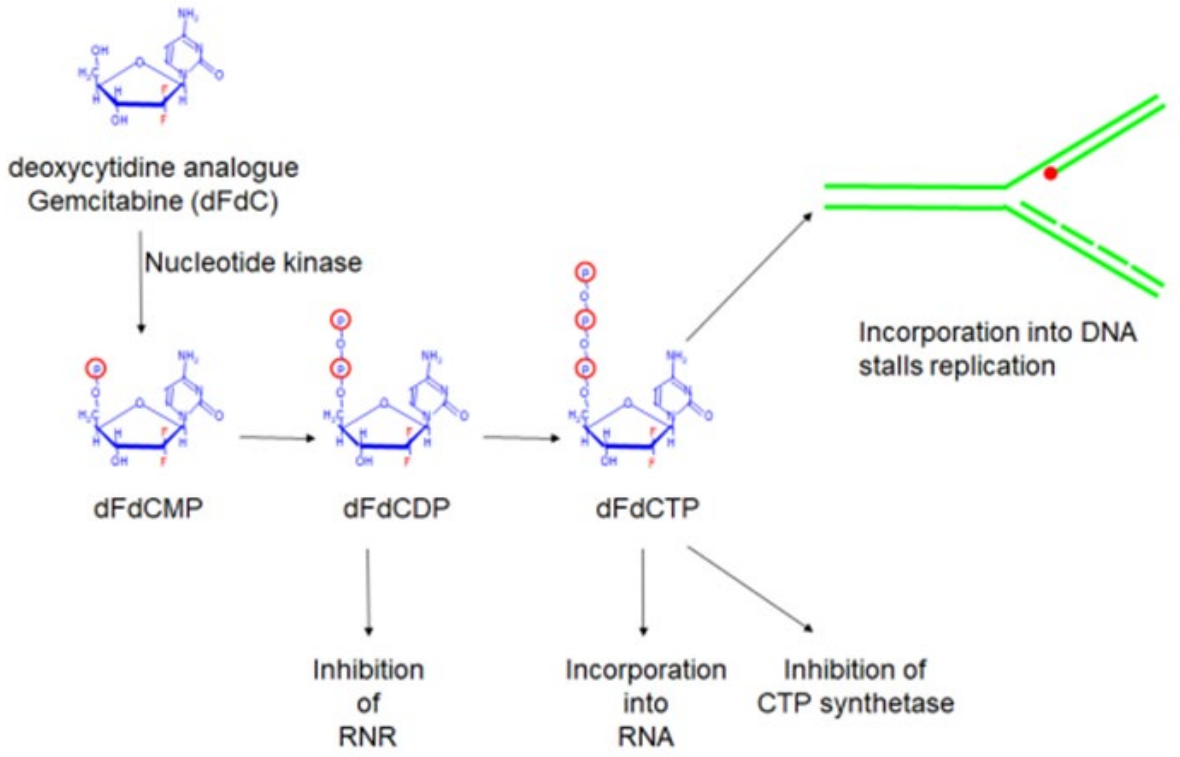

Figure 1.6 Mechanism of action of Gemcitabine.

dFdC is a prodrug which is triphosphorylated by a series of kinases. Incorporation of the triphosphate form (dFdCTP) into nascent DNA causes fork stalling. The diphosphate form (dFdCDP) also acts to inhibit the ribonucleotide reductase (RNR) enzyme, lowering the pool of endogenous nucleotides, in favour of increased Gemcitabine incorporation. Picture created by Dr. Edgar Hartsuiker.

1.5 The Replication Stress Response

Persistent replication stress is a significant contributor to GI; therefore, the cells employ specialised networks that deal with RS facilitating the restart of the forks (which will be discussed in detail in section 1.9.3) and by extent resumption of normal cell cycle progression or programmed cell death.

When a replication fork is stalled, a signalling cascade is activated to initiate the S-phase checkpoint, which prevents S-phase progression until the stress is resolved and the fork can be restarted. Upon fork stalling, the RF helicase (which includes MCM helicase and several other factors), runs ahead of the stalled replication fork and unwinds the DNA to form a tract of single stranded DNA (ssDNA) [164]. The ssDNA is then bound with high affinity by RPA [165] which serves as a platform for the recruitment of a variety of proteins including Ataxia Telangiectasia and Rad3-related (ATR)-interacting protein (ATRIP) [166], the 9-1-1 DNA clamp complex (RAD9-RAD1-HUS1) [167], Topoisomerase II Binding Protein 1 (TOPBP1) [168], and Ewing Tumor-Associated Antigen 1 (ETAA1) [169]. These proteins function in concert to activate the ATR kinase and induce the replication checkpoint, ultimately promoting RF stability. ATRIP binds to ATR forming an ATR–ATRIP heterodimer [170]. The ATR-ATRIP complex directly interacts with ssDNA-bound RPA, promoting ATR localization to the sites of damage [171]. The pre-mRNA processing factor 19 (PRP19) facilitates ubiquitylation of RPA, further ATRIP binding to damaged DNA [172], and partial ATR activation [173]. The ATRIP–ATR complex (assisted by RPA) then interacts with the -1-1 DNA clamp complex [174] which is then phosphorylated, causing the association of DNA topoisomerase 2-binding protein 1 (TOPBP1) with the FATC domain of ATR [175] and driving ATR activation [176]. TOPBP1 can also interact with phosphorylated or unphosphorylated 9-1-1, and this interaction is regulated by Rad9, Rad1 and Hus1 interacting nuclear orphan (RHINO) [177], which further activates ATR [178].

One of the main ATR targets is checkpoint kinase 1 (CHK1) which in turn phosphorylates all members of the CDC25 phosphatase family; CDC25C on S216, leading to its cytoplasmic sequestration and G2-M checkpoint activation [179]; CDC25A on multiple sites, targeting it for degradation and S and G2 checkpoint activation [180–182], as well as CDC25B on S230 under unperturbed conditions, preventing premature initiation of mitosis [183]. CDC25 proteins in turn inhibit CDKs causing cell cycle arrest, stabilisation of stalled forks and inhibition of origin firing to inhibit excessive ssDNA formation [184].

Despite the replication stress response to stabilise and restart the fork, RFs may fail to restart if RS persists. Failure to stabilize RFs may lead to their collapse and potentially cause DNA damage [185]. Just as organisms have evolved a RS response, they have also developed an elegant and specialised DNA damage response system, that detects DNA lesions and promotes their removal/ repair. It is thus imperative that the replicative stress response is orchestrated with DNA damage response pathway to maintain genome stability.

1.6 DNA damage response systems

It has been estimated that around 10.000 DNA lesions occur daily in every cell from both endogenous and exogenous sources. Endogenous sources of DNA damage include hydrolysis, oxidation, alkylation as well as oxygen reactive species while exogenous sources include environmental, physical and chemical agents (UV, IR and alkylating and crosslinking agents) [186]. Consequently, organisms have evolved elaborate mechanisms to deal with different kinds of damage [187]. Repair of damaged DNA is mediated by a series of complex protein networks, collectively known as the DNA damage response (DDR). The DDR consists of sensors that act to detect the damage, mediator proteins activated by the sensors that transmit and expand signals within the network, as well as effector proteins that elicit and define the cellular response [188].

The DDR is orchestrated in large part by a family of highly-conserved protein kinases – the Phosphatidylinositol-3-Kinase-like Kinase family (PIKKs) [189]. The Ataxia-Telangiectasia-Mutated (ATM) and Ataxia Telangiectasia and Rad3-related (ATR) and DNA-dependent Protein Kinase (DNA-PK), are key regulators of the DDR response and among the first responders to DNA damage. Each kinase acts via distinct mechanisms, responding to specific types of damage in a cell cycle-regulated manner; ATM is largely activated at DSBs during G1 whereas ATR is activated by a broad spectrum of DNA damage including DSBs, base adducts and crosslinks during S phase [190]. Under physiological, non-stressed conditions, ATM exists in an inactive, multimeric state [191]. Following DNA damage, one of the main proteins to be activated is ATM. ATM activation occurs by autophosphorylation and acetylation resulting in simultaneous dissociation of the ATM homodimers and increased kinase activity. In particular, ATM is auto-

phosphorylated in its conserved FRAP-ATM-TRRAP (FAT) domain on Ser 1981 [191]. This phosphorylation also contributes to the stability of the protein [192]. ATM is also auto-phosphorylated at Ser367 and Ser1893 which further contributes to its activation [193]. Acetylation of ATM at K3016 is required for autophosphorylation and monomerization upon DNA damage [194]. Despite the initial activation of ATM, it is the MRN complex (see section 1.7) that contributes to full ATM activation [195]. Activated ATM then phosphorylates the core histone variant H2AX which in its turn binds to MDC1. The latter recruits a plethora of DDR factors, and it further activates the MRN-ATM pathway amplifying the DDR signal [196] .

Once both ATR and ATM are activated, they phosphorylate CHK1 and CHK2 kinases respectively, however this specificity is not absolute, as crosstalk between these two kinases and their substrates has been reported [181,197]. Activated CHK1 and CHK2 then phosphorylate a myriad of downstream effectors including E2F1, BRCA1, p53 and several cyclins to mediate cell cycle halting, apoptosis, and DNA damage repair and tolerance mechanisms [196] (Figure 1.7).

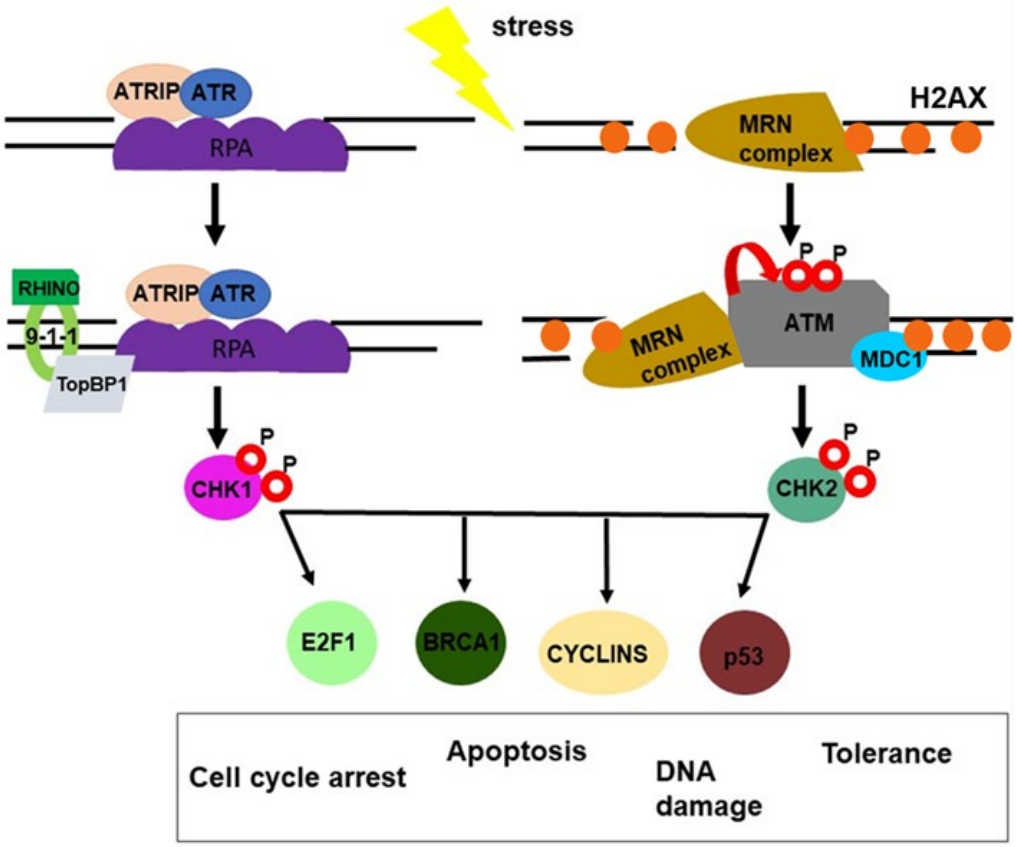

Figure 1.7 ATR and ATM activation.

During RS, RPA binds to ssDNA facilitating the formation of an ATR–ATRIP complex which interacts with the 9-1-1 complex. Activated ATR phosphorylates and activates the downstream effector kinase CHK1. Upon DNA damage, the MRN complex is recruited to the sites of damage and facilitates the autophosphorylation of ATM which in turn phosphorylates the core histone H2AX and activates MDC1. MDC1 then activates more DDR factors including the downstream effector kinase CHK2. Activated CHK1 and CHK2 kinases phosphorylate a range of other factors that initiate cell cycle checkpoints and determine cell fate.

However, some overlapping functions between ATM and ATR have been documented. ATR acts during DSBs through a mechanism that involves ATM and the meiotic recombination 11 (MRE11)–(RAD50) Double Strand Break Repair Protein – Nijmegen breakage syndrome 1 (NBS1) (MRN) complex [198,199], the latter of which will be discussed in detail in the following section. Unlike ATM and DNA-PK, ATR is essential for replication in both human and mouse cells [170,200,201].

1.7 DNA repair mechanisms

Upon DNA damage, a robust DNA damage response is initiated which is cell cycle and damage type specific. The main DNA repair mechanisms include; Base Excision Repair (BER) for small, no-helix distorting base lesions which can be typically caused by oxidation, hydrolysis, deamination or methylation, Nucleotide Excision Repair (NER) for bulky, helix-distorting lesions caused by UV light (6-4 photoproducts and cyclobutane pyrimidine dimers), environmental mutagens and chemotherapeutic agents (i.e., Cisplatin), DNA Double Strand Break (DSB) repair for breaks in both DNA strands (which will be further discussed below) and mismatch repair (MMR) for DNA mismatches [186].

1.7.1 Double strand break repair mechanisms

DSBs are one of the most deleterious types of DNA damage, as both DNA strands are disrupted. If DSBs are left unrepaired they can result in loss of genetic material or chromosomal rearrangement or cell death which can promote tumourigenesis [202]. However, DSBs also participate in normal physiological processes including immunoglobulin heavy chain (IgH) class switch recombination (CSR) and V(D)J recombination for the development of B cells and T cells [203].

Repair of DSBs can be achieved via homologous recombination (HR), classical non-homologous end joining (c-NHEJ), alternative end joining pathway(s) (a-EJ) wherein DNA polymerase θ (polθ) is the predominant (albeit not exclusive) mediator thus also known as TMEJ and single-strand annealing (SSA) (Figure 1.8). The main two pathways of DSB repair are HR and c-NHEJ which are highly conserved throughout eukaryotic evolution.

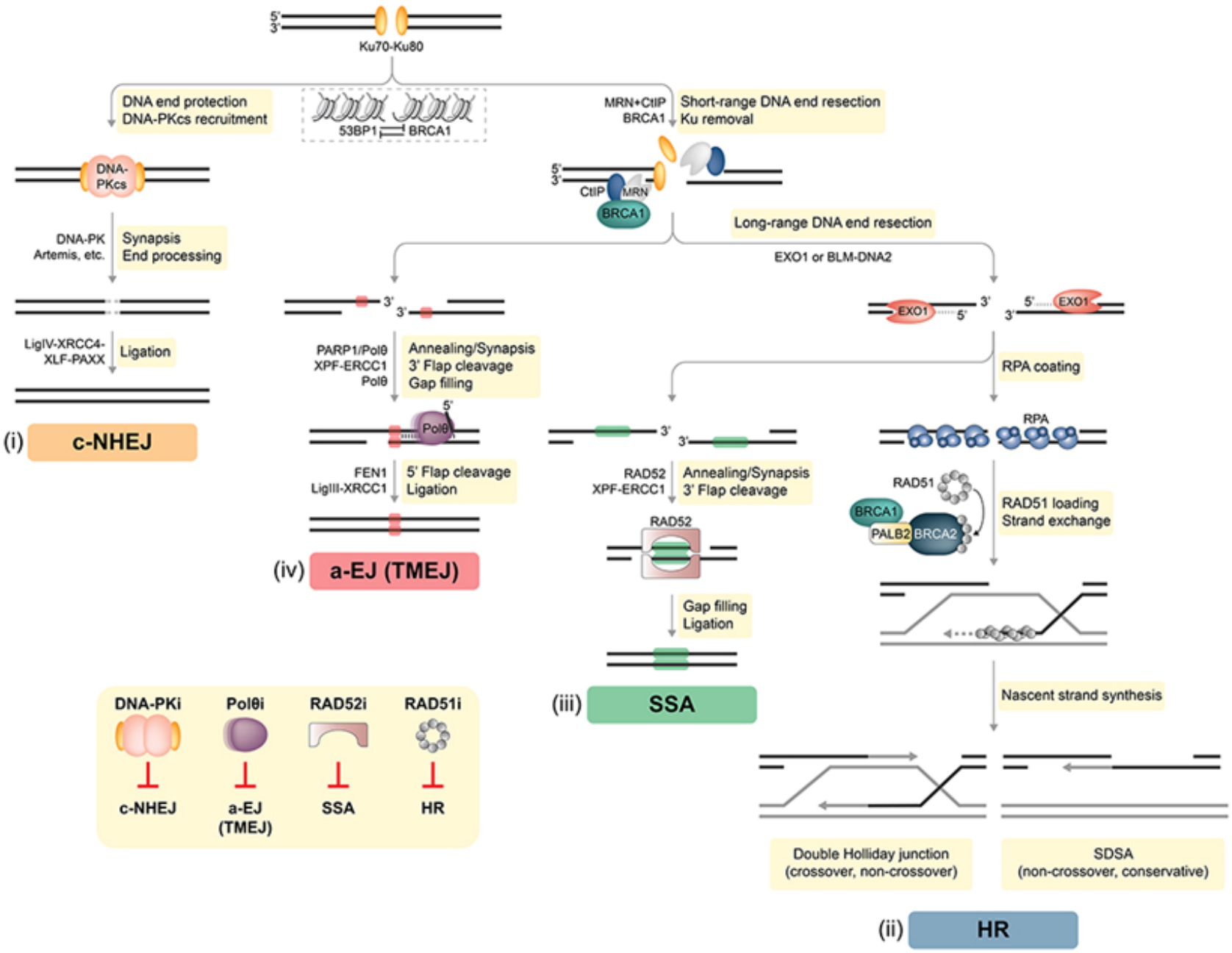
Ku70-Ku80
DNA end protection
DNA-PKcs recruitment
53BP1
BRCA1
MRN+CtIP
BRCA1
Short-range DNA end resection
Ku removal
DNA-PKcs
DNA-PK
Artemis, etc.
Synapsis
End processing
LigIV-XRCC4-
XLF-PAXX
Ligation
(i) c-NHEJ
CtIP
MRN
BRCA1
Long-range DNA end resection
EXO1 or BLM-DNA2
EXO1
PARP1/Polθ
XPF-ERCC1
Polθ
Annealing/Synapsis
3' Flap cleavage
Gap filling
FEN1
LigIII-XRCC1
5' Flap cleavage
Ligation
(iv) a-EJ (TMEJ)
RPA coating
RPA
RAD52
XPF-ERCC1
Annealing/Synapsis
3' Flap cleavage
RAD52
Gap filling
Ligation
(iii) SSA
RAD51
BRCA1
PALB2
BRCA2
RAD51 loading
Strand exchange
Nascent strand synthesis
Double Holliday junction
(crossover, non-crossover)
SDSA
(non-crossover, conservative)
(ii) HR
DNA-PKi
Polθi
RAD52i
RAD51i
c-NHEJ
a-EJ
(TMEJ)
SSA
HR

Figure 1.8 DSB repair pathways.

The main two DSB repair pathways are classical non-homologous end joining (c-NHEJ) and homologous recombination (HR) pathway. In addition, DSBs can be repaired by alternative pathways including alternative end joining (a-EJ) also known as DNA polymerase theta-mediated end joining (TMEJ) and single strand annealing (SSA). I) During c-NHEJ, Ku70/80 proteins bind to DSB, facilitating the recruitment of DNA-dependent protein kinase catalytic subunit (DNA-PKcs), and form DNA-PK holoenzyme bringing the broken DNA ends together (synapsis) which are then trimmed by nucleases such as Artemis. Ligation is achieved by ligase IV complex which includes XRCC4 and XLF ligases. II) HR is initiated by the binding of the MRE11-RAD50-NBS1 (MRN) complex to DNA breaks and together with CTIP and BRCA1, they are responsible for short range DNA resection. Long range resection is then followed by exonuclease 1 (EXO1) or Bloom's syndrome (BLM) helicase facilitated by DNA2 nuclease resulting in a 3'overhang intermediate which is then coated by RPA. The BRCA1-PALB2-BRCA2 complex allows RAD51 to bind to ssDNA forming RAD51 nucleofilaments and displacing RPA. RAD51 binding facilitates strand invasion which leads to either "synthesis-dependent strand annealing" (SDSA), or Holliday junction intermediates. III) SSA uses homologous repeat sequences (20–25 bp) which are found between repetitive elements (green boxes) in the genome. Strand annealing is then achieved by RAD52, and DNA is cleaved by XPF-ERCC1. It is yet to be elucidated which proteins are responsible for gap filling and ligation. IV) A-EJ (also known as TMEJ) uses short microhomologies of 2–20 bp (red boxes) to join the two DNA strands. DNA polymerase θ (Polθ) is recruited to DSBs by PARP for DNA synthesis. Flap processing is achieved by flap endonuclease 1 (FEN1) while ligase 3 (LIG3) closes the gaps. Figure taken from [202].

The choice of pathway is dependent on the structure of the broken DNA ends, the phase of the cell cycle as well as the cell type. NHEJ is an error prone process that mediates repair in all phases of the cell cycle by directly religating the two DNA broken strands with no regard for homology causing DNA loss and mutations [204,205]. In contrast, HR, SSA and a-EJ require 5'→3' nucleolytic degradation to generate ssDNA overhangs. HR is an accurate repair process which uses the intact sister chromatid as a template and is limited to the S and G2 phases of the cell cycle. In addition, HR is the main repair mechanism in yeast and simpler eukaryotes that have compact genomes and a small portion of repetitive sequences whereas NHEJ is a more effective and rapid mechanism in mammals in which repetitive regions are more abundant [64]. SSA is an error prone process, and it requires annealing of longer complementary sequence (more than 50bp) in resected overhangs.

1.7.1.1 Non-Homologous End Joining (NHEJ)

In NHEJ, the DSB is firstly recognised by the Ku70/80 heterodimer in a sequence-independent manner. The heterodimer is comprised of Ku70 and Ku80 proteins and has a high affinity for double-stranded termini. Upon binding, it acts as a platform for the recruitment of other NHEJ proteins to DSBs including DNA-dependent protein kinase, catalytic subunit (DNA-PKcs) [206], X-ray cross complementing protein 4 (XRCC4), DNA Ligase IV [207], XRCC4-like factor (XLF) [208], and Aprataxin-and-PNK-like factor (APLF) [209,210]. Upon recruitment, Ku binds to DNA-PKcs, forming a DNA-PK holoenzyme [211]. DNA-PKcs is a member of the phosphatidylinositol-3 (PI-3) kinase-like kinases which phosphorylate XRCC4 and also bridge the two broken DNA ends enhancing the efficiency of the process [212]. There are several proteins responsible for DNA resection during NHEJ including Artemis, Werner Syndrome Protein (WRN), and APLF. Artemis has a 5′ endonucleases activity, a 5′→3′ exonuclease activity and the ability to remove 3′-phosphoglycolate groups from DNA termini [213,214]. WRN interacts with both the Ku heterodimer and XRCC4 causing the stimulation of the 3′ →5′ exonuclease but not 3′ →5′ helicase of WRN [215,216]. APLF has an endonuclease and a 3′→5′ exonuclease activity. Nucleotide synthesis is achieved by the Pol X family polymerases, including polymerases λ and μ with the former having a template-independent activity [217] and the later synthesising across the discontinuous template [218]. Finally DNA ligase IV complex, including XRCC4 and XLF, is responsible for ligation of either strand of the DSB [219]. XRCC4 stabilizes Ligase IV stimulating its ligation activity through adenylation [220]. The paralog of XRCC4 and XLF human (PAXX) protein, which is member of the XRCC4 family, is also recruited to the sites of DNA damage and promotes Ku-dependent DNA ligation in vitro upon its interaction with Ku proteins (Figure 1.9).

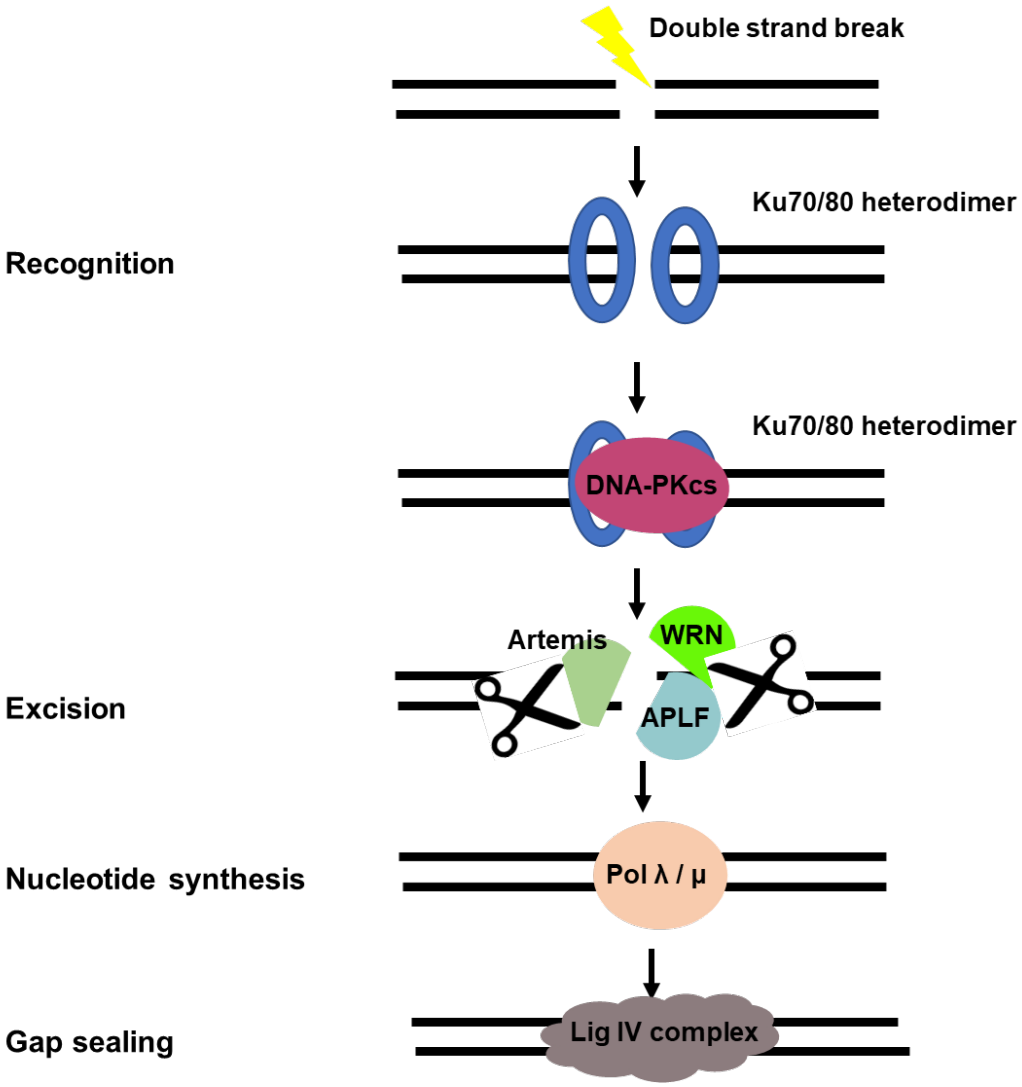

Figure 1.9 Schematic representation of NHEJ in repair mechanism.

The lesion is recognised by the Ku70/80 heterodimer which acts as a platform for the recruitment of DNA-PKcs. Lesion excision is performed by several proteins including Artemis, WRN and APLF which have endo and exonuclease activities. Polymerase λ and μ are responsible for synthesising new nucleotides. Finally, the nick is filled by the ligase IV complex.

1.7.1.2 Homologous Recombination (HR)

A key step in HR is the creation of 3' single stranded DNA overhangs which are generated via the nucleolytic resection of the DSB ends (Figure 1.10 excision step). MRE11 is a crucial nuclease, which acts in association with phosphorylated CtIP to resect ~200–300 nucleotides away from the DSB by endonucleolytic cleavage followed by 3'→5' exonucleolytic degradation back towards the DNA end [221]. CtIP is indispensable for endonucleolytic incision by MRE11 [222]. The endonucleolytic cleavage sites are also entry sites for DNA2 and EXO1 nucleases that act downstream the MRN in the 5'→3' direction extending the resected tracts to produce 3' intermediates in conjunction with BLM or WRN proteins [223–226]. BLM and WRN are thought to act epistatically with DNA2 in order to promote long range resection [227]. More specifically, WRN physically interacts with DNA2 to mediate 5'→3' resection, a process which is dependent on RPA [225]. In addition, an interaction between CtIP and BLM has been shown to increase the helicase activity of the latter, and to enhance the cleavage activity of DNA2 to promote long range resection. This suggests that CtIP is implicated in many facets of DNA resection beyond MRE11 regulation [228].

The second step of HR involves the binding of heterotrimeric RPA to the newly-formed 3' ssDNA [229]. RPA removes secondary structures from ssDNA ends and is subsequently displaced in order to allow RAD51 to bind to the ssDNA [230]. This step is facilitated by BRCA2 which is a protein with several functional domains, of which a set of eight 35-residue motifs (known as BRC repeats), enable it to bind with RAD51. Indeed, BRCA2 sequesters RAD51 as a monomer bound to BRC1-8 repeats, mobilises, and activates it to the sites of damage facilitating the formation of nucleoprotein filaments. In addition to BRC repeats, a sequence of approximately 200 amino acids (aa) in the C-terminal domain interacts directly with RAD51 filaments and stabilises them [231]. The RAD51 nucleoprotein filament interacts with the undamaged strand and undergoes strand exchange wherein the 3' ssDNA tails invade the intact DNA duplex and displaces one of the strands generating a D-loop structure. The latter provides a 3′ end which will be used for the next step, DNA synthesis. Having the undamaged strand as a DNA template, DNA polymerase synthesises nucleotides generating two Holliday junctions (HJ). The HJ must be processed by resolvases or dissolvases to fulfil efficient segregation and this can lead

to crossover or non-crossover products respectively. The strands are then ligated by ligase I [232]. The HR pathway is summarised in (Figure 1.10).

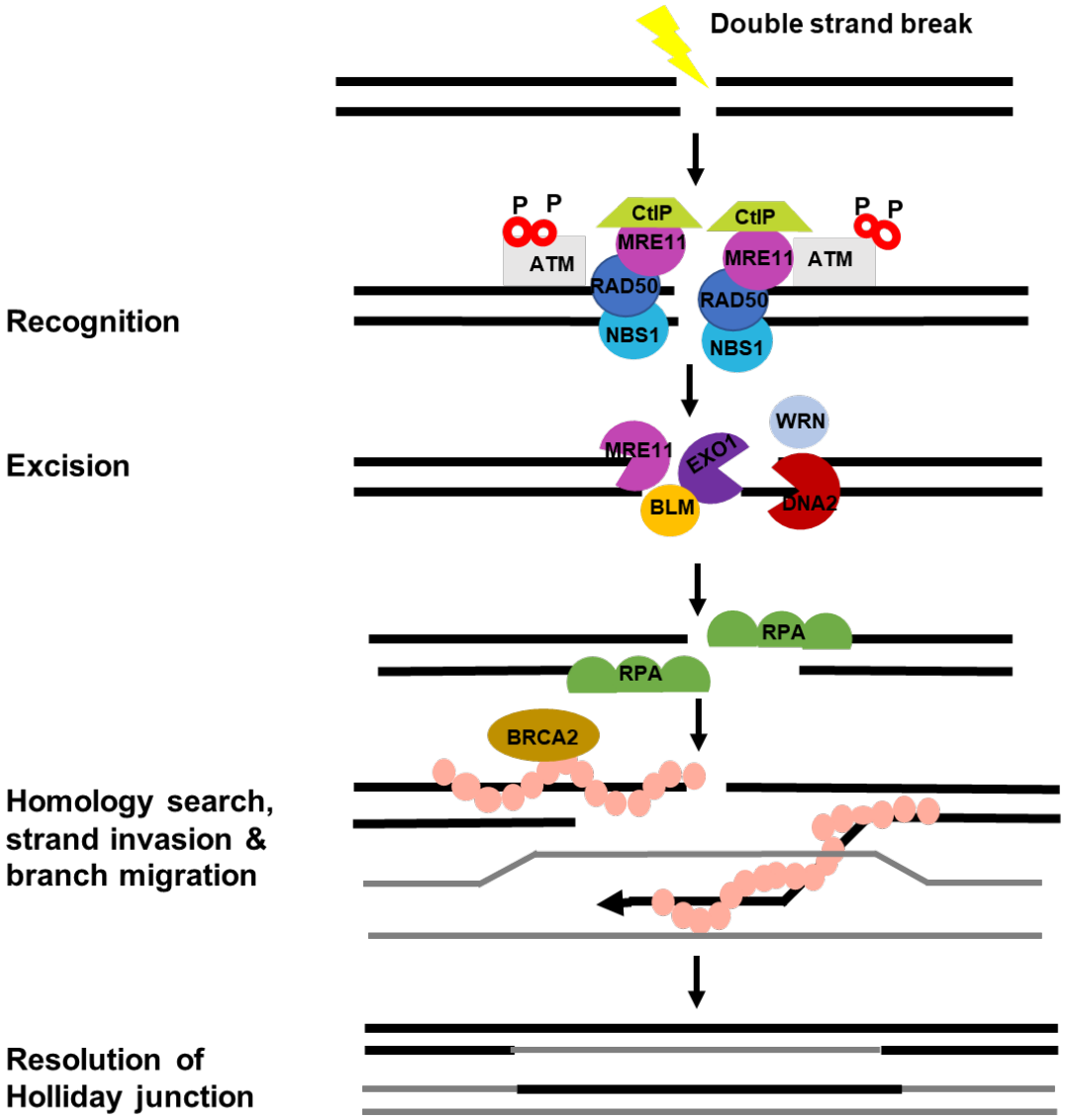

Figure 1.10 Schematic representation of HR repair mechanism.

The MRN complex is rapidly recruited to the sites of damage and recognises DSBs. MRN is also required for activation of ATM which acts as a damage sensor. MRE11 exhibits endo and exonuclease activities, the former of which requires CtIP binding. The endo-nucleolytic cleavage sites facilitate the recruitment of EXO1 and DNA2 nucleases that act downstream the MRN complex in the 5'→3' direction. RPA is bound to ssDNA which is then displaced by BRCA2 that loads RAD51 to the sites of damage. RAD51 then forms nucleoprotein filaments facilitating strand exchange and generating two Holliday junctions which are further processed.

1.7.1.3 Theta mediated end joining (TMEJ)

Multiple names have been given to the a-EJ pathway including a-NHEJ, microhomology-mediated end joining (MMEJ) and more recently TMEJ, in which polθ is required. Being an ‘’alternative’’ pathway, it acts as a ‘’back up’’ to repair DSBs in cells deficient for c-NHEJ but also contributes to the survival of HR-deficient cancer cells [233,234]. TMEJ does not require Ku, XRCC4 or LIG4; ssDNA overhangs are poorly recognised by Ku and thus are inefficiently repaired by NHEJ [235–237]. polθ preferentially joins ends such that deletions in repair products extend to microhomologies in flanking DNA. However, not all a-EJ events are microhomology-mediated and the use of microhomologies is also observed in other repair pathways (i.e., NHEJ) [238]. Poly (ADP-ribose) polymerase 1 (PARP1) deficient cells or cells treated with PARP1 inhibitors caused a reduced recruitment of polθ [239,240] but it is still unknown whether PARylation has a direct role in recruiting polθ. Screening for factors essential for a-EJ demonstrated the involvement of several Fanconi anaemia proteins [241]. PARP1 competes with Ku to bind to DSBs, recruiting MRN complex and CtIP which perform end resection [242–244]. The 9-1-1 complex has also been shown to be implicated in TMEJ by regulating resection before end recognition [245] . RPA is displaced by embryonic stem cell-specific 5-hydroxymethylcytosine-binding protein (HMCES) which binds to ssDNA and favours TMEJ [246]. *In vitro* studies showed that microhomologies should be 3 bp or more for TMEJ to take place with both copies of the microhomology located within 15 nucleotides of the 3′ end [247]. Helicase-like domain (HelD) and a carboxy-terminal polymerase domain (PolD) of polθ form a homodimer [248] or homotetramer [249] that mediate end pairing. HelD promotes polθ translocation alongside the ssDNA which ‘searches’ for microhomologies starting from the 3′ end [247]. *In vitro* studies have shown that polθ is unlikely to sufficiently complete on its own TMEJ with more than 100 nucleotides [250–252], while Polδ has been shown to be implicated in more processive synthesis [253,254]. Flap processing is achieved by DNA2 [241] or FEN1 [255] and ligation primarily by ligase 3 (LIG3) [256] although ligase 1 (LIG1) can also function to seal DNA ends in this context [257].

1.7.1.4 Single strand annealing (SSA)

SSA has similarities to TMEJ, in that it uses homologous repeat sequences that flank a DSB. The original SSA model [258] involves DNA end resection, which is dependent on CtIP [259], generating 3' overhangs. A variety of negative regulators of DNA resection have been documented including H2AX, RNF168, 53BP1, and the Mammalian Rap1-interacting factor 1 (RIF1) [260–262]. In contrast to TMEJ, RAD52 is indispensable for SSA as it anneals the 3' ssDNA ends which form a synapsed intermediate structure. RAD52 is important for repeat-mediated rearrangements that involve long regions of homology. The intermediate structure is then ligated which in its turn requires cleavage of the 3' ssDNA by ERCC1-XPF and gap filling by polymerases. In contrast to TMEJ, RAD52 is indispensable for SSA. SSA is also an error prone mechanism resulting in loss of the genetic material. The length of microhomologies dictates the choice of pathway over HR, TMEJ and SSA [263].

1.8 Structure of MRN complex

The highly conserved MRX/MRN complex (MRE11-RAD50-XRS2 in yeast; MRE11-RAD50-NBS1 in mammals) is a key player of genome integrity as it regulates both signalling and repair functionalities of the DNA damage response in a variety of contexts from DSBs to stalled RFs, abnormal telomeres and viruses [264]. The MRX complex was initially identified in yeast screening for genes implicated in meiotic recombination, and resistance to DNA damage caused by UV light and X-rays [265–267]. The MRN complex acts at the core of the DSB repair mechanism and orchestrates multiple facets of DSB repair, including damage detection, checkpoint activation and repair of the lesion. In particular, it senses DSBs and directly binds to DNA without sequence specificity [268], it functions as co-activator of DSB-induced cell cycle checkpoint signalling, and as an effector of DNA damage pathways in HR, NHEJ and TMEJ repair mechanisms [269,270] and it is responsible for telomere maintenance by facilitating the recruitment of telomerase to telomeres [271,272].

The structural biology of the MRN complex has been extensively studied through a plethora of techniques including X-ray crystallography, small-angle X-ray scattering (SAXS), analytical ultracentrifugation, inductively coupled plasma mass spectrometry

(ICP-MS), dynamic light scattering (DLS), atomic force microscopy (AFM) and electron microscopy (EM). Insights gleaned from these studies are discussed in detail below.

The core of the MRN complex includes MRE11 and RAD50 (MR) which form a heterotetramer composed of an MRE11 dimer and two RAD50 subunits ($MRE11_2RAD50_2$) [273,274]. MR forms a globular DNA binding domain, and NBS1/XRS2 binds to the complex by directly interacting with MRE11 leading to an overall stoichiometry of $MRE11_2RAD50_2NBS1_2$ [275] although there have been some debate over the number of NBS1 subunits interacting with the MR complex [276,277] (Figure 1.11). MR is conserved in all biological kingdoms in contrast to NBS1, which is conserved only in eukaryotes [278].

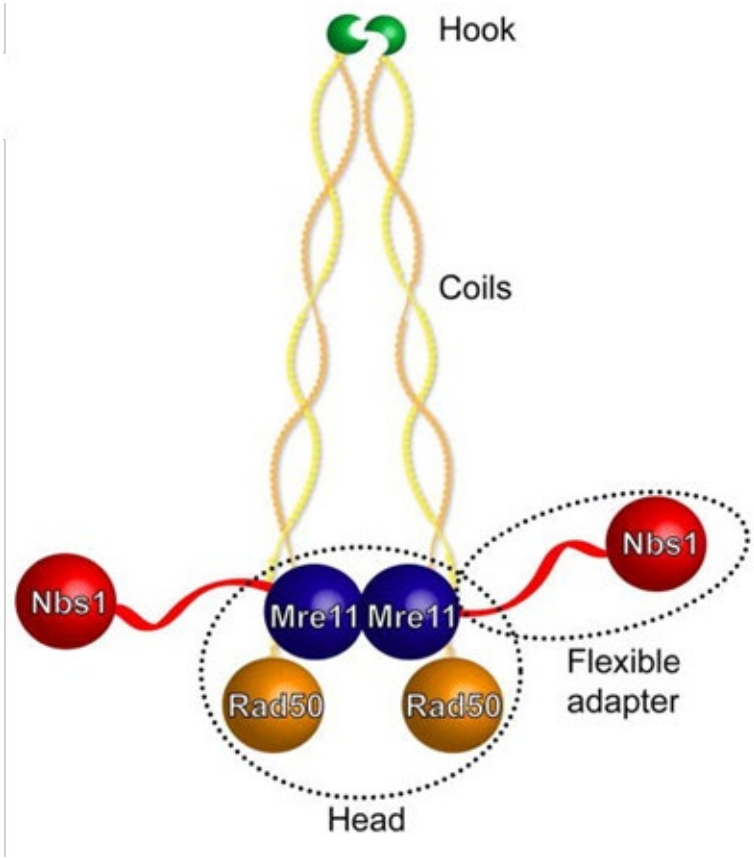

Figure 1.11 Structure of MRN complex.

The MRN complex forms a heterotetramer comprised of a dimer of MRE11 and two Rad50 ABC ATPase domains (dotted circles) forming the head of the complex, the “coil” and “hook” part that encompasses the region of Rad50 separating the N- and C-terminal ABC ATPase halves, and the NBS1 “flexible adapter” (dotted circles) that is responsible for signalling pathways. Figure taken from [274].

RAD50 belongs to the ABC-ATPase superfamily, and it is the largest member of the MRN complex, consisting of 1312 aa in humans. The structure of RAD50 is implicated in both the DNA-binding and DNA end-bridging activities of the complex. The N- and C-terminal domains of the protein form a bipartite (ABC)-type ATP-binding cassette (the ''head'') which include the Walker A and B motifs respectively that bind and unwind dsDNA [279]. The Walker A/B motifs are separated by two long (600–900 aa) antiparallel coiled-coil regions with a flexible central hinge extending the length of the protein up to ~500 Å from the head domain [280] and mediating intramolecular interactions [268,273]. The RAD50 long coiled-coil domain tethers the two broken DNA ends. In the presence of ATP, the N-terminus of one RAD50 molecule interacts with the C-terminus of the other and vice-versa, to form functional ATPase active sites. Each RAD50 molecule also contains a conserved Cys-X-X-Cys motif (known as Zn hook), which is found at the apex of the coil-coil domain and is responsible for tethering the broken DNA ends. The Cys-X-X-Cys motif also facilitates RAD50 dimerization via the coordination of a zinc ion [281] and adjacent interfaces [282]. The ATP-binding motifs and ATPase activity of RAD50 are important for the nuclease activity of MRE11 and control switching between the exonuclease/endonuclease activities of MRE11 [283,284].

MRE11 is a multifunctional protein of 708 aa exhibiting both 5'→3' endonuclease (within the DNA) and 3'→5 exonuclease (at the ends of DNA) activities that excise both ssDNA and dsDNA [285,286]. However, the 5'-terminated DNA strand must be resected to produce the 3' ssDNA overhang for HR repair. MRE11 lacks the 5'→3' exonuclease activity to catalyse this, suggesting the involvement of other DSB processing factors [287]. MRE11 is able to form dimers and large multimers with itself [288], and can interact independently with both RAD50 and NBS1 [289]. The N-terminal domain of MRE11 contains the nuclease and capping domains, whereas the C-terminal section contains the DNA binding and GAR (glycine-arginine-rich) domains [269,290]. The latter has been shown to be colocalized with γ-H2AX and it is implicated in determining the localisation of MRE11 in DNA damage foci [291]. MRE11 is also regulated by a series of post-translational modifications. For example, Polo-Like Kinase 1 (PLK1) phosphorylates MRE11 at Ser649, which primes MRE11 for Casein Kinase II (CK2)-mediated phosphorylation on Ser688. These two phosphorylation events are reported to prevent loading of the MRN complex to sites of damage and regulate activation of the ATM/CHK2 pathway [292]. CK2 also phosphorylates

MRE11 at Ser558/661 and Ser688/689, and this phosphorylated form of MRE11 directly interacts with the subunit of the heat-shock protein 90 co-chaperone R2TP complex (Rvb1p-Rvb2p-Tah1p-Pih1p in yeast and RUVBL1-RUVBL2-RPAP3-PIH1D1 in humans), PIH1D1. Depletion of PIH1D1 and alanine substitution of MRE11 at Ser688/689 affects MRE11 stability, while depletion of R2TP leads to decreased MRN complex levels in human and murine cells [293].

NBS1 is a 754 aa protein, and while it does not have any enzymatic activity, it binds and recruits other proteins that facilitate certain specific functions of the MR complex. This includes the ATM kinase, the MDC1 adaptor protein [294,295] and the MRE11 endonuclease cofactor CtIP [296]. The N-terminus of the protein includes a forkhead-associated (FHA) domain and two breast cancer associated 1 C–terminus (BRCT) domains. The C-terminus of NBS1 directly interacts with ATM and MRE11 [211,297]. NBS1 recruits ATM to DNA damage sites, suggesting that NBS1 can also function as an upstream damage sensor for ATM signalling [211,298]. Mutation, knockdown, degradation, or mislocalisation of MRN components leads to defective ATM signalling [298–301]. However, ATM can be also activated independently of the MRN complex; for example during oxidative stress [302]. The interaction of NBS1 and MRE11 promotes MRN nuclear localisation [276], as only NBS1 harbours a nuclear localisation sequence, which is important for the activation of the HR pathway [303]. Additionally, the C-terminus of NBS1 is implicated in promoting HR repair via its interaction with the ring finger protein 20 (RNF20) [304], and it has also been reported to bind RAD18 to regulate translesion DNA synthesis (TLS) [305] (TLS is described in discussion 7.1) (Figure 1.12).

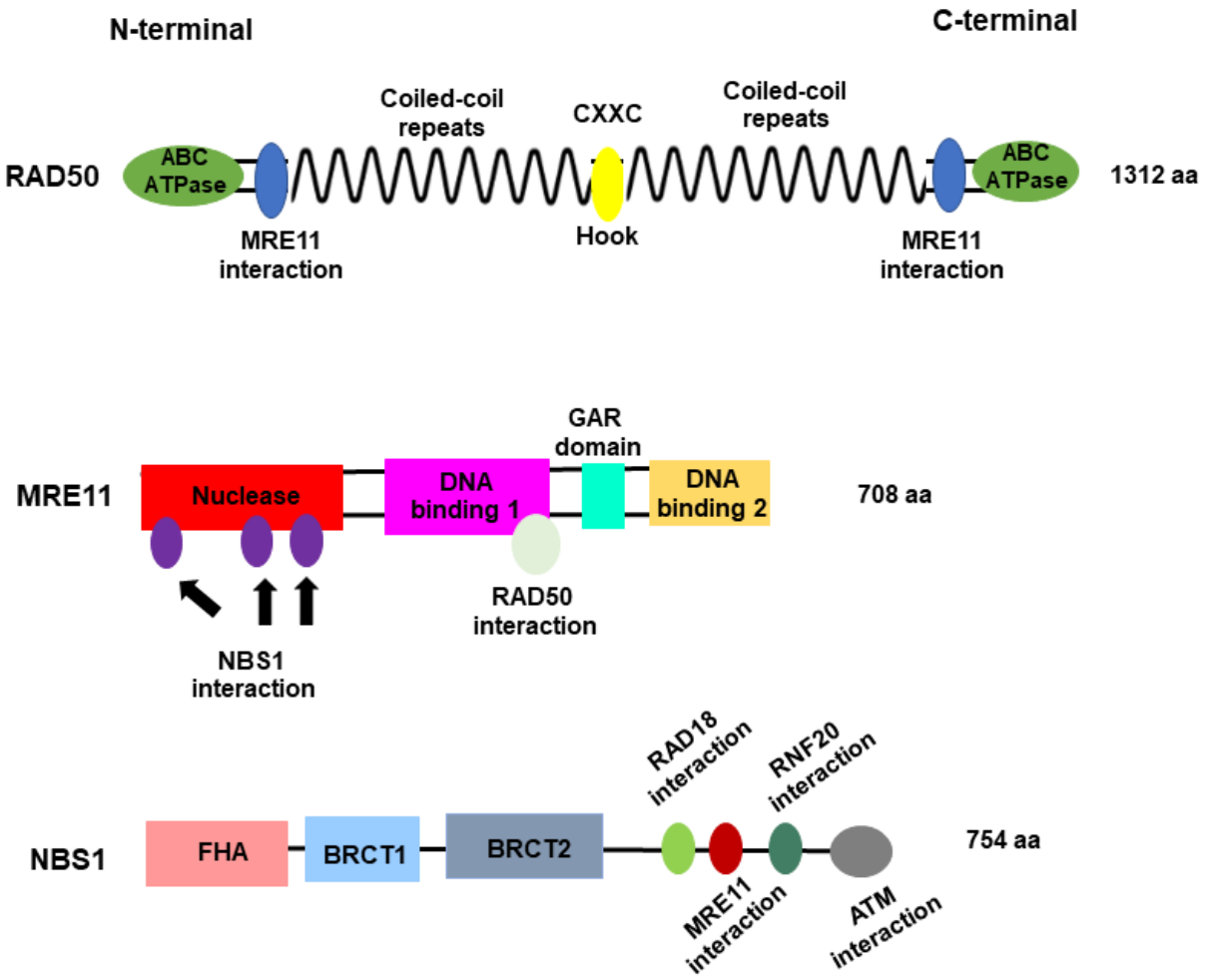

Figure 1.12 Domains of RAD50, MRE11 and NBS1 genes.

RAD50 contains two ABC-type ATPase domains and two central antiparallel coiled-coil regions which bring the N-terminal (Walker A) and the C-terminal (Walker B) domains into close proximity. The apex of the coil-to-coil domain contains a conserved Cys-X-X-Cys motif which has a hook shape facilitating RAD50 dimerization via cysteine-mediated zinc ion coordination. The N-terminal part of MRE11 includes the nuclease and capping domains whereas the C-terminal includes two DNA binding domains and GAR domains. NBS1 contains a structured N–terminus with a FHA domain followed by dual BRCT domains. The C-terminal part of the protein has an extended structure and does not contain recognizable structural sequences, but it is responsible for the interaction of NBS1 with other proteins including RAD18, MRE11, RNF20 and ATM. Figure taken from [312].

Once ATM is activated, it phosphorylates all members of the MRN complex; NBS1 at Ser278, Ser343, Ser397 and Ser615 to regulates the S-phase checkpoint and cell survival after DNA damage [197,306–308], RAD50 at Ser635 which is important for ATM-dependent signalling through structural maintenance of chromosomes protein1 (SMC1) for DNA repair and cell cycle checkpoint control [309], and MRE11 at Ser676 and Ser678 which controls the extent of DNA resection [310].

Upon ATP binding, the complex has a compact, rigid, and closed conformation in which the N and C terminal ATPase regions of RAD50 interact with each other *in trans* and form a groove that can accommodate dsDNA. In this way, dsDNA is inaccessible to MRE11. However, upon ATP hydrolysis or when the complex is in an ATP-free conformation, MRN is activated and it undergoes conformational changes; RAD50 ATPase subunits are flexible and open allowing MRE11 activity [311,312] (Figure 1.13). This ATP hydrolysis cycle might be responsible for regulating the duration of MRN binding to a substrate or a product although the exact mechanism is yet to be elucidated.

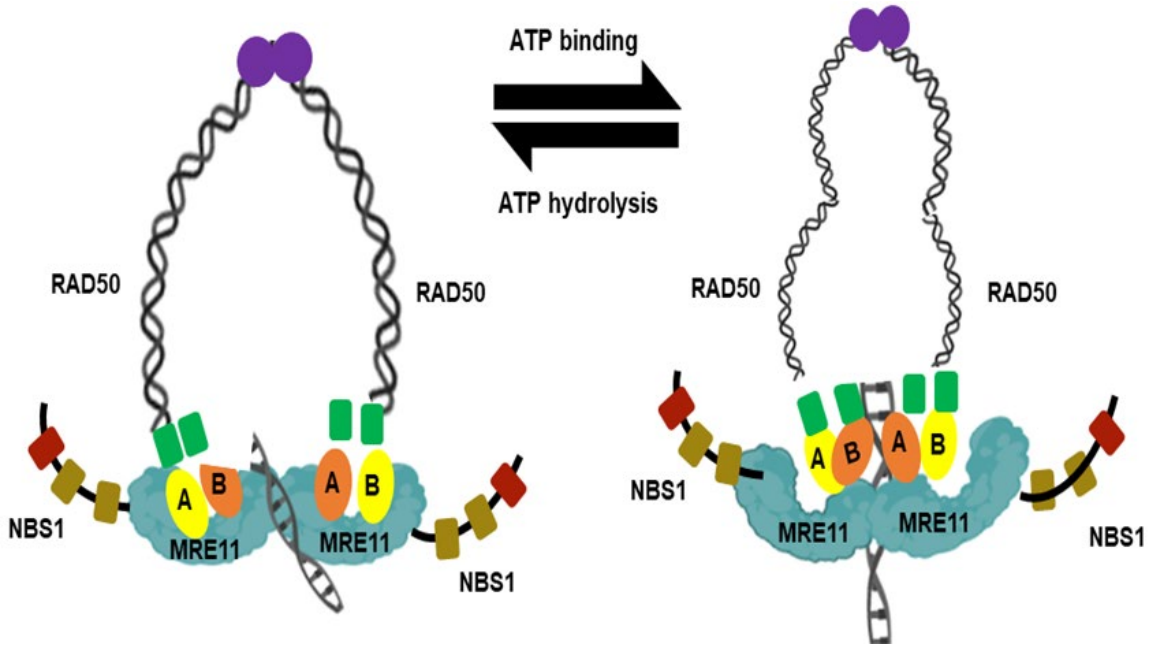

Figure 1.13 Structure and configuration of the MRN complex upon ATP hydrolysis.

Prior to ATP hydrolysis, the configuration of the complex is compact, rigid, and closed preventing MRE11 to access the DNA. However, upon hydrolysis, the MRN complex changes its conformation obtaining an open structure where MRE11 can exhibit its endo and exonuclease activities. Figure taken from [312].

1.8.1 Alterations of MRN complex and cancer

The MRN complex plays a pivotal role in different aspects of the DNA damage response, and each of its component proteins has important biological functions. All three proteins are indispensable for life, since null mutations in any of the genes results in embryonic lethality in murine and stem cell models [313–316]. Also, loss of function mutations in any of the MRN genes are causative for different diseases associated with GI; a) MRE11 mutations cause Ataxia-Telangiectasia (A-T)–like disorder (ATLD) which is rare and with the main clinical characteristic being cerebellar ataxia, b) NBS1 mutations cause Nijmegen breakage syndrome (NBS) characterised by microcephaly, growth retardation, immunodeficiency, and c) RAD50 mutations cause NBS-like disorder with similar clinical manifestations to NBS syndrome [300,317,318] as well as increased risk of haematological cancers [319]. Importantly, these mutations provide significant evidence for the role of MRN in the DDR pathway as patients with these mutations exhibited chromosomal instability, radio-sensitivity, radio-resistant DNA synthesis, cell cycle defects and tumour predisposition [320]. In addition, reduced expression of RAD50, MRE11 and NBS1 was shown in around 3%, 7% and 10% of breast carcinomas, respectively [321] and all genes have been identified as moderate-penetrance breast cancer-susceptibility genes [322]. Lack of MRN complex has been observed in patients with epithelial ovarian cancer [323]. Importantly, MRN may be synthetic lethal when combined with poly(ADP-ribose) glycohydrolase (PARG) inhibition [324] opening a possible therapeutic window to target MRN-defective cancers by inhibiting PARG [325].

1.9 Mechanisms of fork integrity

As already mentioned, RFs are constantly challenged via a series of endogenous and exogenous stresses, many of which modify the DNA backbone or the bases themselves. These impediments can cause RS. Slow or arrested forks can activate mutagenic DNA repair pathways as well as error prone fork restart. In the case of prolonged replication stress, stalled RFs can undergo irreversible fork breakage, which eventually results to GI [326]. However, cells have acquired fork protection mechanisms to deal with the stress and rescue the fork by stabilising, repairing and restarting [327,328] (Figure 1.14).

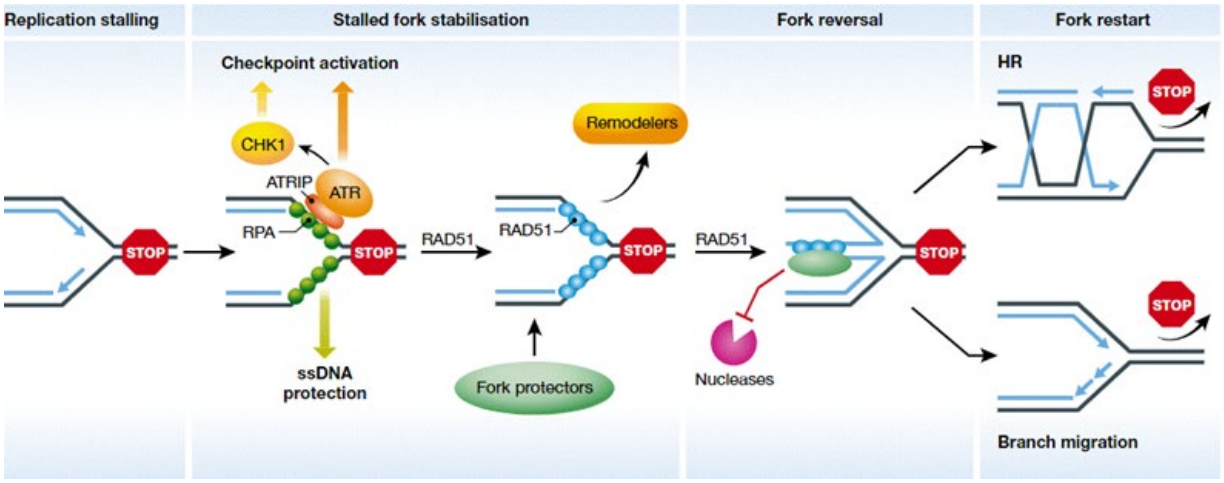

Figure 1.14 Model of fork protection mechanisms.

Upon fork stalling, RPA coats ssDNA forming a ssDNA-RPA complex which activates the checkpoint machinery and downstream pathway for fork recovery. RPA is replaced by RAD51 and with the help of SMARCAL1 and other factors, fork reversal occurs. Protection of reversed forks from deleterious degradation is achieved by a variety of fork protectors before they restart either through HR or branch migration. Figure taken from [328].

1.9.1 Fork reversal

Fork reversal is the process wherein RFs are remodelled via reannealing of the nascent strands to generate a four-way junction structure reminiscent of Holliday junction, also known as a ‘’chicken foot’’ structure (Figure 1.15). This prevents collision of the fork with physical impediments allowing time for the lesion either to be removed before the reversed fork starts, or bypassed through tolerance mechanisms [329]. Reversal also brings any nearby lesion into the context of dsDNA, which may be essential for repair/removal.

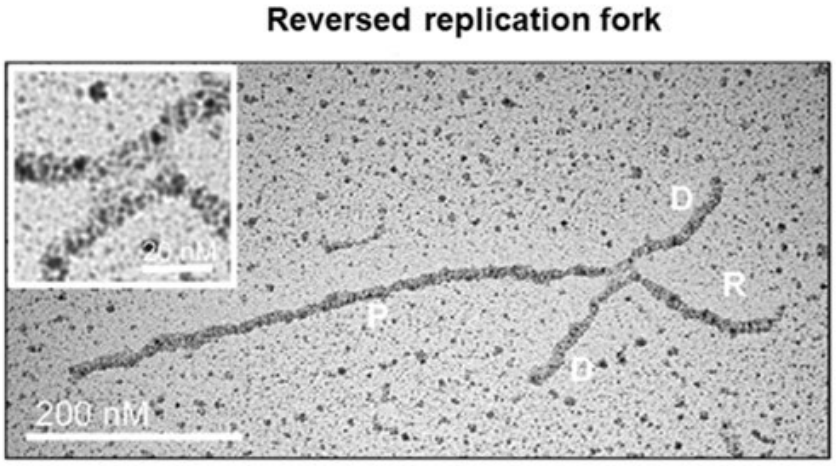

Figure 1.15 Replication fork reversal.

Electron micrograph of a reversed fork. P: parental strand, D: daughter strand, R: Reversed arm. Figure adapted from [328].

Interestingly, this change in DNA configuration was firstly identified more than 40 years ago through electron microscopy [330]. However due to the difficulty in observing this phenomenon, little attention was given until genetic and biochemical techniques were used in prokaryotic systems confirming the existence of reversed forks [331–333]. Over the last two decades, experimental evidence has shown that reversed forks also exist in higher eukaryotic systems [334] .

Fork reversal can occur in response to diverse genotoxic stresses, for example by poisoning of type I topoisomerase in human cells, mouse embryonic fibroblasts (MEFs) and *Xenopus laevis* egg extracts [335]. In addition to topoisomerase poisons, sublethal doses of genotoxic agents including ICL-inducing agents [mitomycin C (MMC), Cisplatin], DNA synthesis inhibitors [(aphidicolin, hydroxyurea (HU)], and base-damaging agents (methyl methanesulfonate, hydrogen peroxide, UV irradiation) also cause replication fork reversal without detectable breaks in chromosomes [336].

Many proteins are implicated in the physical process of fork reversal, including several found mutated in human cancers [329,337]. Among these core reversal factors is RPA which

binds to the regressed arms of RFs ssDNA in order to prevent the formation of secondary structures that may be an impediment for further fork processing [338,339]. RPA also propagates stress signals to activate the checkpoint pathway that includes TOPBP1-dependent and ETAA1-dependent pathways [340,341]. Phosphorylation of RPA causes a shift from replicative DNA synthesis to reparative DNA synthesis [342,343]. However, RPA must be removed for the template strands to re-form the DNA duplex [344].

A DNA translocase of the sucrose nonfermenting 2 (SNF2) family, SWI/SNF-related matrix-associated actin-dependent regulator of chromatin subfamily A-like protein 1 (SMARCAL1) is recruited to stalled replication forks via its interaction with RPA [345,346]. RPA directs SMARCAL1 to selectively remodel the fork stimulating SMARCAL1 activity, when SMARCAL1 is bound to the leading template strand, and inhibiting its function when bound to the lagging strand [344]. SMARCAL1 binds to DNA via its ATPase and HepA-related protein (HARP) domains. It is then phosphorylated by ATR on Ser652, which reduces its ATPase activity and its fork remodelling activities [347].

Zinc Finger RANBP2-Type Containing 3 (ZRANB3) also belongs to the SNF2 family, and it has similar sequence to SMARCAL1. In contrast to SMARCAL1, ZRANB3 is recruited to stalled RFs via its interaction with ubiquitinated PCNA instead of RPA [348,349]. Another SNF2 family member called Helicase-like Transcription Factor (HLTF) have also shown to perform fork reversal in *vitro* and in *vivo*. SMARCAL1, ZRANB3, and HLTF recognize different types of fork structures in *vitro*, indicating that different factors might mediate fork reversal, depending on the type of replication intermediate involved [344,350,351]. In addition, SMARCAL1 or ZRANB3 depletion does not fully abolish reversed fork formation [352–354] suggesting that fork reversal is not controlled by a single protein, and that different structures may be formed even under the same type of challenge. Moreover, other DNA translocases, including RAD54 [355] and FANCM [356], are implicated in fork reversal in *vitro*, supporting the theory that many factors may play a role in fork reversal.

RAD51 is a crucial fork reversal factor. RAD51 is best known as a major HR recombinase. However, it also regulates fork reversal, in a role that is genetically separate from its role in HR, and is also independent of BRCA2 [354,357]. Depletion of RAD51 abolishes replication slowing upon MMC and Camptothecin (CPT) treatment and leads to a significant induction of DSBs even in untreated cells [336]. The mechanism behind this action may be the following; 1) upon RAD51 binding to ssDNA of the stalled fork, RAD51 interacts with

other proteins including SMARCAL1 and ZRANB3 that cause reversal or 2) RAD51 binding to the ssDNA end captures the reversed fork and drives the equilibrium towards fork reversal [358]. Interestingly, fork reversal is not impaired in BRCA1/2-mutant cells or in cells expressing the RAD51 mutant, RAD51-T131P, [352–354] which destabilizes RAD51 nucleofilaments, [359] suggesting that BRCA1/2 protect reversed forks, by loading RAD51 onto ssDNA tails generated upon fork reversal. Interestingly, PARP1 depletion prior to BRCA1/2 loss restores stalled fork stability and confers synthetic viability in mouse embryonic stem cells. In addition, PARP inhibitors prevent fork reversal by favouring ReCQ-mediated fork bypass [360].

1.9.2 Fork protection

Upon fork reversal, ssDNA tracts are formed in the regressed nascent DNA arms, which are susceptible to the action of nucleases including MRE11, EXO1, DNA2 and MUS81 [224,361–363]. Nuclease-dependent DNA degradation is important, although not indispensable, for fork restart, although inappropriate nuclease activity can compromise genome integrity. In the absence of BRCA1/2 or RAD51, RFs are extensively degraded by MRE11 and EXO1 [364,365]. BRCA2 is not required for fork reversal but it protects stalled forks from nucleolytic degradation. Importantly this function is genetically separable from its role in HR repair. Indeed, BRCA2 binds to RAD51 through its C-terminal domain mediating coating of RAD51 onto ssDNA and stabilisation of RAD51-ssDNA filaments, hence conferring fork protection [364]. In addition, proteins of the FA pathway have been shown to protect stalled fork from nucleolytic degradation within the BRCA2-RAD51 pathway. FANCD2-deficient cells also exhibit shortened nascent strands upon HU treatment. FANCD2 has a similar role to BRCA2, promoting RAD51 nucleofilament formation at stalled forks and therefore preventing degradation [366]. Another factor called BOD1L was also found to stabilise RAD51 preventing DNA degradation [367]. Interestingly, fork protection can also be achieved independently of the RAD51-BRCA2 pathway as a new protein called ABRO1 was shown to be important for fork integrity by inhibiting degradation mediated by DNA2 nuclease/WRN helicase [368].

1.9.3 Fork restart

Replication restart is an important aspect of genome maintenance. Ongoing work is shedding light on sophisticated and robust mechanisms that cells employ for fork restart, with a plethora of proteins participating in this process [369]. Indeed, cells depleted of RAD51 exhibit an increased number of forks that do not restart replication upon HU treatment suggesting the pivotal role of RAD51 in this process [370]. The BLM helicase has also been implicated in fork restart through its helicase activity in cells treated with the DNA polymerase inhibitor aphidicolin or HU. Reduced fork restart was also observed in BLM deficient cells [371]. Another study proposed two different fork restart pathways; 1) employing 53BP1 through a fork cleavage-free pathway and 2) employing BRCA1 through a break-induced replication (BIR) pathway facilitated by the SLX-MUS complex [372].

RIF1 has also been documented to play a role in both fork protection and fork restart processes. Its role in fork protection is independent of its function in NHEJ but dependent on its interaction with Protein Phosphatase 1 (PP1). Indeed, RIF1 protects forks from DNA2 mediated resection through its CI and CII domains that are responsible for its interaction with PP1. Deficiency in RIF1 also caused delay in fork restart which was independent of the 53BP1-mediated fork restart pathway [373]. In addition, RECQ1 helicase and PARP were shown to regulate fork restart regardless the type of stress [336]. DNA2 nuclease assisted by WRN helicase process the replication intermediates and facilitate fork restart, and this pathway is different from the EXO1, MRE11, and CtIP pathway [374]. Finally, the binding partner of WRN, known as Werner helicase interacting protein 1 (WRNIP1) [375], was shown to cooperate with RAD51 for fork protection and restart. Interestingly, fork protection was not dependent on the ATPase activity of the protein, however it was important for fork recovery. In particular, WRNIP1 stabilises RAD51 and prevents excessive MRE11 degradation [376] . A summary of the proteins implicated in fork reversal, protection and restart are shown in (Figure 1.16).

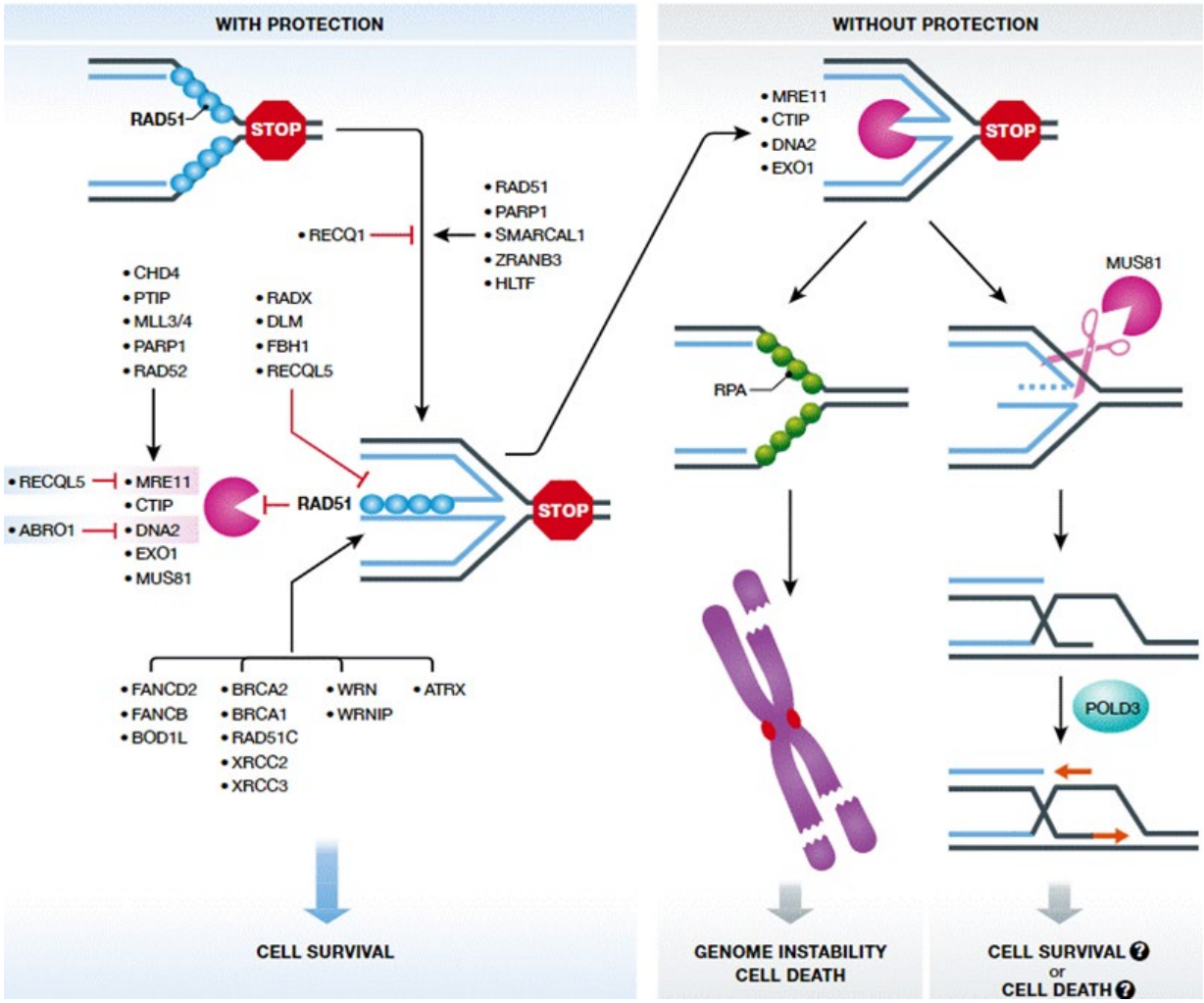

Figure 1.16 Schematic representation of proteins implicated in fork reversal, protection, and restart.

Some of the proteins implicated in fork reversal are RAD51, SMARCAL1, ZRANB3 and HLTF. PARP1 maintains stalled forks in a regressed state by countering RECQ1 helicase. MRE11 is recruited by PARP1, RAD52, PTIP-MLL3/4 and CHD4 to perform DNA resection. Other nucleases also act including EXO1, DNA2 and MUS81 the latter of which depends on EZH2. However, protective factors protect the forks from excessive degradation by the aforementioned nucleases, that can lead to genome instability, by different pathways mainly through the RAD51 nucleofilaments. RAD51 is negatively regulated by RADX which also affects fork stability. When forks are cleaved by MUS81, BIR is activated, but how this pathway contributes to fork protection is yet to be elucidated. Figure taken from [369].

1.10 MRN Interacting Protein (MRNIP)

The Staples laboratory recently identified the novel DNA repair factor MRN Interacting Protein (C5ORF45/MRNIP) as a novel replication fork protection factor [301]. MRNIP is a 37 kDa protein with no obvious enzymatic activity and it interacts with the MRN complex. Recent data from the laboratory demonstrates that MRNIP directly interacts with MRE11 *in vitro*. Preliminary data also suggests that MRNIP may mediate MRE11 phosphorylation in response to DNA damage, at sites reported to regulate resection, although this requires further investigation. Structurally, MRNIP is predicted to be comprised of a small zinc finger-like N-terminal domain, and its C-terminus consists of tracts of intrinsically disordered sequences. MRNIP is rapidly recruited to sites of damaged DNA, promoting MRN function in cells exposed to IR [301]. Depletion of MRNIP leads to impaired radiation-induced MRN chromatin loading, causing decreased DNA resection and defective ATM signalling [301]. In addition, MRNIP is predicted to be phosphorylated at multiple residues. Phosphorylation of Ser115 promotes MRNIP nuclear localization [301]. Published proteomics data agrees with Staples laboratory mass spectrometry findings in identifying Ser217 as a site of abundant phosphorylation [377,378].

Recently, a group identified MRNIP underlying liquid-liquid phase separation (LLPS) in *vivo* and in *vitro* [379] with the intrinsically disordered region 1 being essential for this process. LLPS is a mechanism used to explain the formation of membraneless organelles and is linked to DNA damage repair [380,381]. MRNIP phase separation-derived condensates enhance the recognition of damaged DNA by the MRN complex and DNA end resection. In addition, the same group showed that high MRNIP expression was correlated with radioresistance and shorter survival time in patients with colorectal cancer [379]. Another study showed that MRNIP is required for spermatocyte DSB repair, chromosome synapsis, and male fertility [382]. In particular, MRNIP deficient mice showed lower sperm count and motility and impaired spermatogenesis. MRNIP KO spermatocytes showed decreased level of MRN complex and disrupted meiotic cDNA (DMC1) and RAD51 loading was compromised rendering MRNIP responsible for homologous recombination by interacting with the MRN complex in meiosis [382]. The most recent paper showed that MRNIP KO male mice were sterile which is in accordance with the literature, however, female fertility was unaffected with MRNIP loss suggesting that

MRNIP is a sexually dimorphic marker exclusive to male meiosis [383]. MRNIP loss leads to reduced sex body formation, and defective meiotic sex chromosome inactivation (MSCI) [383].

1.11 Project Aims

The project was conducted in order to shed light on important aspects of MRNIP function. In particular, our first aims were to assess whether MRNIP is involved in the cellular response to break-inducing agents such as CPT, HU and several nucleoside analogues and how MRNIP functions during DNA replication stress. Previous work from the Staples laboratory suggests that MRNIP, like BRCA2, protects stalled replication forks from DNA2 and MRE11-dependent degradation by directly interacting with MRE11 and inhibiting its exonuclease activity [384]. Nucleoside analogues are commonly used to treat cancer types in which subsets of patients suffer from tumours carrying pathogenic mutations in DNA repair factors like BRCA2 (e.g. Pancreatic ductal adenocarcinoma (PDAC) [385] and we hypothesised that a similar therapeutic approach could be applied for patients with MRNIP mutations. Interestingly, the nuclease activity of MRE11 removes Gemcitabine from genomic DNA [386]. However, at present we have no information about how dysregulation of MRE11 in MRNIP-deficient cells might modulate the response to nucleoside analogues treatment.

As already mentioned, MRNIP is phosphorylated at multiple residues. However, there is no evidence for a role for Ser217 in modulating MRNIP function. Therefore, our next aim was to examine the role of Ser217 phosphorylation and a number of other confirmed and putative MRE11 and MRNIP post-translational modification sites in the response to genotoxic chemotherapies. Likewise, the kinase that drives Ser217 phosphorylation is unknown, although analysis of the residues surrounding the site suggests the involvement of a proline-directed kinase such as a member of the Mitogen-Activated Protein Kinase (MAPK) or CDK families. Such cell cycle-specific MRNIP phosphorylation could theoretically provide a means of modulating MRE11 activity at different sites, or during different cell cycle stages.

Our last aim was to assess possible interactors of MRNIP. We therefore carried out an interaction study via mass spectrometric analysis of MRNIP immune complexes and probed the functionality of confirmed interactions.

CHAPTER II

2 MATERIALS & METHODS

2.1 Materials

Table 1: Reagents and buffers

Reagents	Composition
x1 Phosphate buffered saline (PBS)	137 mM NaCl, 2.7 mM KCL, 1.4 mM NaH_2PO_4 and 4.3 mM KH_2P0_4
Permeabilization buffer-immunofluorescence	1% Bovine Serum Albumin (BSA) fraction V , 0.1% Triton X-100 in x1PBS
Blocking solution-immunofluorescence	3% BSA in x1PBS
Blocking solution -western blot	1) x1PBS, 0.1% Tween-20, 5% milk powder 2) x1PBS, 0.1% Tween-20, 5% BSA 3) x1PBS, 0.1% Tween-20, 1% BSA
Blocking solution- DNA fibre assay	3% BSA in x1PBS, 0.1% Triton X-100 in x1PBS
Cell lysis buffer- protein extraction	150 mM NaCl, 50 mM Tris-HCL pH 7.6, 1% Triton X-100, 1 mM EDTA supplemented with benzonase to concentration of 50 U/µl
Cell lysis buffer - immunoprecipitation	200 mM NaCl, 50 mM Tris-HCl pH 7.4, 1% Triton X-100, 2 mM $MgCl_2$ supplemented with Complete Roche protease inhibitors and Phos-Stop™ inhibitors
Fixation solution-immunofluorescence	4% Paraformaldehyde in x1PBS
KCM	500 mM KCl, 150 mM $CaCl_2$, 250 mM $MgCl_2$
Transfer buffer- western blotting	25 mM Tris pH 8.3 and 0.192 M glycine
Wash buffer- western blotting	x1PBS, 0.1% Tween-20
Spreading buffer-DNA fibre assay	200 mM Tris, pH 7.4, 500 mM EDTA, 0.5% SDS

Table 2: Chemotherapeutic drugs

Drugs	Company	Product code
Hydroxyurea	Calbiochem	127-07-1
Camptothecin	Merck	C9911
Gemcitabine	Discovery Fine Chemicals	122111-03-9
Fludarabine	Sigma	F2273
Clofarabine	Sigma	C7495
Cytarabine	Discovery Fine Chemicals	205-705-9
Cisplatin	Calbiochem	CAS 15663-27-1
Cyclohexamide	Sigma	CAS 66-81-9

Table 3: Primary antibodies

Antibody	Reference number	Host species	Blocking solution	Dilution	Company
Alpha-Tubulin	T6199	Mouse	5% Milk in PBS-T	1:10000	Sigma-Aldrich
GAPDH	sc-47724	Mouse	5% Milk in PBS-T	1:5000	Santa Cruz
CDK4 (DCS-31)	sc-56277	Mouse	5% Milk in PBS-T	1:1000	Santa Cruz
CHIP (C-10)	sc-133083	Mouse	5% Milk in PBS-T	1:1000	Santa Cruz
MTA30 (2G10/3)	sc-53382	Mouse	5% Milk in PBS-T	1:1000	Santa Cruz
DNA2	PA5-66086	Rabbit	5% Milk in PBS-T	1:1000	Thermo Fisher Scientific
MRE11	NB100-142	Rabbit	5% Milk in PBS-T	1:1000	Novus Biologicals
Keap1 (G-2)	sc-365626	Mouse	5% Milk in PBS-T	1:1000	Santa Cruz

FK2	BML-PW8810	Mouse	5% Milk in PBS-T	1:1000	Enzo Life Sciences
Phospho-MRE11 (Ser676)	#4859	Rabbit	5% BSA in TBS-T	1:1000	Cell signalling
FLAG tag	ab1162	Rabbit	5% Milk in PBS-T	1:1000	Abcam
C5orf45	ab150917	Rabbit	5% BSA in PBS-T	1:400	Abcam
C5orf45	50-286-093	Rabbit	5% Milk in PBS-T	1:1000	Aviva Systems Biology
C5orf45	in house	Rabbit	5% Milk in PBS-T	1:1000	Dundee Cell Products
DYNLL1	sc-136287	Mouse	5% Milk in PBS-T	1:1000	Santa Cruz
Phospho-CHK1 S345 (133D3)	#2348	Rabbit	5% BSA in TBS-T	1:1000	Cell signalling
CHK1 (2G1D5)	#2360	Mouse	5% Milk in PBS-T	1:1000	Cell signalling
53BP1	Ab21083	Rabbit	3% BSA in PBS	1:2000	Cell signalling
Phospho-Histone H2A.X	PA5-28778	Mouse	3% BSA in PBS	1:1000	Thermo Fisher Scientific
BrdU (B44)	347580	Mouse	3% BSA in PBS	1:100	BD Biosciences

Table 4: Secondary antibodies

Antibody	Reference number	Host species	Blocking solution	Dilution	Company
Alexa Fluor 488	A48269	Rat	3% BSA in PBS	1:1000	Invitrogen
Alexa Fluor 546	A11030	Mouse	3% BSA in PBS	1:1000	Invitrogen
DAPI	62248	-	3% BSA in PBS	1:1000	Thermo Fisher Scientific
Alexa Fluor 594	A11012	Mouse	3% BSA in PBS	1:1000	Invitrogen
Alexa Fluor 555	A32727	Rabbit	3% BSA in PBS	1:1000	Invitrogen

2.2 Methods

2.2.1 Cell culture

All cells were cultured in their respective medium supplemented with 10% FBS unless otherwise stated and cultured at 37°C in the presence of 5% CO2 to a maximum of 80% confluency prior to passage. Cells were passaged by washing with DPBS (Sigma) before incubation with Trypsin-EDTA solution (Sigma) for 5 min at 37°C and detached cells were collected in fresh media. The cells were cultured for a maximum of six weeks and were cryopreserved in FBS with 10% dimethyl sulfoxide (DMSO) and stored in -80°C for short term or liquid nitrogen for long term. The cell lines alongside their characteristics used for this project are shown in the table below (Table 5).

Table 5: Cell lines used in the study

Cell line	Cell type/ tissue	Culture medium
HeLa	Epithelial/ uterus; cervix	DMEM
HCTT116	Epithelial/ large intestine; colon	DMEM
HEK 293	Epithelial/ kidney; embryo	DMEM
LN18	Glioblastoma/ brain, cerebrum; right temporal lobe	DMEM
T98G	Glioblastoma/brain	DMEM
U251	Glioblastoma/brain	DMEM
U138	Glioblastoma/brain	DMEM
UACC1598	Epithelial-like/ovary	DMEM/F12
COV362	Mucinous/ovary	DMEM +15% FBS
TOV-21G	Epithelial/ovary	DMEM
TOV-112D	Epithelial/ovary	DMEM
UWB1-289	Papillary serous epithelial like/ovary	DMEM/F12
A2780	Epithelial/ovary	RPMI 1640
SCOV3	Epithelial/ovary; ascites	McCoy's 5A
OVCAR3	Epithelial/ovary	RPMI 1640 + 20% FBS
U2OS	Epithelial/bone	DMEM
HEK 293 T	Epithelial/kidney; embryo	DMEM
hTERT RPE-1	Epithelial/Eye; Pigmented epithelium; Retina	DMEM/F12
U2OS	Epithelial/osteosarcoma	DMEM

2.2.2 Poly-D-lysine coating

Due to reduced attachment of MRNIP KO cells, all cell culture plates were coated with Poly-D-lysine (ThermoFisher Scientific) which was diluted 1:1 with sterile DPBS at a working solution of 50 µg/ml before any experiment was performed. In particular, the culture vessel was coated with Poly-D-lysine and incubated for an hour at room temperature. The culture surface was then rinsed thrice with distilled water and left uncovered in the laminar hood to fully dry for 2 hours. Plates were then used according to the needs of experiments or stored tightly wrapped with Parafilm™ film at 4°C and used within one week of coating .

2.2.3 RNAi Transfections

Transfection of cells was performed when cells were 30-40% confluent with 10-50nM siRNA (MWG Biotech) and Lipofectamine RNAimax (Invitrogen) for 48 hours according to the manufacturer's instructions. The siRNA sequences alongside their target which were used for this project are shown below (Table 6).

Table 6: siRNA sequences

Target	siRNA sequence (sense)
control	5'-UAAGGCUAUGAAGAGAUAC-3'
MRNIP 19	5'-GCAAACAGCCUUCAUCCAA-3'
MRNIP 21	5'-GUUAGGAGGGACAGGGUUC-3'
SMARCAL1	5'-GCUUUGACCUUCUUAGCAA-3'
PRIMPOL1	5'- GAGGAAACCGUUGUCCUCAGUGUAU-3
MRE11 UTR	5'-GAACCUGGUCCCAGAGGAG-3'
DNA2	5-'ACAGUUGCCUGCAUUCUAA-3'
MUS81	5'-CAGCCCUGGUGGAUCGAUA-3'
CHIP	5'-CGCUGGUGGCCGUGUAUUA-3'

2.2.4 Cell lysate preparation (for Western Blotting)

Cells were washed twice with cold x1PBS and lysed in lysis buffer (50 mM Tris-HCl pH 7.4, 200 mM NaCl, 1% Triton X-100, 1 mM EDTA and 1 mM $MgCl_2$) supplemented with 50U/µl benzonase (Novagen), Complete protease inhibitors and PhosStop™ phosphatase inhibitors (Roche). Lysed cells were collected with a scraper and transferred to Eppendorf tubes. Samples were then incubated for 20 min on ice and centrifuged at 16,000*g* for 10 min at 4°C to eliminate debris. Bicinchoninic acid assay (BCA assay) alongside a NanoDrop™ 2000/2000c Spectrophotometer (Thermo Fisher Scientific) were used for determining protein concentration.

2.2.5 SDS - PAGE (Polyacrylamide Gel Electrophoresis)

Cell lysates were denatured in SDS loading dye (Invitrogen) at 70°C for 10 min prior to loading into Bolt™ 4-12% gradient Bis-Tris gels (Invitrogen). Gels were run in Bolt running buffer (Invitrogen) for 2 hours at 90V and analysed by western blotting. PageRuler™ Prestained Protein Ladder was also used as a standard marker ranging from 10 to 250 kDa.

2.2.6 Western Blotting

Following protein separation through SDS-PAGE, wet transfer onto an Immobilon-FL PVDF membrane (Millipore) was performed at 30 V for 120 min in transfer buffer (Invitrogen supplemented with 20% methanol) using the XCell II Blot Module (Thermo Fisher Scientific). The PVDF membrane was then blocked in blocking solution (x1 PBS-0.1% Tween-20 (Sigma) containing 5% milk powder or 3% BSA and 0.1% Tween-20) for at least 30 min at room temperature. Primary antibody diluted in blocking solution to the relevant concentration was used at 4°C overnight on a rocking platform. The following day, the membrane was washed thrice for 5 min with x1PBS- 0.1% Tween-20 and probed with the relevant secondary antibody at 1:5000 ratio for 1 hour at room temperature in gentle agitation. The membrane was washed again prior to imaging using the ChemiDoc Imaging system (Biorad). Quantification of the protein levels was performed using ImageJ

drawing profile plots and labelling the peaks for each band. The relative density of each peak was then calculated which was compared to the standard band.

2.2.7 Silver staining

The gel was initially washed twice with ultrapure water for 5 min and fixed twice in 30% ethanol:10% acetic acid solution (i.e., 6:3:1 water: ethanol: acetic acid) for 15 min. The gel was then washed twice in 10% ethanol for 5 min before it was washed twice in ultrapure water for 5 min. The gel was then incubated in Sensitiser Working solution (Pierce™ Silver Stain Kit) by mixing 1 part of Silver Stain Sensitiser with 500 parts of ultrapure water for exactly 1 minute, washed with two changes of ultrapure water for 1 min each, following incubation with Stain Working Solution by mixing 1 part of Silver Stain Enhancer with 50 parts of Silver Stain for 30 min. The gel was then washed with two changes of ultrapure water for 20 sec each and the Developer Working Solution was added to the gel until protein bands appear. When the desired band intensity was reached, the Developer Working Solution was replaced by Stop Solution (5% acetic acid). Finally, the Stop Solution was replaced with ultrapure water in which the gel was incubated for 10 min.

2.2.8 Cycloheximide Chase

Cells were incubated in medium supplemented with 30µg/ml of cycloheximide for 6 hours before lysis, resolution, and detection by SDS-PAGE as described above.

2.2.9 MTT growth assay

Cells were plated in 6-well plates at a density of 100,000 cells/well (in a total volume of 200µl/well) for parental and 150,000 cells/well for MRNIP KO backgrounds. 24 hours later, they were transfected with the appropriate siRNAs if required in quadruplicate. After 48 hours, cells were replated on 96-well plates at a density of 1000 cells/well for parental and 1800 cells/well for MRNIP KO backgrounds. The following day, they were treated

with chemotherapeutic agents if necessary. After further 96 hours, 3-(4,5-dimethylthiazol-2-yl)-2,5-diphenyl tetrazolium bromide (MTT) reagent was added at a final concentration of 1 mg/ml at 37°C for 4 hours. The medium was removed and replaced with 100μl of dimethyl sulfoxide (DMSO) to solubilize the formazan product and its absorbance was assessed by quantifying optical density at 540 nm using the ELx800 Absorbance Microplate Reader supporting the GEN5 software. Results were normalized to untreated controls.

2.2.10 Clonogenic survival assay

Cells were plated in 6-well plates at a density of 100,000 cells/well for parental and 150,000 cells/well for MRNIP KO backgrounds. The following day, they were transfected with the appropriate siRNAs for 48 hours and they were reseeded onto 10-cm tissue culture dishes at 1000 cells for parental and 1800 cells for MRNIP KO backgrounds in duplicate for each condition. 24 hours later, cells were treated with the indicated concentrations of drugs for 24 hours. Fresh medium was then added, and cells were incubated for 10-12 days until colonies were formed. Colonies were then fixed and stained with 0.5% crystal violet stain solution in 50/50 methanol/water for an hour at room temperature and rinsed with water. Colonies were manually counted, photographed and results were normalised to the untreated controls for each transfection and plotted as percentage survival.

2.2.11 Genomic DNA isolation

Genomic DNA was isolated from HeLa and HCT116 cells using a DNeasy blood and tissue kit (Qiagen) according to the manufacturer's instructions. Briefly, cells were lysed using Proteinase K. 200μl of buffer AL was then added to the tube and mixed by vortexing it. 200μl of ethanol was added to precipitate the DNA and lysates were loaded onto the DNeasy Mini spin column and spun at 6000*g* for a min. The flow-through was then discarded and the column was placed in a new 2ml collection tube where 500μl of AW1 buffer was added. The column was centrifuged for another min before it was placed in a new tube and 500μl of AW2 was added and centrifuged for a further 3 min at 20.000*g*. The flow-through was then discarded and the column was placed in a new tube where

DNA was eluted by adding 20µl of AE buffer to the centre of the column, incubated for a min and centrifuged at 600*g*.

Real-time polymerase chain reaction (PCR) was performed using Taqman Universal PCR mix (Applied Biosystems) under the following conditions: polymerase activation at 95°C for 1min, denaturation at 95°C for 15 sec, annealing at 60°C for 15 sec and extension at 72°C for 10 sec over 35 cycles.

2.2.12 Generation of stable cell lines

Stable HEK 293 Flp-In TREX cell lines expressing doxycycline-inducible FLAG-MRNIP were produced by co-transfecting with pObpA-Flp recombinase and pDEST-Flag/FRT/TO-MRNIP according to the Flp-In manufacturer's instructions (Invitrogen). 1 µg/ml doxycycline was then added for 24 hours to induce the expression of FLAG which was verified by western blotting using anti-FLAG antibody.

2.2.13 Cloning and Site Directed Mutagenesis of MRE11

MRE11 was amplified using KOD Hot Start DNA polymerase according to manufacturer's instructions with the cycling conditions (35 cycles) being the following: polymerase activation at 95°C for 2 min, denaturation at 95°C for 2 min, annealing at 95°C for 2 min, extension at 70°C for 2 min. The following primers were used:

MRE11 Forward: 5' TGG TGA TCT TTT TGA TGA AAA TAA GCC CT 3'

MRE11 Reverse: 5' AGG GCT TAT TTT CAT CAA AAA GAT CAC CA 3'

A sample of the PCR product was run on 1% agarose gel in x1TAE running buffer for 1 hour at 150V and the rest of it was recombined using BP clonase into the Gateway Entry vector p221DONR.

Site directed mutagenesis was carried out using appropriate mutagenic primers:

H63D MRE11 Forward: 5' GGT GGT GAT CTT TTT GAT GAA AT AAG CCC 3'

H63D MRE11 Reverse: 5’ GGG CTT ATT TTC ATC AAA AAG ATC ACC ACC 5’

SS676/678DD MRE11 Forward: 5’ CAG CAA AAT CAT GGA CCA GGA TCA AG 3’

SS676/678DD MRE11 Reverse: 5’ CTT GAT CCT GGT CCA TGA TTT TGC T 3’

SS676/678AA MRE11 Forward: 5’ CAG CAA AAT CAT GGC CCA GGC TCA AG 3’

SS676/678AA MRE11 Reverse: 5’ CTT GAG CCT GGG CCA TGA TTT TGC TG 3’

KOD polymerase-based reaction was then performed according to manufacturer’s instructions using the p221DONR-MRE11 clone as a template. Cycling conditions of the PCR were the following: polymerase activation at 95°C for 2 min, denaturation at 95°C for 2 min, annealing at 95°C for 2 min, extension at 70°C for 2 min. The PCR product was digested overnight at room temperature using DpnI before bacterial transformation and sequence verification using the following primers was performed:

MRE11 seq 1: 5’ CTC AAA GAC TGC TGT TGT GTC AGC 3’

M13 Forward: 5’ GTA AAA CGA CGG CCA GT 3’

MRE11 GateWay Forward: 5’ GGG GAC AAG TTT GTA CAA AAA…GAG TAC TGC AGA TGC ACT TGA 3’

MRE11 GateWay Reverse: 5’ GGG GAC CAC TTT GTA CAA GAA… CTT CTA TTT CTT CTT AAA 3’

Mutants were then recombined into GateWay destination vectors as outlined in the manufacturer’s instructions. All plasmids were sequenced to verify the presence of mutant MRE11, which was then co-transfected into MRNIP KO HeLa cells with the pObpA recombinase plasmid.

In addition, the Horejsi laboratory (Barts Cancer Institute) provided us with MRE11 constructs encoding alanine mutants of MRE11 CK2 and PLK1 phosphorylation sites (Ser 558, 561, 649, 688 and 689), which were cloned and used to generate stable cell lines in HeLa MRNIP KO cells using the GateWay system as described above.

2.2.14 Transformation of competent bacteria

100 µl of Competent E.coli DH5α and One Shot ™ Stbl3™ (Thermo Fisher Scientific) bacteria were thawed on ice. DH5α bacteria were mixed with x5 KCM, distilled water and plasmid DNA for 20 min on ice followed by 10 min incubation at room temperature. Pre-warmed LB media were then added to the bacteria and incubated at 37ºC for 1 hour with rotation. The bacteria were then spun down at 3000*rpm* for 2 min to pellet and plated on LB-agar containing the appropriate antibiotic: Ampicillin (Sigma) at final concentration 100 µg/mL and Kanamycin (Sigma) at 500µg/ml.

One Shot ™ Stbl3™ bacteria were mixed with plasmid DNA and incubated for 2 min on ice and heat shocked for 30 sec at 42 ºC. Incubation on ice for 2 min was then followed prior to incubation with S.O.C medium (G-biosciences) for 1 hour at 37ºC with shaking. One Shot ™ Stbl3™ bacteria were then plated on LB-agar plates with appropriate antibiotic.

For both types of strains, plates were incubated overnight at 37ºC, and the resultant colonies were inoculated into LB broth supplement with the appropriate antibiotic.

2.2.15 Purification of plasmid DNA

Plasmid DNA was purified using the Qiagen miniprep kit and DNA was isolated according to the manufacturer's instructions. Briefly, the bacterial overnight culture was pelleted by centrifugation at 250*g* for 5 min at room temperature. The bacterial pellet was then resuspended in 250µl of Buffer A1 and transferred to a microcentrifuge tube, to which 250µl of Buffer A2 was added and mixed thoroughly by inverting the tube until it is clear. 300µl of Buffer A3 was then added to the tube, which was centrifuged for 10 min at 11,000*g*. The supernatant was then loaded to a QIAprep spin column and centrifuged for 1 min at 11,000*g*, then the flow-through was discarded, and 500µl of Buffer AW was added to wash the QIAprep spin column. Centrifugation was then followed for a further min before the flow-through was discarded. 600µl of A4 buffer was then added, centrifuged for a min and flow-through was discarded. The QIAprep spin column was transferred to a new collection tube and spun for a further min to remove any residual wash buffer. To elute the DNA, 50µl of Buffer AE was added to the centre of the QIAprep

spin column, left to stand for a min at room temperature, and centrifuged for a further min. The amount of plasmid DNA was measured using a Nanodrop 2000 (Thermo-Scientific) and sequenced.

2.2.16 DNA Sequencing

Plasmid DNA was verified using the Eurofins Mix2Seq kit: 15µl of Plasmid DNA with a concentration of between 50-100ng/µl was added to the provided sequencing tubes, then 2µl of the SeqPrimer with a concentration of 10pmol/µl was added and the sample was sent for Sanger sequencing.

2.2.17 DNA transfection

DNA transfections were carried out using Lipofectamine™ 2000 transfection reagent (Thermo Fisher Scientific) according to the manufacturer's instructions. Cells were transfected when 80% confluency was reached. For each transfection sample, 1µg of plasmid DNA was used with 1µg of pObpA recombinase plasmid. Cells were then incubated for 24 hours prior to testing for protein expression.

2.2.18 RNA extraction

RNA was isolated using Qiagen kit according to manufacturer's instructions. Briefly, cells were washed with x1PBS and lysed with the appropriate volume of APL buffer for 5 min at room temperature. The lysate was then pipetted into an AllPrep spin column and spun for a min at 8000*g*. The flow-through was dropwise pipetted onto the centre of the slanted gel bed in the Protein Cleanup spin column and spun at 240*g* for 3 min. The AllPrep spin column was then placed in a new 2 ml collection tube and 350µl of Buffer RLT was then added to the column and centrifuged for a min at 8000*g*. 350µl of 70% ethanol was added to the flow-through and mixed well by pipetting up and down several times. 700µl of the sample, including any precipitate that may have formed, was added to an RNeasy spin column inside a 2 ml collection tube and centrifuged for a min at 8000*g*. The flow-through was discarded. 700µl of Buffer RW1 was added to the RNeasy® spin column and

centrifuged for 30 sec at 8000*g* to wash the spin column membrane where flow-through was discarded again. 500µl of Buffer RPE was then added to the RNeasy spin column, centrifuged for 30 sec at 8000*g* discarding the flow-through. The RNeasy spin column was again centrifuged for another min at full speed to remove residual wash buffer. Finally, 30-50µl of RNase-free water was directly pipetted onto the spin column membrane and then centrifuged for a min at 8000*g* to elute RNA.

2.2.19 Reverse transcription Polymerase Chain Reaction (RT-PCR)

Isolated RNA was reverse-transcribed using the QIAGEN® OneStep RT-PCR Kit according to the manufacturer's instructions. A reaction mix including QIAGEN OneStep x5 RT-PCR Buffer, dNTP, primers, RNAase- free water, QIAGEN OneStep x2 RT-PCR Enzyme Mix was prepared and 2µg was used. The cycling conditions for RT-PCR are as follows: reverse transcription for 30 min at 50°C, initial PCR activation for 15 min at 95°C, denaturation for 1 min at 94°C, annealing for 1 min at 60°C, extension for 1 min at 72°C for 40 cycles.

2.2.20 Immunofluorescence

Cells were seeded in 24-well plates in round coverslips and transfected with the appropriate siRNAs or treated with chemotherapeutic agents if necessary. Cells were then fixed with 4% paraformaldehyde for 10 min at 4°C, permeabilised in x1PBS containing 0.5% Triton X-100 for 5 min at room temperature, blocked in 3% BSA in x1PBS for 30 min and incubated with primary antibody overnight at 4°C. The following day, cells were washed in x1PBS and incubated with fluorescence-conjugated secondary antibodies; Alexa Fluor™ 594 anti-mouse (Invitrogen) and Alexa Fluor™ anti-rabbit (Invitrogen) diluted in 3% BSA in x1PBS with 1µg/ml of DAPI for 1 hour at room temperature in the dark. Cells were then washed in x1PBS, and coverslips were mounted cell-side down in Shandon Immu-Mount medium (ThermoFisher Scientific). Slides were then imaged with a Zeiss LSM710 confocal microscope at x40 or x63 magnification and images were analysed using Zen software (Zeiss).

2.2.21 Immunoprecipitation

Cell lysis was performed in lysis buffer as descried above. For purification of FLAG-tagged proteins, lysates were incubated with 30µl of M2-anti FLAG beads (Sigma) overnight at 4°C. For immunoprecipitations using endogenous antibodies, 2-5µg of the relevant antibody was incubated with the sample and A/G beads (Santa Cruz Biotechnology) overnight at 4°C. The following day, beads were pelleted and washed three times in lysis buffer with the last wash in x1PBS supplemented with Complete protease inhibitors and PhosStop™ phosphatase inhibitors (Roche). For FLAG-tagged proteins, elution was performed by incubating with 100ng/ml x3 FLAG peptide (Sigma) diluted in x1PBS supplemented with Complete protease inhibitors and PhosStop™ phosphatase inhibitors (Roche) according to manufacturer's instructions. Elution for immunoprecipitations with endogenous antibodies was performed by heating the beads at 70°C for 10 min with SDS loading dye (Invitrogen).

2.2.22 DNA Fibre Assay

Cells were seeded in 6 well plates and transfected with the appropriate siRNAs if appropriate, then treated with 25µM CldU (Sigma) and 250µM IdU (Sigma) for 20 min each following a 4-hour treatment with 4mM of HU or 1mM of Gemcitabine. Cells were then collected with ice cold x1PBS, diluted at a concentration of $1x10^6$ cells/ml and spun at maximum speed for 5 min. 2.5µl of ice cold cell suspension was added on a positively charged slide and 7.5µl of spreading buffer (200 mM Tris, pH 7.4, 500 mM EDTA, and 0.5% SDS) was added to the same spot of the cells in a circular movement and incubated for 5 min at room temperature. The slides were then tilted at 45° and left to be air-dried for 20 min resulting in a white line across the slide, prior to fixation in methanol/acetic acid (3:1) for 10 min at room temperature. The slides were then air-dried overnight. The following day, DNA fibres were rehydrated twice with distilled water and denatured with 2.5M HCl for an hour in a Coplin jar. Slides were then washed x1PBS and incubated with blocking solution (3% BSA/PBS containing 0.1% Triton X-100) for an hour. Slides were washed again with x1PBS before they were incubated with primary antibodies rat anti-BrdU (Abcam) and mouse anti-BrdU (BD Biosciences) diluted in blocking solution for 2.5 hours in a humid chamber to avoid drying in the dark. Slides were then washed with

x1PBS and incubated with secondary antibodies diluted in blocking solution, anti-rat AF555 and donkey anti-mouse AF488 for an hour in a humid chamber in the dark. Slides were washed thrice with x1PBS prior to sealing with nail varnish. At least 200 DNA fibres per sample were visualised on a Zeiss LSM710 confocal microscope using Zen software and analysed with ImageJ.

2.2.23 Statistical analysis

One-way ANOVA was used to compare the means of three or more groups of data and two-way ANOVA was used to assess the interrelationship of two independent variables on a dependent variable. Standard deviation was calculated and reported on the graphs as error bars as described in the figure legends. A statistically significant value is defined as $P \leq 0.05$. The level of significance is represented as * $P<0.05$, ** $P<0.01$, *** $P<0.001$ and **** $P<0.001$. Excel and GraphPad Prism were used to plot the graphs.

CHAPTER III

3 RESULTS

3.1 The role of MRNIP in the response to Camptothecin and Hydroxyurea.

Prior work suggests a role for the novel DNA repair factor MRNIP in DSB repair and replication fork protection with MRNIP also being identified in eluates from Isolation of Proteins on Nascent DNA (iPOND) experiments [384]. In *vitro*, MRNIP limits MRE11 exonuclease activity, and loss of MRNIP leads to MRE11-dependent degradation of nascent DNA at reversed forks [384]. MRNIP-depleted cells were also demonstrated to be sensitive to IR [387], however, it is unclear to which other forms of genotoxic stress MRNIP-deficient cells may be sensitive, which was the first aim of this project. Furthermore, prior to this project, all work involving loss-of-function of MRNIP was carried out using siRNA-mediated MRNIP depletion, which has a number of drawbacks including incomplete knockdown and off-target effects on other cellular factors. Therefore, we resolved to employ Clustered Regularly Interspaced Short Palindromic Repeats (CRISPR-Cas9)-mediated MRNIP knockout (KO) cell lines and the parental cells from which they were derived to further assess the role of MRNIP in chemosensitivity. A variety of chemotherapeutic drugs were used in this project including the RNR inhibitor HU, the topoisomerase 1 (TOP1) inhibitor CPT as well as nucleoside analogues Gemcitabine, Cytarabine, Clofarabine and Fludarabine. MRE11 is involved in processing Top1 cleavage complexes following CPT treatment [388–390], in DNA end resection following HU treatment [362,384,391], and in the removal of Gemcitabine from stalled forks [386,392]. As such, there is ample precedent for further investigations into the potential role of MRNIP in regulating the cellular response to a wider series of chemotherapeutic agents.

3.2 MRNIP promotes CPT resistance by limiting DNA damage.

To study the effects of MRNIP loss on the cellular response to other genotoxins, we used recently generated Flp-In TREX HeLa and HCT116 MRNIP KO cell lines available in the Staples laboratory, in which Exon 3 of MRNIP was the gRNA target. Stable MRNIP KO CRISPR clones were created using Santa Cruz Biotechnology CRISPR-Cas9 (sc-412131-KO-2) and HDR plasmids (sc-412131-HDR-2), the map of which is shown in (Figure 3.1), according to the manufacturer's protocol. Polymerase Chain Reaction (PCR) was employed to confirm the disruption of the MRNIP gene. Primer pairs were designed spanning exons 1, 2 or 3, the size and sequence of which are displayed in Table 7.

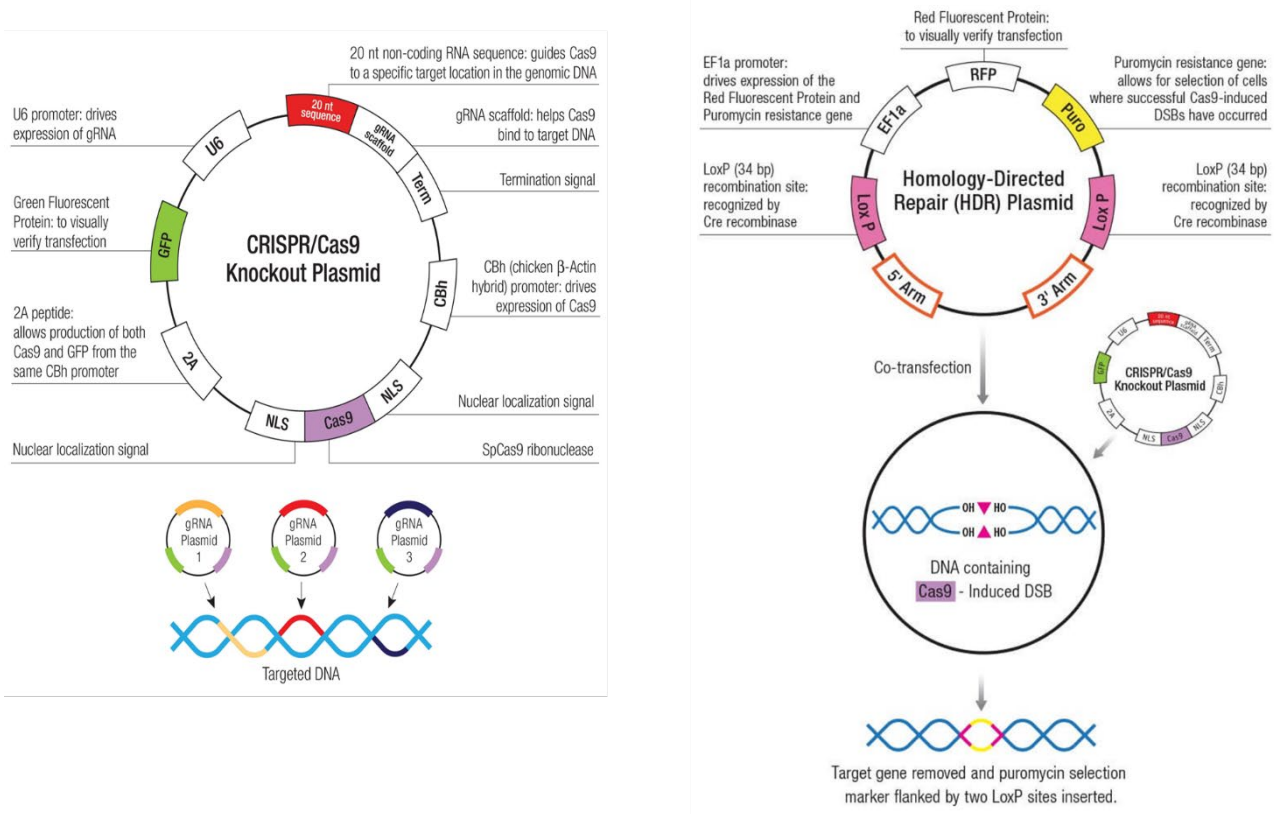

Figure 3.1 MRNIP CRISPR plasmids.

(Left) CRISPR/Cas9 KO Plasmids include guide RNA sequences (20 nucleotides) that are specific to MRNIP from the GeCKO (v2) library. These guide RNA sequences direct the Cas9 protein to create a site-specific double strand break in the genomic DNA. (Right) Selection of cells containing DSB induced by the Cas9 enzyme is undertaken by co-transfection with MRNIP HDR plasmid. Figure taken from Samta Cruz website; https://www.scbt.com/p/mrnip-crispr-knockout-and-activation-products-h.

Table 7: Size of MRNIP exons and sequence of primers

No. of exons	Length (bp)	Sequence
1	87	For: 5' GGA GCA CGG ACG CCG CCG CG 3' Rev: 5' GCA GAG CGC ACG CGC TTG GCT G 3'
2	60	For: 5' GTT CCC CTT GTG CTT GGC AC 3' Rev: 5' TGC CCG CCA CCA TGC CTG GC 3'
3	89	For: 5' GGA GCT GGA CAT GAC TCC TG 3' Rev: 5' GGC ATC ATA AAG GGT CTG CA 3'

PCR using primers spanning Exons 1 and 2 yielded a product of the expected size, indicating that these exons were largely intact. PCR using primers spanning Exon 3 consistently yielded no product. Primers targeting the actin gene were used as a loading control, and this control reaction yielded a product using the identical samples as a template. This indicates that Exon 3 of the MRNIP gene was successfully disrupted by the CRISPR-Cas9 targeting protocol (Figure 3.2).

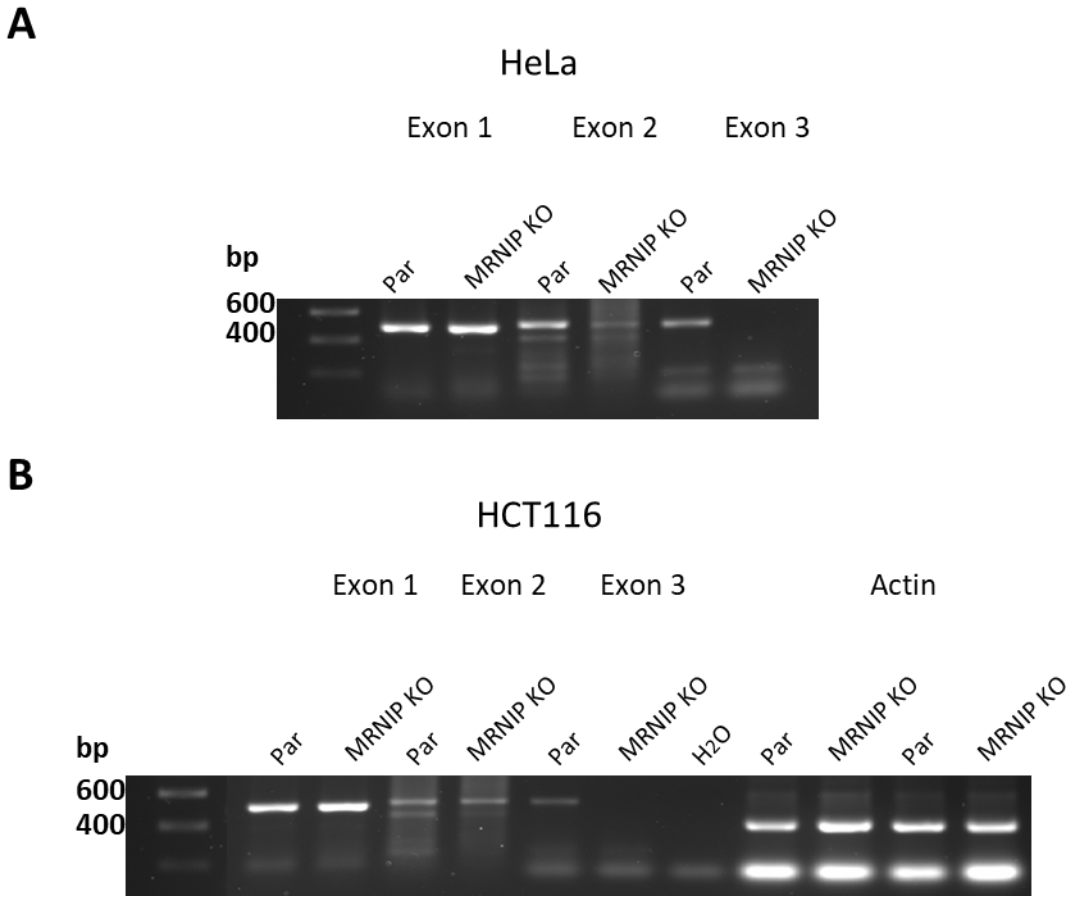

Figure 3.2 Genetic deletion of MRNIP using CRISPR-Cas9.

Genomic DNA was isolated from A) parental (Par) and derivative MRNIP KO (MRNIP KO) HeLa and B) parental and derivative MRNIP KO HCT116 cell lines and PCR reactions using primers targeting Exons 1, 2 and 3 of MRNIP were performed. Actin and H_2O only samples were used as controls.

We also performed western blotting using whole cell extracts from parental and derivative MRNIP KO HeLa and HCT116 lines to examine the levels of MRNIP protein in these samples. We tested two commercial MRNIP antibodies; from Abcam and Aviva Systems Biology, as well as an in-house antibody generated by Dundee Cell Products. We also included a MRNIP KO line stably expressing doxycycline-inducible N-terminally FLAG-tagged MRNIP, to test whether the antibodies used are capable of detecting overexpressed, tagged MRNIP. In blots probed with all three antibodies, bands of the expected molecular weight (~40 kDa) were observed. However, not all of these antibodies appeared to specifically recognise MRNIP; for example, there was no loss of signal in blots generated from MRNIP KO cell extracts probed with a MRNIP antibody from Abcam or the band observed at the expected size was non-specific (Figure 3.3 *A)*.

Conversely, both our in-house antibody and an Aviva Systems antibody recognised a weak band of the expected weight, which was absent in lysates derived from MRNIP KO cells (Figure 3.3 A, B). Testing of MRNIP KO cells expressing FLAG-MRNIP demonstrated that our in-house antibody efficiently detected overexpressed MRNIP, and that under these conditions, endogenous MRNIP is just barely detectable (Figure 3.3 B, C). We could have also examined RNA levels of MRNIP in parental and MRNIP KO samples performing RT-PCR to confirm MRNIP loss in the MRNIP KO samples. Collectively, we believe that we have achieved disruption of the MRNIP gene via CRISPR in these cell lines although we cannot exclude the possibility of some MRNIP being present in the MRNIP KO cell lines.

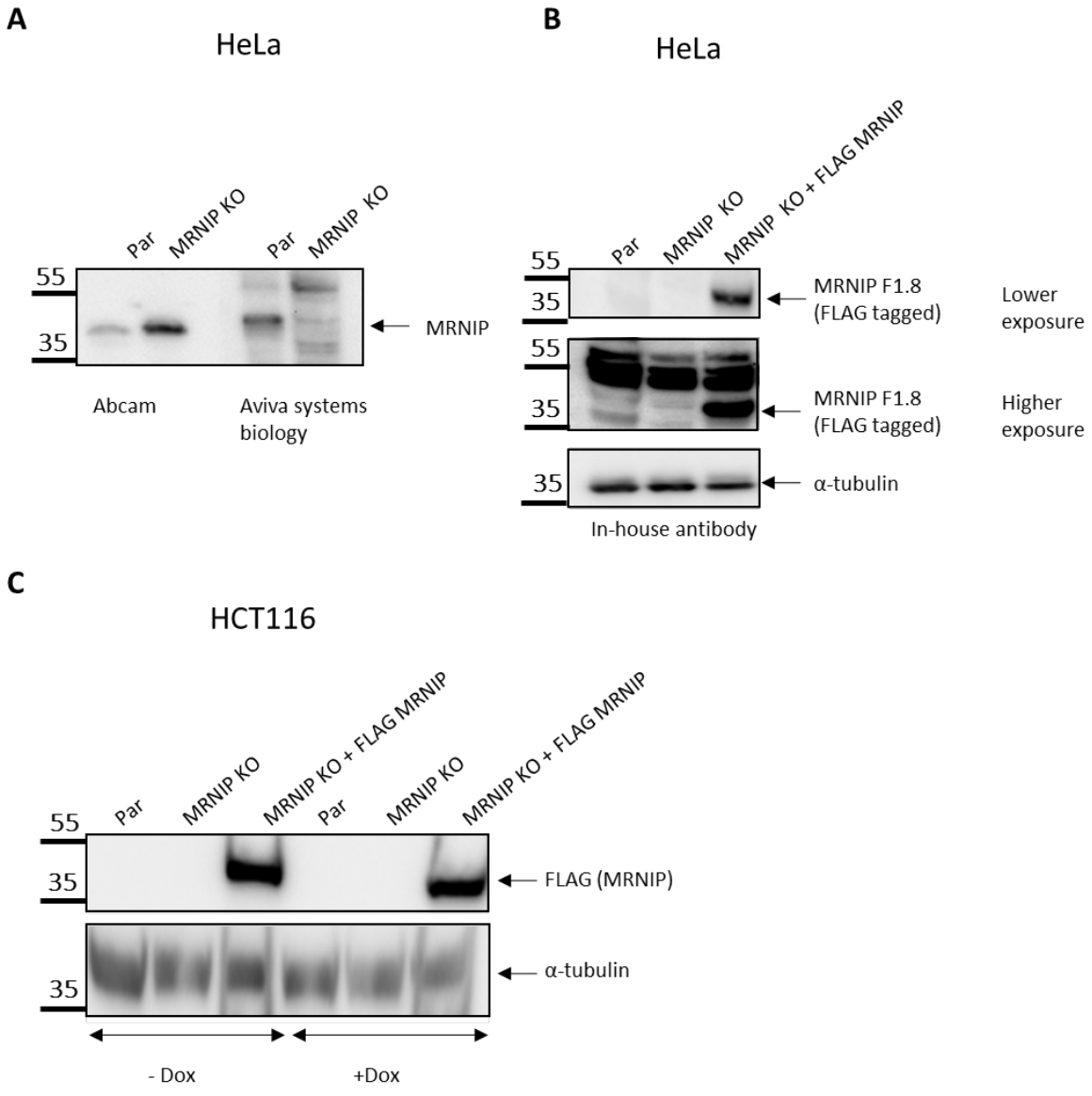

Figure 3.3 Validation of MRNIP antibody.

Whole cell extracts were prepared from A) parental (Par) HeLa, derivative MRNIP KO (MRNIP KO) cells, B) parental HeLa, derivative MRNIP KO cells and derivative MRNIP KO cells stably overexpressing FLAG MRNIP (MRNIP KO + FLAG MRNIP) and C) parental HCT116, derivative MRNIP KO and derivative MRNIP KO cells stably overexpressing FLAG MRNIP. Lysates were resolved by western blotting and probed with a range of customised and commercial antibodies raised against MRNIP (Abcam, Aviva Systems Biology, Dundee Cell Products) or FLAG. Blots are representative from three experiments (n=3).

DNA topoisomerases are crucial enzymes that maintain the topological state of DNA, and which have proved attractive targets for the development of effective anti-cancer agents. Topoisomerases are classified based on whether they create single (TOP-1) or double stranded (TOP-2) breaks. TOP-1 encircles the DNA like a clamp and nicks the sugar phosphate backbone of one strand of DNA, in the absence of an energy cofactor (ATP), enabling the broken strand to rotate around the TOP1-bound DNA strand. Once the DNA is relaxed, TOP1 religates the breaks by forming a covalent enzyme-DNA intermediate between the topoisomerase catalytic tyrosine and the end of the broken DNA [393].

For the last two decades, topoisomerase poisons have been widely used for the treatment of various cancers including colorectal, pancreatic, breast, gastric and small cell lung cancer. CPT is a potent TOP-1 poison that binds to the TOP1-DNA complex and blocks the re-joining step of the cleavage/religation reaction of TOP-1, resulting in accumulation of the covalent reaction intermediate. This complex acts as an impediment to replication fork progression, leading to the generation of single-ended DNA double strand breaks (seDSBs) and ultimately cell death.

Given the emerging role of MRNIP as a regulator of MRE11, and the published literature indicating a crucial role for MRE11 in mediating resection of seDSBs induced by the topoisomerase I poison CPT [335,394,395], we next assessed whether MRNIP loss alters CPT resistance. To achieve this, we performed an MTT (3-(4,5-dimethylthiazol-2-yl)-2,5-diphenyltetrazolium bromide) assay as a crude measure of cell viability.

Parental HeLa (Figure 3.4 *A)* and HCT116 (Figure 3.4 B), derivative MRNIP KO and MRNIP KO cells stably overexpressing FLAG MRNIP were treated with various concentrations of CPT for 96 hours, prior to incubation with MTT reagent and subsequent

analysis by spectrophotometry at 560 nm. CRISPR-mediated deletion of MRNIP sensitized both cell lines to CPT treatment, which is in accordance with the findings of our latest publication [384]. In addition, rescue of the phenotype was observed in MRNIP KO cell lines engineered to stably re-express FLAG-tagged MRNIP, demonstrating that the observed drug sensitivity in MRNIP KO lines is a direct consequence of MRNIP deletion and not a side effect of spurious off-target Cas9 activity (Figure 3.4 *A,B)*.

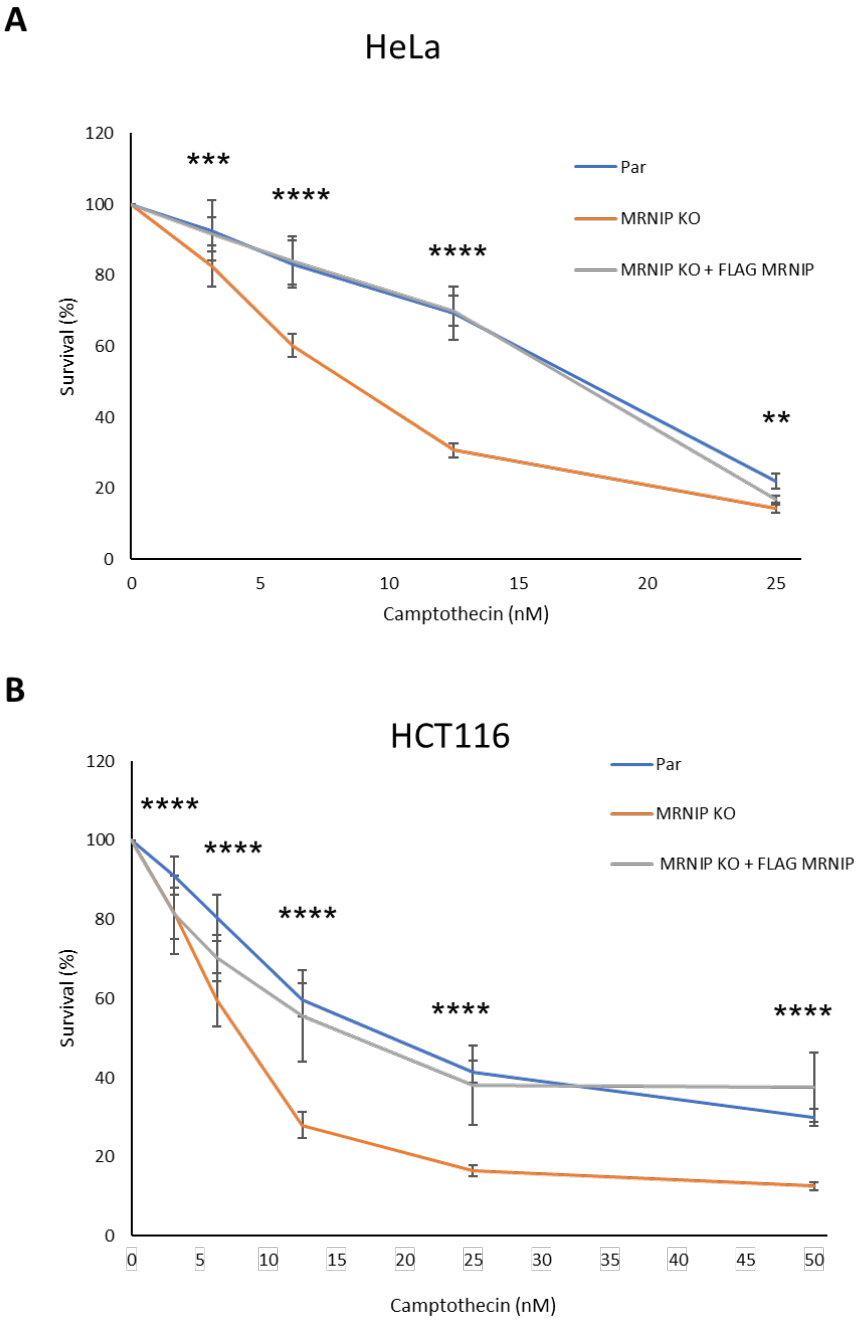

Figure 3.4 MRNIP KO cells are sensitive to CPT treatment.

A) Parental (Par) HeLa and B) HCT116 cells, derivative MRNIP KO (MRNIP KO) cells and MRNIP KO cells stably expressing FLAG-MRNIP (MRNIP KO + FLAG MRNIP) were treated with the indicated concentrations of CPT. After 96 hours, an MTT assay was performed, and results were normalised to untreated controls. Data represent the mean from three experiments (n=3), and errors displayed represent SD. Statistical significance was determined by two-way ANOVA with Tukey correction for multiple comparisons. **P ≤0.01, ***P ≤0.001, ****P ≤0.0001.

Given that MRNIP KO cells are sensitive to HU [384] and CPT, we next tested whether DNA damage levels are further elevated in HU and CPT treated MRNIP KO HeLa and HCT116 cells, relative to their wild-type counterparts. We also employed MRNIP KO cells stably overexpressing doxycycline-inducible FLAG-tagged MRNIP, to ensure that any phenotype observed could specifically be rescued by reintroduction of MRNIP. We initially assessed the prevalence of γH2AX and 53BP1 foci via indirect immunofluorescence following treatment with 3mM of HU for 6 hours to induce replication stress in HeLa cells. Cells were identified as foci-positive when they exhibited more than 5 foci (Figure 3.5 A). As expected, HU treatment of both parental and MRNIP KO HeLa cells resulted in an increase in the frequency of foci-positive cells. A statistically significant increase in γH2AX and 53BP1 foci was observed in both unperturbed and HU treated MRNIP KO HeLa cells when compared to parental control lines and overexpression of FLAG-tagged MRNIP rescued elevated DNA damage for both markers (Figure 3.5 *B)*.

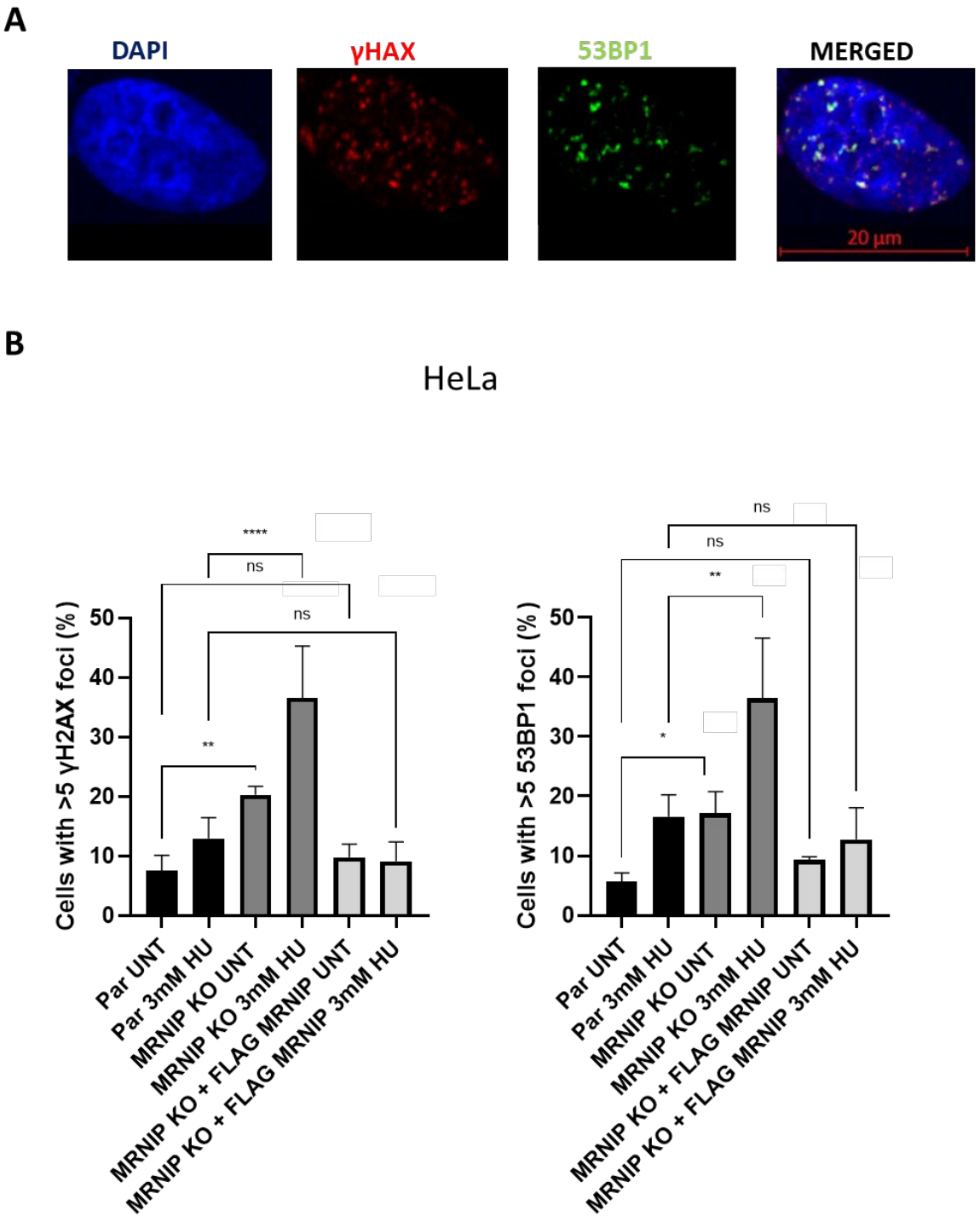

Figure 3.5 MRNIP KO cells exhibit increased DNA damage foci upon HU treatment.

A) Representative images of cells with more than five γH2AX and 53BP1 foci which were scored as positive. Scale bar 20µm. B) Parental (Par) HeLa, derivative MRNIP KO (MRNIP KO) cells and MRNIP KO cells stably expressing FLAG-MRNIP (MRNIP KO + FLAG MRNIP) were mock treated (UNT) or treated with 3mM HU for 6 hours, fixed, stained with DNA damage markers γH2AX and 53BP1 and counterstained with DAPI. Data represent the mean from three experiments (n=3), and errors displayed represent SD. Statistical significance was determined by two-way ANOVA with Tukey correction for multiple comparisons. ns; not statistical, *P ≤0.005, **P ≤0.01, ****P ≤0.0001.

In addition, HeLa and HCT116 cells were treated with a low (50nM) (Figure 3.6 A) and a high (1μM) (Figure 3.6 B) dose of CPT. MRNIP KO HeLa cells exhibited elevated γH2AX and 53BP1 foci compared to the parental cells following treatment of low and high dose of CPT for 2 hours and overexpression of FLAG-tagged MRNIP rescued elevated DNA damage levels (Figure 3.6 A, B).

A

HeLa

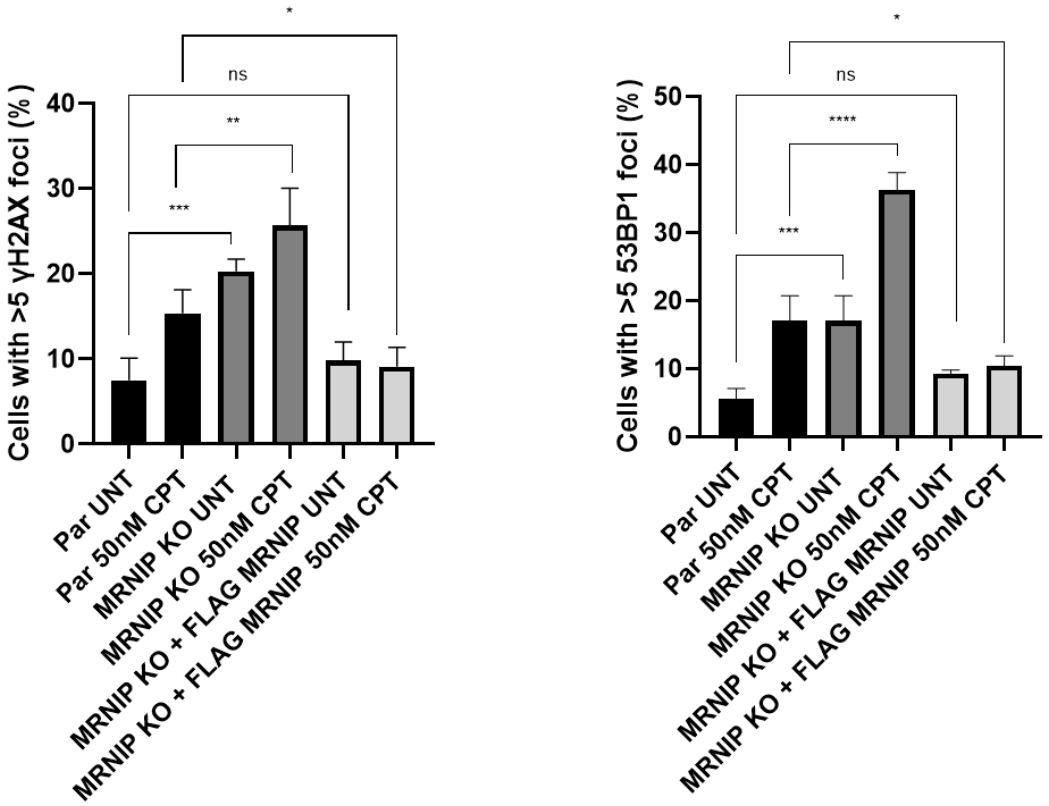
Cells with >5 γH2AX foci (%)
0
10
20
30
40
*
ns
**
***
Par UNT
Par 50nM CPT
MRNIP KO UNT
MRNIP KO 50nM CPT
MRNIP KO + FLAG MRNIP UNT
MRNIP KO + FLAG MRNIP 50nM CPT
Cells with >5 53BP1 foci (%)
0
10
20
30
40
50
*
ns
****
***
Par UNT
Par 50nM CPT
MRNIP KO UNT
MRNIP KO 50nM CPT
MRNIP KO + FLAG MRNIP UNT
MRNIP KO + FLAG MRNIP 50nM CPT

B

HeLa

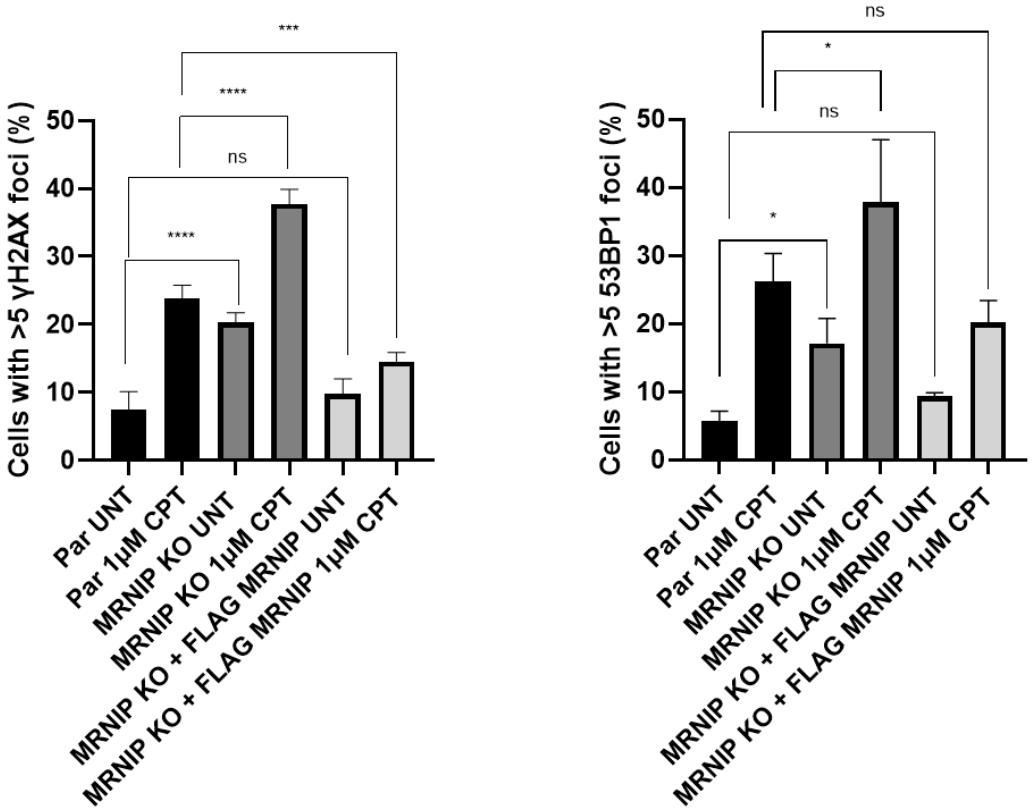
Cells with >5 γH2AX foci (%)
0
10
20
30
40
50
***
****
ns
****
Par UNT
Par 1μM CPT
MRNIP KO UNT
MRNIP KO 1μM CPT
MRNIP KO + FLAG MRNIP UNT
MRNIP KO + FLAG MRNIP 1μM CPT
Cells with >5 53BP1 foci (%)
0
10
20
30
40
50
ns
*
ns
*
Par UNT
Par 1μM CPT
MRNIP KO UNT
MRNIP KO 1μM CPT
MRNIP KO + FLAG MRNIP UNT
MRNIP KO + FLAG MRNIP 1μM CPT

Figure 3.6 HeLa MRNIP KO cells exhibit increased DNA damage foci upon CPT treatment.

A) Parental (Par) HeLa, derivative MRNIP KO (MRNIP KO) cells and derivative MRNIP KO cells stably expressing FLAG MRNIP (MRNIP KO + FLAG MRNIP) were mock treated (UNT) or treated with 50nM of CPT for 2 hours B) Parental HeLa, derivative MRNIP KO cells and derivative MRNIP KO cells stably expressing FLAG MRNIP were mock treated (UNT) or treated with 1μM of CPT for 2 hours fixed, stained with DNA damage markers γH2AX and 53BP1 and counterstained with DAPI. Data represent the mean from three experiments (n=3) and errors displayed represent SD. Statistical significance was determined by two-way ANOVA with Tukey correction for multiple comparisons. ns; not statistical, *P ≤0.005, **P ≤0.01, ***P ≤0.001, ****P ≤0.0001.

Similar phenotypes were obtained for the HCT116 cell line with higher levels of DNA damage being observed in MRNIP KO cells treated with 1μM of CPT compared to the controls which were rescued with overexpression of FLAG-tagged MRNIP (Figure 3.7).

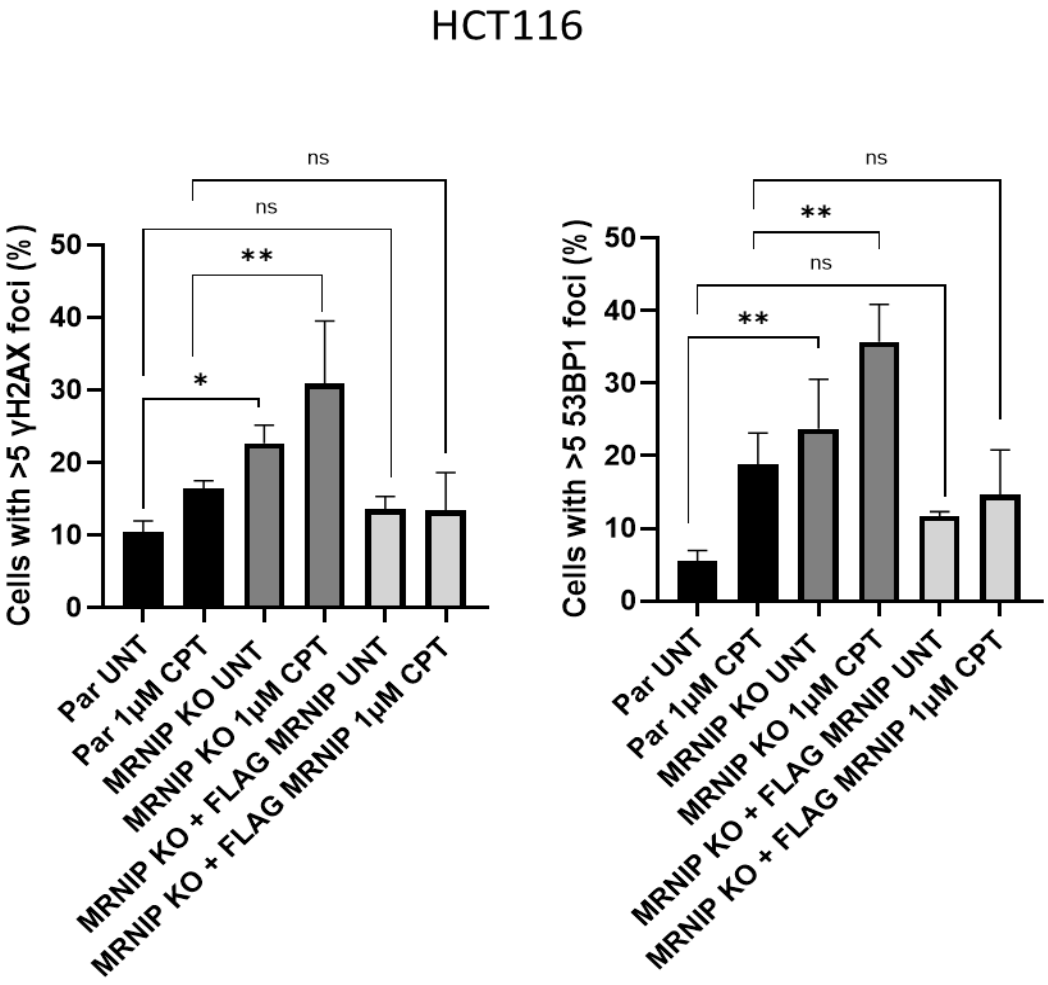

Figure 3.7 HCT116 MRNIP KO cells exhibit increased DNA damage foci upon CPT treatment.

Parental HCT116, derivative MRNIP KO cells and derivative MRNIP KO cells stably expressing FLAG MRNIP were mock treated (UNT) or treated with 1μM of CPT for 2 hours fixed, stained with DNA damage markers γH2AX and 53BP1 and counterstained with DAPI. Data represent the mean from three experiments and errors displayed represent SD. Statistical significance was determined by two-way ANOVA with Tukey correction for multiple comparisons, (n=3). ns: not statistical, *P ≤0.05, **P ≤0.01.

These experiments suggest that elevated levels of DNA damage can be rapidly induced by HU and CPT treatments of MRNIP KO cells.

3.3 Several sequence features of MRNIP contribute to MRNIP-mediated CPT resistance.

Following the observation that MRNIP KO cells were sensitive to CPT, we next examined CPT sensitivity in HeLa cells stably expressing tetracycline-inducible FLAG-tagged MRNIP housing mutations at established and putative sites of functional importance. This included mutations at potential sites of phosphorylation by MAPKs/CDKs (Ser217), a likely PIKK phosphorylation site (Ser115), as well as two potential ubiquitination sites (K58/129R), or four cysteines (cysteines 12,15,31,34) predicted by AlphaFold to form the metal ion-coordinating core of the N-terminal Zinc Finger domain. We also included the Δ25 mutant, which lacks a motif with some similarity to the N-terminal domain of the MRN interactor CtIP, and which is proven to be non-functional in the context of the repair of radiation-induced DNA damage [384] (Table 8). We generated MRNIP KO cell lines stably expressing these mutants, and initially tested their expression via western blotting using an anti-FLAG antibody, which as expected exclusively recognised overexpressed FLAG-tagged MRNIP. Tubulin was included as a loading control.

Table 8: Types of MRNIP mutations

Name of mutation	Type of mutation
S217A	Inhibition of phosphorylation at Ser217
S115A	Inhibition of phosphorylation at Ser115
S115D	Mimicking phosphorylation at Ser115
Δ25	Absence of KELWS sequence
C4A	Substitution of cysteines 12,15,31,34 in putative ZNF domain
K58/129R	Substitution of putative ubiquitination sites

Notably, MRNIP KO cells with stably incorporated FLAG-tagged WT MRNIP expressed protein even in the absence of doxycycline. Such 'leaky' expression was unexpected, but to compensate in all future experiments, doxycycline was added to all samples including parental controls and MRNIP KO cells. The FLAG-S115D band displayed slightly reduced electrophoretic transit, as expected given the introduction of a negative charge, although both the FLAG-S115A and S217A bands appeared to run at the same height as the FLAG-WT band, suggesting minimal phosphorylation of these sites under these conditions. Consistent with the loss of a 25 amino acid sequence, the band corresponding to the Δ25 mutant ran slightly lower, confirming the absence of the KELWS sequence. Interestingly, we observed elevated protein levels following arginine substitution of putative ubiquitination sites K58 and K129 (Figure 3.8) suggesting possible involvement of these sites in mediating ubiquitin-proteasome-dependent degradation of MRNIP.

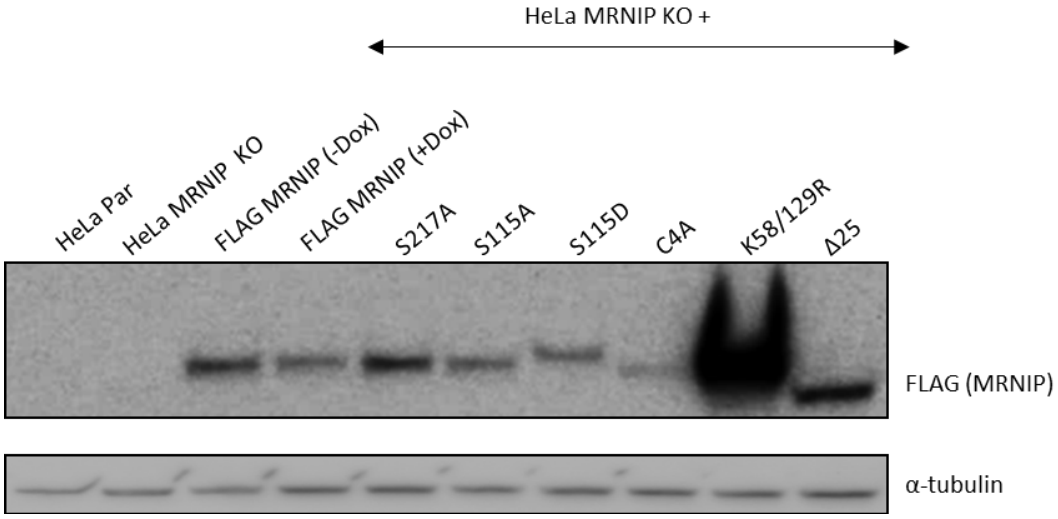

Figure 3.8 Expression of mutated forms of MRNIP at different sites in HeLa MRNIP KO cells.

MRNIP expression was induced upon doxycycline treatment at least 24 hours and whole cell extracts from HeLa parental (Par), derivative MRNIP KO (MRNIP KO), and MRNIP KO cells stably expressing FLAG-WT (FLAG MRNIP) or mutant MRNIP including the following substitutions: inhibiting phosphorylation at Ser217 (S217A), and at Ser115 (S115A), mimicking phosphorylation at Ser115 (S115D), substitution of cysteines 12,15,31,34 in the putative zinc finger domain (C4A), substitution of putative ubiquitination sites K58/129 (K58/129R) as well as disruption of the KELWS sequence (Δ25) were prepared. Lysates were resolved by western blotting and probed for MRNIP and α-tubulin as a loading control.

We next investigated the functionality of these altered versions of MRNIP in the context of survival following CPT treatment. Again, an MTT assay was performed following incubation of cells with a range of CPT concentrations. Doxycycline was added to all samples. As observed previously, MRNIP KO cells were sensitive to CPT, and this sensitivity was fully rescued by stable reintroduction of FLAG-tagged WT MRNIP. Ectopic expression of the S217A mutant only partially rescued survival, with a significant increase in survival observable only at 12.5nM of CPT and not to the same extent as in parental cells (Figure 3.9 A).

Overexpression of the C4A mutant further exacerbated CPT sensitivity at all concentrations of CPT tested, suggesting that elevated expression of a MRNIP mutant incapable of metal ion co-ordination has a dominant negative effect on cell survival. A

similar effect was observed in cells expressing the K58/129R double mutant, raising the possibility that modification of these sites plays an important role in MRNIP function in response to CPT-induced DNA damage (Figure 3.9 B*)*. MRNIP KO cells expressing alanine or glutamic acid substitutions of Ser115 displayed similar survival curves to control MRNIP KO cells, implying that dynamic phosphorylation of this site might be required for MRNIP function (Figure 3.9 C).

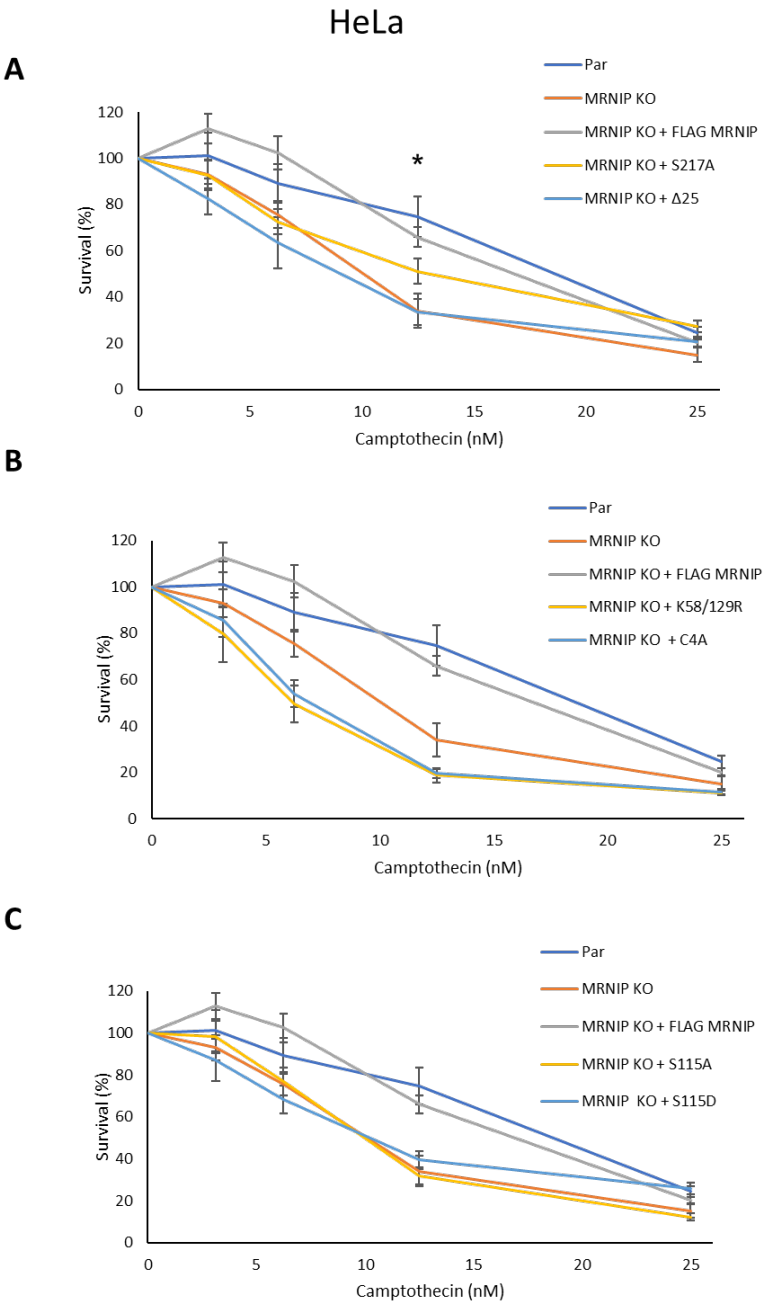

Figure 3.9 HeLa MRNIP KO cells expressing mutated forms of MRNIP at different sites are sensitive to CPT.

A) Parental (Par) HeLa, derivative MRNIP KO (MRNIP KO) cells, derivative MRNIP KO cells stably expressing FLAG MRNIP (MRNIP KO + FLAG MRNIP) and MRNIP KO cells expressing S217A and Δ25 MRNIP mutants, B) MRNIP KO cells expressing C4A and K58/129R double MRNIP mutants and C) MRNIP KO cells expressing alanine (S217A) or glutamic acid substitutions of Ser115 (S217D) were treated with the indicated concentrations of CPT. After 96 hours, an MTT assay was performed, and results were normalised to untreated controls. Data represent the mean from three experiments (n=3) and errors displayed represent SD. Statistical significance was determined by two-way ANOVA with Tukey correction for multiple comparisons. *P ≤0.05.

3.4 Ser217 and K58/129R are not required for MRNIP-mediated protection of nascent DNA.

The Staples laboratory previously demonstrated that disruption of Ser115, the Zinc Finger cysteines and the KELWS motif does not result in impaired protection of nascent DNA at HU-stalled replication forks [297]. Therefore, we also employed DNA fibre assays to test whether FLAG-tagged S217A and K58/129R mutants (mutants that had not been tested in the previous publication thus chosen for this project) can function effectively in fork protection. Briefly, cells were labelled with CldU (green label) and IdU (red label) thymidine analogues for 20 min each, followed by prolonged fork stalling with a high dose of HU (3mM) (Figure 3.10 *A)*. The fork is considered as protected from nucleolytic degradation when the length of both tracts is equal, while shortening of the IdU tract indicates a deprotected fork that has likely been degraded by the action of one or more nucleases. Notably, only forks that include contiguous CldU-IdU signals were included in our analysis, to ensure that any phenotype observed is due to nucleolytic resection of stalled replication forks, and not premature termination events. As expected in line with published findings [384], in samples derived from MRNIP KO cells the IdU:CldU ratio dropped to approximately 0.7, demonstrating nascent DNA degradation in response to prolonged stalling in the presence of HU. Both parental and derivative MRNIP KO cells expressing FLAG tagged MRNIP maintained a IdU:CldU ratio of approximately 1 following HU treatment, demonstrating that reintroduction of MRNIP fully rescues nascent DNA protection. However, neither the Ser217A nor the K58/129R mutant displayed a defect in fork protection, as they exhibited a IdU:CldU ratio of approximately 1 which was similar to the parental cell line (Figure 3.10 *B)*. This suggests that neither these residues, nor their modification contribute to the function of MRNIP in the context of protection of HU-stalled forks and serves to highlight mechanistic differences between the distinct roles of MRNIP at DNA breaks and reversed forks.

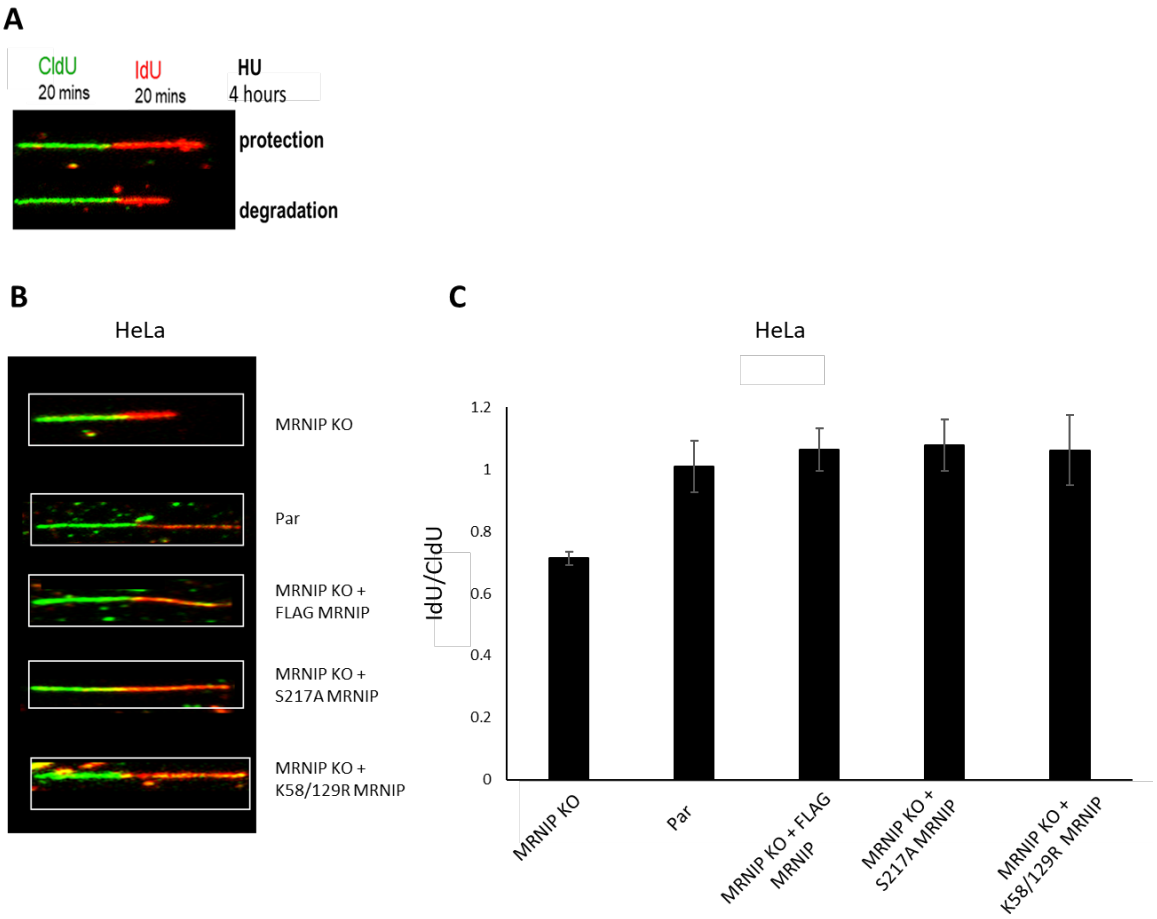

Figure 3.10 Ser217 and K58/129R are not required for MRNIP-mediated protection of nascent DNA.

A) Schematic representation of the experimental set up. B) Parental (Par) HeLa, derivative MRNIP KO (MRNIP KO), derivative MRNIP KO cells stably expressing FLAG MRNIP (MRNIP KO + FLAG MRNIP), S217A and K58/129R MRNIP mutants were labelled with CldU for 20 min, then IdU for 20 min followed by a 4 hours 3mM HU treatment. C) Fork degradation was assessed via the IdU:CldU tract length ratio. Data represent the mean from two experiments (n=2). At least 200 fibres were measured for each condition.

In conclusion, our findings indicate that MRNIP prevents DNA damage accumulation in cycling but otherwise unperturbed HeLa and HCT116 cells, and that cells depleted of MRNIP are sensitive to HU and CPT. Several sequence motifs in MRNIP play important roles in mediating resistance to CPT. However, neither Ser217 nor the putative ubiquitination sites lysine 58 and 129 play important roles in mediating fork protection.

CHAPTER IV

4 The role of MRE11 phosphorylation in the protection of nascent DNA by MRNIP.

In the absence of fork protection factors such as RAD51 and BRCA1/2, stalled forks undergo MRE11-dependent degradation, which has been suggested to lead to chromosomal instability [336,357,362,396]. However, how MRE11 is regulated in this context is poorly understood. ATM phosphorylates MRE11 at serine 676 and 678, limiting radiation-induced DSB resection [310]. In addition, PIH1D1 - a component of the Heat-Shock Protein 90 (HSP90) cochaperone R2TP – is reported to directly interact with MRE11 phosphorylated by PLK1 and CK2 at serines 558/561 and 688/689 to regulate MRE11 stability and chromatin association [292,293]. In addition, PLK1 is reported to prime MRE11 phosphorylation at serine 649, which in its turn promotes CK2-mediated phosphorylation of MRE11 at serine 688. Phosphorylation of MRE11 at S649/S688 is reported to inhibit binding of the MRN complex to damaged DNA and counteracts ATM signalling and DNA repair [292]. In response to IR, MRNIP promotes ATM activation, and the phosphorylation of multiple ATM targets including KAP1 and p53 [301]. A recent study from the Lukas laboratory also demonstrated that Ser676/678 phosphorylation is required for MRE11-dependent nascent DNA degradation in certain contexts [397].

Based on this prior research, we hypothesised that MRNIP promotes ATM-mediated phosphorylation of MRE11, and that altered MRE11 phosphorylation in MRNIP KO cells modulates nascent DNA degradation. To investigate this, we tested MRE11 phosphorylation in MRNIP KO cells, and generated MRE11 mutants to test their role in protection of nascent DNA at stalled replication forks, using MRNIP KO cells as a model system. These mutations:

- Disrupt MRE11 phosphorylation at Ser558/561, Ser649, Ser688/689 and Ser676/678 (Ser>Ala).
- Mimic phosphorylation at Ser676/678 (Ser>Glu).
- Disrupt the exonuclease activity of MRE11 (H63D).

4.1 MRNIP promotes MRE11 phosphorylation.

Initially, we treated parental and derivative MRNIP KO HeLa cells with either HU or CPT and assessed MRE11 phosphorylation via western blotting with an antibody raised against Ser676 phospho-peptide, available commercially from Cell Signalling. This batch of antibody performed well, and we observed MRE11 phosphorylation in response to both HU and CPT treatments in WT HeLa cells. In contrast, MRE11 phosphorylation was barely detectable in lysates derived from MRNIP KO cells, suggesting a role for MRNIP in mediating MRE11 phosphorylation in response to replication stress and DNA break formation (Figure 4.1).

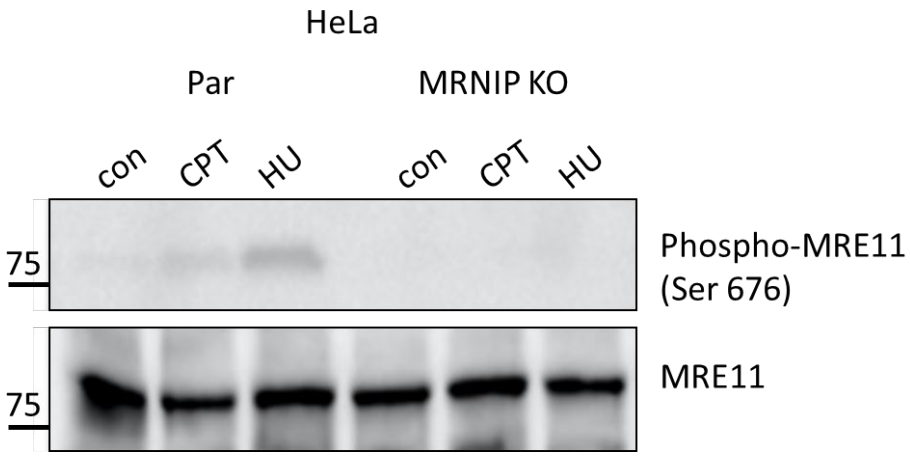

Figure 4.1 Phosphorylation of MRE11 at serine 676 is absent in HeLa MRNIP KO cells after CPT and HU treatments.

Whole cell extracts from parental (Par) and derivative MRNIP KO (MRNIP KO) HeLa cells were treated with 1μM CPT (CPT) for 3 hours and 3mM HU (HU) for 6 hours, lysed and blotted for phosphorylated MRE11 (Ser 676) and total MRE11. Experiment was performed once (n=1) as subsequent antibody batches failed to return an exploitable signal. Figure was created by Dr. Staples.

However, subsequent batches of this antibody did not perform well, and the degradation in antibody quality was confirmed by other laboratories (Lukas lab, personal communication). Our subsequent attempts to examine MRE11 phosphorylation in whole cell extracts derived from HeLa and MRNIP KO cells following treatment with HU (3 mM, 6 hrs) resulted in detection of only a very faint band (Figure 4.2 A). Assuming this poor blot quality could be improved by increasing the amount of source material and reducing non-specific background, we performed MRE11 immunoprecipitations in HeLa and U2OS cells treated with HU or CPT, followed by western blotting with the phospho-MRE11 antibody (Ser 676) (Figure 4.2 B,C). MRE11 was manifoldly enriched following immunoprecipitation. Unfortunately, again no band was detected in input samples derived from whole cell extracts and blotting for phospho-MRE11(Ser 676) in MRE11 immune complexes yielded several bands that did not increase following HU or CPT treatments (Figure 4.2 B, C).

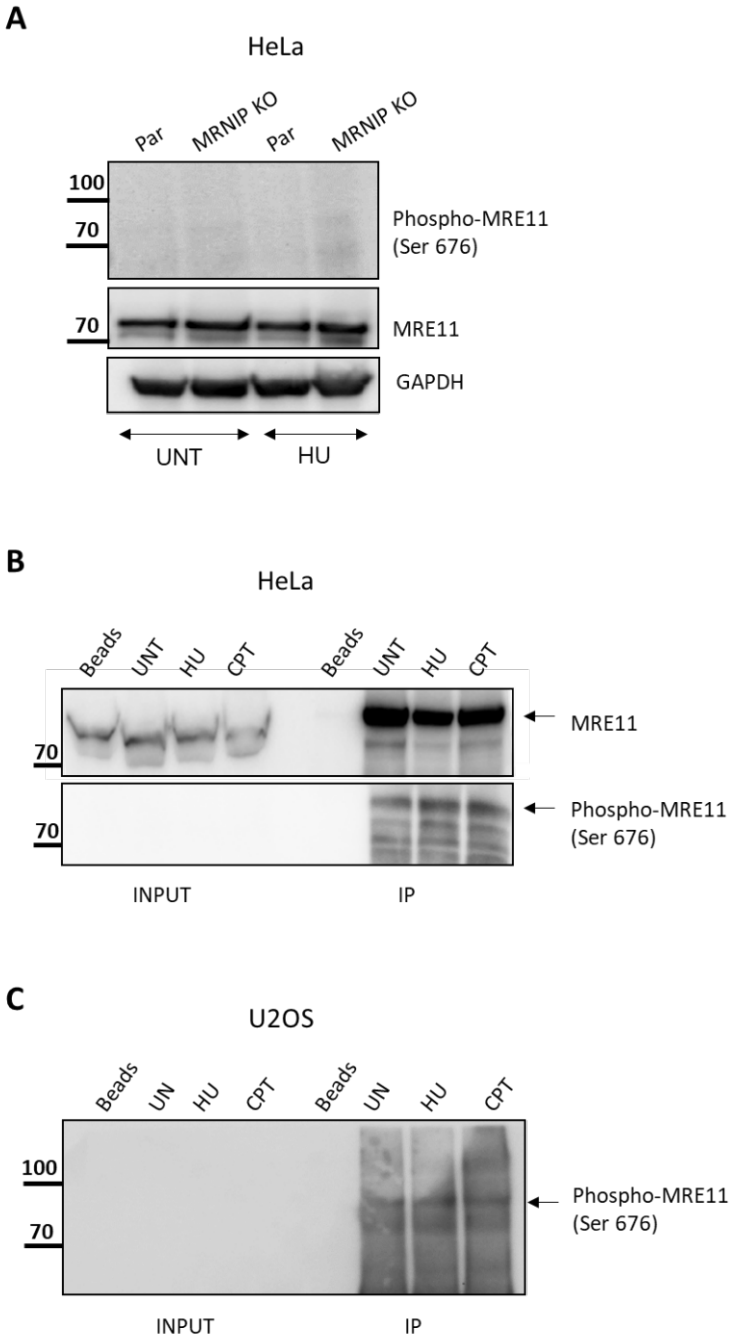

Figure 4.2 Levels of MRE11 and phosphorylated MRE11 in HeLa and U2OS cells.

A) Whole cell extracts from HeLa parental (Par) and derivative MRNIP KO (MRNIP KO) were mock treated (UNT) or treated with 3mM HU (HU) for 6 hours, lysed and western blotting was performed using the relevant antibodies. B) Levels of total MRE11 and phosphorylated MRE11 (Ser 676) in HeLa and C) U2OS cells performing immunoprecipitation using FLAG antibody. Cells were treated with beads only (Beads), mock treated (UNT), treated with 3mM HU for 6 hours (HU) and 1μM CPT for 3 hours (CPT), lysed and immunoprecipitated with MRE11 antibody. Eluates were resolved by SDS-PAGE and probed for the relevant antibodies.

According to the results, we concluded that the new batch of phospho-MRE11 antibody was of insufficient quality, and subsequent attempts to improve on this work by purchasing new aliquots of antibody from different batches proved unsuccessful. A future approach to assess the phosphorylation at Ser676/678 would be to use Phos-Tag gels testing wilt type and MRE11 mutant at this residue. Despite these disappointing findings, we were encouraged by our early data suggesting that MRE11 phosphorylation induced by DNA damage and replication stress is defective in MRNIP KO cells. Based on this, we resolved to assess whether alanine or aspartic acid substitution of Ser676/678 ameliorates or accentuates the nascent DNA degradation phenotype observed in MRNIP KO cells.

4.2 Generation of MRE11 mutants.

Based on the preliminary data that phosphorylation of MRE11 at serine 676 was absent in MRNIP KO cells after CPT and HU treatments, and the previous work from the Lavin laboratory demonstrating that alanine substitution of MRE11 at Ser 676/678 results in increased DNA end resection [310], we generated a series of MRE11 mutants. MRE11 was firstly amplified by PCR and recombined using BP clonase into the Gateway Entry vector p221DONR. Mutations were then introduced by whole-plasmid Site-Directed Mutagenesis and sequenced before recombining into the Gateway destination vector pDEST-T/O-FLAG. These mutants were confirmed by Sanger sequencing with no further mutations being present. This approach included alanine substitutions of MRE11 at Ser 676/678, and the H63D mutant (Figure 4.3) which was reported as exonuclease-dead by a previous group showing that the exonuclease activity of MRE11 was essential for DNA resection [398]. It is important to note that all prior evidence as well as previous work from this laboratory implicating MRE11 in nascent DNA degradation was based on pharmacological MRE11 inhibition using Mirin or PFM39 [221,384]. Therefore, it is advantageous to prove the involvement of particular factors via both pharmacological and genetic means.

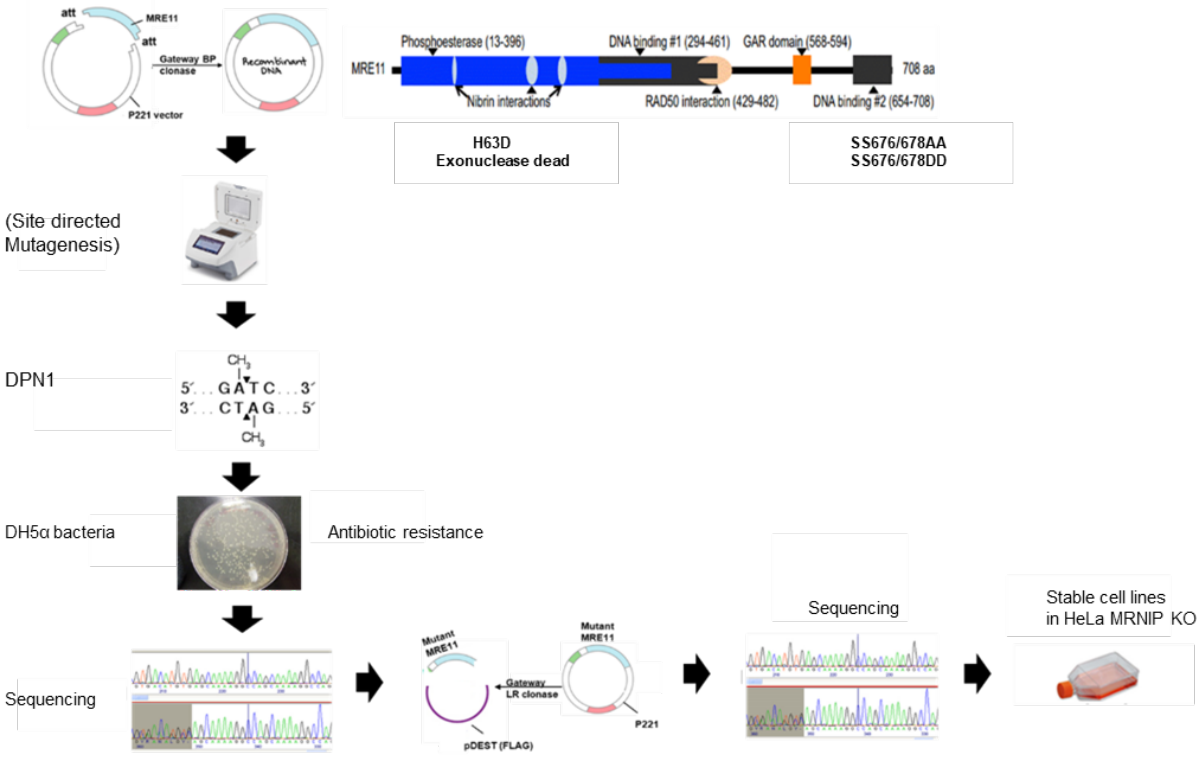

Figure 4.3 Schematic representation of the process used in the generation of stable cell lines expressing MRE11 mutants using the Gateway system.

MRE11 is composed of a phosphodiesterase domain in its N-terminus that harbours endonuclease and exonuclease activities and interaction sites with NBS1, DNA binding sites that are scattered throughout the centre, a RAD50 binding motif and a glycine-arginine-rich (GAR) motif that participates in DNA binding in *vitro* and it is responsible for localizing MRE11 to sites of damage.

The Gateway system was used for the generation of mutants starting with the PCR-mediated generation of an MRE11 ORF that contains attB1 and attB2 sites. Corresponding attP1 and attP2 recombination sites are present in the recipient vector, p221. MRE11 fragment and vector were mixed with BP clonase to produce an entry vector containing attL1 and attL2 sites. Site Directed Mutagenesis was performed using mutagenic primers, followed by treatment with the DpnI enzyme, which cleaves only methylated sites present in the template DNA. The product was then transformed into DH5α bacteria and sequenced for verification. The entry vector was then mixed with LR clonase mix and the destination vector, pDEST-FRT/TO-FLAG, containing attR1 and attR2 sites. The product was then sequenced and stably integrated into Flp-In sites present in Flp-In HeLa MRNIP KO cells, via co-transfection with a plasmid encoding the pObpA recombinase.

We generated a series of MRNIP KO HeLa cell lines stably expressing FLAG-tagged WT MRE11, and Ser676/678Ala, Ser676/678Asp and His63Asp mutants of MRE11. MRE11 Ser676/678 phosphorylation status was tested in these stable cell lines via immunoprecipitation using FLAG-M2 Sepharose beads and blotting for phospho-MRE11 following treatment with 1μM CPT for 3 hours. As expected, FLAG-tagged Ser676/678Ala MRE11 was undetectable, indicating that the site substitution was successful (Figure 4.4). The His63Asp and Ser676/678Asp mutants were detected, as predicted, confirming that loss of exonuclease activity does not affect MRE11 phosphorylation at these sites.

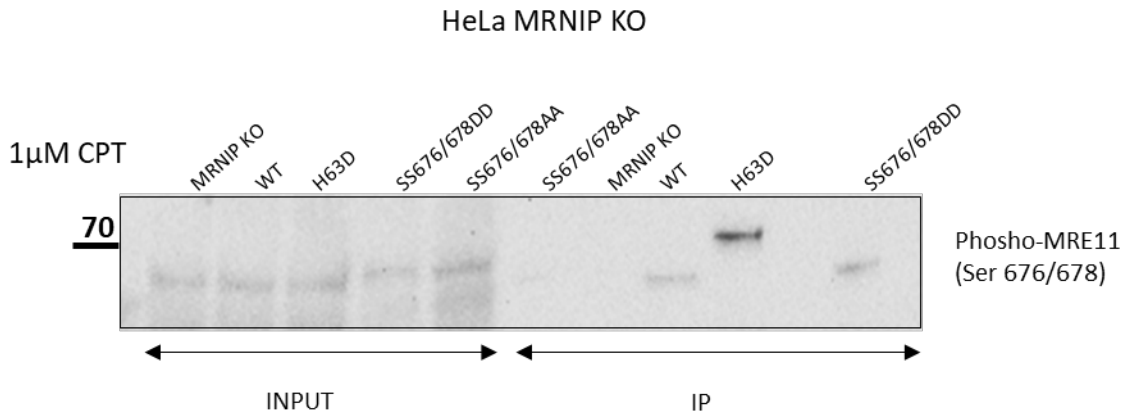

Figure 4.4 Levels of phosphorylated MRE11 in HeLa MRNIP KO cells expressing mutated forms of MRE11 phosphorylation sites.

Hela MRNIP KO (MRNIP KO), MRNIP KO cells expressing FLAG-tagged wild type MRE11 (WT), Ser676/678Ala (SS676/678AA), Ser676/678Asp (SS676/678DD) and His63Asp (H63D) mutants were treated with 1μM CPT for 3 hours, lysed and immunoprecipitated with MRE11 antibody. Eluates were resolved by SDS-PAGE and probed for phosphorylated MRE11 at serines 676/678. Experiment was performed once (n=1) as consequent antibody batches failed to return an exploitable signal.

The His63Asp mutant displayed reduced electrophoretic mobility, and sequencing of the plasmid revealed that due to the presence of repeat sequences near the portion of the cDNA encoding the MRE11 C-terminal region, a recombination event had occurred, leading to the contiguous duplication of part of the MRE11 sequence. To circumvent this problem, we employed *E. coli* Stbl3 bacteria to propagate the H63D-containing plasmid. This is a hybrid strain derived from *E. coli* K12 and *E. coli* B, which contains a mutation in the bacterial recombinase RecA. This mutation limits the potential for unwanted recombination between repeat sequences. This approach was successful for us, since new preparations of the pDEST-FLAG-MRE11 H63D plasmid did not contain the unwanted repeat sequence, and the encoded protein displayed the expected electrophoretic mobility when stably expressed in MRNIP KO cells (Figure 4.5).

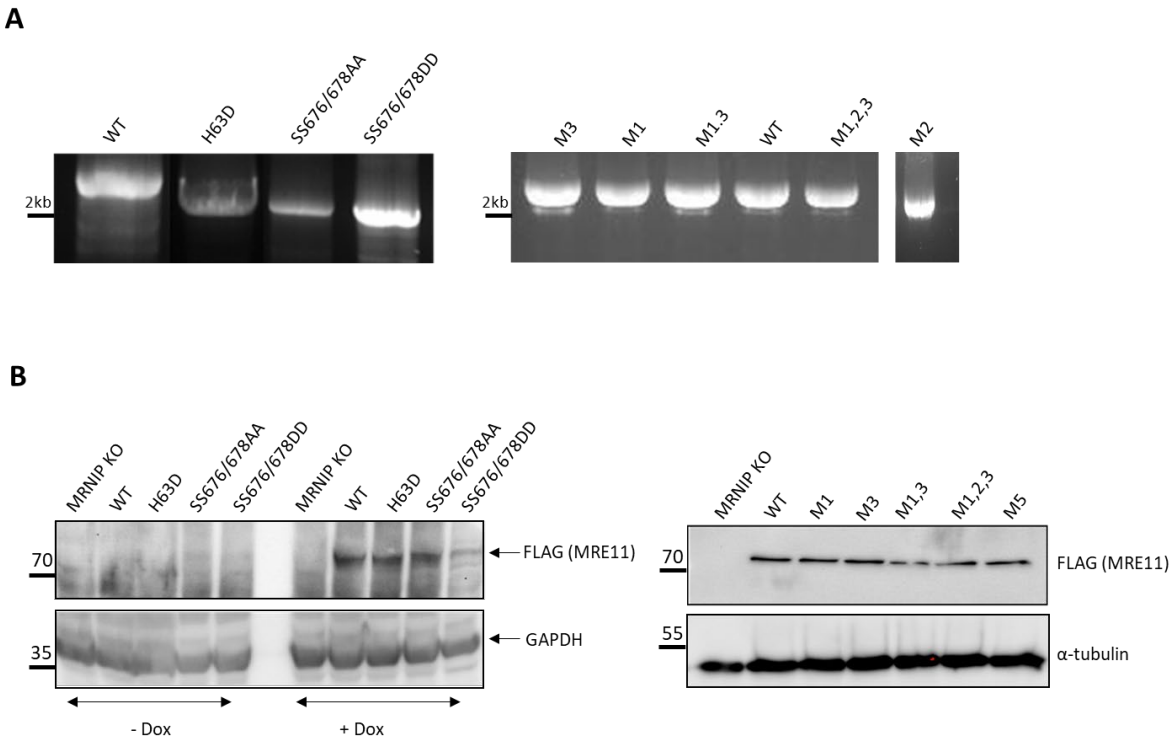

Figure 4.5 Levels of MRE11 in HeLa MRNIP KO cells expressing mutated forms of MRE11 phosphorylation sites.

A) Amplified PCR products of wild type (WT) MRE11, Ser676/678Ala (SS676/678AA), Ser676/678Asp (SS676/678DD), His63Asp (H63D), M1 (SS556/561AA), M2 (S649A), M3 (SS688/689AA), M1,3, M1,2,3 and M5 (S649A, S556/561AA, SS688/689AA, SS676/678AA) MRE11 mutants being generated by using the pDONR221 plasmid backbone, were run in 1% agarose gel. B) Whole cell extracts from MRNIP KO (MRNIP KO), MRNIP KO cells stably expressing FLAG-tagged wild type (WT) MRE11, Ser676/678Ala (SS676/678AA), Ser676/678Asp (SS676/678DD), His63Asp (H63D), M1 (SS556/561SAA), M2 (S649A), M3 (SS688/689AA), M1,3, M1,2,3 and M5 (S649A, S556/561AA, SS688/689AA, SS676/678AA) MRE11 mutants were mock treated (-Dox) or treated with doxycycline (+Dox) for at least 24 hours to induce MRE11 expression, lysed and blotted for the relevant antibodies.

To probe the role of MRE11 phosphorylation more widely in regulating function, the Horejsi laboratory (Barts Cancer Institute) provided us with MRE11 constructs encoding alanine mutants of MRE11 CK2 and PLK1 phosphorylation sites (Ser 558, 561, 649, 688 and 689), which were cloned and used to generate stable cell lines in HeLa MRNIP KO cells as described above. The phosphorylation sites substituted to construct mutants for this project are displayed in Table 9, along with associated functions and the kinases known to target these sites.

Table 9: Types of MRE11 mutations

Type of mutation	Reported Function	Kinase
Ser 558/561 (M1)	• Interacts with PIH1D • MRE11 stability	CK2
Ser 649 (M2)	• Primes CK2 dependent MRE11 phosphorylation at Ser 688 • Inhibits loading of MRN complex to sites of damage	PLK1
Ser 676/678	• Cell survival • HR repair • DNA resection	ATM
Ser 688/689 (M3)	• Inhibits loading of MRN complex to sites of damage • MRE11 stability • Interaction with PIH1D	CK2
H63	• DNA resection	-

4.3 MRE11 phosphorylation is a crucial determinant of nascent DNA degradation at stalled replication forks.

To decipher the role of MRE11 phosphorylation in fork stability, we employed the DNA fibre assay. To reduce levels of endogenous MRE11, we used an siRNA targeting the untranslated region of MRE11, to ensure that the siRNA used did not target mRNA transcribed from the mutant cDNAs introduced (Figure 4.6 A). We verified knockdown of MRE11 in HeLa MRNIP KO cells 48 hours post-transfection by western blotting, confirming that our knockdown protocol resulted in an approximately 60% reduction, according to densitometry (ImageJ), in endogenous MRE11 levels (Figure 4.6 B). Replication fork protection was assessed as before, via sequential CldU and IdU labelling followed by chronic HU treatment and DNA fibre analysis. As expected, MRNIP KO cells displayed nascent DNA degradation, which was reversed by depletion of MRE11, consistent with previous reports that degradation at these sites is inhibited by Mirin and PFM39 [384]. Stable expression of FLAG-tagged WT MRE11 restored nascent DNA degradation. Strikingly, the H63D exonuclease-dead mutant of MRE11 failed to restore DNA degradation under these conditions, consistent with prior reports implicating the exonuclease but not the endonuclease activity of MRE11 in degradation of reversed replication forks [357,364]. Furthermore, the Ser676/678Asp mutant of MRE11 also failed to restore DNA degradation, in contrast to published reports that phosphorylation of these sites is required for degradation [310]. Finally, the Ser676/678Ala mutant functioned similarly to WT MRE11 in this context, suggesting that phosphorylation of these sites is not required for MRE11 function in degradation of nascent DNA at reversed replication forks *per se* (Figure 4.6 C). Given the findings, we propose that MRNIP-mediated MRE11 phosphorylation at Ser 676/678 limits nascent DNA resection at reversed forks.

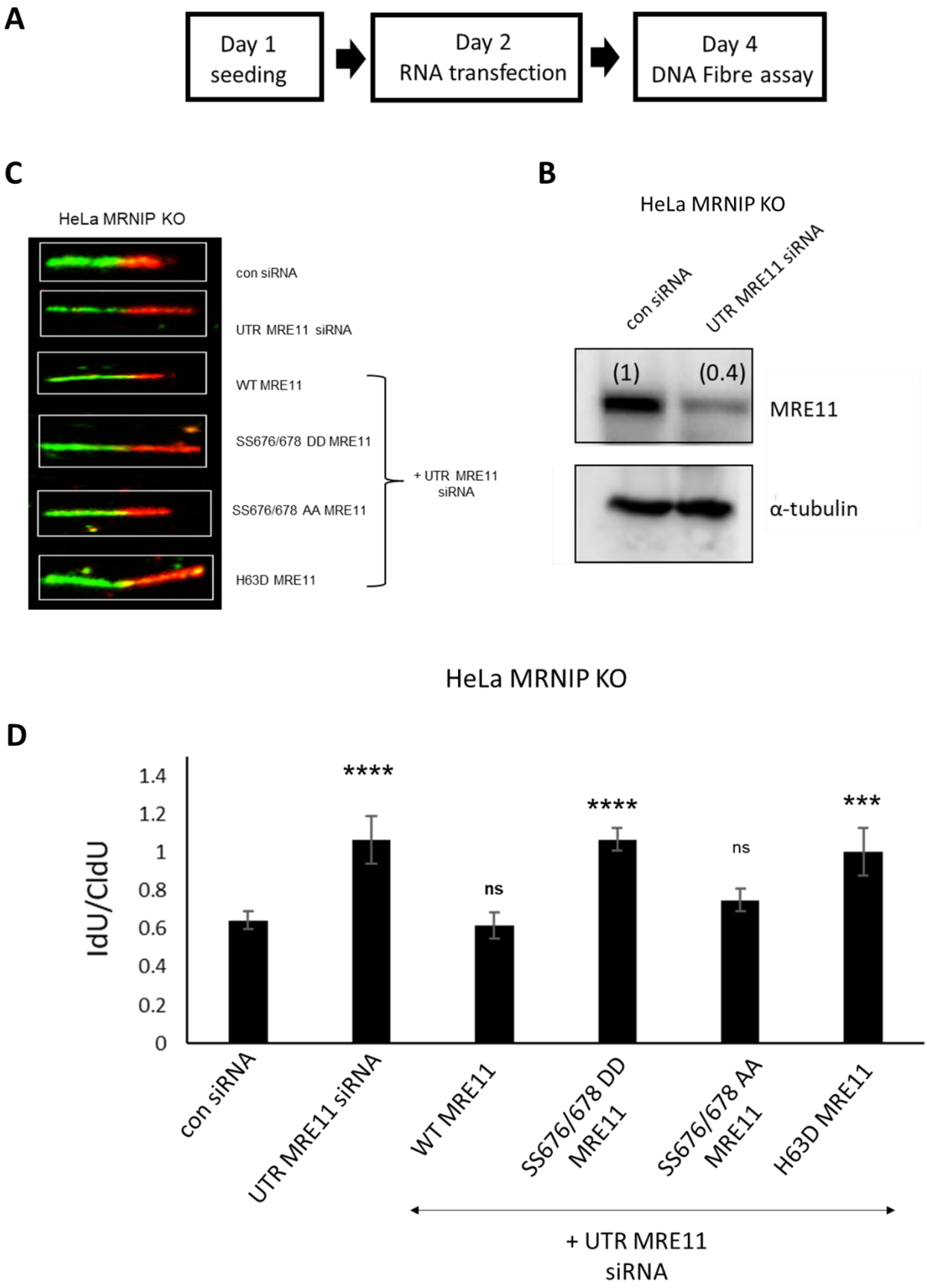
A
Day 1
seeding
Day 2
RNA transfection
Day 4
DNA Fibre assay
C
HeLa MRNIP KO
con siRNA
UTR MRE11 siRNA
WT MRE11
SS676/678 DD MRE11
SS676/678 AA MRE11
H63D MRE11
+ UTR MRE11
siRNA
B
HeLa MRNIP KO
con siRNA
UTR MRE11 siRNA
(1)
(0.4)
MRE11
α-tubulin
HeLa MRNIP KO
D
IdU/CldU
1.4
1.2
1
0.8
0.6
0.4
0.2
0
****
ns
****
ns
***
con siRNA
UTR MRE11 siRNA
WT MRE11
SS676/678 DD
MRE11
SS676/678 AA
MRE11
H63D MRE11
+ UTR MRE11
siRNA

Figure 4.6 Phosphomimetic substitution of MRE11 Ser676/8 rescues DNA degradation.

A) Schematic representation of the experimental set up. Cells were transfected with a non-targeting control siRNA (con siRNA) or siRNA that targets the 5' untranslated region of MRE11 (UTR MRE11 siRNA) for 48 hours and DNA fibre assay was performed. B) Confirmation of knockdown. HeLa MRNIP KO cells were transfected with a non-targeting control siRNA (con siRNA) or siRNA that targets the 5' untranslated region of MRE11 (UTR MRE11 siRNA) for 48 hours, lysed and blotted for MRE11 and α-tubulin as a loading control. Numbers in brackets indicate the relative levels of proteins as determined via ImageJ analysis. C) Representative examples of DNA fibres at indicated conditions. HeLa MRNIP KO cells and MRNIP KO cells engineered with FLAG tagged wild type (WT) MRE11, Ser676/678Ala (SS676/678AA), Ser676/678Asp (SS676/678DD) and His63Asp (H63D) MRE11 mutants were transfected with a non-targeting control siRNA (con siRNA) or siRNA that targets the 5' untranslated region of MRE11 (UTR MRE11 siRNA). Nascent DNA was then labelled with CldU for 20 min, IdU for 20 min and treated with 3mM HU for 4 hours. D) Fork degradation was assessed via the IdU:CldU tract length ratio. At least 200 DNA fibres were measured for each condition. Data represent the mean from four experiments (n=4). Statistical significance was determined by one-way ANOVA with Tukey correction for multiple comparisons. ns: not statistical, ***P≤0.001, ****P ≤ 0.0001.

We conclude that MRNIP functions to promote MRE11 phosphorylation at Ser 676/678 and hypothesise that this event limits MRE11 chromatin association/DNA binding of MRE11 to prevent aberrant resection of nascent DNA at reversed replication forks. Schematic representation of the model is given in (Figure 4.7). Further work is required to prove this hypothesis (see Discussion). Our evidence also confirms a specific role for the exonuclease function of MRE11 in degradation of nascent DNA.

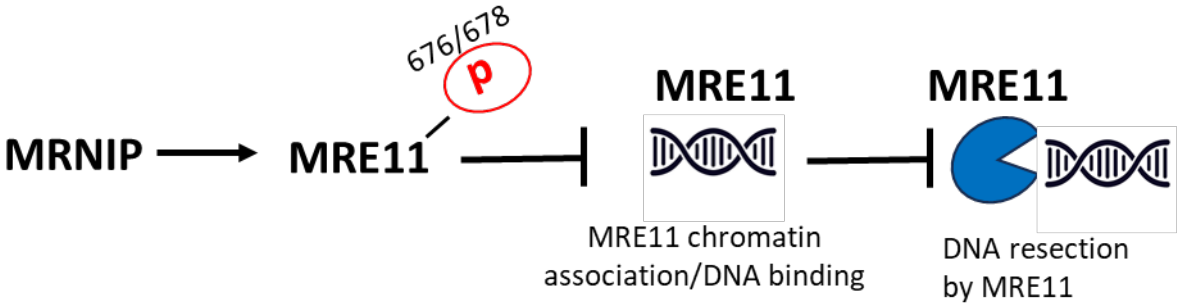

Figure 4.7. Proposed model of MRNIP regulating MRE11 phosphorylation at serines 676 and 678.

MRNIP promotes phosphorylation of MRE11 at Ser676/678 which compromises the ability of MRE11 to associate to the chromatin and bind to DNA, therefore inhibiting DNA resection

MRE11 is also phosphorylated by PLK1 and CK2, and to assess the contribution of these phosphorylation sites to MRE11 function at reversed forks in MRNIP-deficient cells, we performed DNA fibre assays in MRNIP KO cells stably expressing alanine substitutions of Ser558/561 (M1), Ser649 (M2), or Ser688/689 (M3), as well as a combination M1-M3 mutant in which all three PLK1/CK2 sites were substituted, and a mutant in which M1-M3 sites were substituted in addition to the two PIKK sites at Ser676/678 (M5). This latter, complex mutant housing a total of 7 alanine substitutions was generated to build on a recent interesting observation from collaborator Prof. Petr Cejka (Bellinzona), who demonstrated that dephosphorylation of MRE11 *in vitro* unexpectedly led to elevated exonuclease activity.

As before, we depleted MRE11 using an untranslated region (UTR)-directed siRNA in MRNIP KO cells stably expressing FLAG-WT, M1, M2, M3, M1-3 and M5 MRE11, and performed DNA degradation fibre assays using HU. Representative images of fibres for each condition are shown in (Figure 4.8 A). As expected, the IdU:CldU ratio in MRNIP KO cells was reduced to 0.6, indicating the presence of DNA degradation. Depletion of MRE11 resulted in a significant rescue of this phenotype, and restoration of WT MRE11 restored degradation. Strikingly, the M1, M2, M3 and M1-3 mutants all failed to restore degradation, suggesting that PLK1/CK2-mediated phosphorylation facilitates MRE11 function at deprotected forks in MRNIP-deficient cells. This observation conflicts with previous findings that PLK1/CK2-mediated MRE11 phosphorylation at serine 558/561 and 688/689 inhibits MRN loading and chromatin association [292,293], although one notes that these prior observations were conducted in cells exposed to ionising radiation.

In an apparent paradox, the M5 mutant housing mutations of all PIKK, CK2 and PLK1 sites restored nascent DNA degradation in MRNIP-deficient cells to the same extent as WT MRE11, indicating that while partial dephosphorylation of this region of MRE11 impairs activity at these sites, wider dephosphorylation results in restoration of MRE11 function, at least in the context of stalled, reversed forks (Figure 4.8 B).

These findings suggest that dynamic cycles of phosphorylation and dephosphorylation regulate MRE11 activity in the context of stalled replication forks, suggest the presence of multiple cell cycle-regulated inputs, for example via PLK1, and posit the possibility that dephosphorylation of Ser676/678 might provide a means of rapidly activating MRE11 in the absence of PLK1/CK2-mediated phosphorylation of the 558/561 and 649/688/689

clusters – for example during G1 or S-phase when PLK1 activity is minimal. As future experiment, we could investigate if chromatin binding or DNA binding is compromised in cells expressing mutant forms of MRE11.

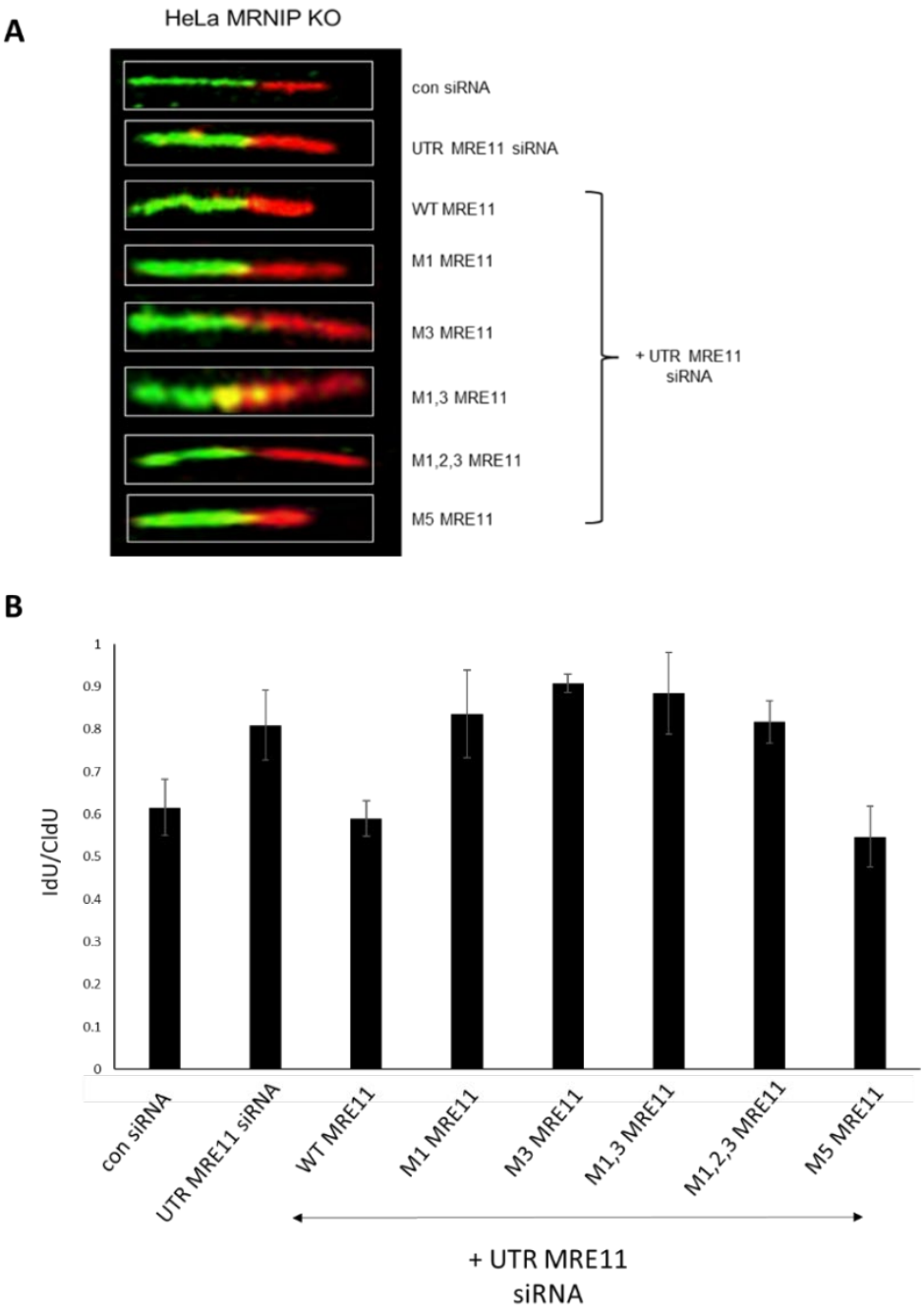

Figure 4.8. Alanine substitution of CK2, PLK1 and PIKK phosphorylation sites in MRE11 restores extensive DNA resection.

A) Representative examples of DNA fibres. HeLa MRNIP KO cells and HeLa MRNIP KO cells engineered with FLAG tagged wild type (WT) MRE11, M1 (SS556/561AA), M2 (S649A), M3 (SS688/689AA), M1,3, M1,2,3 and M5 (S649A, S556/561AA, SS688/689AA, SS676/678AA) MRE11 mutants were transfected with a non-targeting control siRNA (con siRNA) or an siRNA that targets the 5' untranslated region of MRE11 (UTR MRE11 siRNA). Nascent DNA was then labelled with CldU for 20 min, IdU for 20 min and treated with 3mM HU for 4 hours. B) Fork degradation was assessed via the IdU:CldU tract length ratio. At least 200 DNA fibres were counted for each condition. Data represent the mean from two experiments (n=2).

CHAPTER V

5 The role of MRNIP in regulating the cellular response to nucleoside analogues.

Previous work from the Staples laboratory demonstrated a direct interaction of MRNIP with MRE11, and *in vitro* MRNIP-mediated repression of MRE11 exonuclease activity [384]. In addition, recent work from two different laboratories found that MRE11 exonuclease activity, assisted by the CtIP-BRCA1 complex, is responsible for removing Gemcitabine from replicating DNA [386,392]. However, the exact mechanism of MRE11 activity in the context of nucleoside analogues is yet to be elucidated. Therefore, we aimed to shed light in the role of MRNIP in regulating MRE11 activity in response to Gemcitabine treatment.

5.1 MRNIP promotes Gemcitabine sensitivity and causes elevated DNA damage in HeLa and HCT116 cells upon Gemcitabine treatment.

To investigate whether MRNIP modulates cell survival in response to Gemcitabine, we performed MTT assay in HeLa (Figure 5.1 A) and HCT116 (Figure 5.1 B) parental and derivative MRNIP KO cells treated with various concentrations of Gemcitabine for 96 hours. Surprisingly, MRNIP KO cells were resistant to Gemcitabine in both cell lines with HCT116 cells exhibiting a stronger phenotype. We observed more than 80% death in HCT116 cells even at the lowest concentration of Gemcitabine used, in contrast to MRNIP KO cells, in which survival was minimally impacted even at the highest concentration used (Figure 5.1 B). Gemcitabine sensitivity was fully restored in MRNIP KO cells stably expressing FLAG-MRNIP in both cell lines (Figure 5.1 A, B). In addition, survival of parental HeLa cells was approximately 40% less than that observed in MRNIP KO cells by the end of the treatment (Figure 5.1 A).

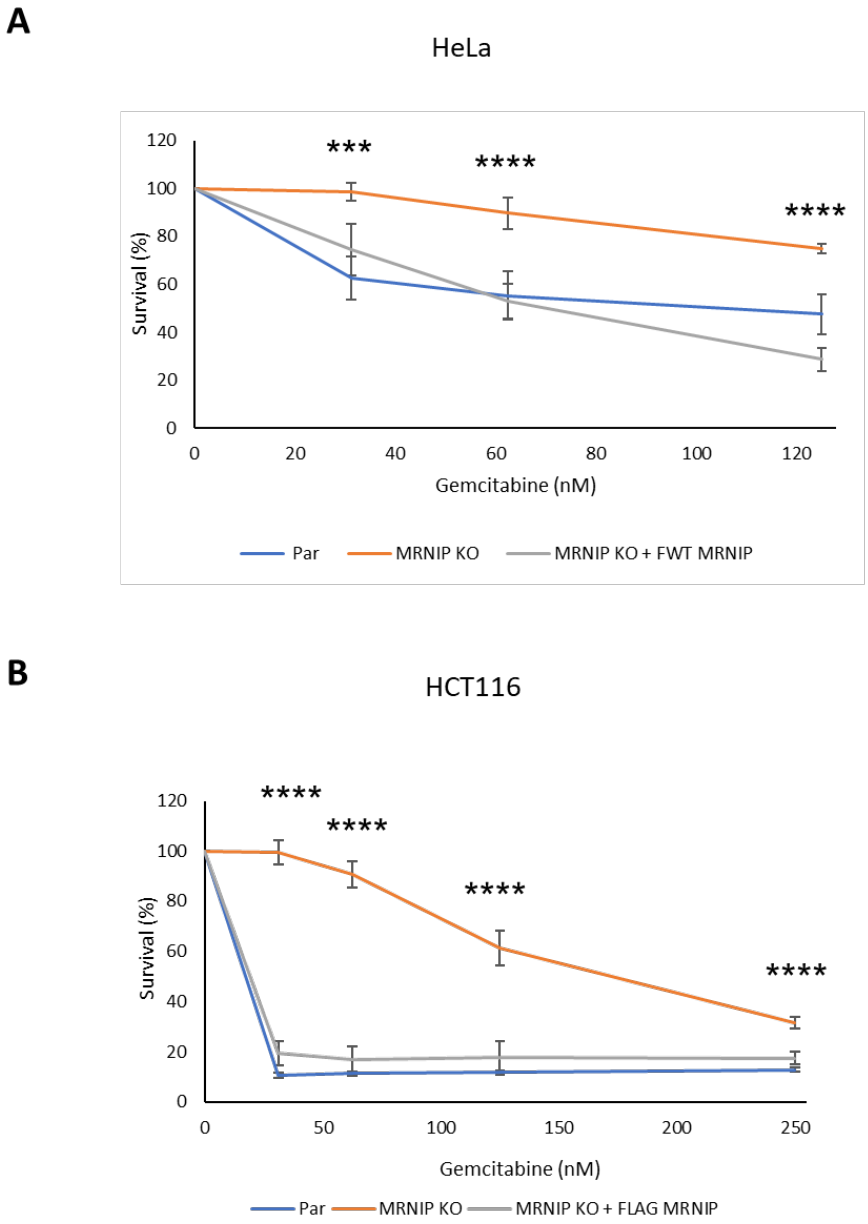

Figure 5.1 MRNIP KO derivative HeLa and HCT116 cells are resistant to Gemcitabine.

A) HeLa parental (Par), derivative MRNIP KO (MRNIP KO) and derivative MRNIP KO cells stably expressing FLAG-MRNIP (MRNIP KO + FLAG MRNIP). B) HCT116 parental, derivative MRNIP KO and derivative MRNIP KO cells stably expressing FLAG-MRNIP were treated with the indicated concentrations of Gemcitabine. After 96 hours, an MTT assay was performed, and results were normalised to untreated controls. Data represent the mean from three experiments (n=3), and errors displayed represent SD. Statistical significance was determined by two-way ANOVA with Tukey correction for multiple comparisons. ***P ≤0.001, ****P ≤ 0.0001.

Given that MRNIP KO cells are resistant to Gemcitabine, we next examined DNA damage levels in Gemcitabine treated HeLa MRNIP KO cells. We also employed MRNIP KO cells stably expressing doxycycline-inducible FLAG-tagged MRNIP, to ensure that any phenotype observed could specifically be rescued by reintroduction of MRNIP. We assessed the prevalence of γH2AX and 53BP1 foci via indirect immunofluorescence following treatment with 100nM of Gemcitabine for 4 and 24 hours. Cells were identified as foci-positive when they exhibited more than 5 foci. A statistically significant increase in both markers was observed in MRNIP KO cells compared to the parental line under unperturbed conditions and rescue of the phenotype was observed in cells re-expressing FLAG tagged MRNIP (Figure 5.2 A, B). Treatment with 100nM of Gemcitabine for 4 hours of parental and derivative MRNIP KO HCT116 cells did not cause a statistically significant increase of either marker and the phenotype was rescuable when re-expressing FLAG tagged MRNIP (Figure 5.2 A). Gemcitabine acts in S phase and the doubling time of HCT116 cells is 18 hours suggesting that the cells will not be in S phase within 4 hours therefore the treatment is not long enough to cause breaks. However, a longer treatment (24 hours) with the same Gemcitabine concentration led to a statistically significant increase in γH2AX in parental but not MRNIP KO cells. Rescue of the phenotype for both markers was observed in MRNIP KO cells re-expressing FLAG tagged MRNIP (Figure 5.2 B).

A

HCT116

4 hours

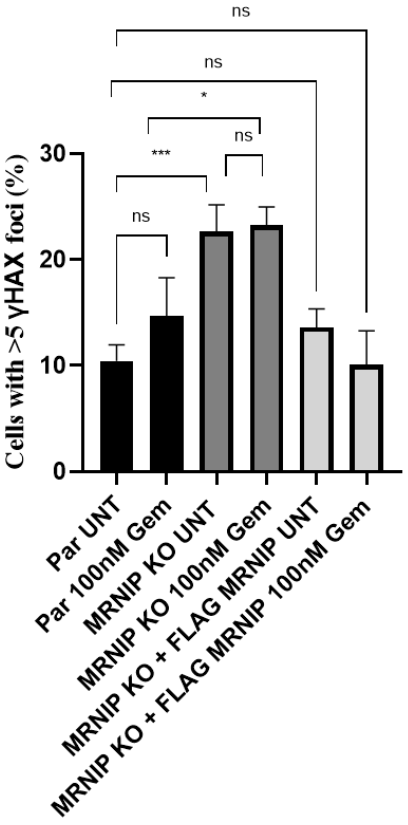

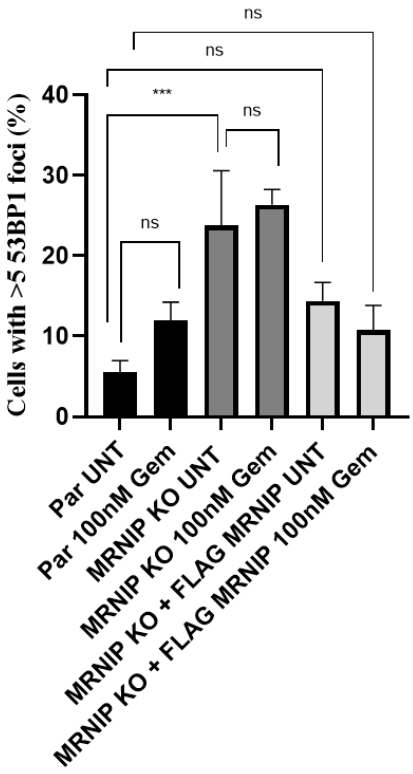

B

24 hours

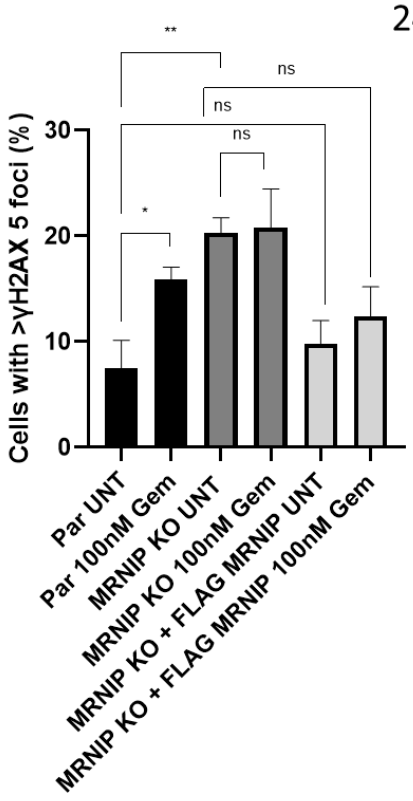

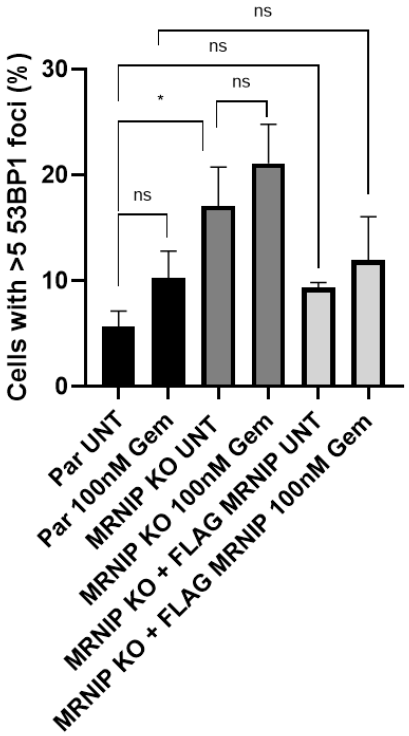

Figure 5.2 HCT116 cells but not derivative MRNIP KO cells exhibit increased frequency of DNA damage foci following Gemcitabine treatment after 24 hours.

A) Parental (Par) HCT116, derivative MRNIP KO (MRNIP KO) and MRNIP KO cells stably expressing FLAG-MRNIP (MRNIP KO + FLAG MRNIP) were treated with 100nM of Gemcitabine for 4 and B) 24 hours, fixed, stained with DNA damage markers γH2AX and 53BP1 and counterstained with DAPI. Cells with more than five γH2AX foci were scored as positive. Data represent the mean from three experiments (n=3) and errors displayed represent SD. Statistical significance was determined by two-way ANOVA with Tukey correction for multiple comparisons. ns: not statistical, *P≤0.05, **P ≤0.01, ***P ≤0.001.

We also assessed the prevalence of γH2AX and 53BP1 foci via indirect immunofluorescence following a higher dose of Gemcitabine (1μM) for 4 and 24 hours. No statistically significant increase in either marker was again observed in MRNIP KO cells while increase of 53BP1 foci only was seen in parental cells following a 4 hour of 1μM treatment of Gemcitabine (Figure 5.3 A). A longer treatment of the same dose of Gemcitabine did not result in an increase of either marker in MRNIP KO cells but it caused an increase in the 53BP1 foci in parental cells (Figure 5.3 B).

A

HCT116

4 hours

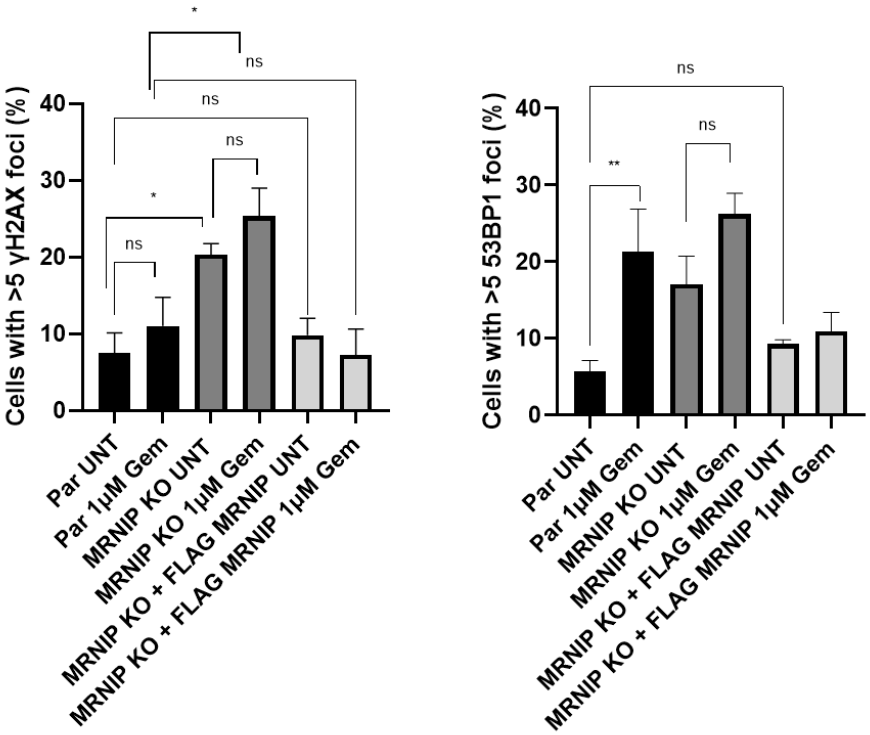

B

24 hours

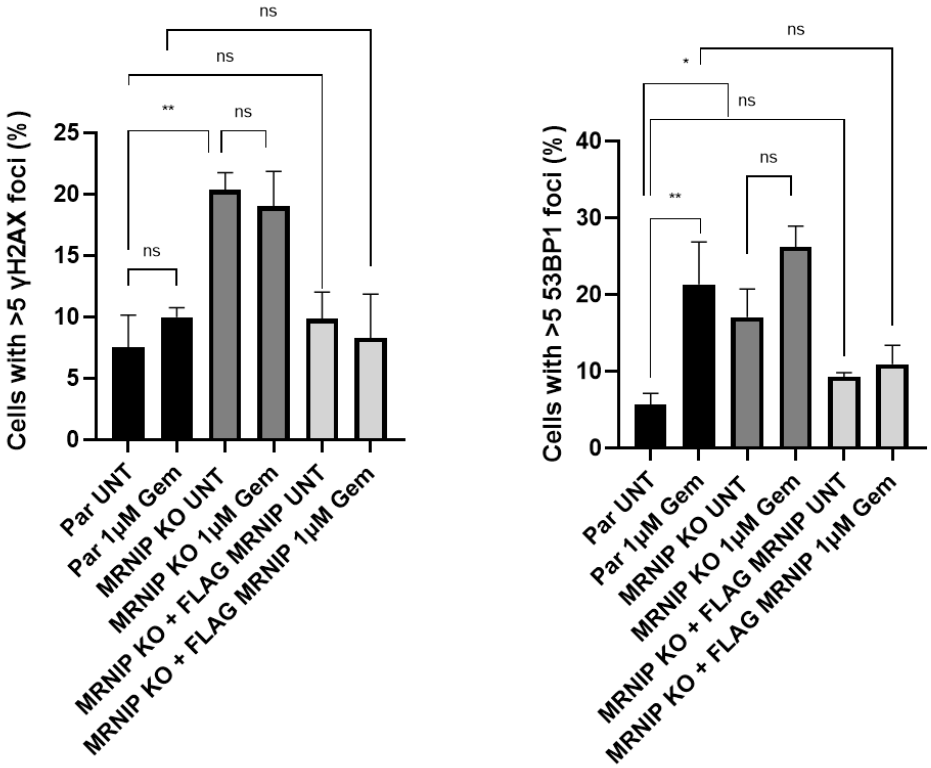

Figure 5.3 HCT116 cells but not derivative MRNIP KO cells exhibit increased frequency of DNA damage foci following Gemcitabine treatment after 24 hours.

A) Parental (Par) HCT116, derivative MRNIP KO (MRNIP KO) and MRNIP KO cells stably expressing FLAG-MRNIP (MRNIP KO + FLAG MRNIP) treated with 1μM of Gemcitabine for 4 and B) 24 hours, fixed, stained with DNA damage markers γH2AX and 53BP1 and counterstained with DAPI. Cells with more than five γH2AX foci were scored as positive. Data represent the mean from three experiments (n=3) and errors displayed represent SD. Statistical significance was determined by two-way ANOVA with Tukey correction for multiple comparisons.ns: not statistical, *P ≤0.05 **P ≤0.01.

These experiments suggest that MRNIP loss confers chemoresistance to Gemcitabine and limits further DNA damage in cells treated with Gemcitabine for 24 hours.

5.2 Alanine substitution of MRNIP at Ser 217 reverses MRNIP-mediated Gemcitabine sensitivity.

To assess the potential role of MRNIP post-translational modifications in the Gemcitabine response, we next assessed Gemcitabine sensitivity by performing MTT assays. Parental, derivative MRNIP KO, derivative MRNIP KO cells stably expressing tetracycline-inducible FLAG-tagged WT or mutant MRNIP were treated with a range of Gemcitabine concentrations. These stable cell lines express versions of MRNIP harbouring mutations of the potential phosphorylation sites Ser217 and Ser115, of two potential ubiquitination sites K58/129R, and of four predicted metal ion-coordinating cysteines C4A, as well as the Δ25 mutant. Again, MRNIP KO cells were resistant to Gemcitabine relative to parental cells, and cells stably expressing FLAG-tagged WT MRNIP exhibited sensitivity profiles similar to the parental line. Strikingly, expression of a Ser 217 alanine substitution mutant of MRNIP rescued Gemcitabine sensitivity in a MRNIP KO background, suggesting that Ser 217 phosphorylation is important for MRNIP function in this context (Figure 5.4 A). Expression of the C4A, K58/129R and Δ25 mutants in MRNIP KO cells led to Gemcitabine sensitivity profiles similar to the parental cells suggesting that these sites do not play an important role in MRNIP function in response to Gemcitabine treatment (Figure 5.4 A+B). In addition, no difference in drug sensitivity was observed between the mutants mimicking and inhibiting phosphorylation of MRNIP at Ser115, a phenomenon also observed after CPT treatment (Figure 5.4 C).

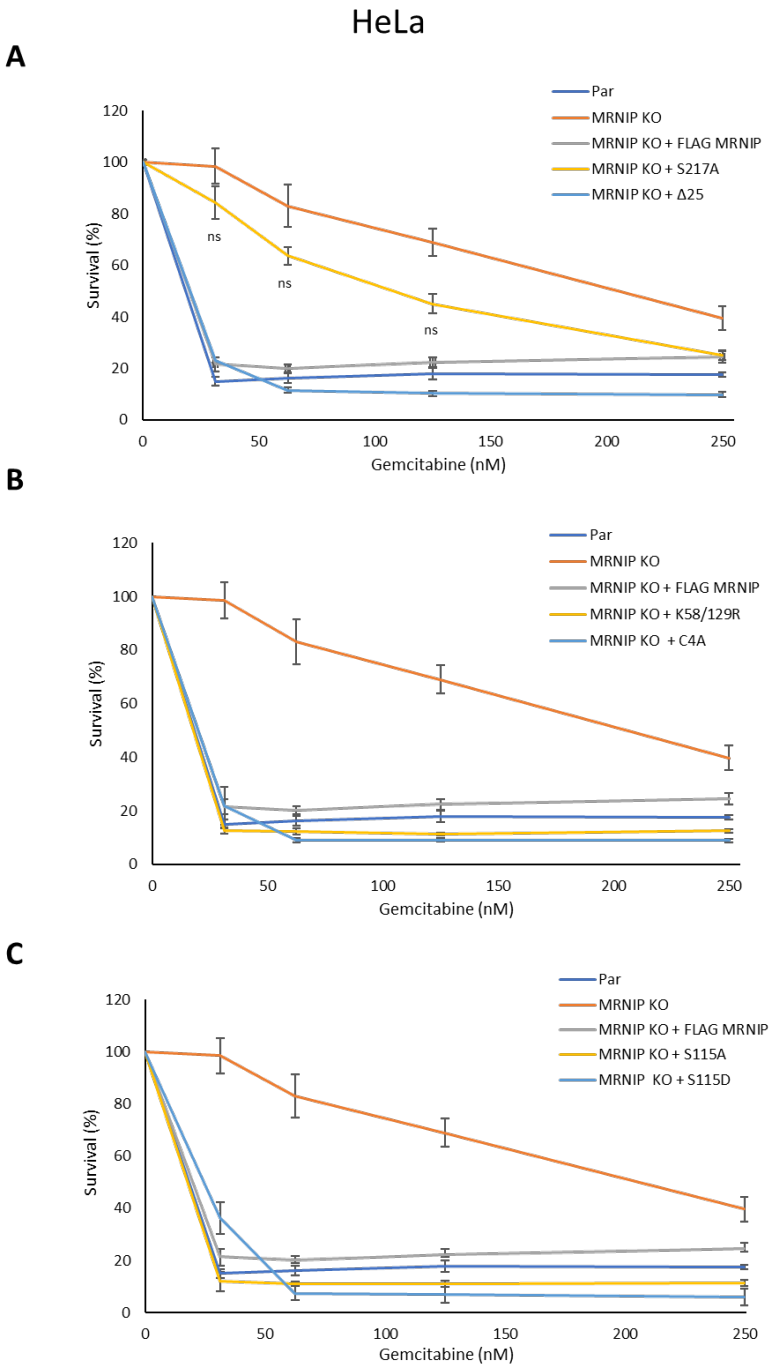

Figure 5.4 Ser 217 phosphorylation is important for MRNIP function for Gemcitabine sensitivity.

A) Parental (Par) HeLa, derivative MRNIP KO (MRNIP KO) cells, derivative MRNIP KO cells stably expressing FLAG MRNIP (MRNIP KO + FLAG MRNIP), and MRNIP KO cells expressing S217A and Δ25 MRNIP mutants, B) MRNIP KO cells expressing C4A and K58/129R double MRNIP mutants and C) MRNIP KO cells expressing alanine (S217A) or glutamic acid substitutions of Ser115 (S217D) were treated with the indicated concentrations of Gemcitabine. After 96 hours, an MTT assay was performed, and results were normalised to untreated controls. Data represent the mean from three experiments (n=3) and errors displayed represent SD. Statistical significance was determined by two-way ANOVA with Tukey correction for multiple comparisons. ns: not statistical.

5.3 MRNIP confers sensitivity to Gemcitabine and Cytarabine but resistance to Clofarabine and Fludarabine.

Given that HeLa and HCT116 MRNIP KO cells are resistant to the chain terminating nucleoside analogue Gemcitabine, we next assessed cell survival in these cells performing an MTT assay using different concentrations of a variety of nucleoside analogues including Cytarabine, Clofarabine and Fludarabine. HeLa MRNIP KO cells were resistant to Cytarabine (Figure 5.5 A) as well as Gemcitabine (Figure 5.5 B). However, HeLa MRNIP KO cells exhibited sensitivity to Clofarabine (Figure 5.5 C) and Fludarabine (Figure 5.5 D).

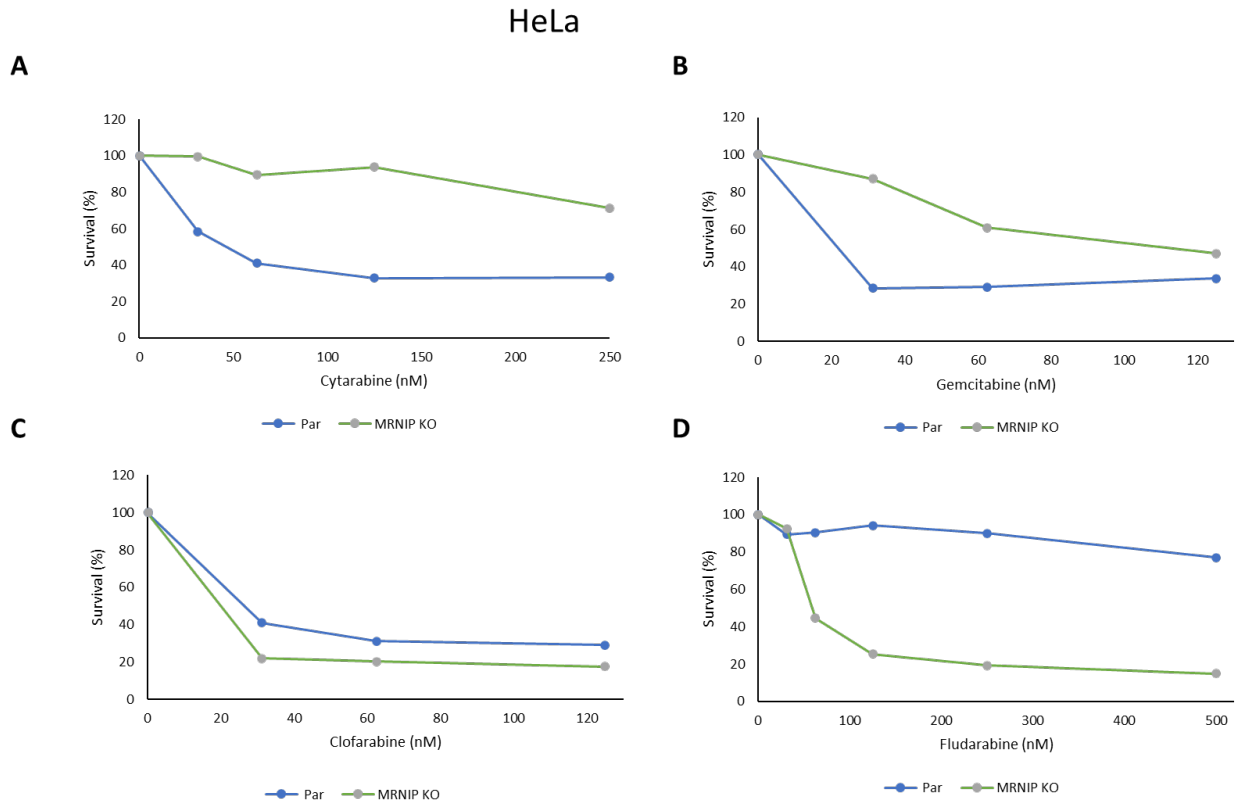

Figure 5.5 MRNIP KO HeLa cells are resistant to Gemcitabine and Cytarabine but sensitive to Clofarabine and Fludarabine.

Parental (Par) HeLa and derivative MRNIP KO (MRNIP KO) cells were treated with the indicated concentrations of A) Cytarabine, B) Gemcitabine, C) Clofarabine and D) Fludarabine. After 96 hours, an MTT assay was performed, and results were normalised to untreated controls. Data represent one experiment (n=1).

In addition, we examined cell survival following the same treatments in HCT116 cells and derivative MRNIP KO cells, performing an MTT as before. Again, we found that MRNIP KO cells were resistant to Cytarabine (Figure 5.6 A) and Gemcitabine (Figure 5.6 B) but were sensitive to Clofarabine (Figure 5.6 C) and Fludarabine (Figure 5.6 D). Although all nucleoside analogues share the same mode of activation i.e., after uptake they are triphosphorylated and incorporated into the DNA, mainly causing the block of DNA synthesis (but also many other effects), they differ in structure; Gemcitabine and Cytarabine are pyrimidine nucleoside analogues while Clofarabine and Fludarabine are purine nucleoside analogues. In addition, other factors may determine this varied response, such as differential incorporation of the nucleoside analogues by a primase or its removal by a polymerase or the extent of interference with nucleotide metabolism (see Discussion 7.1)

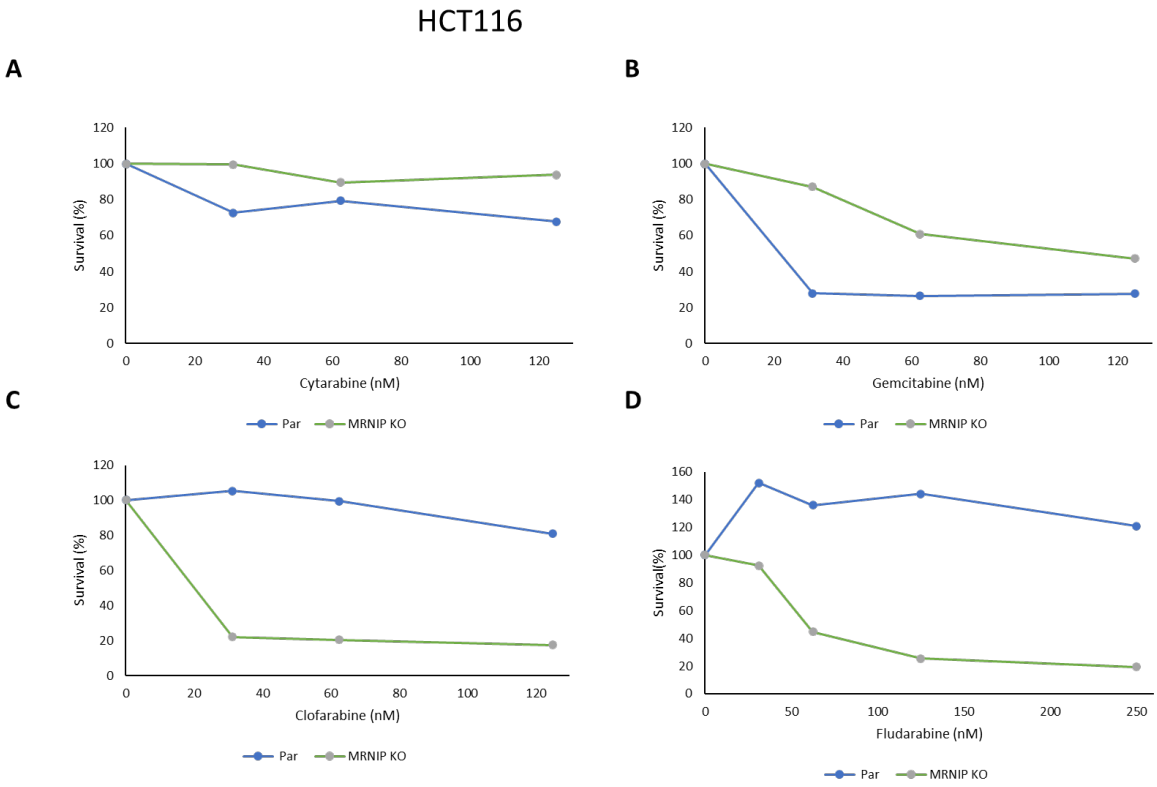

Figure 5.6 MRNIP KO HCT116 cells are resistant to Gemcitabine and Cytarabine but sensitive to Clofarabine and Fludarabine.

Parental (Par) HCT116 and derivative MRNIP KO (MRNIP KO) cells were treated with the indicated concentrations of A) Cytarabine, B) Gemcitabine, C) Clofarabine and D) Fludarabine. After 96 hours, an MTT assay was performed, and results were normalised to untreated controls. Data represent one experiment (n=1).

5.4 The role of MRNIP in fork degradation in cells treated with Gemcitabine.

Given that HeLa cells are sensitive to Gemcitabine treatment, we next examined nascent DNA degradation in HeLa cells by performing DNA fibre assays based on sequential CldU and IdU labelling followed by a 4 hour HU (3mM) or Gemcitabine (1μM) treatments, as tested before (Figure 5.7 A). Representative images of DNA fibres for each condition are shown in (Figure 5.7 B). Interestingly, nascent DNA was deprotected in parental HeLa cells following Gemcitabine but not HU treatments (Figure 5.7 C). The same phenotype was also observed in U2OS cells (Figure 5.7 D).

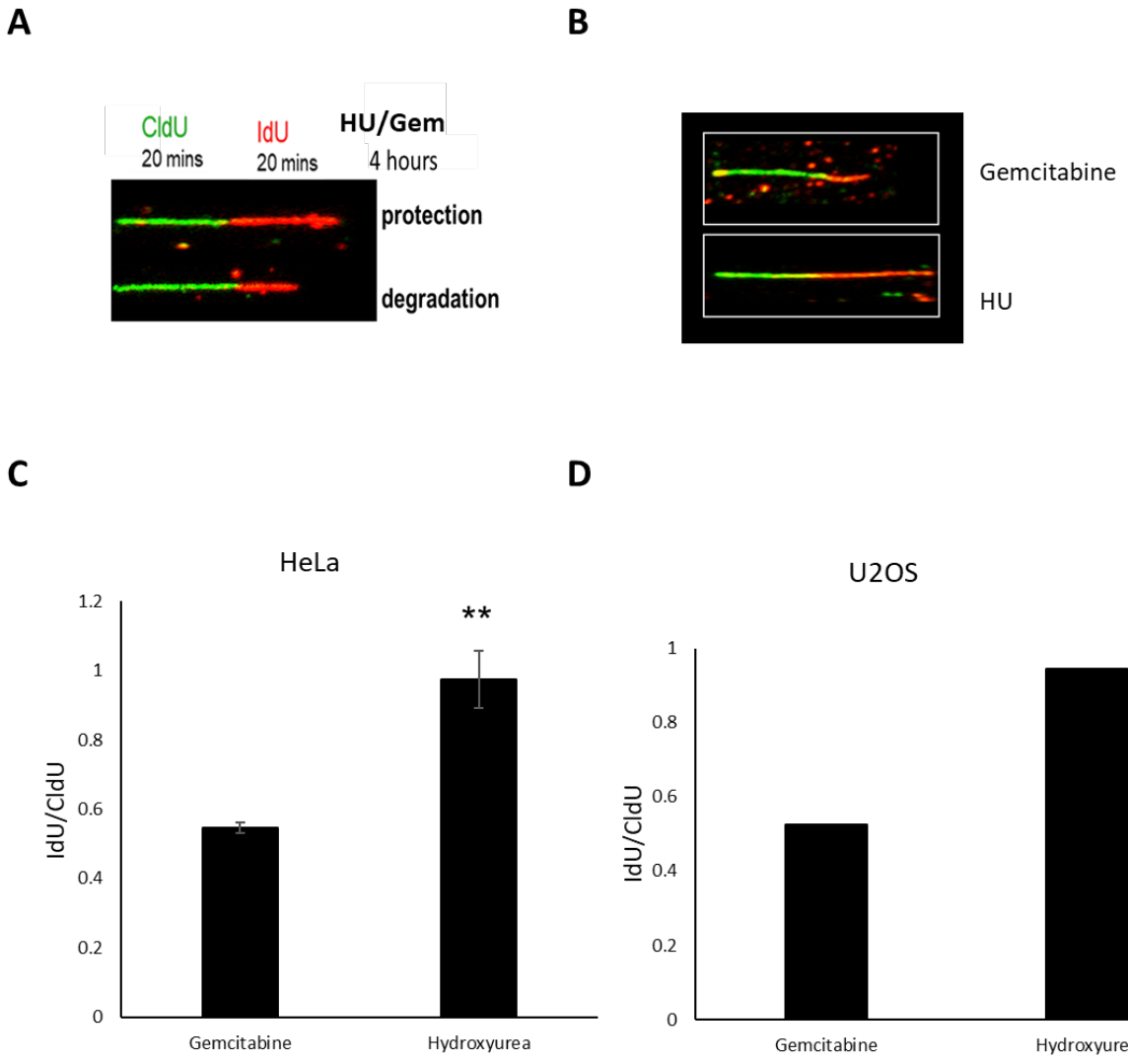

Figure 5.7 Gemcitabine causes nascent DNA degradation in HeLa and U2OS cells.

A) HeLa and U2OS cells were treated with 1μM Gemcitabine or 3mM HU for 4 hours prior to labelling with CldU and IdU for 20 min each. B) Representative examples of DNA fibres at indicated conditions. Fork degradation was assessed via the IdU:CldU tract length ratio in C) HeLa and D) U2OS cells. At least 200 DNA fibres were counted per condition. Treatment with HU is the control sample as the degradation phenotype has already been established previously in the laboratory. Data from HeLa cells represent the mean from three experiments (n=3) and error bars displayed represent SD. Statistical significance was determined by one-way ANOVA with Tukey correction for multiple comparisons **P ≤ 0.01. Data from U2OS cells represent one experiment (n=1).

This is rather atypical, in that replication tract shortening is usually observed in response to other agents only after loss of function of an important protective factor. This finding suggests that a nucleolytic event, or a series of events occurs during the Gemcitabine response, even in genetically unperturbed conditions. We conducted some follow up (below) to try gain mechanistic insight, although this avenue of study requires significant further work, which is beyond the scope of my work here. In addition, it would be interesting to examine in the future DNA degradation in the same cell lines followed by Clofarabine and Fludarabine treatments.

Spurred on by this finding, we next aimed to identify the nuclease responsible for nascent DNA degradation after Gemcitabine treatment. We used siRNAs to deplete various nucleases including DNA2, MUS81 and MRE11 for 48 hours and then performed DNA fibre assays after 4 hours of high-dose Gemcitabine treatment to initiate both chain termination and dNTP pool perturbation (Figure 5.8 A). Knockdown of each nuclease was confirmed by western blotting (Figure 5.8 B). Surprisingly, our data suggested that the main nucleases DNA2, MRE11 and MUS81 do not seem to drive Gemcitabine-induced nascent DNA degradation (Figure 5.8 C). However, the experiment was poorly controlled as we did not include MRNIP or BRCA2 KO HeLa cells treated with HU, which would confirm whether depletion of each nuclease was efficient enough to affect function at these sites.

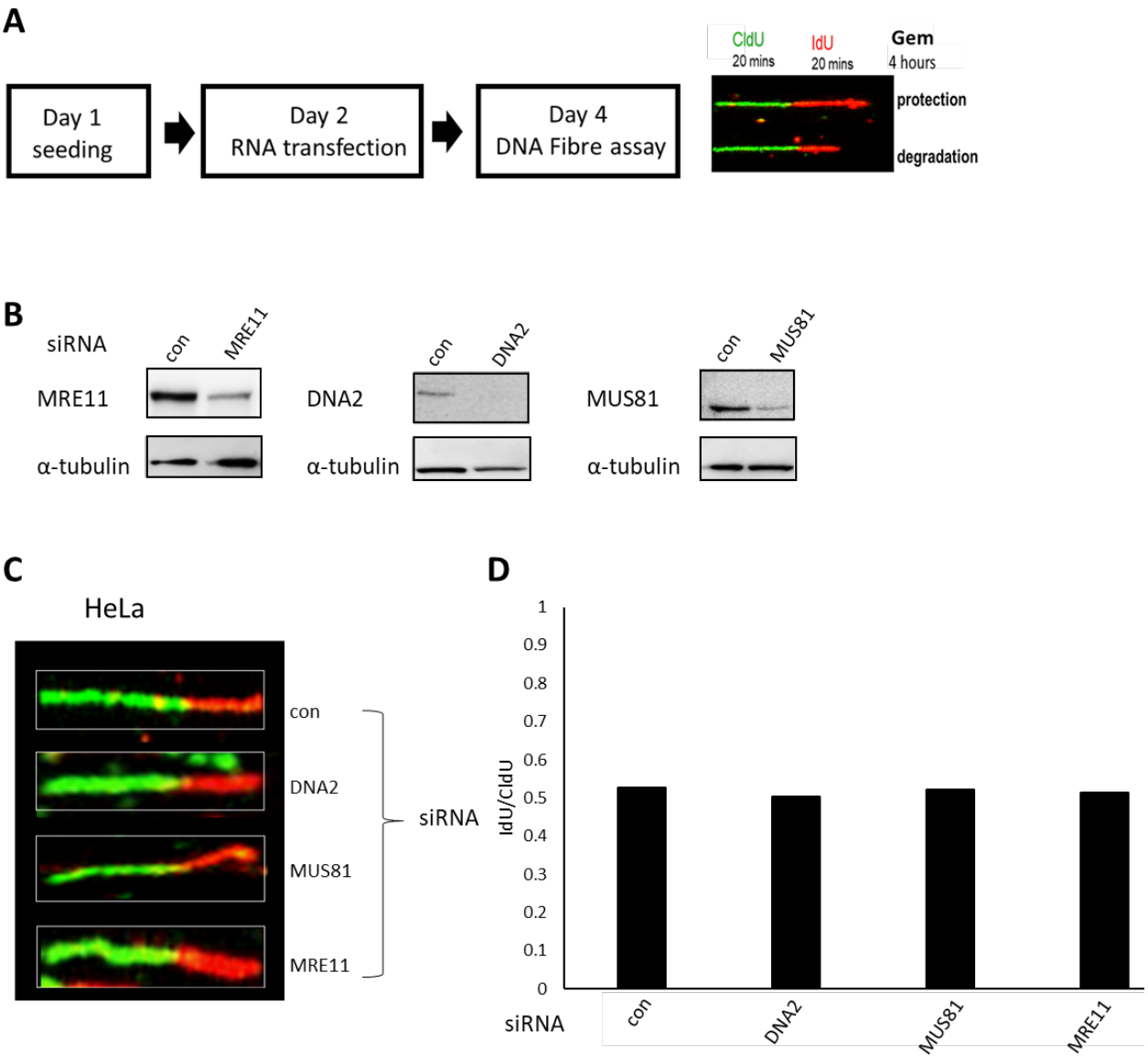

Figure 5.8 DNA2, MRE11 and MUS81 do not contribute to fork degradation following Gemcitabine treatment.

A) Schematic representation of the experimental set up. HeLa cells were transfected with a non-targeting control siRNA (con siRNA), or siRNA targeting DNA2, MUS81 and MRE11 nucleases for 48 hours and treated with 1μM Gemcitabine for 4 hours prior to labelling with CldU for 20 min and IdU for another 20 min. B) Confirmation of MRE11 UTR siRNA knockdown. Whole cell extracts from HeLa cells were transfected with a non-targeting control siRNA (con siRNA), or siRNA targeting DNA2, MUS81 and MRE11 nucleases for 48 hours, lysed and blotted for the relevant antibodies. C) Representative examples of DNA fibres at indicated conditions. D) Fork degradation was assessed via the IdU:CldU tract length ratio. Data represent one experiment (n=1). At least 200 fibres were counted for each condition.

Based on the finding that HeLa and U2OS parental cell lines exhibit deprotected forks after Gemcitabine treatment, we next examined DNA degradation in HeLa MRNIP KO cells by performing DNA fibre assays as previously done following Gemcitabine treatment for 4 hours (Figure 5.9 A). Representative images of DNA fibres for each condition are shown in (Figure 5.9 B). Interestingly, HeLa MRNIP KO cells exhibited a ratio of IdU/CldU of approximately 1 (Figure 5.9 C).

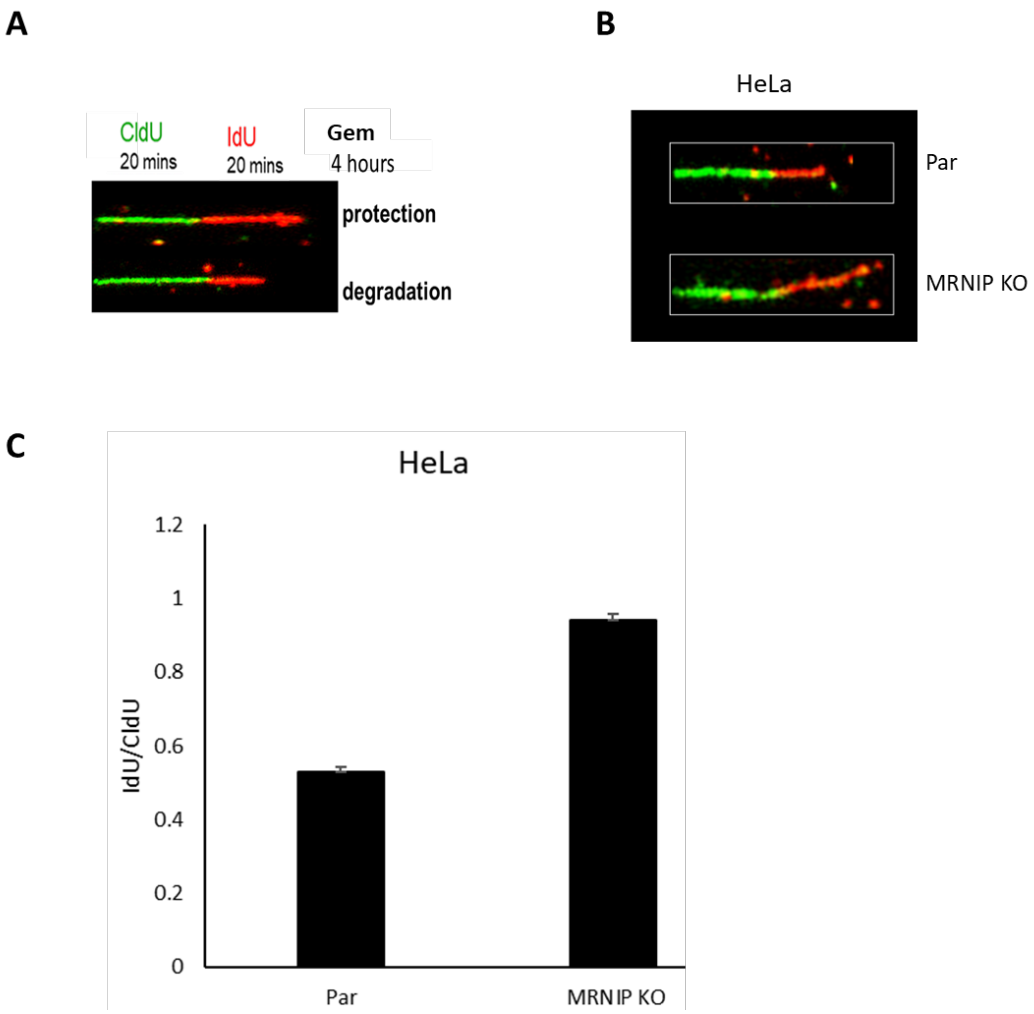

Figure 5.9 HeLa KO cells exhibit protected forks following Gemcitabine treatment.

A) HeLa parental (Par) and derivative MRNIP KO (MRNIP KO) cells were treated with 1μM Gemcitabine for 4 hours prior to labelling with CldU and IdU for 20 min. B) Representative examples of DNA fibres at indicated conditions. C) Fork degradation was assessed via the IdU:CldU tract length ratio. Data represent the mean of two experiments (n=2). At least 200 fibres were counted for each condition.

5.5 MRNIP levels in ovarian and glioblastoma cell lines.

Given that HeLa and HCT116 MRNIP KO cells are resistant to Gemcitabine, we next aimed to examine the role of MRNIP in a variety of cell lines challenged with other chemotherapies. Our laboratory recently found that MRNIP, similar to BRCA2, suppresses daughter strand gaps (DSGs) in treated cells with cisplatin and PARP inhibitors. The latter have revolutionised the treatment of patients with BRCA-deficient ovarian epithelial tumours [399]. MRNIP is reported to be under expressed in approximately 6% of ovarian cancers (COSMIC). For this reason, we tested the expression of MRNIP in a variety of ovarian (OC) and glioblastoma cell lines by western blotting. Our findings indicate that MRNIP is widely expressed in multiple cancer types (Figure 5.10, B C, D). However, MRNIP is notably undetectable in a subset of High-Grade Ovarian Serous Adenocarcinoma cell lines including UWB1-289 and OVCAR-3 (Figure 5.10 A, B), and in glioblastoma U138 cells (Figure 5.10 C).

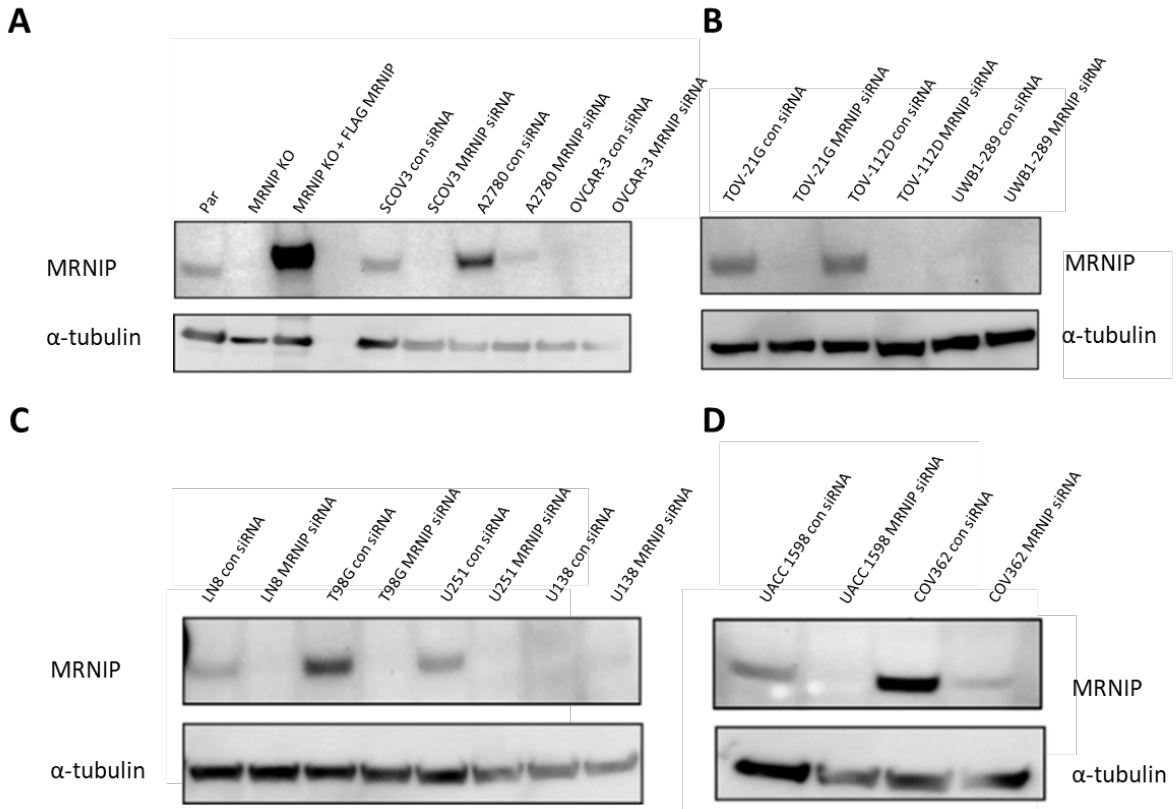

Figure 5.10 MRNIP expression in ovarian and glioblastoma cells.

A) Whole cell extracts from parental (Par) HeLa, derivative MRNIP KO (MRNIP KO) and derivative MRNIP KO stably expressing FLAG-tagged MRNIP (MRNIP KO + FLAG MRNIP), SCOV3, A2780, OVCAR-3 ovarian cell lines, B) TOV-21G, TOV-112D, UWB1-289 ovarian cell lines C) LN8, T98G, U251, U138 glioblastoma cell lines and D) UACC1598, COV362 ovarian cell lines were transfected with non-targeting control siRNA (con siRNA) or siRNA targeting MRNIP (MRNIP siRNA) for 48 hours. Cell lysates were then resolved by western blotting and probed for MRNIP and α-tubulin as a loading control.

We selected A2780, one of the many cell lines strongly expressing MRNIP as well as two cell lines, UWB1-289 and OVCAR-3, that did not seem to express MRNIP (Figure 5.10 A and B) to measure MRNIP mRNA levels via qRT-PCR. We found that MRNIP mRNA levels were lower in UWB1-289 and OVCAR-3 compared to A2780 (Figure 5.11 A). In addition, we tested MRNIP mRNA levels in HeLa and U2OS cells, and in A2780 and OVCAR-3 cells which were depleted of MRNIP. We found that A2780 was the cell line with the highest expression of MRNIP mRNA, while HeLa cells contained the lowest (Figure 5.11 B). These results also verified the specificity of the MRNIP probe, and the efficacy of the siRNA used to target MRNIP mRNA.

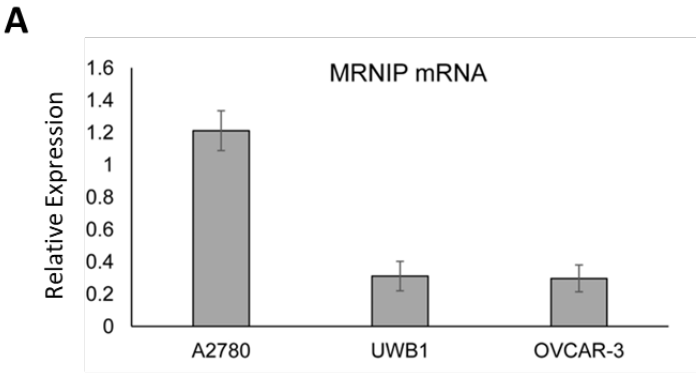

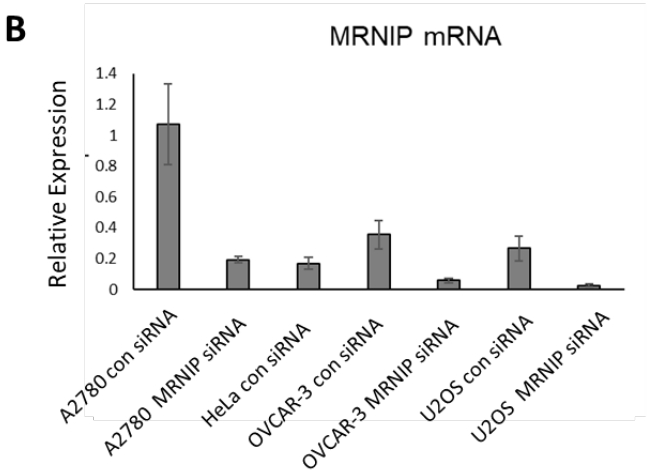

Figure 5.11 Relative mRNA expression of MRNIP.

A) RNA was isolated from A2780, OVCAR-3 and UWB1-289 cells, and reverse transcribed using oligo (dT) primers. qRT-PCR was performed using probes targeting MRNIP, and Ct values were normalised to those obtained from a reference probe. B) HeLa, A2780, OVCAR-3 and U2OS cells were transfected with a non-targeting control siRNA (con siRNA) or an siRNA targeting MRNIP (MRNIP siRNA). Total RNA was isolated, and qRT-PCR was performed as in (A). Experiments were performed in triplicates, and error bars shown represent the standard error of the mean. Experiment was performed once (n=1).

5.6 The role of MRNIP in response to a variety of chemotherapeutic agents in A2780 and COV362 OC lines.

Given that MRNIP is well-expressed in A2780 and COV362 cells, we next investigated the role of MRNIP in these lines following treatment with different classes of genotoxic drugs; the RNR inhibitor HU, the DNA cross-linkers MMC and Cisplatin, the DNA-PK inhibitor NU7441 and the chain terminator Gemcitabine. Depletion of MRNIP in A2780 cells resulted in sensitivity to HU (Figure 5.12 A), NU7441 (Figure 5.12 D) and Cisplatin (Figure 5.12 E) but resistance to Gemcitabine (Figure 5.12 C). This latter finding is consistent with the Gemcitabine resistance observed in MRNIP KO HeLa and HCT116 cells. In contrast, MRNIP-depleted A2780 cells were not sensitive to MMC at the concentrations used (Figure 5.12 B).

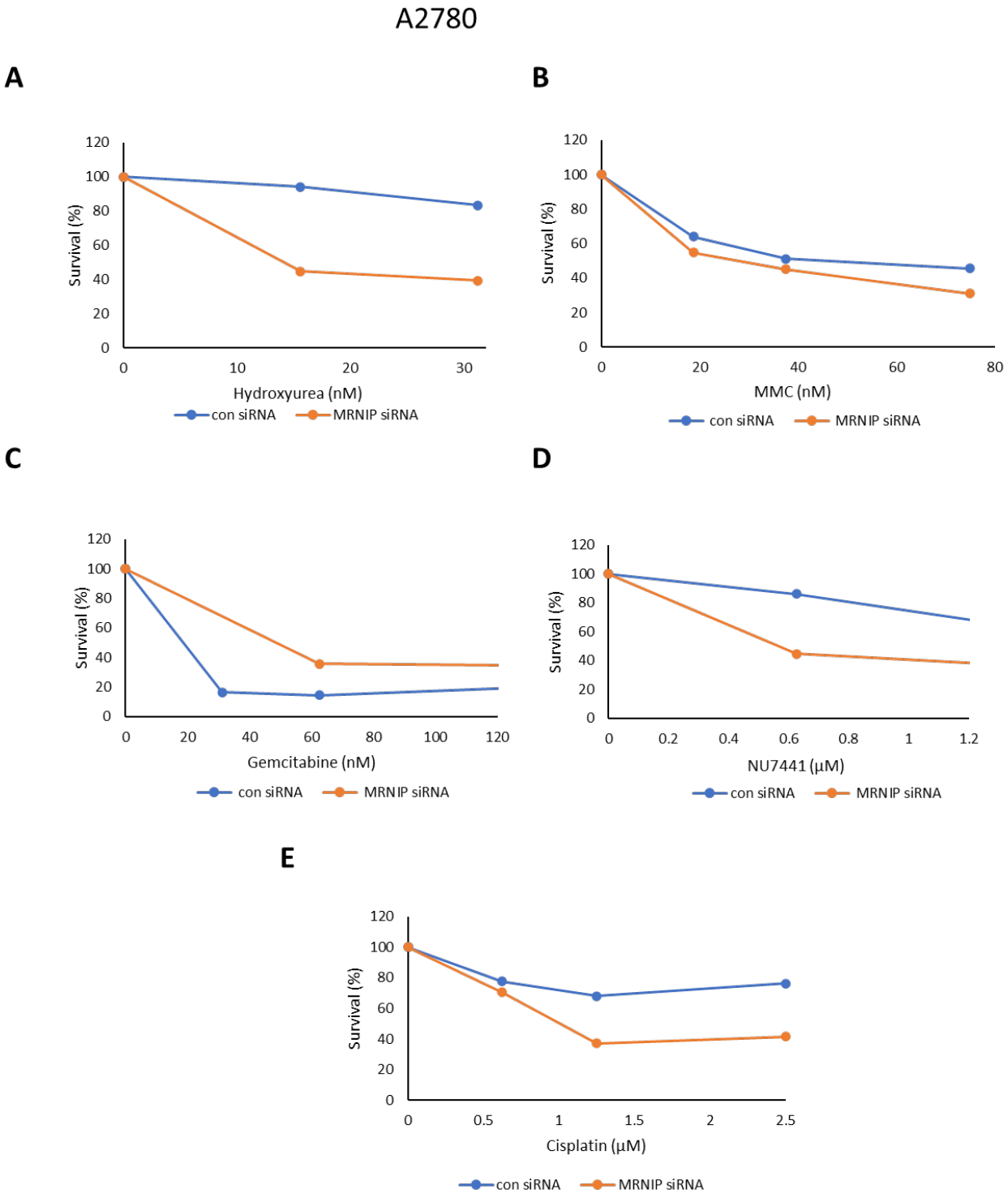

Figure 5.12 MRNIP confers resistance to HU, NU7441 and Cisplatin but sensitivity to Gemcitabine in A2780 cells.

A2780 cells were transfected with a non-targeting control siRNA (con siRNA) or an siRNA that targets MRNIP (MRNIP siRNA) for 48 hours and treated with different concentrations of A) HU, B) MMC, C) Gemcitabine, D) NU7441 and E) Cisplatin. After 96 hours, an MTT assay was performed, and results were normalised to untreated controls. Data represent one repeat (n=1).

However, MRNIP depletion in COV362 cells caused sensitivity to both HU (Figure 5.13 A) and MMC (Figure 5.13 B). In contrast to A2780 cells, MRNIP-depleted COV362 cells exhibited resistance to NU7441 (Figure 5.13 C).

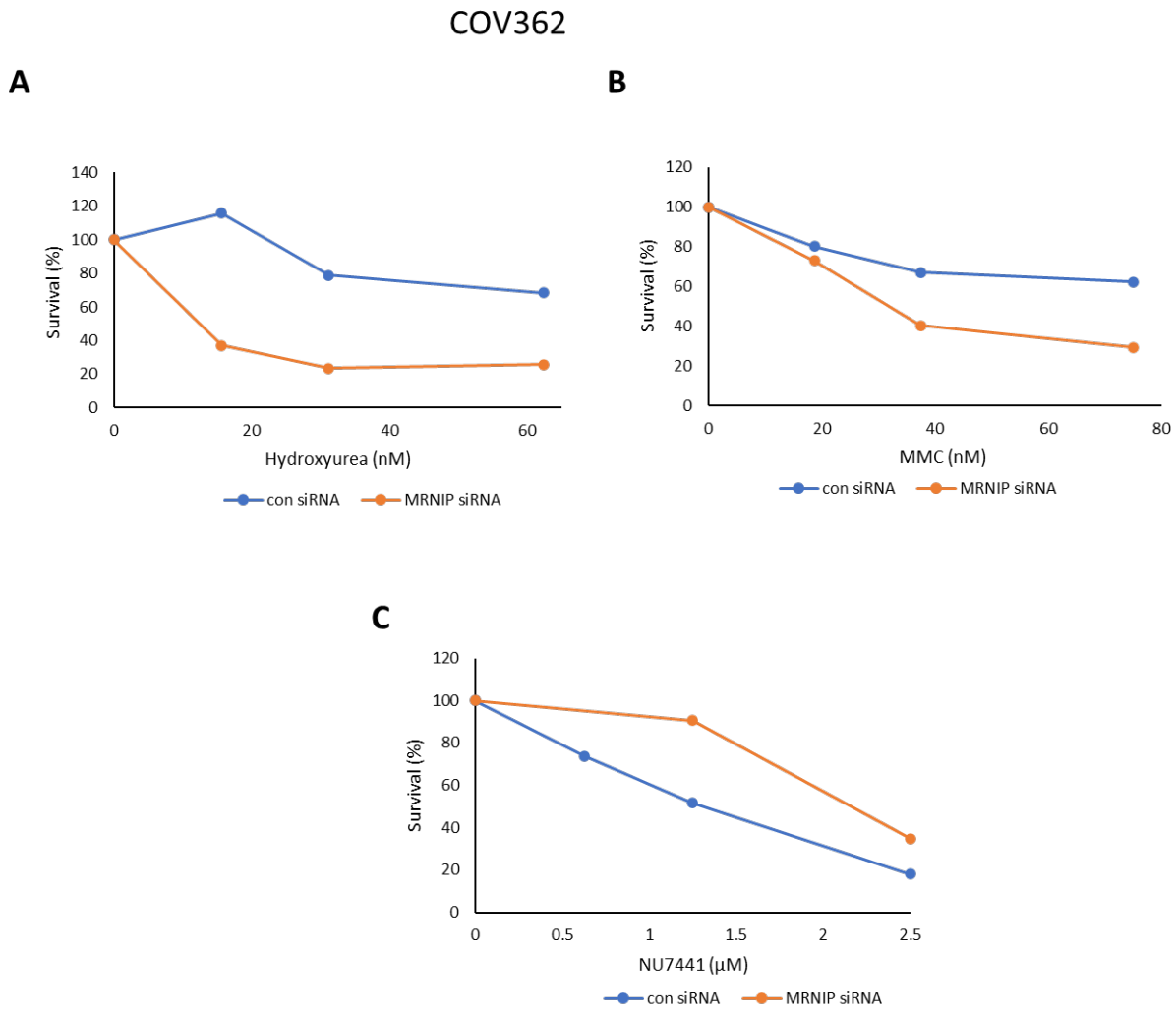

Figure 5.13 MRNIP confers resistance to HU and MMC but sensitivity to NU7441 in COV362 cells.

COV362 cells were transfected with a non-targeting control siRNA (con siRNA) or an siRNA that targets MRNIP (MRNIP siRNA) for 48 hours and treated with different concentrations of A) HU, B) MMC and C) NU7441. After 96 hours, an MTT assay was performed, and results were normalised to untreated controls. Data represent one repeat (n=1).

In conclusion, this work demonstrates that MRNIP loss or depletion confers Gemcitabine resistance in a variety of cell lines, possibly by limiting nucleolytic resection of the stalled fork (Figure 5.9). Our data also suggest a functional role for Ser217 in mediating Gemcitabine sensitivity (Figure 5.4). These findings will be the subject of ongoing work in the Staples laboratory.

CHAPTER VI

6 Identification of MRNIP interactors.

According to previous work from Staples laboratory, MRNIP physically interacts with and regulates MRE11 [384] and given the apparent roles of MRNIP in the replication stress response, we aimed to identify replication- stress specific MRNIP interactors that might shed additional mechanistic light on MRNIP function.

6.1 A functional interaction between MRNIP and CDK4.

We used the modified immortalized human embryonic kidney Flp-In TREX HEK 293 cells to generate a stable cell line that expresses C-terminally FLAG-tagged MRNIP. We confirmed MRNIP-FLAG overexpression by western blotting. Tubulin was used as a loading control (Figure 6.1).

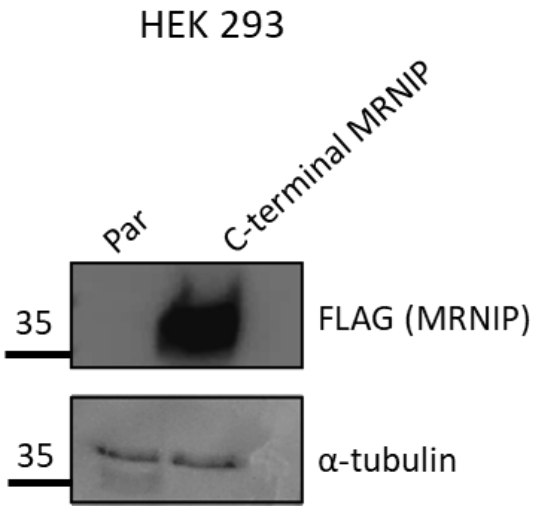

Figure 6.1 Expression of MRNIP in HEK 293 cell line.

Whole cell extracts form Flp-In TREX HEK 293 parental (Par) and a derivative line expressing C-terminally FLAG-tagged MRNIP (C-terminal MRNIP) were prepared, and lysates were used for western blotting to probe for FLAG antibody and α-tubulin as a loading control.

In order to attempt to identify novel MRNIP interactions we treated 10x150mm plates of MRNIP-FLAG HEK 293 cells per sample with 3mM HU for 4 hours or 1μM CPT for 2 hours, and performed large-scale immunoprecipitations using FLAG M2 beads, performing elution of FLAG immune complexes via competition with a 3X FLAG peptide. Parental HEK 293 cells served as a control (Figure 6.2 A). We tested phosphorylation of the kinase CHK1 at Ser345 in input samples to demonstrate successful treatment with CPT and HU, and western blotting confirmed that CHK1 phosphorylation was markedly elevated following both treatments. Total CHK1 was used as a loading control (Figure 6.2 B). These samples were then analysed by mass spectrometry by Dr Kate Heesom of Bristol University proteomics facility.

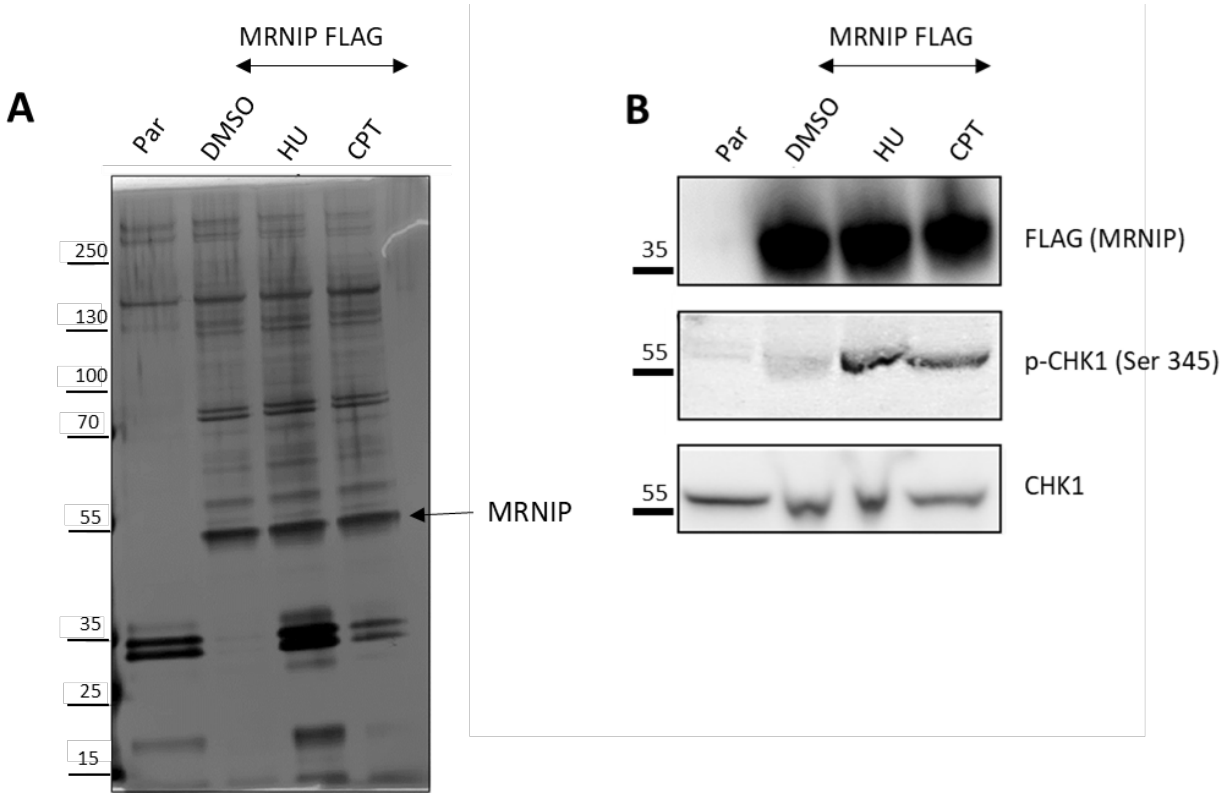

Figure 6.2 MRNIP interactors from Mass spectrometry analysis.

A) Silver staining of HEK 293 parental (Par) cells and a derivative line expressing C-terminally FLAG-tagged MRNIP (MRNIP FLAG). Cells were mock treated (DMSO) or treated with 3mM HU (HU) for 4 hours and 1μM CPT (CPT) for 2 hours, lysed and immunoprecipitated with FLAG antibody. B) Eluates were resolved by SDS-PAGE and probed by the indicated antibodies.

Mass spectrometry findings revealed three top hits in addition to the MRN complex: CDK4, KEAP1 and DYNNL1. To attempt to confirm these putative interactions, we then performed a repeat immunoprecipitation in HEK 293 cells, and in HEK 293 cells expressing C-terminally FLAG-tagged MRNIP treated with 3mM HU for 4 hours and 1μM CPT for 2 hours and probed with the relevant antibodies. Western blotting confirmed that only CDK4 interacts with MRNIP – no bands were observed in eluates from FLAG immune complexes for either DYNNL1 or KEAP1. As expected, we also observed an interaction between MRNIP and MRE11 (Figure 6.3). Reciprocal immunoprecipitation in HEK 293 and HEK 293 cells expressing C-terminally FLAG-tagged MRNIP probing for CDK4 could have also been performed to confirm interaction of MRNIP with CDK4, but time was limited.

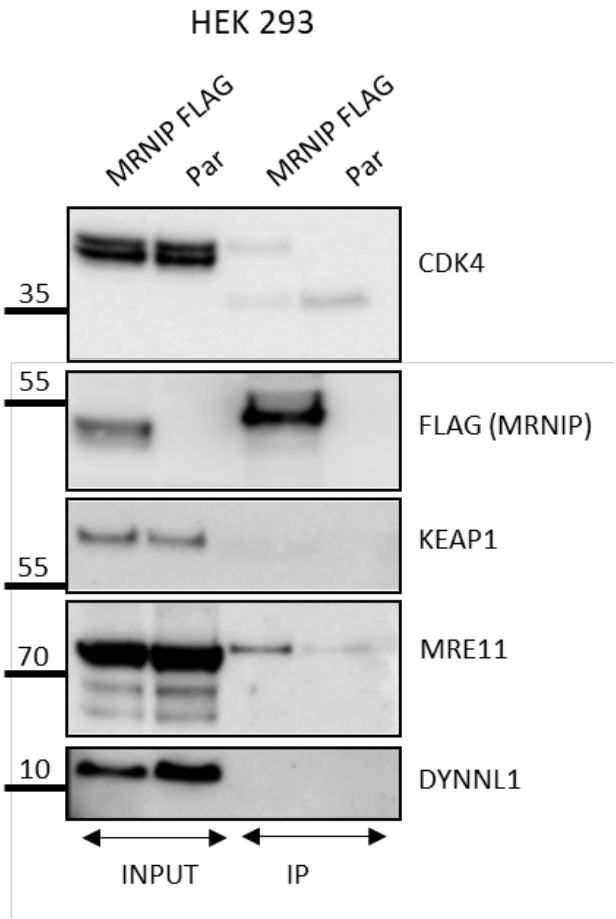

Figure 6.3 CDK4 interacts with MRNIP.

HEK 293 parental (Par) cells and HEK 293 cells expressing C-terminally FLAG-tagged MRNIP (MRNIP FLAG) were lysed, and the extracts were immunoprecipitated with FLAG antibody conjugated to agarose beads. Eluates were resolved by SDS-PAGE and probed with the indicative antibodies.

6.2 CDK4 levels are elevated in MRNIP KO cells.

Given that CDK4 (discussed in section 1.3 of the introduction) likely interacts with MRNIP, our next goal was to assess the levels of CDK4 in HeLa and HCT116 cells in which MRNIP was either knocked out via CRISPR-Cas9 or depleted via siRNA. MRNIP KO cells stably expressing FLAG-tagged MRNIP were included to test whether any alterations in CDK4 levels in MRNIP KO cells could be rescued by restoration of MRNIP expression. Consistently (based on three independent repeats), CDK4 levels were increased in the absence of MRNIP (by CRISPR (Figure 6.4 A) and siRNA (Figure 6.4 B) in both cell lines compared to the control. This could potentially be because an increased number of MRNIP KO cells were observed in G1 phase (personal communication Dr. Staples), though this enrichment was slight and is unlikely to be sufficient to lead to the alterations observed. The latter observation needs to be repeated. In addition, normal levels of CDK4 were restored in MRNIP KO cells expressing FLAG-tagged MRNIP (Figure 6.4 A, B).

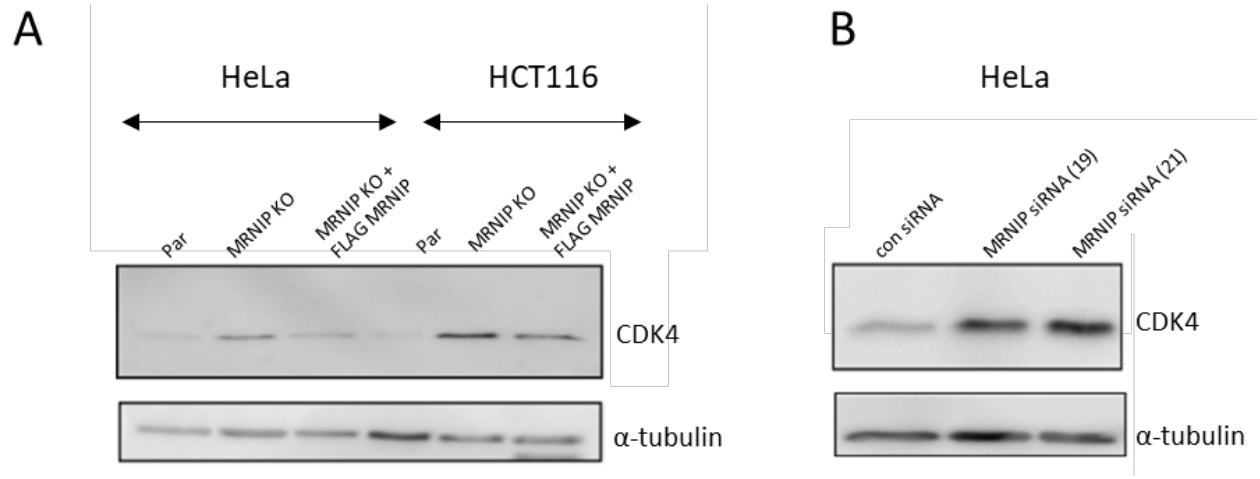

Figure 6.4 CDK4 levels in HeLa and HCT116 cell lines.

A) Whole cell extracts from HeLa and HCT116 parental (Par), derivative MRNIP KO (MRNIP KO), and MRNIP KO cell stably expressing FLAG-tagged MRNIP (MRNIP KO + FLAG MRNIP) were prepared, and lysates were used for western blotting to prob for CDK4 and α-tubulin as a loading control. Experiment was conducted four times (n=4). B) HeLa cells were transfected with non-targeting control siRNA (con siRNA) or with two different siRNA targeting MRNIP [MRNIP siRNA (19) and (21)] for 48 hours, lysed and blotted for CDK4 and α-tubulin as a loading control. Experiment was conducted three times (n=3).

Based on the observation that CDK4 expression was increased in MRNIP KO cells, we next investigated whether MRNIP regulates CDK4 stability. We therefore treated parental HeLa and HCT116 cells and derivative MRNIP KO cells with the protein synthesis inhibitor cycloheximide (CHX) for up to 8 hours, then lysed the cells and blotted for CDK4. In parental cells, a steady decrease in CDK4 levels was observed over the time course. In contrast, CDK4 remained stable in MRNIP KO cells even after 8 hours of CHX treatment. CDK4 was degraded by 70% (Figure 6.5 A) and 40% (Figure 6.5 B*)* in parental HeLa and HCT116 cells respectively by the end point of the treatment according to protein quantification by ImageJ. The differences observed in the extent of degradation might be cell type specific.

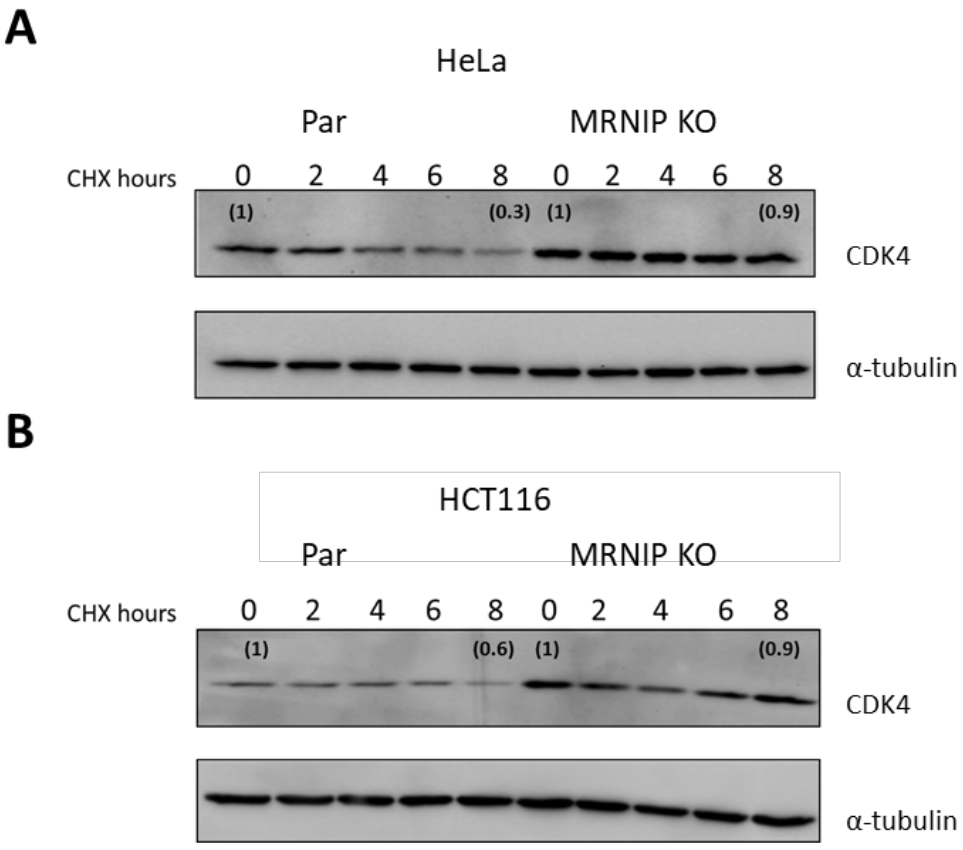

Figure 6.5 CDK4 is degraded in HeLa and HCT116 parental but not derivative MRNIP KO cell lines.

Whole cell extracts from A) HeLa and B) HCT116 parental (Par) and derivative MRNIP KO (MRNIP KO) cells were treated with 30 µg/ml CHX for the indicated hours, lysed, and probed for CDK4 and α-tubulin as a loading control. Numbers in brackets indicate the relative levels of proteins as determined via ImageJ analysis.

We then investigated whether CDK4 levels in HeLa MRNIP KO cells change throughout the cell cycle. MRNIP KO cells were treated with thymidine (double thymidine block), nocodazole and lovastatin to arrest cells in S, G2/M and G1 phases of the cell cycle respectively, then were lysed and blotted for CDK4. The levels of CDK4 in HeLa MRNIP KO cells remained unchanged throughout the cell cycle. Cyclins A and E were increased in cells treated with Lovastatin, suggesting that these treatments had been to some degree effective *(Figure 6.6).* Unfortunately, we were unable to confirm the efficacy of the other treatments using Fluorescence-activated Cell Sorting (FACS) analysis due to technical problems with our flow cytometer. We also examined CDK4 levels only in MRNIP KO cells where CDK4 levels were elevated, and we did not use parental cells as a control.

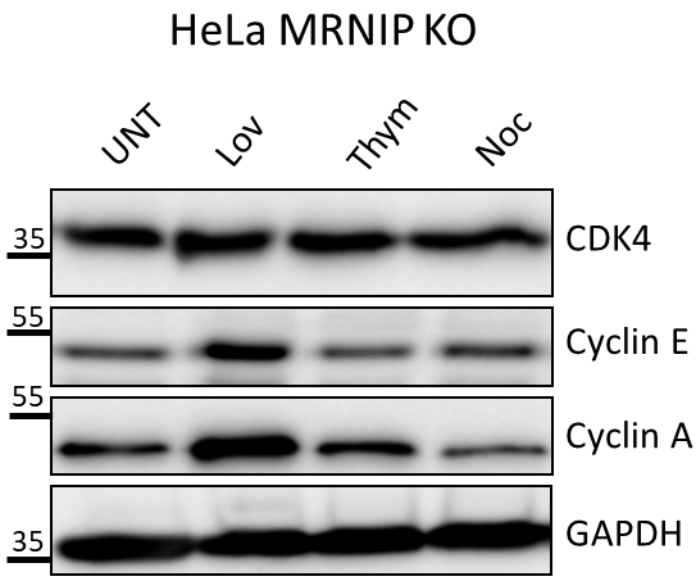

Figure 6.6 CDK4 levels remain unchanged throughout the cell cycle in HeLa MRNIP KO cells.

Whole cell extracts from HeLa MRNIP KO cells were mock treated (UNT) or treated with 2mM thymidine (Thym) for 16 hours, washed and treated again for another 14 hours (double block), 40μM Lovastatin (Lov) overnight and 30mM Nocadazole (Noc) overnight to arrest cells in S, G2/M and G1 phases respectively, lysed and blotted for CDK4, Cyclins A and E. GAPDH was used as a loading control.

We next examined whether CDK4 degradation is dependent on the proteosome by performing western blotting of lysates derived from parental HeLa and derivative MRNIP KO cells treated with the proteasomal inhibitor MG132. We observed no difference in CDK4 levels between the untreated and treated cells possibly suggesting, but not excluding the possibility, that bulk CDK4 degradation is proteasome-independent. Lysates were reprobed with an anti-Ubiquitin FK2 antibody to confirm the efficacy of the treatment (Figure 6.7), however this data suggested that the MG132 treatment did not work effectively. As a future experiment, we could investigate the ubiquitination of immunoprecipitated CDK4 in parental and MRNIP KO cells following proteosome inhibition.

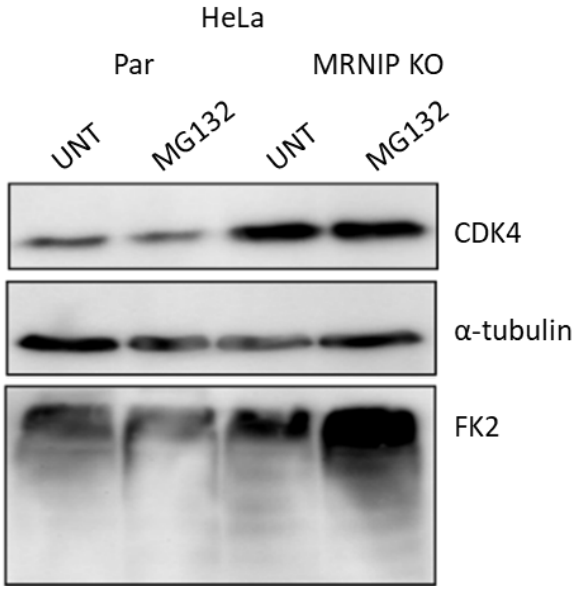

Figure 6.7 CDK4 degradation is unaltered by MG132 treatment.

Whole cell extracts from HeLa parental (Par) and derivative MRNIP KO (MRNIP KO) cells were mock treated (UNT) or treated with 5μM MG132 (MG132) for 8 hours, then were lysed and resolved by SDS-PAGE followed by blotting with the indicated antibodies.

6.3 MRNIP may mediate CHIP-dependent CDK4 degradation.

According to a recent publication, the E3 ubiquitin ligase CHIP drives CDK4 degradation following endoplasmic reticulum stress [400]. Therefore, we assessed CDK4 levels in HeLa parental and derivative MRNIP KO cells depleted of CHIP. We found that CDK4 levels were significantly elevated following CHIP depletion in parental HeLa cells, whereas the already-elevated levels of CDK4 in MRNIP KO cells remained unchanged following CHIP depletion. This suggests that MRNIP may mediate CHIP-dependent degradation of CDK4 (Figure 6.8). It is important to note that we did not confirm knockdown of CHIP using a CHIP antibody via western blotting. This is an interesting phenotype but requires further investigation.

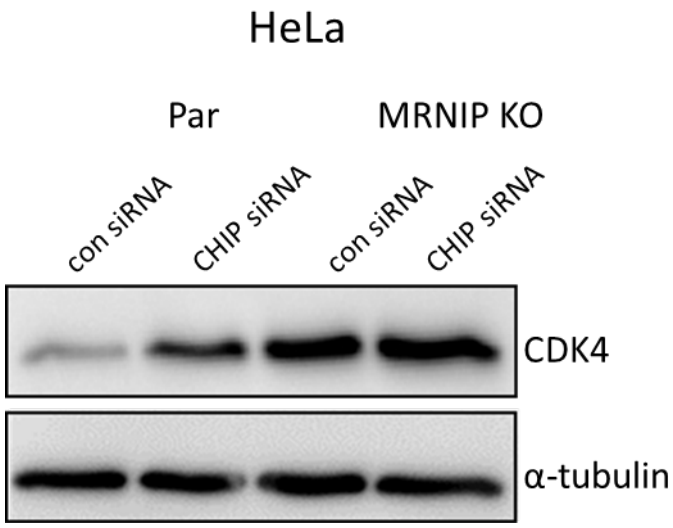

Figure 6.8 MRNIP may mediate CHIP-dependent CDK4 degradation in HeLa cells.

Whole cell extracts from HeLa parental (Par) and derivative MRNIP KO (MRNIP KO) cells were transfected with non-targeting siRNA (con siRNA) or siRNA that targets CHIP (CHIP siRNA) for 48 hours, lysed and blotted for CDK4 and α-tubulin as a loading control.

In conclusion, we found that CDK4 interacts with MRNIP and that in the absence of MRNIP, CDK4 levels are increased.

6.4 MRNIP depletion leads to increased CDK4 levels in RPE-1 cells.

Based on the observation that CDK4 levels are increased in several cancerous cell lines ablated of MRNIP, we next examined CDK4 levels in non-cancerous retinal RPE-1 cells depleted of MRNIP using two different siRNAs. We observed increased CDK4 levels in RPE-1 cells depleted of MRNIP, like the alterations previously observed in cancerous cells (Figure 6.9 A). A recent study showed that CDK4 determines cell size through regulating cell growth duration and rate [401]. Work from the Saurin laboratory suggests that enlarged cells experience DNA damage during S-phase following release from CDK4 inhibitor-mediated G1 cell cycle blockade [402]. Based on these observations, we tested cell survival in RPE-1 cells which were depleted of MRNIP using two different siRNAs and treated the cells with the CDK4 inhibitor Palbociclib either for 2 or 4 days and released into normal media for an additional 2 days. In both scenarios, cells depleted of MRNIP exhibited Palbociclib sensitivity compared to cells transfected with non-targeting control siRNA (Figure 6.9 B).

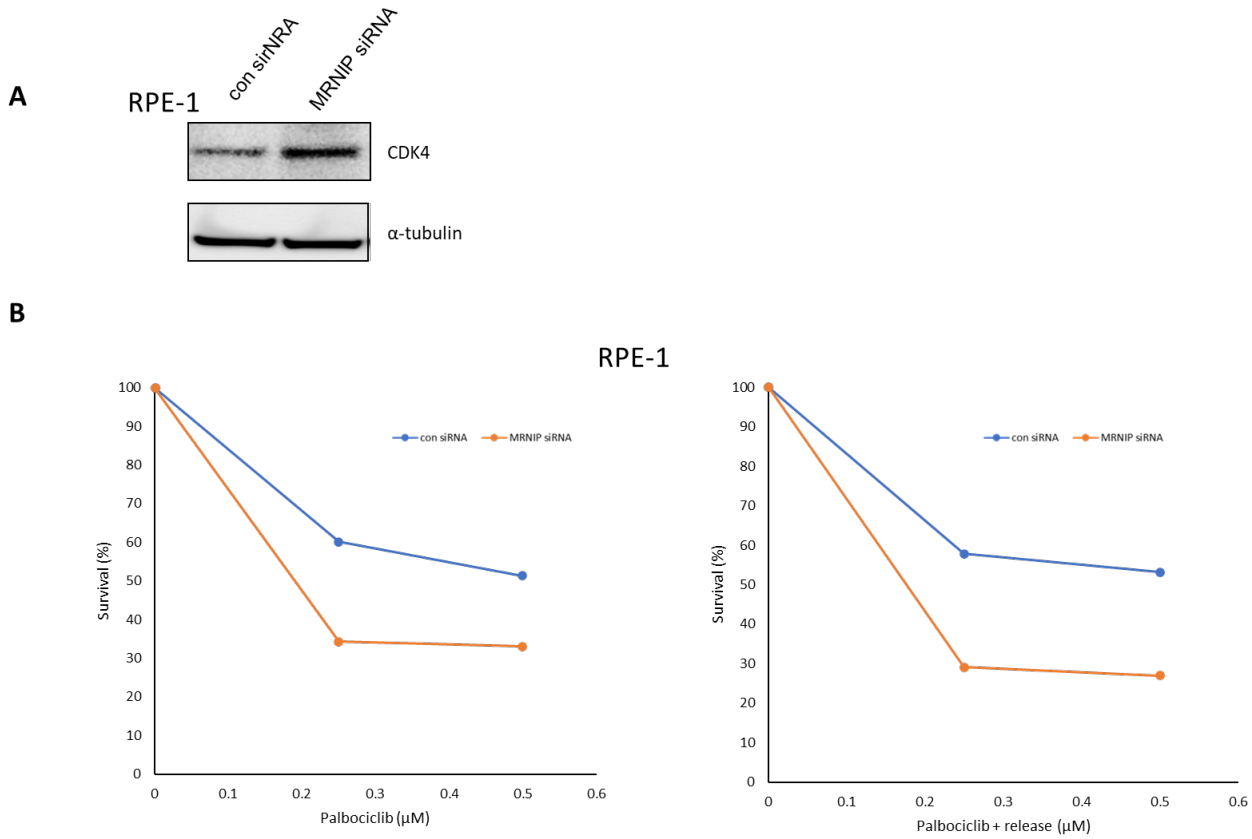

Figure 6.9 RPE-1 MRNIP KO cells are sensitive to the CDK4/6 inhibitor Palbociclib.

A) RPE-1 cells were transfected with a non-targeting control siRNA (con siRNA) or an siRNA that targets MRNIP (MRNIP siRNA) for 48 hours, lysed and blotted for CDK4 and α-tubulin as a loading control. B) RPE-1 cells were transfected with a non-targeting control siRNA (con siRNA) or an siRNA that targets MRNIP (MRNIP siRNA) for 48 hours and treated for 4 days with different concentrations of Palbociclib or treated for 2 days with Palbociclib which was released into normal media for an additional 2 days. An MTT assay was then performed, and results were normalised to untreated controls. Data represent one experiment (n=1).

Several mechanisms may be at play here – enhanced CDK4 levels have been reported to drive resistance to CDK inhibition, while enhanced replicative stress can lead to chemosensitivity. We hypothesise that since MRNIP acts protectively during replication stress, combination treatment with Palbociclib leads to enhanced DNA damage and reduced viability, overriding any mild resistance phenotype associated with enhanced CDK4 levels in MRNIP-depleted cells. This requires further investigation.

6.5 MRE11 drives Gemcitabine resistance in MRNIP KO HCT116 cells.

This study found that MRNIP KO cells are resistant to Gemcitabine treatment. This is interesting in the light of recent work from the Hartsuiker laboratory demonstrating that MRE11 removes Gemcitabine from DNA [386]. Therefore, we examined cell survival performing an MTT assay in parental HCT116 and derivative MRNIP KO cells which were depleted of MRE11 for 48 hours and treated with various concentrations of Gemcitabine for a further 96 hours. We confirmed that HCT116 MRNIP KO cells were resistant to Gemcitabine and that loss of MRE11 re-sensitised cells to Gemcitabine (Figure 6.10 A), supporting our model that hyperactive MRE11 drives Gemcitabine resistance in MRNIP KO cells. We confirmed a 60% loss of MRE11 protein (which seemed to be enough to show the resistant phenotype) by western blotting in HCT116 cells transfected with an siRNA targeting the 5' untranslated region of MRE11 (Figure 6.10 B). Mirin could have also been used for this experiment to confirm our model.

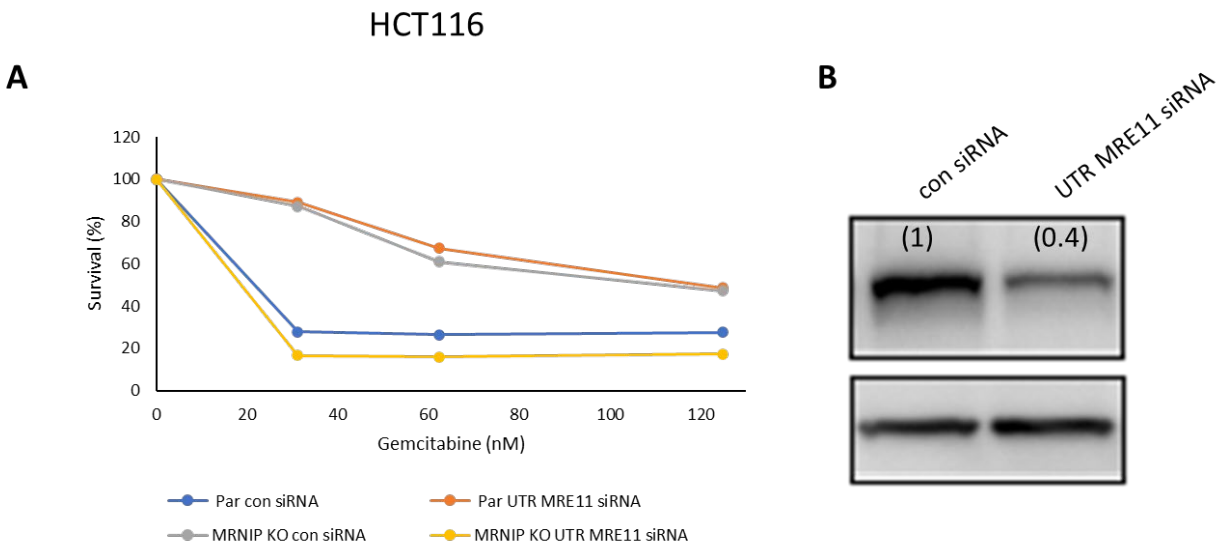

Figure 6.10 MRE11 confers resistance to Gemcitabine in HCT116 MRNIP KO cells.

A) HCT116 parental (Par) and derivative MRNIP KO (MRNIP KO) cells were transfected with a non-targeting control siRNA (con siRNA) or an siRNA that targets 5' untranslated region of MRE11 (UTR MRE11 siRNA) for 48 hours and treated with different concentrations of Gemcitabine. After 96 hours, an MTT assay was performed, and results were normalised to untreated controls. Data represent one experiment (n=1). B) Confirmation of knockdown. HCT116 cells were transfected with a non-targeting control siRNA (con siRNA) or siRNA that targets the 5' untranslated region of MRE11 (UTR MRE11 siRNA) for 48 hours, lysed and blotted for MRE11 and α-tubulin as a loading control. Numbers in brackets indicate the relative levels of proteins as determined by ImageJ analysis.

6.6 The role of MRNIP and PRIMPOL in ssDNA gap formation/processing.

Recent findings from our laboratory and others strongly suggest that ssDNA gaps that have been accumulated due to PRIMPOL repriming underpin chemosensitivity of BRCA1 and BRCA2-deficient cells [403–405]. Despite these advances, how MRE11 activity is regulated in these different contexts is remarkably poorly understood.

Unpublished data from Dr. Staples lab showed that PRIMPOL and MRE11-dependent ssDNA gaps are formed in MRNIP KO cells and that PRIMPOL-mediated repriming drives sensitivity to the PARP inhibitor, Olaparib in MRNIP KO cells. A recent study also found that multiple doses of Cisplatin supress fork degradation in BRCA-deficient cells

and this is due to the activity of PRIMPOL through its *de novo* priming action causing ssDNA gaps behind the forks [406].

Based on these results, we performed clonogenic assays in HCT116 parental and derivative MRNIP KO cell lines depleted of PRIMPOL and treated with Cisplatin or Gemcitabine for 24 hours, followed by release into normal media. MRNIP KO cells were sensitive to Cisplatin and resistant to Gemcitabine which is in accordance with our previous findings. Depletion of PRIMPOL caused sensitivity in MRNIP KO lines treated with Gemcitabine (Figure 6.11A) but not Cisplatin (Figure 6.11B) suggesting that PRIMPOL-mediated repriming drives Gemcitabine resistance, but does not determine cisplatin sensitivity in a MRNIP-deficient background. Representative pictures of colonies formed are shown in (Figure 6.11 C). We also verified knockdown of PRIMPOL by western blotting (Figure 6.11D).

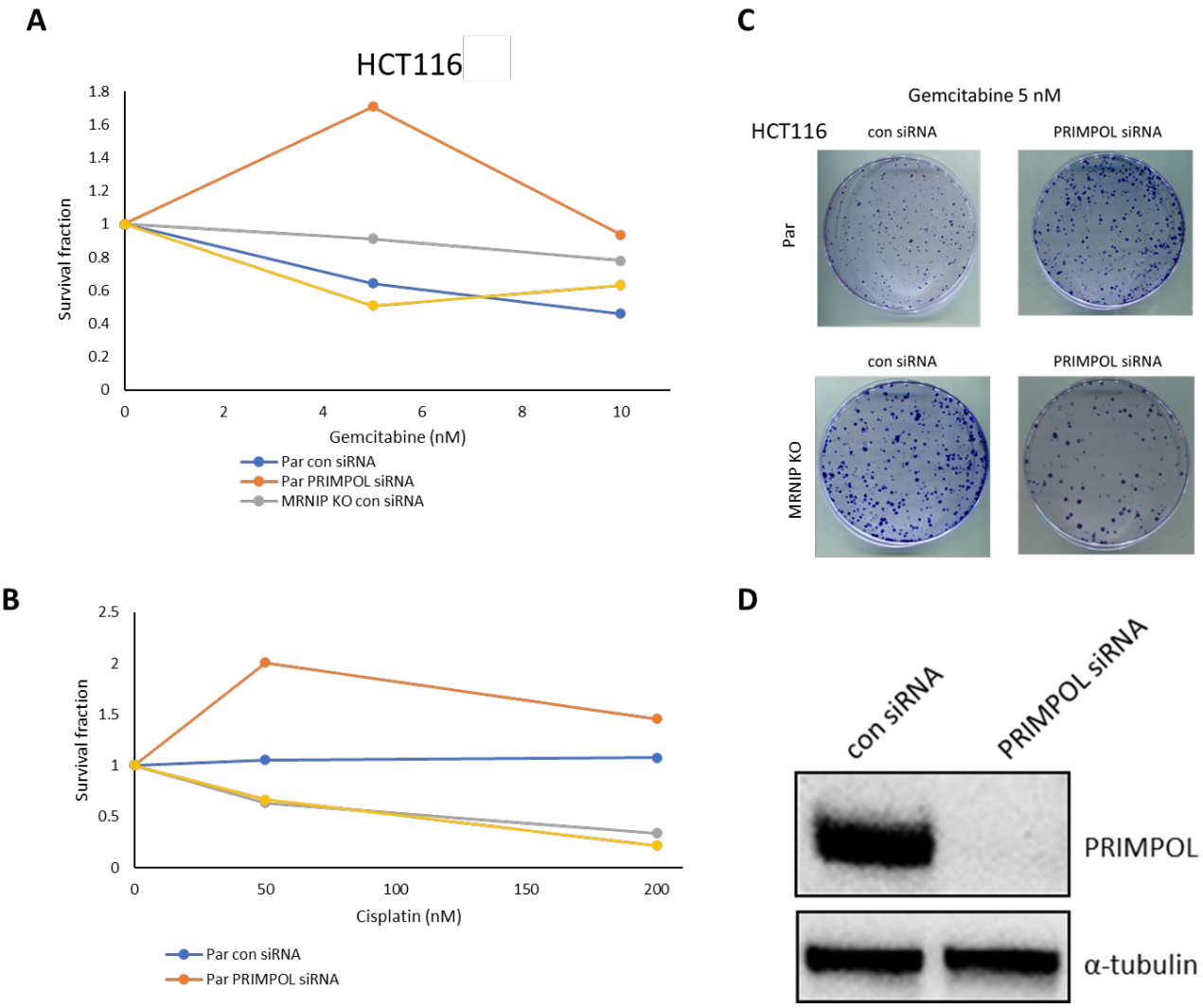

Figure 6.11 PRIMPOL drives resistance to Gemcitabine in HCT116 MRNIP KO cells.

HCT116 parental (Par) and derivative MRNIP KO (MRNIP KO) cells were transfected with non-targeting control siRNA (con siRNA) or an siRNA targeting PRIMPOL (PRIMPOL siRNA) for 48 hours, treated with A) 5 and 10nM Gemcitabine and B) 50 and 200nM Cisplatin for 24 hours, and colonies were left to develop for 10 days. Colonies were manually counted, photographed and results were normalised to the untreated controls for each transfection and plotted as percentage survival. Data represent one experiment (n=1). C) Representative images of colonies formed. D) Confirmation of PRIMPOL siRNA knockdown in HCT116 cells. HCT116 cells were transfected with a non-targeting control siRNA (con siRNA) or siRNA that targets PRIMPOL (PRIMPOL siRNA) for 48 hours, lysed and blotted for PRIMPOL and α-tubulin as a loading control.

CHAPTER VII

7 DISCUSSION

7.1 MRNIP: A novel regulator of chemosensitivity.

Our lab identified MRNIP, a protein that interacts with the MRN complex and promotes MRN complex chromatin association and efficient ATM signalling during the DDR response [384]. MRNIP acts a genome maintenance factor by promoting DNA DSB repair, and our more recent studies have uncovered a novel role for MRNIP as a novel fork protection factor. MRNIP limits the exonuclease activity of MRE11 *in vitro* [384]. In addition, MRNIP-deficient cells are sensitive to replication stress agents such as HU, and DSB-inducers such as IR [384]. However, the mechanisms underpinning MRNIP-mediated MRE11 repression remain largely unknown, and likewise whether MRNIP-deficient cells are sensitive to other classes of replication stress and DNA damage-inducing agents remains untested.

This project employed two MRNIP KO cell lines generated by CRISPR-Cas9 technology in two different backgrounds: HeLa cells (cervical cancer) and HCT116 cells (colorectal cancer), with the aim of testing the potential role of MRNIP in mediating resistance to other classes of chemotherapy. We tested these lines via a series of PCRs spanning each individual MRNIP exon. While exons 1 and 2 appeared intact, exon 3 was disrupted in MRNIP KO cells, suggesting that this was the site of insertion of the puromycin cassette (Figure 3.2). Loss of MRNIP protein was confirmed by western blotting (Figure 3.3). Exons 1 and 2 are relatively short and collectively could theoretically encode a 51 amino acid protein encompassing much of the N-terminal zinc finger domain. However, such a truncated mRNA is likely to be destroyed by nonsense-mediated decay. Northern Blot or using TaqMan probes that span exon 1-2 boundary and exon 2-3 boundary could have also been performed to confirm disruption of exon 3 in MRNIP KO cell lines. MRNIP interacts with MRE11, which functions in conjunction with phosphorylated CtIP to promote seDSB resection by counteracting Ku70/80 [394,395,407]. Therefore, we hypothesised that MRNIP might regulate MRE11 in the context of CPT-induced seDSBs. We therefore assessed cell survival in CPT-treated WT and MRNIP KO cells. This study confirmed that MRNIP KO HeLa and HCT116 cells are sensitive to CPT, and this

phenotype was fully rescuable by restoration of MRNIP in MRNIP KO cells, suggesting that the effect observed was due to MRNIP loss (Figure 3.4). These data provided effective validation of MRNIP as a chemoresistance factor. The inclusion of the rescue experiment was an important control, given the extensive reports that Cas9 action can lead to a variety of off-target effects [408–412].

To our surprise, MRNIP KO cells are resistant to the nucleoside analogues Gemcitabine and Cytarabine (Figure 5.1 A,B), (Figure 5.5 A,B), (Figure 5.6 A,B) but sensitive to the nucleoside analogues Fludarabine and Clofarabine (Figure 5.5 C,D), (Figure 5.6 C,D). One possible explanation for Gemcitabine resistance in MRNIP KO cells is that hyperactive MRE11 removes Gemcitabine more efficiently from stalled forks, thus promoting the completion of replication and cell survival. Another explanation for the resistant phenotype after Gemcitabine treatment in MRNIP-deficient cells could be that these cells do not perform HR as efficiently. Previous studies have found that Chinese hamster ovary cell lines deficient in HR and BER [413] and the FANCC deficient pancreatic cancer cell line PL11 [414] were resistant to Gemcitabine compared to HR-proficient cell lines. Another recent study showed that HR intermediates formed after Gemcitabine treatment are converted into DSBs, causing cell death [415]. In addition, a more recent study found that BRCA2-deficient cells are more resistant to Gemcitabine treatment compared to BRCA2-restored cells, and the authors suggest that in the absence of HR, another pathway that does not involve extensive DNA synthesis such as alternative nonhomologous end-joining, might be implicated in the repair of Gemcitabine induced breaks [416]. Based on these findings, we speculate that in the absence of MRNIP, no toxic HR intermediates are formed, which favours cell survival. Another explanation for Gemcitabine resistance in MRNIP-deficient cells may be related to the incorporation of Gemcitabine and Cytarabine by PRIMPOL [417], a RNA/DNA primase with DNA/RNA primase and DNA polymerase activity [418], and which has been implicated in tolerance to CTNAs [419]. PRIMPOL reprimes after CTNA-induced lesions by performing close-coupled *de novo* synthesis of primer strands *in vitro* [419]. However, there is no previous evidence that PRIMPOL incorporates Clofarabine or Fludarabine which may justify the sensitivity observed in MRNIP KO cells following Clofarabine and Fludarabine but not Gemcitabine and Cytarabine treatments. We could test this performing single turnover kinetic assays with recombinant PRIMPOL in the presence of 5 mM $MnCl_2$ or $MgCl_2$ as performed

before [417] (with Gemcitabine and Cytarabine treatments) under Clofarabine and Fludarabine treatments.

Indeed, clonogenic experiments included in this study showed that PRIMPOL siRNA reverses resistance to Gemcitabine in MRNIP KO cells (Figure 6.11), suggesting that enhanced survival in MRNIP KO cells is dependent on replication repriming. We hypothesise that excessive repriming driven by PRIMPOL-mediated CTNA incorporation leads to short DNA fragments that cannot efficiently template-switch. Loss of MRNIP leads to MRE11 hyperactivation, digestion of these fragments and restoration of template switching (TS). TS as well as TLS are DNA damage tolerance mechanisms. TS is an error-free process that involves the use of the undamaged template from the sister chromatid for synthesising DNA in a recombination-dependent manner. On the contrary TLS is an error prone process where one or more of the TLS DNA polymerases synthesise nucleotides opposite and past the DNA lesion prior to the action of the replicative DNA polymerase [420]. A model suggested by Dr. Staples is shown below (Figure 7.1).

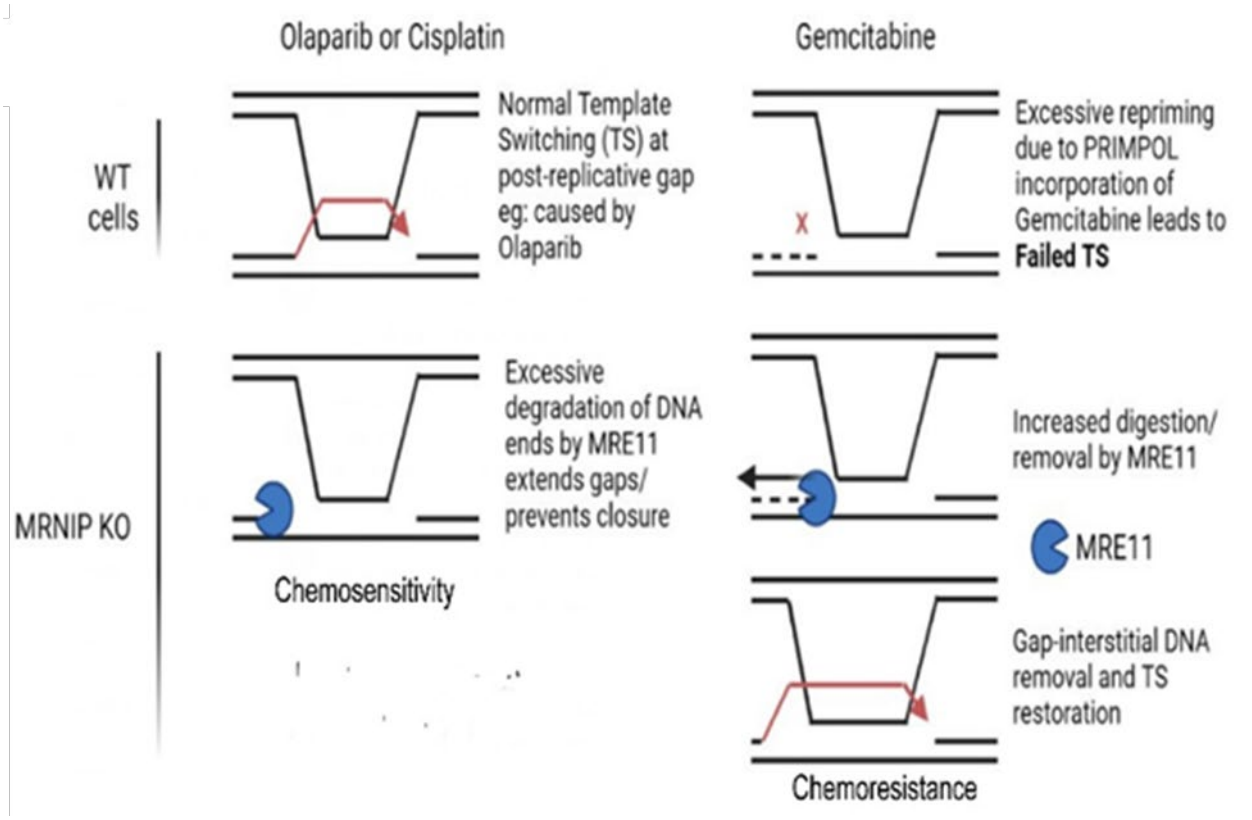

Figure 7.1 Proposed model demonstrating enhanced template switching (TS) consequent to MRE11 hyperactivation in MRNIP KO cells.

(Left) Wild type cells undergo normal TS following Olaparib or Cisplatin treatments as a mechanism of damage tolerance. On the contrary, hyperactive MRE11 -due to loss of MRNIP- (MRNIP controls MRE11 exonuclease activity) in MRNIP KO cells leads to excessive degradation of DNA ends. (Right) PRIMPOL can incorporate Gemcitabine and Cytarabine, which could lead to excessive re-priming and the formation of consecutive DSGs spaced by short stretches of interstitial DNA, which are likely poor substrates for TS-mediated gap filling. Model proposed and drawn by Dr. Staples.

In keeping with this hypothesis, PRIMPOL and MRE11-dependent ssDNA gaps are detectable in Gemcitabine-treated MRNIP KO cells only after depletion of the template switching factor UBC13 (Staples laboratory, unpublished data). A model suggested by Dr. Staples is shown below (Figure 7.2).

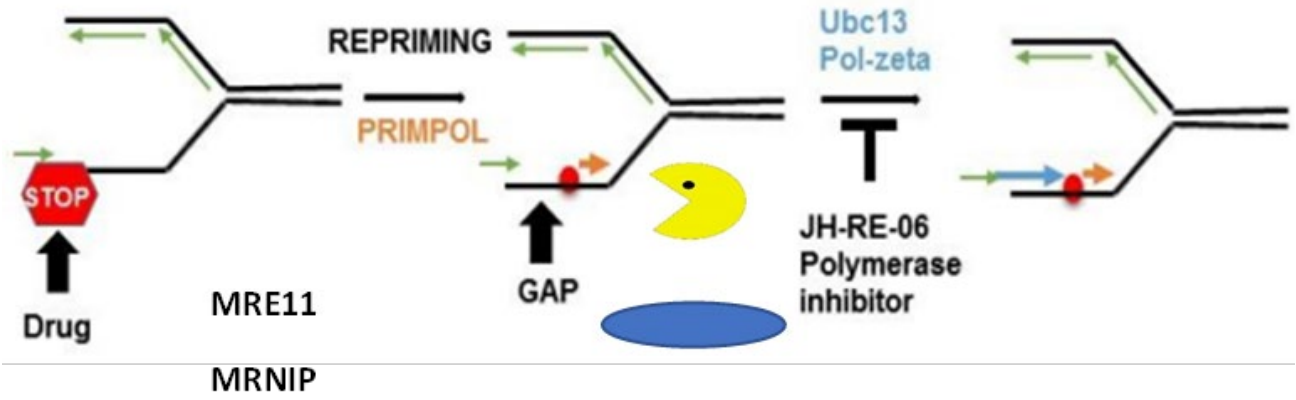

Figure 7.2 MRNIP represses MRE11 activity at ssDNA gaps formed by repriming in response to Cisplatin or Olaparib.

Replication obstacles lead to repriming by the primase-polymerase PRIMPOL, leaving behind a ssDNA gap that is protected from MRE11 nuclease action by BRCA1/2 (not shown). These gaps are filled by Pol-zeta, via UBC13-dependent Template Switching or by Trans-Lesion Synthesis. Cells lacking MRNIP exhibit elevated PRIMPOL and MRE11 ssDNA gaps following Cisplatin or Olaparib treatment. Our data suggest that MRNIP-mediated MRE11 repression also functions to protect these gaps, facilitating eventual gap closure and chemoresistance. Model suggested and drawn by Dr. Staples.

In addition, Gemcitabine can be incorporated into RNA to a lesser extent but the biological consequences of this have not been widely studied. According to one study, the sensitivity of different cell lines to Gemcitabine was related to its incorporation into RNA [421] and therefore it would also be of interest to evaluate Gemcitabine levels in both nascent DNA and RNA in MRNIP KO cells.

In addition, it has been shown that the exonuclease activity of DNA Polymerase ε plays an important role in cellular tolerance to Cytarabine [422], however due to the ‘’ masked’’ chain termination (extra nucleotide is masked and polymerase cannot start synthesis) mode of Gemcitabine action, some suggest that the Polymerase ε exonuclease cannot remove Gemcitabine from the DNA. However, recent work from the Hartsuiker lab showed that DNA polymerase ε exonuclease activity is implicated in Gemcitabine resistance in DT40 cells (personal communication). In addition, a study found that the exonuclease of human DNA polymerase ε removed Fludarabine from DNA with difficulty and that this excision results in the formation of a "dead end complex (complex formed between Fludarabine and DNA polymerase) [423] possibly explaining the sensitivity observed in MRNIP KO cells following Fludarabine but not Gemcitabine or Cytarabine treatments. Therefore, the synergistic action of PRIMPOL repriming and MRE11 or polymerase ε-mediated removal of Gemcitabine and Cytarabine from stalled forks might be responsible for the resistant phenotype observed in MRNIP KO cells.

In addition, Gemcitabine and Cytarabine are weak inhibitors of DNA polymerases [424] while the triphosphate form of Clofarabine and Fludarabine are potent inhibitors of both DNA polymerase α and RNR [425] therefore it is likely that DNA replication cannot be resumed at Clofarabine and Fludarabine stalled forks as DNA polymerase is inhibited explaining the sensitivity observed in MRNIP KO cells following Clofarabine and Fludarabine treatments. The fact that MRNIP KO cells are resistant to Cytarabine, which causes chain termination but not RNR inhibition, leads us to suspect that the resistance phenotype is directly related to the chain termination effect. Sensitivity to Clofarabine and Fludarabine may be similar in nature to the sensitivity observed in MRNIP KO cells in response to HU.

It is also important to note that it is not yet known whether Gemcitabine causes fork reversal, and whether reversed forks are the major site of Gemcitabine removal by MRE11 (given that fork reversal reveals an end that nucleases can act upon). To

elucidate this, we could employ siRNA to deplete known fork reversal factors including FBH1, SMARCAL1, ZRANB3, and HLTF and examine sensitivity of MRNIP KO cells after Gemcitabine treatment. Furthermore, we must also consider the possibility that some DNA synthesis occurs in the presence of high-dose Gemcitabine in MRNIP KO cells, since perturbations to dNTP pools are less extreme following Gemcitabine treatment, when compared with the HU treatment that forms the basis of the typical nascent DNA degradation assay.

7.2 Different sequence motifs in MRNIP are implicated in resistance to CPT and sensitivity to Gemcitabine.

Following our survival experiments with MRNIP KO cells after CPT and Gemcitabine treatment, we then tested survival of MRNIP KO cells stably expressing tetracycline-inducible FLAG-tagged MRNIP mutated at different sites under the same treatment conditions. We confirmed MRNIP expression in all cells, a rescue of the phenotype in cells overexpressing flag-tagged MRNIP, however, we observed a ''leakage'' in MRNIP expression in cells expressing FLAG-tagged MRNIP in the absence of doxycycline treatment (Figure 3.8). This could be due to a mutation in the promoter region resulting in MRNIP expression being constitutively ''ON''. Control cells were therefore also treated with doxycycline to avoid off-target effects. In addition, we observed that the band corresponding for FLAG-S115A mutant runs at the same height as the FLAG-WT suggesting that MRNIP is not highly phosphorylated on Ser115 after doxycycline treatment (Figure 3.8). This could be explained by the fact that doxycycline might not induce phosphorylation at this site, or that MRNIP phosphorylation might be in a small but important fraction of MRNIP, or that MRNIP phosphorylation is transient and cannot be immediately identified by band shifts via western blotting. The Staples laboratory is currently generating a phospho-specific antibody to investigate this further.

Our MTT assays showed that substituting serine 217 to alanine rescued CPT sensitivity (Figure 3.9 A) and Gemcitabine resistance (Figure 5.4A) in MRNIP KO cells. However, previous results from the Staples laboratory showed that alanine substitution of Ser217 did not have a role in MRNIP-mediated fork protection following HU treatment [384]. In addition, we showed in our previous paper that S115A and Δ25 MRNIP mutants cannot complement MRNIP loss following exposure to IR [384] or CPT (Figure 3.9 A,C). Both CPT and IR induce DSBs; single-ended and double-ended, respectively. Given our results, we suggest that Ser115 phosphorylation and the KELWS sequence contribute to MRNIP function in DSB repair but are dispensable for protection of reversed forks. The differential involvement of these phosphorylation sites suggests the presence of distinct and context-dependent regulatory mechanisms that control MRNIP function. In the context of IR-induced DNA damage, MRNIP controls MRN complex chromatin loading, yet HU-dependent MRE11 loading is unaffected by MRNIP loss. We hypothesise that the KELWS sequence and post-translational modification at Ser115 are important for MRNIP-

mediated MRN chromatin loading. There is no real evidence for the involvement of the entire MRN complex in nucleolytic resection of nascent DNA at gaps or reversed forks. Perhaps MRNIP phosphorylation specifically promotes chromatin loading of the MRN complex but cannot alter MRE11 loading in the context of replication.

It is important to mention that it is not yet known which kinase(s) phosphorylate MRNIP at Ser217, although several proline-directed kinases including CDKs, MAPKs, Glycogen synthase kinase (GSK) or Jun N-terminal kinase (JNK) are possible candidates. However, Ser217 is a good candidate for a non-canonical CDK1 site, and therefore we hypothesise that this phosphorylation event could represent a mechanism of cell cycle dependent MRE11 regulation by MRNIP.

We are currently in the process of raising an antibody against Ser217 to facilitate assessment of phosphorylation at this site and will also employ small-molecule inhibitors to identify the kinase(s) involved. We will also perform pulldown experiments using biotinylated peptides and phosphopeptides incubated with nuclear extracts, followed by mass spectrometry analysis. In addition, we will perform proteomics in cells expressing MRNIP and MRE11 mutants to assess how phosphorylation regulates the protein-protein contacts made by these factors during DNA damage and replication stress.

7.3 Role of MRNIP in DNA damage response.

To better understand the link between cell survival and DNA damage, we assessed DNA damage levels in HeLa and HCT116 MRNIP KO cells acutely treated with HU to induce replication stress (Figure 3.5) as well as low and high concentrations of CPT (Figure 3.6, Figure 3.7). HeLa and HCT116 MRNIP KO cells exhibited increased levels of DNA damage, as assessed by γH2AX and 53BP1 markers even in the absence of genotoxic treatment, confirming that MRNIP is implicated in the suppression of DNA damage in cycling, otherwise unchallenged cancer cells. Overexpression of FLAG-tagged MRNIP in MRNIP KO cells led to fewer DNA damage foci, suggesting that the response observed in MRNIP KO cells was due to the loss of MRNIP and was not a consequence of other off target effects. Increased DNA damage levels were also observed when MRNIP KO cells were treated with HU (Figure 3.5) and both doses of CPT in both HeLa and HCT116 cell lines compared to the control (Figure 3.6, Figure 3.7), while overexpression of FLAG-tagged MRNIP in MRNIP KO cells led to an even lower number of foci than was observed in the parental line, indicating that MRNIP overexpression may be able to further suppress DNA damage (Figure 3.5, Figure 3.6, Figure 3.7). It would be interesting to examine DNA damage levels in MRNIP KO cells treated with a longer exposure to CPT as the above experiments were conducted following a 2-hour incubation (the cells did not have enough time to enter S phase) with the drug. In addition, treatment of cells and subsequent release of the drug could form the basis of another future experiment to assess how the cell deals with RS after having recovered from treatment.

We also assessed DNA damage levels in HCT116 and derivative MRNIP KO cells treated with low (Figure 5.2) and high concentrations (Figure 5.3) of Gemcitabine for 4 and 24 hours. Longer exposure of even 100nM of Gemcitabine caused increased DNA damage levels (γH2AX marker only) in parental but not derivative MRNIP KO cells which tallies with the resistant phenotype observed in MRNIP KO cells following Gemcitabine treatment (Figure 5.2B).

7.4 Role of MRNIP in determining nascent DNA degradation after HU and Gemcitabine treatment.

It is well established that several DNA repair factors have roles at the replication fork which are genetically separatable roles from their canonical role in HR-mediated repair [354,357,364,365,426]. In particular, BRCA1/2 protect stalled forks from MRE11-dependent DNA resection following treatment with HU or platinating chemotherapies [365]. Our lab showed that MRNIP represses MRE11 exonuclease activity *in vitro* and that MRNIP acts as a novel replication fork protection factor [384] . Loss of MRNIP leads to MRE11-mediated nascent DNA degradation in cells treated with HU, a phenotype that was rescued by MRE11 inhibition (Mirin or PFM39), prevention of fork remodelling (SMARCAL1) or depletion of the MRE11 recruitment factor Pax transcription activation domain-interacting protein (PTIP) [384]. However, my work demonstrates that substitution of serine 217 to alanine and substitution of lysines 58 and 129 to arginine did not affect fork protection following HU treatment (Figure 3.10). It is important to note that we did not test whether the nascent DNA degradation phenotypes observed in Gemcitabine-treated cells are modulated by alanine substitution of Ser217. We are currently assessing the dynamics of replication in Gemcitabine-treated MRNIP KO cells. Given that we also more recently observed the formation of UBC13-dependent ssDNA gaps in Gemcitabine-treated MRNIP KO cells (unpublished data), it is possible that MRNIP phosphorylation at this site might not occur during S phase but at a later cell cycle phase; for example, CDK1 is inactive during S phase. CDK1 is a proline-directed kinase that preferentially phosphorylates the consensus sequence S/T-P-x-K/R (where x is any amino acid), although it also phosphorylates the minimal consensus sequence S/T-P [427]. We hypothesise that MRNIP might be phosphorylated at Ser217 by CDK1 in G2 and potentially regulate MRE11 in the context of ssDNA gaps that have persisted into G2. This will be tested in future using the S1 nuclease-linked DNA fibre assay [384]. This is a modified version of the DNA fibre assay that uses the S1 nuclease, an enzyme that specifically cleaves ssDNA. In the case of post-replicative ssDNA gaps, the S1 enzyme will act by cleaving those gaps eventually causing shorter tracts which as be used as a read-out.

Paradoxically, Gemcitabine-treated HeLa and U2OS cells exhibited reduced replication tract length following chronic incubation with high-dose Gemcitabine (Figure 5.7), yet our

data suggests that the main nucleases typically involved in resection of stalled forks (MRE11, MUS81 or DNA2) are not involved in mediating this degradation event (Figure 5.8). However, the experiment was poorly controlled as we did not include control samples such as MRNIP KO cells treated with HU, which would have demonstrated that the depletion of each factor was sufficient to elicit a phenotype. It is also important to note that Gemcitabine diphosphate acts by inhibiting RNR and by causing chain-termination. This dual mode of action could theoretically explain the degradation phenotype observed in genetically unperturbed cells. To investigate whether the degradation phenotype is due to the combination of RNR inhibition and chain termination, or to chain termination alone, we could assess degradation of nascent DNA in HeLa and U2OS cells after Cytarabine treatment, since Cytarabine causes chain termination but does not inhibit RNR. Another distinct aspect of CTNA incorporation relative to other chemotherapies is that it is incorporated directly into the daughter strands instead of introducing parental strand modifications. As already mentioned, it is yet to be elucidated if forks reverse after Gemcitabine treatment, and this could be revealed by electron microscopy or by depleting fork reversal factors including SMARCAL1, ZRNB3 or HLTF.

Another candidate for resecting DNA in HeLa and U2OS cells treated with Gemcitabine is Polε, which alongside Polδ, are the only polymerases with 3'-5' exonuclease activities [428]. It has also been shown that Polε is implicated in the removal of Cytarabine [429] contributing to Cytarabine tolerance [422]. Personal communication from the Hartsuiker laboratory showed that mirin increased Gemcitabine sensitivity in a DT40 Polε exonuclease mutant [430] , a mutation that is found in 7-12% of endometrial cancers and 1–2% of colorectal cancers [431–433]. Due to limited time, we were unable to examine fork dynamics through DNA fibre assays in Gemcitabine-treated DT40 wild type and Polε exonuclease mutants, but it is worth investigating in the future.

Interestingly, MRNIP loss reduced nascent DNA degradation in response to Gemcitabine (Figure 5.9). One hypothesis that fits with this observation would be that DNA degradation is due to recombination-dependent effects. In the absence of MRNIP, Holliday Junction Resolvases may not effectively cut DNA. Although we did not find a phenotypic difference in cells depleted of MUS81, we cannot exclude the possibility that MUS81 might cut DNA at Gemcitabine-stalled forks, as suggested in the case of HU-stalled forks [370], as the experiment was poorly controlled. Likewise, we did not test the involvement of the SLX4 or GEN1 resolvases. Another hypothesis explaining enhanced fork protection in MRNIP

KO cells could be that MRNIP acts as a switch for Polε to act as a polymerase or exonuclease; when MRNIP is present, Polε acts as an exonuclease and therefore forks are degraded in HeLa and U2OS cells while when MRNIP is absent; Polε acts as a polymerase therefore MRNIP KO cells exhibit protected forks. To assess that we could mutate Polε polymerase and/or exonuclease activities in parental and MRNIP KO cells and assess their degradation phenotype after Gemcitabine treatment. One must also consider the possibility that the phenotype in MRNIP KO cells represents increased DNA synthesis, rather than reduced degradation of nascent DNA.

7.5 Phosphorylation of MRE11 dictates the extent of DNA resection.

Unpublished data from our laboratory demonstrated that phosphorylation of MRE11 at Ser676 was undetectable in HeLa MRNIP KO cells when treated with HU and CPT compared to WT parental cells (Figure 4.1). Unfortunately, although we detected basal MRE11 levels, we were unable to consistently detect phosphorylation of MRE11 in either HeLa or U2OS cells despite our efforts to optimise the conditions of the antibody and following advice from our collaborators (Figure 4.2). Before this problem arose, we constructed mutants that mimic and ablate MRE11 phosphorylation at Ser676/678, and an MRE11 exonuclease-dead mutant of MRE11 and generated stable MRNIP KO cell lines expressing FLAG-tagged WT or mutant MRE11 (Figure 4.3). Within this system, we were able to confirm the phosphorylation of ectopic MRE11 at Ser676, and that the antibody did not detect the 676/678 alanine mutant (Figure 4.4). This indicates that the antibody does function specifically but is unable to detect what may be limited levels of endogenous MRE11 phosphorylation. Our work using the H63D mutant of MRE11 in the context of replication fork protection is novel, as to date all prior evidence implicating MRE11 exonuclease activity in the degradation of nascent DNA has been gathered via pharmacological inhibition of MRE11, for example by the use of Mirin or PFM39 [221,384]. Construction of stable cell lines expressing an exonuclease-dead MRE11 mutant, which has been confirmed through sequencing and previously used [395] , would be advantageous as results can be confirmed through both genetic and pharmacological means. In addition, MRE11 is phosphorylated at SQ/TQ sites, which are targets of ATM, ATR and PIKK kinases, and this modification inactivates the MRN complex by facilitating its dissociation from chromatin, and thus contributing to checkpoint recovery [434]. Several studies have suggested ATM to be the kinase responsible for phosphorylating MRE11 in response to DSBs [435–439]. Indeed, one study demonstrated that MRE11 is phosphorylated at Ser 676/678 by ATM post-IR [310], although the kinase(s) that is/are implicated in MRE11 phosphorylation in response to other agents such as HU or CPT are unknown. Previous research has shown that the ribosomal S6 kinase (RSK) phosphorylates MRE11 at Ser 676 *in vitro* and *in vivo* and this phosphorylation prevents MRE11 binding to dsDNA and inhibits ATM activation [440].

To investigate which kinase is responsible for MRE11 phosphorylation at Ser 676/678, we could treat HeLa and derivative MRNIP KO cells with PIKK inhibitors or deplete ATM, ATR

or DNA-PK and examine the phosphorylation of MRE11 at Ser 676/678 after HU or CPT stimulus. In addition, it would be interesting to examine the phosphatases that might be involved. A recent study using the CausalPath method showed that MRE11 (alongside ATM and ATR) is activated when Protein Phosphatase, Mg2+/Mn2+ dependent 1D (PPM1D) is inhibited [441]. CausalPath is a computational method that was recently developed in order to analyse proteomic datasets generating causal hypotheses by aligning the observed changes with literature knowledge [442] .

Our collaborators from the Horejsi laboratory (Barts Cancer Institute) provided us with MRE11 constructs encoding alanine mutants of several CK2 and PLK1 phosphorylation sites in MRE11 (Ser558, 561, 649, 688 and 689), which were used to generate stable cell lines in HeLa MRNIP KO (Figure 4.5) and to consequently investigate the role of these sites in regulating MRE11-mediated degradation of nascent DNA at reversed replication forks stalled by chronic HU treatment. All sites tested were required for nascent DNA degradation, suggesting that MRE11 phosphorylation at these sites facilitates its function in resecting nascent DNA during replication stress (Figure 4.8). These results contradict with the finding that phosphorylation of MRE11 at S649/S688 causes release of the MRN complex from DNA and inactivates both ATM–Chk2 and ATR–Chk1 pathways [292]. This contradiction could be explained by the different nature of the stimulus used; this project exposed the cells to HU while previous research studied nascent degradation following IR exposure. These different post-translational modifications might act in a context-dependent manner at breaks or stalled forks. If this is the case, it fits broadly with our observations that MRNIP promotes IR-induced chromatin loading of MRN, but not HU-induced MRE11 chromatin association and so functions in a context-dependent manner.

Interestingly, we found that mimicking MRE11 phosphorylation at Ser676/678 in MRNIP KO cells fully rescued nascent DNA degradation (Figure 4.6). This result was in contrast to a recent paper which showed that MRE11 phosphorylation at 676/678 is required for nascent DNA degradation in a BRCA2-deficient background [397]. This apparent conflict might reflect the fact that MRE11 phosphorylation is defective in MRNIP KO cells, and that this defect may underpin the degradation phenotypes observed in MRNIP-deficient cells.

Unpublished *in vitro* studies from our collaborators in the Cejka laboratory showed that a phosphomimetic Ser676/678 mutant (S676/678E) exhibited reduced DNA cleavage compared to wild type MRE11, and that bulk inhibition of MRE11 phosphorylation resulted

in elevated exonucleolytic DNA resection. Indeed, combinatorial alanine substitution of PIKK, CK2 and PLK1 phosphorylation sites led to a fork degradation profile similar to wild type MRE11 (Figure 4.8), suggesting that a functionally active enzyme can be restored by specific dephosphorylation of the PIKK sites. These findings also suggest that MRE11 is functionally inactivated in the absence of CK2/PLK1 phosphorylation, and this may be a mechanism to limit MRE11 activity in the early stages of the cell cycle, when PLK1 activity is low [443] and HR-mediated repair cannot be performed due to the absence of a sister chromatid. One could hypothesise that dephosphorylation of the PIKK sites might provide a mechanism to rapidly activate MRE11. These sites are implicated in DNA binding; therefore, we hypothesise that different combinations of phosphorylation (or lack thereof) can differentially impact DNA binding, and thus effective nuclease function. As a future experiment, we should focus on chromatin association of these different MRE11 mutants following induction of DSBs by IR or replication stress by HU treatment. A proposed model is shown in (Figure 7.3).

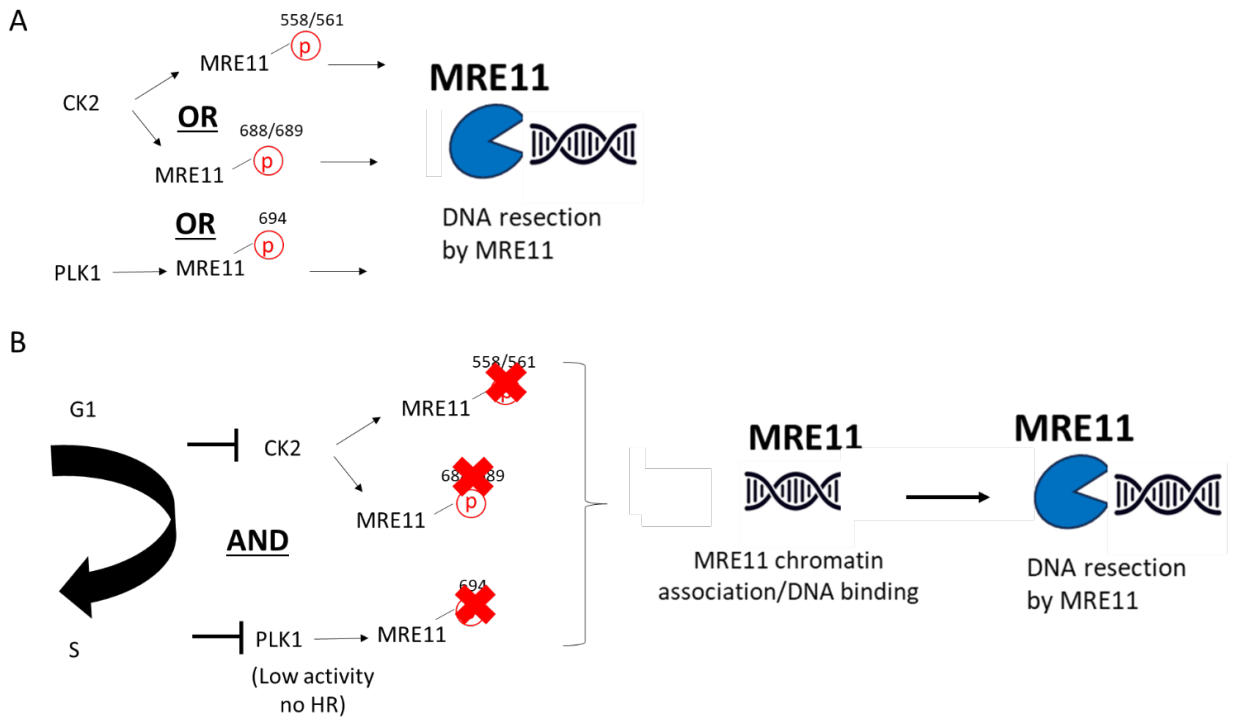

Figure 7.3 Proposed model where different phosphorylation of MRE11 can impact its DNA binding and by extent its nuclease action.

A) CK2 phosphorylates MRE11 at serines 558/561 and 688/689 and PLK1 phosphorylates MRE11 at serine 694 [292,293] which are individually essential for DNA resection. B) When CK2 and PLK1 are inactivated, for example during the early stage of the cell cycle where PLK1 activity is low [443] and HR cannot be performed, MRE11 is bound to chromatin/DNA which in its turn, favours DNA end resection.

As future experiments, we could inhibit or deplete (siRNA) CK2 and PLK1, the kinases responsible for MRE11 phosphorylation at serines 558,561, 649, 688 and 689 and perform S1-linked DNA fibre assays to monitor DSG formation in HeLa cells. In addition, we could perform S1-linked DNA fibre assays in MRNIP KO cells expressing MRE11 mutants following treatment with a range of chemotherapies including Cisplatin, Olaparib or Gemcitabine to assess the effect of these treatments on DSG formation.

CK2 is implicated in many cellular processes including DNA damage and repair. More specifically, multiple studies have shown that CK2 phosphorylates a variety of DNA repair proteins including XRCC1 [444,445], MDC1 [446,447], RAD51 [448], the deubiquitylase OTUB1 [449],

the MLH1 component of the DNA mismatch repair complex MutLα[450], and CTP1 [451]. A study published this year showed that CK2 is also important for ATR-mediated S phase checkpoint activation in response to DNA replication stress, for binding of claspin (CLSPN) and CDC45 to chromatin as well as fork recovery of HU stalled forks [452]. However, CK2 kinase has also been shown to have a role in late G2/M as it phosphorylates MUS81 at serine 87 after mild replication stress [453], while another group found that CPT sensitivity in a variety of cancerous and non-cancerous cell lines was correlated to high CK2 sensitivity [454].

PLK1 has also been associated with controlling various cellular processes. Indeed, activation of PLK1 via the synergistic action of Aura and Bora causes CDK1 activation and mitotic entry [455] while a study using Xenopus laevis egg extracts found that PLK1 depletion caused increased CHK1 phosphorylation and decreased CDK2 activity, demonstrating a possible role of PLK1 in inhibiting the ATR/CHK1-dependent S phase checkpoint [456]. Silencing PLK11 in cell carcinoma models and treatment with an active CPT11 metabolite SN38 caused increased anti proliferative and pro apoptotic results [457].

7.6 CDK4 is a MRNIP interactor.

In our attempt to identify novel MRNIP interactors, we immunoprecipitated MRNIP-FLAG from HEK 293 cells treated with HU or CPT and analysed the eluates by Orbitrap mass spectrometry (Figure 6.2) (orbitrap is an ion trap mass analyser that consists of two outer electrodes and a central electrode, which enable it to act as both an analyser and detector). This study revealed 3 possible novel MRNIP interactors but we could identify only CDK4 in follow-up immunoprecipitation experiments (Figure 6.3). The complete structure of MRNIP has not yet been identified, although its N-terminal domain is predicted to contain a zinc finger. A recent paper showed that knockdown of zinc finger protein 384 (ZNF384) inhibited G1/S transition in hepatocellular carcinoma cells and significantly reduced the expression of cyclin D1 [458], the binding partner of CDK4. Perhaps MRNIP interacts with CDK4 via its zinc finger. In addition, it is possible that MRNIP might modulate the interaction between CDK4 and its binding partner cyclin D1 causing cell cycle arrest similarly to the zinc finger transcription factor INSM1 [459]. Indeed, cell cycle profile analysis showed an increased proportion of cells in G1 in MRNIP KO compared to the control (personal communication with Dr. Staples). We could test whether MRNIP can affect the CDK4-CyclinD1 interaction by performing co-immunoprecipitation of CyclinD1/CDK4 in MRNIP KO cells. In addition, we could use FLAG-tagged MRNIP mutants lacking the N-terminal region (63-343) to perform co-immunoprecipitation and investigate whether the N-terminal of MRNIP mediates interaction with CDK4.

In addition, CDK4 is a proline-directed kinase, and MRNIP is phosphorylated by a proline-directed kinase at Ser217; therefore, CDK4 is potential candidate kinase for MRNIP phosphorylation at this site. CDK4 displays a less-stringent S/T-P-X consensus compared to other CDKs [460] therefore, Ser217 may be a non-canonical CDK4 site. One might hypothesise that MRNIP phosphorylation by CDK4 could inhibit HR in G1 to ensure that mitotic recombination occurs solely between sister chromatids, as was recently described as a function of the USP11/KEAP1 network [461].

In addition, we found that CDK4 levels were higher in MRNIP-depleted or KO cells and remained stable throughout the cell cycle (Figure 6.4). Interestingly, CDK4 was not degraded in MRNIP KO cells after CHX treatment in contrast to parental lines (Figure 6.5), suggesting that MRNIP regulates CDK4 degradation. As a future experiment we could

perform a cycloheximide chase in FLAG-tagged MRNIP mutants lacking the N-terminal region (63-343) to investigate the stability of CDK4.

Based on the recent paper that the E3 ligase CHIP promotes CDK4 degradation [400], we depleted CHIP from parental HeLa and MRNIP KO cells and examined the extent of CDK4 degradation. We found that depletion of CHIP in HeLa cells restored CDK4 levels (Figure 6.8), suggesting that MRNIP regulates CHIP-mediated CDK4 degradation. Surprisingly, CDK4 degradation was unaffected by MG132 treatment as CDK4 levels were not altered after treatment (Figure 6.7). This finding contradicts with the literature that has shown that CCAAT/enhancer binding protein alpha (C/EBPa) enhances the formation of CDK4-ubiquitin conjugates and induces CDK4 proteosome dependent degradation in several tissue models [462]. A more recent study showed that CDK4 is degraded by the anaphase-promoting complex/cyclosome (APC/C) during metaphase-anaphase transition in HeLa cells, whereas the levels of its partner cyclin D1 remain stable and it is sequestered in cytoplasm [463] .

As a future experiment, we could perform CDK4 immunoprecipitation in HeLa and derivative MRNIP KO cells treated with the proteasomal inhibitor MG132 and blot for FK2 to examine ubiquitination of CDK4. Autophagy could also be a possible mechanism for CDK4 degradation, which could be assessed in the future by using autophagy inhibitors prior to examination of CDK4 levels in MRNIP KO cells. It would also be interesting to examine whether global autophagy is altered in MRNIP-deficient cells.

7.7 MRNIP is absent in certain ovarian cell lines.

According to a recent study, MRNIP is highly expressed in testis, and MRNIP depletion leads to murine male subfertility [382]. MRNIP is also predicted to be under expressed in a subset of ovarian cancers (COSMIC). Our study found that MRNIP is highly expressed in a range of ovarian and glioblastoma cell lines, however, MRNIP was undetectable by western blot in high-grade ovarian serous adenocarcinoma cell lines UWB1-289 and OVCAR-3, and in glioblastoma U138 cells (Figure 5.10). Due to the difficulty in detecting endogenous MRNIP by western blot, we cannot exclude the possibility that UWB1-289, OVCAR-3 and U138 cells express MRNIP at low levels that are simply below the detection threshold of the antibody. It is also unlikely that MRNIP is absent in these cell lines (i.e., due to chromosome alterations) as we did identify MRNIP mRNA in these cells, albeit at reduced levels relative to MRNIP-positive OC lines (Figure 5.11). A possible explanation for observing low MRNIP levels could be DNA methylation. Aberrant DNA methylation-associated transcriptional silencing is widely observed in cancers [464]. It is therefore possible that the promoter that drives MRNIP expression is hypermethylated, leading to downregulation of MRNIP expression. Histone modification is another possible explanation for observing low levels of MRNIP in these cells. Methylation-driven silencing could lead to suppression of MRNIP transcription. To investigate this further, we could employ the **A**ssay for Transposase-**A**ccessible **C**hromatin with high-throughput **seq**uencing (ATAC sequencing) in UWB1-289, OVCAR-3 and U138 cells in order to examine regions of the genome with open or accessible chromatin.

In addition, depletion of MRNIP sensitised both A2780 (Figure 5.12 A) and COV362 (Figure 5.13 A) cells to HU but only COV362 cells to MMC (Figure 5.13 B). The discrepancies in MMC sensitivity between COV362 and A2780 cell lines could be because of cell line differences and if this is the case, higher doses of MCC should be used for A2780 cells. If higher doses of MMC are used and we still observe no differences between control and MRNIP depleted cells, we may suggest that the sensitivity observed following Cisplatin (Figure 5.12 C) but not MMC (Figure 5.12 B) - both of which are cross linking drugs - could be explained by the fact that these drugs cause subtly different types of damage, and that MRNIP is part of one pathway but not the other. Indeed, Cisplatin causes DNA damage of which 90% is intrastrand crosslinks (predominantly crosslinks between adjacent purine

residues on the same strand of the DNA double helix) and less than 5% is ICLs [465]. MMC also causes less than 5% ICLs [466].

In addition, loss of MRNIP sensitised A2780 cells to NU7441 (Figure 5.12 D) but rendered COV362 cells resistant to the same doses of NU7441 (Figure 5.13 C). This could be attributed to cell line-specific differences. However, these are preliminary data, and more repeats are needed alongside clonogenic assays to properly determine the role of MRNIP in chemosensitivity in this context. In addition, DNA damage levels could also be assessed in MRNIP-depleted OC lines by performing indirect immunofluorescence for 53BP1 and γH2AX markers as well as COMET assays. Our ultimate goal is to employ the MRNIP antibody as a probe in ovarian cancer tissue microarrays linked to patient data and assess MRNIP as a potential biomarker for patient survival and chemotherapeutic outcome.

7.8 PRIMPOL promotes resistance to Gemcitabine in MRNIP KO cells.

Following the observation that cells ablated of MRNIP were resistant to Gemcitabine and Cytarabine (Figure 5.1, Figure 5.5 A,B, Figure 5.6 A,B) (and based on a recent paper which demonstrates that MRE11 removes Gemcitabine from DNA [386]) we next assessed the role of MRE11 in HCT116 parental and derivative MRNIP KO cells following Gemcitabine treatment. We found that loss of MRE11 sensitised MRNIP KO cells to Gemcitabine (Figure 6.10) which is in accordance with our theory that in the absence of MRNIP, hyperactive MRE11 digests the nascent DNA and removes the lesion, which then can facilitate repair/fork restart and perhaps promote enhanced post-replicative gap filling.

Following the finding that the primase activity of PRIMPOL is important for cellular tolerance to replication stalling induced by incorporation of CTNAs and that PRIMPOL performs *in vitro* close-coupled repriming downstream of CTNAs and DNA damage lesions [419], we next assessed the role of PRIMPOL in Gemcitabine and Cisplatin sensitivity in HCT116 parental and derivative MRNIP KO cells. We found that PRIMPOL depletion restores sensitivity to MRNIP KO cells following treatment with Gemcitabine (Figure 6.11). This supports our current hypothesis that hyper-resection by MRE11 in MRNIP KO cells can remove short-gapped DNA fragments and restore TS-mediated filling of DSGs generated by repriming (Figure 7.1).

7.9 Conclusions

This project aimed to understand the role of MRNIP, an MRN interactor, in response to different chemotherapeutic drugs as well as the functionality of a series of post-translational modifications of MRE11 and MRNIP. Cells ablated of MRNIP are sensitive to CPT but resistant to Gemcitabine, the latter of which requires Ser217, which may be a potential non-canonical CDK1 site. However, the same site does not affect MRE11-mediated nascent DNA degradation following HU treatment suggesting that this phosphorylation acts in a context dependent manner. In addition, mimicking MRE11 phosphorylation at Ser676/678, which was absent in MRNIP KO cells following HU and CPT treatments, using a phospho-mimetic mutant, prevented DNA degradation suggesting that Ser676/678 is involved in limiting nascent DNA resection at reversed forks. Unexpectedly, DNA degradation was observed in parental cell lines following Gemcitabine treatment which was not due to the action of the major nucleases while MRNIP KO cells exhibited protected forks under the same treatment. Due to poor controls in the experiment, we cannot exclude the possibility of a major nuclease to be responsible for DNA resection in parental cells.

Overall, our work has revealed several important PTMs in both MRNIP and MRE11, which serve to control the activity of these factors in the context of replication. We have also made important advances towards understanding how MRNIP (and by inference MRE11) act in response to different types of replication stress induced by different classes of anti-cancer drugs. Finally, we demonstrate that MRNIP can interact with and destabilise CDK4.

References

1. Sandoval J, Esteller M. Cancer epigenomics: Beyond genomics. *Curr Opin Genet Dev*. 2012;22(1):50-55. doi:10.1016/j.gde.2012.02.008

2. Baylin SB, Jones PA. A decade of exploring the cancer epigenome-biological and translational implications. *Nat Rev Cancer*. 2011;11(10):726-734. doi:10.1038/nrc3130

3. Esteller M. *Molecular Origins of Cancer Epigenetics in Cancer*. Vol 358.; 2008.

4. Smith GL, Lopez-Olivo MA, Advani PG, et al. Financial Burdens of Cancer Treatment: A Systematic Review of Risk Factors and Outcomes. doi:10.6004/jnccn.2019.7305

5. Zaidi AA, Ansari TZ, Khan A. The financial burden of cancer: Estimates from patients undergoing cancer care in a tertiary care hospital. *Int J Equity Health*. 2012;11(1):1-6. doi:10.1186/1475-9276-11-60/TABLES/7

6. Hanahan D, Weinberg RA. The Hallmarks of Cancer. *Cell*. 2000;100(1):57-70. doi:10.1016/S0092-8674(00)81683-9

7. Nistér M, Libermann TA, Betsholtz C, et al. Expression of Messenger RNAs for Platelet-derived Growth Factor and Transforming Growth Factor-α and Their Receptors in Human Malignant Glioma Cell Lines. *Cancer Res*. 1988;48(14):3910-3918.

8. Hermanson M, Funa K, Hartman M, Westermark B, Heldin CH, Nister M. Platelet-derived Growth Factor and Its Receptors in Human Glioma Tissue: Expression of Messenger RNA and Protein Suggests the Presence of Autocrine and Paracrine Loops. *Cancer Res*. 1992;52(11):3213-3219.

9. Keller J, Shroyer KR, Batajoo SK, et al. Combination of phosphorylated and truncated EGFR correlates with higher tumor and nodal stage in head and neck cancer. *Cancer Invest*. 2010;28(10):1054-1062. doi:10.3109/07357907.2010.512602

10. Saeed O, Lopez-Beltran A, Fisher KW, et al. RAS genes in colorectal carcinoma: Pathogenesis, testing guidelines and treatment implications. *J Clin*

Pathol. 2019;72(2):135-139. doi:10.1136/jclinpath-2018-205471

11. Kastan MB, Bartek J. Cell-cycle checkpoints and cancer. *Nat 2004 4327015*. 2004;432(7015):316-323. doi:10.1038/nature03097

12. Sherr CJ, McCormick F. The RB and p53 pathways in cancer. *Cancer Cell*. 2002;2(2):103-112. doi:10.1016/S1535-6108(02)00102-2

13. Okada T, Lopez-Lago M, Giancotti FG. Merlin/NF-2 mediates contact inhibition of growth by suppressing recruitment of Rac to the plasma membrane. *J Cell Biol*. 2005;171(2):361. doi:10.1083/JCB.200503165

14. Curto M, Cole BK, Lallemand D, Liu CH, McClatchey AI. Contact-dependent inhibition of EGFR signaling by Nf2/Merlin. *J Cell Biol*. 2007;177(5):893-903. doi:10.1083/JCB.200703010

15. Hezel AF, Bardeesy N. LKB1; linking cell structure and tumor suppression. *Oncogene 2008 2755*. 2008;27(55):6908-6919. doi:10.1038/onc.2008.342

16. Partanen JI, Nieminen AI, Klefstrom J. 3D view to tumor suppression: lkb1, polarity and the arrest of oncogenic c-myc. *http://dx.doi.org/104161/cc857786*. 2009;8(5):716-724. doi:10.4161/CC.8.5.7786

17. Ikushima H, Miyazono K. TGFβ signalling: a complex web in cancer progression. *Nat Rev Cancer 2010 106*. 2010;10(6):415-424. doi:10.1038/nrc2853

18. Hayflick L. The illusion of cell immortality. *Br J Cancer*. 2000;83(7):841-846. doi:10.1054/bjoc.2000.1296

19. Wright WE, Pereira-smith OM, Shay JW, Hines Boulevard H, anid Phyllis Gough RM. Reversible cellular senescence: implications for immortalization of normal human diploid fibroblasts. *Mol Cell Biol*. 1989;9(7):3088-3092. doi:10.1128/MCB.9.7.3088-3092.1989

20. Jafri MA, Ansari SA, Alqahtani MH, Shay JW. Roles of telomeres and telomerase in cancer, and advances in telomerase-targeted therapies. *Genome Med*. 2016;8(1):1-18. doi:10.1186/s13073-016-0324-x

21. Hoang SM, O'sullivan RJ. Alternative Lengthening of Telomeres: building

bridges to connect chromosome ends. doi:10.1016/j.trecan.2019.12.009

22. Fernald K, Kurokawa M. Evading apoptosis in cancer. 2013. doi:10.1016/j.tcb.2013.07.006

23. O'Brien MA, Kirby R. Apoptosis: A review of pro-apoptotic and anti-apoptotic pathways and dysregulation in disease. *J Vet Emerg Crit Care*. 2008;18(6):572. doi:10.1111/J.1476-4431.2008.00363.X

24. Aubrey BJ, Kelly GL, Janic A, Herold MJ, Strasser A. How does p53 induce apoptosis and how does this relate to p53-mediated tumour suppression? *Cell Death Differ*. 2018;25(1):104-113. doi:10.1038/cdd.2017.169

25. Arcaro A, Guerreiro AS. *The Phosphoinositide 3-Kinase Pathway in Human Cancer: Genetic Alterations and Therapeutic Implications*. Vol 8.; 2007.

26. Hillen F, Griffioen AW. Tumour vascularization: sprouting angiogenesis and beyond. *Cancer Metastasis Rev*. 2007;26(3-4):489. doi:10.1007/S10555-007-9094-7

27. Holmgren L, O'reilly MS, Folkman J. Dormancy of micrometastases: Balanced proliferation and apoptosis in the presence of angiogenesis suppression. *Nat Med*. 1995;1(2):149-153. doi:10.1038/nm0295-149

28. Parangi S, O'Reilly M, Christofori G, et al. Antiangiogenic therapy of transgenic mice impairs de novo tumor growth. *Proc Natl Acad Sci U S A*. 1996;93(5):2002-2007. doi:10.1073/pnas.93.5.2002

29. Bottaro DP, Liotta LA. Out of air is not out of action. *Nature*. 2003;423(6940):593-595. doi:10.1038/423593a

30. Gupta MK, Qin RY. Mechanism and its regulation of tumor-induced angiogenesis. *World J Gastroenterol*. 2003;9(6):1144. doi:10.3748/WJG.V9.I6.1144

31. Van Zijl F, Krupitza G, Mikulits W. Initial steps of metastasis: Cell invasion and endothelial transmigration. *Mutat Res - Rev Mutat Res*. 2011;728(1-2):23-34. doi:10.1016/j.mrrev.2011.05.002

32. Brabletz T, Kalluri R, Nieto MA, Weinberg RA. EMT in cancer. *Nat Rev Cancer*

2018 182. 2018;18(2):128-134. doi:10.1038/nrc.2017.118

33. Jolly MK, Boareto M, Huang B, et al. Implications of the hybrid epithelial/mesenchymal phenotype in metastasis. *Front Oncol*. 2015;5(JUN). doi:10.3389/fonc.2015.00155

34. Jolly MK, Ware KE, Gilja S, Somarelli JA, Levine H. EMT and MET: necessary or permissive for metastasis? *Mol Oncol*. 2017;11(7):755. doi:10.1002/1878-0261.12083

35. Hanahan D, Weinberg RA. Hallmarks of cancer: The next generation. *Cell*. 2011;144(5):646-674. doi:10.1016/j.cell.2011.02.013

36. Eniafe J, Jiang • Shuai. The functional roles of TCA cycle metabolites in cancer. *Oncogene*. 2021;40:3351-3363. doi:10.1038/s41388-020-01639-8

37. Warburg O. The Metabolism of Carcinoma Cells. *J Cancer Res*. 1925;9(1):148-163. doi:10.1158/JCR.1925.148

38. Warburg O, Wind F, Negelein E. THE METABOLISM OF TUMORS IN THE BODY. *J Gen Physiol*. 1927;8(6):519-530. doi:10.1085/JGP.8.6.519

39. Hsu PP, Sabatini DM. Cancer cell metabolism: Warburg and beyond. *Cell*. 2008;134(5):703-707. doi:10.1016/j.cell.2008.08.021

40. Heiden MGV, Cantley LC, Thompson CB. Understanding the warburg effect: The metabolic requirements of cell proliferation. *Science (80-)*. 2009;324(5930):1029-1033. doi:10.1126/science.1160809

41. Jones RG, Thompson CB. Tumor suppressors and cell metabolism: A recipe for cancer growth. *Genes Dev*. 2009;23(5):537-548. doi:10.1101/gad.1756509

42. DeBerardinis RJ, Lum JJ, Hatzivassiliou G, Thompson CB. The Biology of Cancer: Metabolic Reprogramming Fuels Cell Growth and Proliferation. *Cell Metab*. 2008;7(1):11-20. doi:10.1016/j.cmet.2007.10.002

43. Robey RB, Hay N. Is Akt the “Warburg kinase”?-Akt-energy metabolism interactions and oncogenesis. *Semin Cancer Biol*. 2009;19(1):25-31. doi:10.1016/j.semcancer.2008.11.010

44. Elstrom RL, Bauer DE, Buzzai M, et al. Akt stimulates aerobic glycolysis in

cancer cells. *Cancer Res*. 2004;64(11):3892-3899. doi:10.1158/0008-5472.CAN-03-2904

45. Ehrlich P. Uber den jetzigen Stand der Karzinomforschung. *Ned Tijdschr Geneeskd*. 1909;(5):273-290.

46. Schreiber RD, Old LJ, Smyth MJ. Cancer immunoediting: integrating immunity's roles in cancer suppression and promotion. *Science*. 2011;331(6024):1565-1570. doi:10.1126/SCIENCE.1203486

47. Dunn GP, Old LJ, Schreiber RD. The immunobiology of cancer immunosurveillance and immunoediting. *Immunity*. 2004;21(2):137-148. doi:10.1016/J.IMMUNI.2004.07.017

48. Teng MWL, Galon J, Fridman WH, Smyth MJ. From mice to humans: developments in cancer immunoediting. *J Clin Invest*. 2015;125(9):3338-3346. doi:10.1172/JCI80004

49. Rabinovich GA, Gabrilovich D, Sotomayor EM. IMMUNOSUPPRESSIVE STRATEGIES THAT ARE MEDIATED BY TUMOR CELLS. doi:10.1146/annurev.immunol.25.022106.141609

50. de Visser KE, Coussens LM. The inflammatory tumor microenvironment and its impact on cancer development. *Contrib Microbiol*. 2006;13:118-137. doi:10.1159/000092969

51. Lin WW, Karin M. A cytokine-mediated link between innate immunity, inflammation, and cancer. *J Clin Invest*. 2007;117(5):1175-1183. doi:10.1172/JCI31537

52. Lippitz BE. Cytokine patterns in patients with cancer: A systematic review. *Lancet Oncol*. 2013;14(6):e218-e228. doi:10.1016/S1470-2045(12)70582-X

53. Balamurugan K. HIF-1 at the crossroads of hypoxia, inflammation, and cancer. *Int J Cancer*. 2016;138(5):1058-1066. doi:10.1002/ijc.29519

54. Tang D, Tao D, Fang Y, Deng C, Xu Q, Zhou J. TNF-Alpha Promotes Invasion and Metastasis via NF-Kappa B Pathway in Oral Squamous Cell Carcinoma. *Med Sci Monit Basic Res*. 2017;23:141-149. doi:10.12659/msmbr.903910

55. Lonkar P, Dedon PC. Reactive species and DNA damage in chronic inflammation: Reconciling chemical mechanisms and biological fates. *Int J Cancer*. 2011;128(9):1999-2009. doi:10.1002/ijc.25815

56. Güngör N, Godschalk RWL, Pachen DM, Van Schooten FJ, Knaapen AM. Activated neutrophils inhibit nucleotide excision repair in human pulmonary epithelial cells: role of myeloperoxidase. *FASEB J*. 2007;21(10):2359-2367. doi:10.1096/fj.07-8163com

57. Condeelis J, Pollard JW. Macrophages: Obligate partners for tumor cell migration, invasion, and metastasis. *Cell*. 2006;124(2):263-266. doi:10.1016/j.cell.2006.01.007

58. Fu XT, Dai Z, Song K, et al. Macrophage-secreted IL-8 induces epithelial-mesenchymal transition in hepatocellular carcinoma cells by activating the JAK2/STAT3/Snail pathway. *Int J Oncol*. 2015;46(2):587-596. doi:10.3892/ijo.2014.2761

59. Cai J, Xia L, Li J, Ni S, Song H, Wu X. Tumor-associated macrophages derived TGF-β-induced epithelial to mesenchymal transition in colorectal cancer cells through Smad2,3-4/Snail signaling pathway. *Cancer Res Treat*. 2019;51(1):252-256. doi:10.4143/crt.2017.613

60. Gocheva V, Wang HW, Gadea BB, et al. IL-4 induces cathepsin protease activity in tumor-associated macrophages to promote cancer growth and invasion. *Genes Dev*. 2010;24(3):241-255. doi:10.1101/gad.1874010

61. Vasiljeva O, Papazoglou A, Krüger A, et al. Tumor cell-derived and macrophage-derived cathepsin B promotes progression and lung metastasis of mammary cancer. *Cancer Res*. 2006;66(10):5242-5250. doi:10.1158/0008-5472.CAN-05-4463

62. James BP, Sicheng W, Qiang P-H, Marianne Q-J. Secretion of matrix metalloproteinase-9 by macrophages, *in vitro* , in response to *Helicobacter pylori*. *FEMS Immunol Med Microbiol*. 2005;45(2):159-169. doi:10.1016/j.femsim.2005.03.008

63. Gorgoulis VG, Vassiliou LVF, Karakaidos P, et al. Activation of the DNA

damage checkpoint and genomic instability in human precancerous lesions. *Nature*. 2005;434(7035):907-913. doi:10.1038/nature03485

64. Aguilera A, Gómez-González B. Genome instability: A mechanistic view of its causes and consequences. *Nat Rev Genet*. 2008;9(3):204-217. doi:10.1038/nrg2268

65. Langie SAS, Koppen G, Desaulniers D, et al. Causes of genome instability: the effect of low dose chemical exposures in modern society. *Carcinogenesis*. 2015;36. doi:10.1093/carcin/bgv031

66. Knudson AG. Mutation and cancer: statistical study of retinoblastoma. *Proc Natl Acad Sci U S A*. 1971;68(4):820-823. doi:10.1073/pnas.68.4.820

67. Hanel W, Moll UM. Links between mutant p53 and genomic instability. *J Cell Biochem*. 2012;113(2):433-439. doi:10.1002/jcb.23400

68. Li FP, Fraumeni JF. Soft-tissue sarcomas, breast cancer, and other neoplasms. A familial syndrome? *Ann Intern Med*. 1969;71(4):747-752. doi:10.7326/0003-4819-71-4-747

69. Blumenfeld B, Ben-Zimra M, Simon I. Perturbations in the Replication Program Contribute to Genomic Instability in Cancer. *Int J Mol Sci*. 2017;18(6):1138. doi:10.3390/ijms18061138

70. Arlt MF, Durkin SG, Ragland RL, Glover TW. Common fragile sites as targets for chromosome rearrangements. *DNA Repair (Amst)*. 2006;5(9-10):1126-1135. doi:10.1016/j.dnarep.2006.05.010

71. Lehmann AR, McGibbon D, Stefanini M. Xeroderma pigmentosum. *Orphanet J Rare Dis*. 2011;6(1):70. doi:10.1186/1750-1172-6-70

72. Rapin I, Weidenheim K, Lindenbaum Y, et al. Cockayne Syndrome in Adults: Review With Clinical and Pathologic Study of a New Case. *J Child Neurol*. 2006;21(11):991-1006. doi:10.1177/08830738060210110101

73. Pino MS, Mino-Kenudson M, Wildemore BM, et al. Deficient DNA mismatch repair is common in Lynch syndrome-associated colorectal adenomas. *J Mol Diagnostics*. 2009;11(3):238-247. doi:10.2353/jmoldx.2009.080142

74. Murphy MA, Wentzensen N. Frequency of mismatch repair deficiency in ovarian cancer: A systematic review This article is a US Government work and, as such, is in the public domain of the United States of America. *Int J Cancer*. 2011;129(8):1914-1922. doi:10.1002/ijc.25835

75. Fusco N, Lopez G, Corti C, et al. Mismatch Repair Protein Loss as a Prognostic and Predictive Biomarker in Breast Cancers Regardless of Microsatellite Instability. *JNCI Cancer Spectr*. 2018;2(4). doi:10.1093/JNCICS/PKY056

76. Luo J. WRN Protein and Werner Syndrome. *Am Chinese J Med Sci*. 2010;3(4):205. doi:10.7156/v3i4p205

77. Cunniff C, Bassetti JA, Ellis NA. Bloom's Syndrome: Clinical Spectrum, Molecular Pathogenesis, and Cancer Predisposition. *Mol Syndromol*. 2017;8(1):4-23. doi:10.1159/000452082

78. Sumpter R, Levine B. Emerging functions of the Fanconi anemia pathway at a glance. *J Cell Sci*. 2017;130(16):2657-2662. doi:10.1242/jcs.204909

79. Amirifar P, Ranjouri MR, Yazdani R, Abolhassani H, Aghamohammadi A. Ataxia-telangiectasia: A review of clinical features and molecular pathology. *Pediatr Allergy Immunol*. 2019;30(3):277-288. doi:10.1111/pai.13020

80. Faivre L, Le Merrer M, Lyonnet S, et al. Clinical and genetic heterogeneity of Seckel syndrome. *Am J Med Genet*. 2002;112(4):379-383. doi:10.1002/ajmg.10677

81. Heikkinen K, Mansikka V, Karppinen SM, Rapakko K, Winqvist R. Mutation analysis of the ATR gene in breast and ovarian cancer families. *Breast Cancer Res*. 2005;7(4):R495. doi:10.1186/bcr1037

82. Hanahan D. Hallmarks of Cancer: New Dimensions. *Cancer Discov*. 2022;12(1):31-46. doi:10.1158/2159-8290.CD-21-1059

83. Yuan S, Norgard RJ, Stanger BZ. Cellular Plasticity in Cancer. *Cancer Discov*. 2019;9(7):837. doi:10.1158/2159-8290.CD-19-0015

84. Ordóñez-Morán P, Dafflon C, Imajo M, Nishida E, Huelsken J. HOXA5 Counteracts Stem Cell Traits by Inhibiting Wnt Signaling in Colorectal Cancer.

Cancer Cell. 2015;28(6):815-829. doi:10.1016/J.CCELL.2015.11.001

85. Tan SH, Barker N. Stemming Colorectal Cancer Growth and Metastasis: HOXA5 Forces Cancer Stem Cells to Differentiate. *Cancer Cell*. 2015;28(6):683-685. doi:10.1016/J.CCELL.2015.11.004

86. Perekatt AO, Shah PP, Cheung S, et al. SMAD4 suppresses WNt-driven dedifferentiation and oncogenesis in the differentiated gut epithelium. *Cancer Res*. 2018;78(17):4878-4890. doi:10.1158/0008-5472.CAN-18-0043/653209/AM/SMAD4-SUPPRESSES-WNT-DRIVEN-DE-DIFFERENTIATION-AND

87. Kaufman CK, Mosimann C, Fan ZP, et al. A zebrafish melanoma model reveals emergence of neural crest identity during melanoma initiation. *Science*. 2016;351(6272):aad2197. doi:10.1126/SCIENCE.AAD2197

88. Krah NM, Narayanan SM, Yugawa DE, et al. Prevention and Reversion of Pancreatic Tumorigenesis through a Differentiation-Based Mechanism. *Dev Cell*. 2019;50(6):744-754.e4. doi:10.1016/J.DEVCEL.2019.07.012

89. Thienpont B, Van Dyck L, Lambrechts D. Tumors smother their epigenome. *Mol Cell Oncol*. 2016;3(6). doi:10.1080/23723556.2016.1240549

90. Bakir B, Chiarella AM, Pitarresi JR, Rustgi AK. EMT, MET, plasticity and tumor metastasis. *Trends Cell Biol*. 2020;30(10):764. doi:10.1016/J.TCB.2020.07.003

91. Gupta PB, Pastushenko I, Skibinski A, Blanpain C, Kuperwasser C. Phenotypic Plasticity: Driver of Cancer Initiation, Progression, and Therapy Resistance. *Cell Stem Cell*. 2019;24(1):65-78. doi:10.1016/J.STEM.2018.11.011

92. Heyn H, Vidal E, Ferreira HJ, et al. Epigenomic analysis detects aberrant super-enhancer DNA methylation in human cancer. *Genome Biol*. 2016;17(1). doi:10.1186/S13059-016-0879-2

93. Saghafinia S, Mina M, Riggi N, Hanahan D, Ciriello G. Pan-Cancer Landscape of Aberrant DNA Methylation across Human Tumors. *Cell Rep*. 2018;25(4):1066-1080.e8. doi:10.1016/J.CELREP.2018.09.082

94. Audia JE, Campbell RM. Histone Modifications and Cancer. *Cold Spring Harb Perspect Biol*. 2016;8(4). doi:10.1101/CSHPERSPECT.A019521

95. Corces MR, Granja JM, Shams S, et al. The chromatin accessibility landscape of primary human cancers. *Science*. 2018;362(6413). doi:10.1126/SCIENCE.AAV1898

96. Janin M, Coll-SanMartin L, Esteller M. Disruption of the RNA modifications that target the ribosome translation machinery in human cancer. doi:10.1186/s12943-020-01192-8

97. Esteve-Puig R, Bueno-Costa A, Esteller M. Writers, readers and erasers of RNA modifications in cancer. *Cancer Lett*. 2020;474:127-137. doi:10.1016/J.CANLET.2020.01.021

98. Bhatt AP, Redinbo MR, Bultman SJ. The Role of the Microbiome in Cancer Development and Therapy. *CA Cancer J Clin*. 2017;67(4):326. doi:10.3322/CAAC.21398

99. Okumura S, Konishi Y, Narukawa M, et al. Gut bacteria identified in colorectal cancer patients promote tumourigenesis via butyrate secretion. *Nat Commun 2021 121*. 2021;12(1):1-14. doi:10.1038/s41467-021-25965-x

100. Zhang Q, Ma C, Duan Y, et al. Gut Microbiome Directs Hepatocytes to Recruit MDSCs and Promote Cholangiocarcinoma. *Cancer Discov*. 2021;11(5):1248-1267. doi:10.1158/2159-8290.CD-20-0304

101. Lee S, Schmitt CA. The dynamic nature of senescence in cancer. *Nat Cell Biol 2019 211*. 2019;21(1):94-101. doi:10.1038/s41556-018-0249-2

102. Wang B, Kohli J, Demaria M. Senescent Cells in Cancer Therapy: Friends or Foes? *Trends in cancer*. 2020;6(10):838-857. doi:10.1016/J.TRECAN.2020.05.004

103. Kowald A, Passos JF, Kirkwood TBL. On the evolution of cellular senescence. *Aging Cell*. 2020;19(12). doi:10.1111/ACEL.13270

104. Faget D V, Ren Q, Stewart SA. Unmasking senescence: context-dependent effects of SASP in cancer. *Nat Rev Cancer*. doi:10.1038/s41568-019-0156-2

105. Birch J, Gil J. Senescence and the SASP: many therapeutic avenues. *Genes Dev*. 2020;34(23-24):1565-1576. doi:10.1101/GAD.343129.120

106. Alberts B, Johnson A, Lewis J, Raff M, Roberts K, Walter P. DNA Replication Mechanisms. 2002.

107. Randell JCW, Bowers JL, Rodríguez HK, Bell SP. Sequential ATP hydrolysis by Cdc6 and ORC directs loading of the Mcm2-7 helicase. *Mol Cell*. 2006;21(1):29-39. doi:10.1016/j.molcel.2005.11.023

108. Speck C, Chen Z, Li H, Stillman B. ATPase-dependent cooperative binding of ORC and Cdc6 to origin DNA. *Nat Struct Mol Biol*. 2005;12(11):965-971. doi:10.1038/nsmb1002

109. Frigola J, He J, Kinkelin K, et al. Cdt1 stabilizes an open MCM ring for helicase loading. *Nat Commun*. 2017;8. doi:10.1038/ncomms15720

110. Thu YM, Bielinsky AK. Enigmatic roles of Mcm10 in DNA replication. *Trends Biochem Sci*. 2013;38(4):184-194. doi:10.1016/j.tibs.2012.12.003

111. Lodish H, Berk A, Zipursky SL, Matsudaira P, Baltimore D, Darnell J. The Role of Topoisomerases in DNA Replication. 2000.

112. Goedecke W. DNA polymerases. In: *XPharm: The Comprehensive Pharmacology Reference*. Elsevier Inc.; 2007:1-2. doi:10.1016/B978-008055232-3.62996-4

113. Stodola JL, Burgers PM. Resolving individual steps of Okazaki-fragment maturation at a millisecond timescale. *Nat Struct Mol Biol*. 2016;23(5):402-408. doi:10.1038/nsmb.3207

114. McCulloch SD, Kunkel TA. The fidelity of DNA synthesis by eukaryotic replicative and translesion synthesis polymerases. *Cell Res*. 2008;18(1):148-161. doi:10.1038/cr.2008.4

115. Kunkel TA. Evolving views of DNA replication (in)fidelity. In: *Cold Spring Harbor Symposia on Quantitative Biology*. Vol 74. NIH Public Access; 2009:91-101. doi:10.1101/sqb.2009.74.027

116. Nurse P. Cyclin dependent kinases and regulation of the fission yeast cell cycle. *Biol Chem*. 1999;380(7-8):729-733. doi:10.1515/BC.1999.093/MACHINEREADABLECITATION/RIS

117. Nurse P, Thuriaux P. Regulatory genes controlling mitosis in the fission yeast Schizosaccharomyces pombe. *Genetics*. 1980;96(3):627-637. doi:10.1093/GENETICS/96.3.627

118. Nurse P, Thuriaux P, Nasmyth K. *Genetic Control of the Cell Division Cycle in the Fission Yeast Schizosaccharomyces Pombe*. Vol 146.; 1976.

119. Beach D, Durkacz B, Nurse P. *Functionally Homologous Cell Cycle Control Genes in Budding and Fission Yeast*. Vol 300.; 1982.

120. Malumbres M, Barbacid M. Cell cycle, CDKs and cancer: a changing paradigm. *Nat Rev Cancer 2009 93*. 2009;9(3):153-166. doi:10.1038/nrc2602

121. Satyanarayana A, Kaldis P. Mammalian cell-cycle regulation: several Cdks, numerous cyclins and diverse compensatory mechanisms. *Oncogene*. 2009;28:2925-2939. doi:10.1038/onc.2009.170

122. Narasimha AM, Kaulich M, Shapiro GS, Choi YJ, Sicinski P, Dowdy SF. Cyclin D activates the Rb tumor suppressor by mono-phosphorylation. *Elife*. 2014;3. doi:10.7554/ELIFE.02872

123. Baker SJ, Reddy EP. CDK4: A Key Player in the Cell Cycle, Development, and Cancer. *Genes Cancer*. 2012;3(11-12):658-669. doi:10.1177/1947601913478972

124. Shapiro GI. Cyclin-dependent kinase pathways as targets for cancer treatment. *J Clin Oncol*. 2006;24(11):1770-1783. doi:10.1200/JCO.2005.03.7689

125. Ortega S, Malumbres M, Barbacid M. Cyclin D-dependent kinases, INK4 inhibitors and cancer. *Biochim Biophys Acta - Rev Cancer*. 2002;1602(1):73-87. doi:10.1016/S0304-419X(02)00037-9

126. Malumbres M, Barbacid M. Cell cycle, CDKs and cancer: a changing paradigm. *Nat Rev Cancer 2009 93*. 2009;9(3):153-166. doi:10.1038/nrc2602

127. Harper JW, Adams PD. Cyclin-dependent kinases. *Chem Rev*. 2001;101(8):2511-2526. doi:10.1021/CR0001030

128. Schwartz GK, Shah MA. Targeting the cell cycle: A new approach to cancer therapy. *J Clin Oncol*. 2005;23(36):9408-9421. doi:10.1200/JCO.2005.01.5594

129. Sever R, Brugge JS. Signal transduction in cancer. *Cold Spring Harb Perspect Med*. 2015;5(4). doi:10.1101/cshperspect.a006098

130. Marei HE, Althani A, Afifi N, et al. p53 signaling in cancer progression and therapy. *Cancer Cell Int*. 2021;21(1):1-15. doi:10.1186/S12935-021-02396-8/FIGURES/4

131. Branzei D, Foiani M. Maintaining genome stability at the replication fork. *Nat Rev Mol Cell Biol*. 2010;11(3):208-219. doi:10.1038/nrm2852

132. Zeman MK, Cimprich KA. Causes and consequences of replication stress. *Nat Cell Biol*. 2014;16(1):2-9. doi:10.1038/ncb2897

133. Khurana S, Oberdoerffer P. Replication Stress: A Lifetime of Epigenetic Change. *Genes (Basel)*. 2015;6(3):858-877. doi:10.3390/genes6030858

134. Kotsantis P, Petermann E, Boulton SJ. Mechanisms of Oncogene-Induced Replication Stress: Jigsaw Falling into Place. *Cancer Discov*. 2018;8(5):537-555. doi:10.1158/2159-8290.CD-17-1461

135. Macheret M, Halazonetis TD. Intragenic origins due to short G1 phases underlie oncogene-induced DNA replication stress. *Nature*. 2018;555(7694):112-116. doi:10.1038/NATURE25507

136. Bretones G, Delgado MD, León J. Myc and cell cycle control. *Biochim Biophys Acta - Gene Regul Mech*. 2015;1849(5):506-516. doi:10.1016/j.bbagrm.2014.03.013

137. Spruck CH, Won KA, Reed SI. Deregulated cyclin E induces chromosome instability. *Nature*. 1999;401(6750):297-300. doi:10.1038/45836

138. Ekholm-Reed S, Méndez J, Tedesco D, Zetterberg A, Stillman B, Reed SI. Deregulation of cyclin E in human cells interferes with prereplication complex assembly. *J Cell Biol*. 2004;165(6):789-800. doi:10.1083/jcb.200404092

139. Bester AC, Roniger M, Oren YS, et al. Nucleotide deficiency promotes genomic instability in early stages of cancer development. *Cell*. 2011;145(3):435-446. doi:10.1016/j.cell.2011.03.044

140. Jones RM, Mortusewicz O, Afzal I, et al. Increased replication initiation and

conflicts with transcription underlie Cyclin E-induced replication stress. *Oncogene*. 2013;32(32):3744-3753. doi:10.1038/onc.2012.387

141. Shimura T, Ochiai Y, Noma N, Oikawa T, Sano Y, Fukumoto M. Cyclin D1 overexpression perturbs DNA replication and induces replication-associated DNA double-strand breaks in acquired radioresistant cells. *Cell Cycle*. 2013;12(5):773-782. doi:10.4161/cc.23719

142. Liu P, Slater DM, Lenburg M, Nevis K, Cook JG, Vaziri C. Replication licensing promotes cyclin D1 expression and G1 progression in untransformed human cells. *Cell Cycle*. 2009;8(1):125-136. doi:10.4161/cc.8.1.7528

143. Steckel M, Molina-Arcas M, Weigelt B, et al. Determination of synthetic lethal interactions in KRAS oncogene-dependent cancer cells reveals novel therapeutic targeting strategies. *Cell Res*. 2012;22(8):1227-1245. doi:10.1038/cr.2012.82

144. Zimmerman KM, Jones RM, Petermann E, Jeggo PA. Diminished origin-licensing capacity specifically sensitizes tumor cells to replication stress. *Mol Cancer Res*. 2013;11(4):370-380. doi:10.1158/1541-7786.MCR-12-0491

145. Di Micco R, Fumagalli M, Cicalese A, et al. Oncogene-induced senescence is a DNA damage response triggered by DNA hyper-replication. *Nature*. 2006;444(7119):638-642. doi:10.1038/nature05327

146. Singhal G, Leo E, Setty SKG, Pommier Y, Thimmapaya B. Adenovirus E1A Oncogene Induces Rereplication of Cellular DNA and Alters DNA Replication Dynamics. *J Virol*. 2013;87(15):8767-8778. doi:10.1128/jvi.00879-13

147. Kotsantis P, Silva LM, Irmscher S, et al. Increased global transcription activity as a mechanism of replication stress in cancer. *Nat Commun*. 2016;7:13087. doi:10.1038/ncomms13087

148. Labib K, Hodgson B. Replication fork barriers: Pausing for a break or stalling for time? *EMBO Rep*. 2007;8(4):346-353. doi:10.1038/sj.embor.7400940

149. Lucca C, Vanoli F, Cotta-Ramusino C, et al. Checkpoint-mediated control of replisome-fork association and signalling in response to replication pausing. *Oncogene*. 2004;23(6):1206-1213. doi:10.1038/sj.onc.1207199

150. Meister P, Taddei A, Vernis L, Poidevin M, Gasser SM, Baldacci G. Temporal separation of replication and recombination requires the intra-S checkpoint. *J Cell Biol*. 2005;168(4):537-544. doi:10.1083/jcb.200410006

151. Tourrière H, Pasero P. Maintenance of fork integrity at damaged DNA and natural pause sites. *DNA Repair (Amst)*. 2007;6(7):900-913. doi:10.1016/j.dnarep.2007.02.004

152. Cheung-Ong K, Giaever G, Nislow C. DNA-Damaging Agents in Cancer Chemotherapy: Serendipity and Chemical Biology. *Chem Biol*. 2013;20(5):648-659. doi:10.1016/J.CHEMBIOL.2013.04.007

153. Choi J-S, Berdis A. Combating resistance to DNA damaging agents. *Oncoscience*. 2018;5(5-6):134. doi:10.18632/ONCOSCIENCE.423

154. Biersack B. Interplay of non-coding RNAs and approved antimetabolites such as gemcitabine and pemetrexed in mesothelioma. *Non-coding RNA Res*. 2018;3(4):213. doi:10.1016/J.NCRNA.2018.11.001

155. (7) (PDF) Pharmacokinetics and Pharmacodynamics of Plasma Clofarabine and Cellular Clofarabine Triphosphate in Patients with Acute Leukemias. https://www.researchgate.net/publication/8942860_Pharmacokinetics_and_Pharmacodynamics_of_Plasma_Clofarabine_and_Cellular_Clofarabine_Triphosphate_in_Patients_with_Acute_Leukemias/figures?lo=1&utm_source=google&utm_medium=organic. Accessed August 15, 2023.

156. Ciccolini J, Serdjebi C, Peters GJ, Giovannetti E. Pharmacokinetics and pharmacogenetics of Gemcitabine as a mainstay in adult and pediatric oncology: an EORTC-PAMM perspective. *Cancer Chemother Pharmacol*. 2016;78(1):1. doi:10.1007/S00280-016-3003-0

157. Fowler JD, Brown JA, Johnson KA, Suo Z. Kinetic investigation of the inhibitory effect of gemcitabine on DNA polymerization catalyzed by human mitochondrial DNA polymerase. *J Biol Chem*. 2008;283(22):15339-15348. doi:10.1074/jbc.M800310200

158. Jiang HY, Hickey RJ, Abdel-Aziz W, et al. *Effects of Gemcitabine and AraC on in Vitro DNA Synthesis Mediated by the Human Breast Cell DNA Synthesome*.

Vol 45. Springer-Verlag; 2000.

159. Wang J, Lohman GJS, Stubbe J. Enhanced subunit interactions with gemcitabine-5-diphosphate inhibit ribonucleotide reductases. 2007. www.pnas.org/cgi/content/full/. Accessed August 19, 2022.

160. Bergman AM, Pinedo HM, Peters GJ. Determinants of resistance to 2′,2′-difluorodeoxycytidine (gemcitabine). *Drug Resist Updat*. 2002;5(1):19-33. doi:10.1016/S1368-7646(02)00002-X

161. Ruiz van Haperen VWT, Veerman G, Vermorken JB, Peters GJ. 2',2'-Difluoro-deoxycytidine (gemcitabine) incorporation into RNA and DNA of tumour cell lines. *Biochem Pharmacol*. 1993;46(4):762-766. doi:10.1016/0006-2952(93)90566-F

162. Fowler JD, Brown JA, Johnson KA, Suo Z. Kinetic Investigation of the Inhibitory Effect of Gemcitabine on DNA Polymerization Catalyzed by Human Mitochondrial DNA Polymerase. *J Biol Chem*. 2008;283(22):15339. doi:10.1074/JBC.M800310200

163. Toschi L, Finocchiaro G, Bartolini S, Gioia V, Cappuzzo F. Role of gemcitabine in cancer therapy. *Future Oncol*. 2005;1(1):7-17. doi:10.1517/14796694.1.1.7

164. Byun TS, Pacek M, Yee MC, Walter JC, Cimprich KA. Functional uncoupling of MCM helicase and DNA polymerase activities activates the ATR-dependent checkpoint. *Genes Dev*. 2005;19(9):1040-1052. doi:10.1101/gad.1301205

165. Chen R, Wold MS. Replication protein A: Single-stranded DNA's first responder: Dynamic DNA-interactions allow replication protein A to direct single-strand DNA intermediates into different pathways for synthesis or repair Prospects & Overviews R. Chen and M. S. Wold. *BioEssays*. 2014;36(12):1156-1161. doi:10.1002/bies.201400107

166. Saldivar JC, Cortez D, Cimprich KA. The essential kinase ATR: Ensuring faithful duplication of a challenging genome. *Nat Rev Mol Cell Biol*. 2017;18(10):622-636. doi:10.1038/nrm.2017.67

167. Delacroix S, Wagner JM, Kobayashi M, Yamamoto KI, Karnitz LM. The Rad9-Hus1-Rad1 (9-1-1) clamp activates checkpoint signaling via TopBP1. *Genes*

Dev. 2007;21(12):1472-1477. doi:10.1101/gad.1547007

168. Kumagai A, Lee J, Yoo HY, Dunphy WG. TopBP1 Activates the ATR-ATRIP Complex. *Cell*. 2006;124(5):943-955. doi:10.1016/J.CELL.2005.12.041

169. Feng S, Zhao Y, Xu Y, et al. Ewing tumor-associated antigen 1 interacts with replication protein A to promote restart of stalled replication forks. *J Biol Chem*. 2016;291(42):21956-21962. doi:10.1074/jbc.C116.747758

170. Cortez D, Guntuku S, Qin J, Elledge SJ. ATR and ATRIP: Partners in checkpoint signaling. *Science (80-)*. 2001;294(5547):1713-1716. doi:10.1126/science.1065521

171. Zou L, Elledge SJ. Sensing DNA damage through ATRIP recognition of RPA-ssDNA complexes. *Science (80-)*. 2003;300(5625):1542-1548. doi:10.1126/science.1083430

172. Maréchal A, Li JM, Ji XY, et al. PRP19 Transforms into a Sensor of RPA-ssDNA after DNA Damage and Drives ATR Activation via a Ubiquitin-Mediated Circuitry. *Mol Cell*. 2014;53(2):235-246. doi:10.1016/j.molcel.2013.11.002

173. Ashton NW, Bolderson E, Cubeddu L, O'Byrne KJ, Richard DJ. Human single-stranded DNA binding proteins are essential for maintaining genomic stability. *BMC Mol Biol*. 2013;14(1):9. doi:10.1186/1471-2199-14-9

174. Ellison V, Stillman B. Biochemical Characterization of DNA Damage Checkpoint Complexes: Clamp Loader and Clamp Complexes with Specificity for 5′ Recessed DNA. James E. Haber, ed. *PLoS Biol*. 2003;1(2):e33. doi:10.1371/journal.pbio.0000033

175. St.Onge RP, Besley BDA, Pelley JL, Davey S. A role for the phosphorylation of hRad9 in checkpoint signaling. *J Biol Chem*. 2003;278(29):26620-26628. doi:10.1074/jbc.M303134200

176. Choi JH, Lindsey-Boltz LA, Kemp M, Mason AC, Wold MS, Sancar A. Reconstitution of RPA-covered single-stranded DNA-activated ATR-Chk1 signaling. *Proc Natl Acad Sci U S A*. 2010;107(31):13660-13665. doi:10.1073/pnas.1007856107

177. Cotta-Ramusino C, McDonald ER, Hurov K, Sowa ME, Harper JW, Elledge SJ.

A DNA damage response screen identifies RHINO, a 9-1-1 and topBP1 interacting protein required for ATR signaling. *Science (80-)*. 2011;332(6035):1313-1317. doi:10.1126/science.1203430

178. Lindsey-Boltz LA, Kemp MG, Capp C, Sancar A. RHINO forms a stoichiometric complex with the 9-1-1 checkpoint clamp and mediates ATR-Chk1 signaling http://www.tandfonline.com/doi/pdf/10.4161/15384101.2014.967076. *Cell Cycle*. 2015;14(1):99-108. doi:10.4161/15384101.2014.967076

179. Dalal SN, Schweitzer CM, Gan J, Decaprio JA. *Cytoplasmic Localization of Human Cdc25C during Interphase Requires an Intact 14-3-3 Binding Site*. Vol 19.; 1999. http://mcb.asm.org/.

180. Goloudina A, Yamaguchi H, Chervyakova DB, Appella E, Fornace AJ, Bulavin D V. Regulation of human Cdc25A stability by Serine 75 phosphorylation is not sufficient to activate a S phase checkpoint. *Cell Cycle*. 2003;2(5):471-476. doi:10.4161/CC.2.5.482

181. Sørensen CS, Syljuåsen RG, Falck J, et al. Chk1 regulates the S phase checkpoint by coupling the physiological turnover and ionizing radiation-induced accelerated proteolysis of Cdc25A. *Cancer Cell*. 2003;3(3):247-258. doi:10.1016/S1535-6108(03)00048-5

182. Xiao Z, Chen Z, Gunasekera AH, et al. Chk1 Mediates S and G2 Arrests through Cdc25A Degradation in Response to DNA-damaging Agents. *J Biol Chem*. 2003;278(24):21767-21773. doi:10.1074/JBC.M300229200

183. Schmitt E, Boutros R, Froment C, Monsarrat B, Ducommun B, Dozier C. CHK1 phosphorylates CDC25B during the cell cycle in the absence of DNA damage. *J Cell Sci*. 2006;119(20):4269-4275. doi:10.1242/JCS.03200

184. Toledo LI, Altmeyer M, Rask MB, et al. ATR prohibits replication catastrophe by preventing global exhaustion of RPA. *Cell*. 2014;156(1-2):374. doi:10.1016/j.cell.2014.01.001

185. Vesela E, Chroma K, Turi Z, Mistrik M. Common chemical inductors of replication stress: Focus on cell-based studies. *Biomolecules*. 2017;7(1). doi:10.3390/biom7010019

186. Chatterjee N, Walker GC. Mechanisms of DNA damage, repair and mutagenesis. doi:10.1002/em.22087

187. Zhou B-BS, Elledge SJ. The DNA damage response: putting checkpoints in perspective. *Nature*. 2000;408(6811):433-439. doi:10.1038/35044005

188. Harper JW, Elledge SJ. The DNA Damage Response: Ten Years After. *Mol Cell*. 2007;28(5):739-745. doi:10.1016/j.molcel.2007.11.015

189. Maréchal A, Zou L. DNA damage sensing by the ATM and ATR kinases. *Cold Spring Harb Perspect Biol*. 2013;5(9). doi:10.1101/cshperspect.a012716

190. Cimprich KA, Cortez D. ATR: An Essential Regulator of Genome Integrity. *Nat Rev Mol Cell Biol*. 2008;9(8):616. doi:10.1038/NRM2450

191. Bakkenist CJ, Kastan MB. DNA damage activates ATM through intermolecular autophosphorylation and dimer dissociation. *Nature*. 2003;421(6922):499-506. doi:10.1038/nature01368

192. So S, Davis AJ, Chen DJ. Autophosphorylation at serine 1981 stabilizes ATM at DNA damage sites. *J Cell Biol*. 2009;187(7):977-990. doi:10.1083/jcb.200906064

193. Kozlov S V., Graham ME, Peng C, Chen P, Robinson PJ, Lavin MF. Involvement of novel autophosphorylation sites in ATM activation. *EMBO J*. 2006;25(15):3504-3514. doi:10.1038/sj.emboj.7601231

194. Sun Y, Xu Y, Roy K, Price BD. DNA Damage-Induced Acetylation of Lysine 3016 of ATM Activates ATM Kinase Activity. *Mol Cell Biol*. 2007;27(24):8502-8509. doi:10.1128/mcb.01382-07

195. Berkovich E, Monnat RJ, Kastan MB. Roles of ATM and NBS1 in chromatin structure modulation and DNA double-strand break repair. *Nat Cell Biol*. 2007;9(6):683-690. doi:10.1038/ncb1599

196. Reinhardt HC, Yaffe MB. Kinases that control the cell cycle in response to DNA damage: Chk1, Chk2, and MK2. *Curr Opin Cell Biol*. 2009;21(2):245-255. doi:10.1016/j.ceb.2009.01.018

197. Gatei M, Sloper K, Sörensen C, et al. Ataxia-telangiectasia-mutated (ATM) and

NBS1-dependent phosphorylation of Chk1 on Ser-317 in response to ionizing radiation. *J Biol Chem*. 2003;278(17):14806-14811. doi:10.1074/jbc.M210862200

198. Doksani Y, Bermejo R, Fiorani S, Haber JE, Foiani M. Replicon Dynamics, Dormant Origin Firing, and Terminal Fork Integrity after Double-Strand Break Formation. *Cell*. 2009;137(2):247-258. doi:10.1016/j.cell.2009.02.016

199. Jazayeri A, Falck J, Lukas C, et al. ATM- and cell cycle-dependent regulation of ATR in response to DNA double-strand breaks. *Nat Cell Biol*. 2006;8(1):37-45. doi:10.1038/ncb1337

200. De Klein A, Muijtjens M, Van Os R, et al. Targeted disruption of the cell-cycle checkpoint gene ATR leads to early embryonic lethality in mice. *Curr Biol*. 2000;10(8):479-482. doi:10.1016/S0960-9822(00)00447-4

201. Brown EJ, Baltimore D. *ATR Disruption Leads to Chromosomal Fragmentation and Early Embryonic Lethality*.; 2000. www.genesdev.org.

202. Trenner A, Sartori AA. Harnessing DNA Double-Strand Break Repair for Cancer Treatment. *Front Oncol*. 2019;9:1388. doi:10.3389/FONC.2019.01388

203. Lieber MR. Mechanisms of human lymphoid chromosomal translocations. *Nat Rev Cancer*. 2016;16(6):387-398. doi:10.1038/nrc.2016.40

204. Symington LS, Gautier J. Double-Strand Break End Resection and Repair Pathway Choice. *Annu Rev Genet*. 2011;45(1):247-271. doi:10.1146/annurev-genet-110410-132435

205. Wyman C, Kanaar R. DNA Double-Strand Break Repair: All's Well that Ends Well. *Annu Rev Genet*. 2006;40(1):363-383. doi:10.1146/annurev.genet.40.110405.090451

206. Uematsu N, Weterings E, Yano KI, et al. Autophosphorylation of DNA-PKCS regulates its dynamics at DNA double-strand breaks. *J Cell Biol*. 2007;177(2):219-229. doi:10.1083/jcb.200608077

207. Costantini S, Woodbine L, Andreoli L, Jeggo PA, Vindigni A. Interaction of the Ku heterodimer with the DNA ligase IV/Xrcc4 complex and its regulation by DNA-PK. *DNA Repair (Amst)*. 2007;6(6):712-722.

doi:10.1016/j.dnarep.2006.12.007

208. Yano KI, Morotomi-Yano K, Wang SY, et al. Ku recruits XLF to DNA double-strand breaks. *EMBO Rep*. 2008;9(1):91-96. doi:10.1038/sj.embor.7401137

209. Macrae CJ, McCulloch RD, Ylanko J, Durocher D, Koch CA. APLF (C2orf13) facilitates nonhomologous end-joining and undergoes ATM-dependent hyperphosphorylation following ionizing radiation. *DNA Repair (Amst)*. 2008;7(2):292-302. doi:10.1016/j.dnarep.2007.10.008

210. Grundy GJ, Rulten SL, Zeng Z, et al. APLF promotes the assembly and activity of non-homologous end joining protein complexes. *EMBO J*. 2013;32(1):112-125. doi:10.1038/emboj.2012.304

211. Falck J, Coates J, Jackson SP. Conserved modes of recruitment of ATM, ATR and DNA-PKcs to sites of DNA damage. *Nature*. 2005;434(7033):605-611. doi:10.1038/nature03442

212. Jackson SP. SJackson, S. P. (2002). Sensing and repairing DNA double-strand breaks. Carcinogenesis, 23(5), 687-96. Retrieved from http://www.ncbi.nlm.nih.gov/pubmed/12016139ensing and repairing DNA double-strand breaks. *Carcinogenesis*. 2002;23(5):687-696.

213. Ma Y, Pannicke U, Schwarz K, Lieber MR. Hairpin opening and overhang processing by an Artemis/DNA-dependent protein kinase complex in nonhomologous end joining and V(D)J recombination. *Cell*. 2002;108(6):781-794. doi:10.1016/S0092-8674(02)00671-2

214. Povirk LF, Zhou T, Zhou R, Cowan MJ, Yannone SM. Processing of 3′-phosphoglycolate-terminated DNA double strand breaks by artemis nuclease. *J Biol Chem*. 2007;282(6):3547-3558. doi:10.1074/jbc.M607745200

215. Cooper MP, Machwe A, Orren DK, Brosh RM, Ramsden D, Bohr VA. Ku complex interacts with and stimulates the Werner protein. *Genes Dev*. 2000;14(8):907-912.

216. Kusumoto R, Dawut L, Marchetti C, et al. Werner protein cooperates with the XRCC4-DNA ligase IV complex in end-processing. *Biochemistry*. 2008;47(28):7548-7556. doi:10.1021/bi702325t

217. Ramadan K, Shevelev I V., Maga G, Hübscher U. De Novo DNA synthesis by human DNA polymerase λ, DNA polymerase μ and terminal deoxyribonucleotidyl transferase. *J Mol Biol*. 2004;339(2):395-404. doi:10.1016/j.jmb.2004.03.056

218. McElhinny SAN, Havener JM, Garcia-Diaz M, et al. A gradient of template dependence defines distinct biological roles for family X polymerases in nonhomologous end joining. *Mol Cell*. 2005;19(3):357-366. doi:10.1016/j.molcel.2005.06.012

219. Chen L, Trujillo K, Sung P, Tomkinson AE. Interactions of the DNA ligase IV-XRCC4 complex with DNA ends and the DNA-dependent protein kinase. *J Biol Chem*. 2000;275(34):26196-26205. doi:10.1074/jbc.M000491200

220. Grawunder U, Wilm M, Wu X, et al. Activity of DNA ligase IV stimulated by complex formation with XRCC4 protein in mammalian cells. *Nature*. 1997;388(6641):492-495. doi:10.1038/41358

221. Shibata A, Moiani D, Arvai AS, et al. DNA double-strand break repair pathway choice is directed by distinct MRE11 nuclease activities. *Mol Cell*. 2014;53(1):7-18. doi:10.1016/j.molcel.2013.11.003

222. Shuren Liao, Margaret Tammaro, Hong Yan. The structure of ends determines the pathway choice and Mre11 nuclease dependency of DNA double-strand break repair.

223. Daley JM, Tomimatsu N, Hooks G, et al. Specificity of end resection pathways for double-strand break regions containing ribonucleotides and base lesions. *Nat Commun 2020 111*. 2020;11(1):1-12. doi:10.1038/s41467-020-16903-4

224. Iannascoli C, Palermo V, Murfuni I, Franchitto A, Pichierri P. The WRN exonuclease domain protects nascent strands from pathological MRE11/EXO1-dependent degradation. *Nucleic Acids Res*. 2015;43(20):9788-9803. doi:10.1093/nar/gkv836

225. Sturzenegger A, Burdova K, Kanagaraj R, et al. DNA2 cooperates with the WRN and BLM RecQ helicases to mediate long-range DNA end resection in human cells. *J Biol Chem*. 2014;289(39):27314-27326.

doi:10.1074/jbc.M114.578823

226. Nimonkar A V., Genschel J, Kinoshita E, et al. BLM–DNA2–RPA–MRN and EXO1–BLM–RPA–MRN constitute two DNA end resection machineries for human DNA break repair. *Genes Dev*. 2011;25(4):350. doi:10.1101/GAD.2003811

227. Mimitou EP, Symington LS. Sae2, Exo1 and Sgs1 collaborate in DNA double-strand break processing. *Nature*. 2008;455(7214):770-774. doi:10.1038/nature07312

228. Daley JM, Jimenez-Sainz J, Wang W, et al. Enhancement of BLM-DNA2-Mediated Long-Range DNA End Resection by CtIP. *Cell Rep*. 2017;21(2):324-332. doi:10.1016/j.celrep.2017.09.048

229. San Filippo J, Sung P, Klein H. Mechanism of Eukaryotic Homologous Recombination. *Annu Rev Biochem*. 2008;77(1):229-257. doi:10.1146/annurev.biochem.77.061306.125255

230. Symington LS, Rothstein R, Lisby M. Mechanisms and regulation of mitotic recombination in Saccharomyces cerevisiae. *Genetics*. 2014;198(3):795-835. doi:10.1534/genetics.114.166140

231. Rajendra E, Venkitaraman AR. Two modules in the BRC repeats of BRCA2 mediate structural and functional interactions with the RAD51 recombinase. *Nucleic Acids Res*. 2010;38(1):82-96. doi:10.1093/nar/gkp873

232. Douglass Wright W, Shital Shah S, Heyer W-D. Homologous recombination and the repair of DNA double-strand breaks. 2018. doi:10.1074/jbc.TM118.000372

233. Ceccaldi R, Liu JC, Amunugama R, et al. Homologous-recombination-deficient tumours are dependent on Polh-mediated repair. 2015. doi:10.1038/nature14184

234. Mateos-Gomez PA, Gong F, Nair N, Miller KM, Lazzerini-Denchi E, Sfeir A. Mammalian polymerase θ promotes alternative NHEJ and suppresses recombination. *Nature*. 2015;518(7538):254-257. doi:10.1038/NATURE14157

235. Kabotyanski EB, Gomelsky L, Han J-O, Stamato TD, Roth DB. Double-strand

break repair in Ku86-and XRCC4-deficient cells. *Nucleic Acids Res*. 1998;26(23).

236. Boulton SJ, Jackson SP. Identification of a Saccharomyces cerevisiae Ku80 homologue: roles in DNA double strand break rejoining and in telomeric maintenance. *Nucleic Acids Res*. 1996;24(23):4639-4648.

237. Liang F, Jasin M. Ku80-deficient cells exhibit excess degradation of extrachromosomal DNA. *J Biol Chem*. 1996;271(24):14405-14411. doi:10.1074/JBC.271.24.14405

238. Zhao B, Rothenberg E, Ramsden DA, Lieber MR. The molecular basis and disease relevance of non-homologous DNA end joining. *Nat Rev Mol Cell Biol*. 2020;21(12):765. doi:10.1038/S41580-020-00297-8

239. Mateos-Gomez PA, Nair N, Miller KM, Lazzerini-Denchi E, Sfeir A. Mammalian polymerase h promotes alternative NHEJ and suppresses recombination. 2015. doi:10.1038/nature14157

240. Kais Z, Rondinelli B, Holmes A, et al. FANCD2 maintains fork stability in BRCA1/2-deficient tumors and promotes alternative end-joining DNA repair. *Cell Rep*. 2016;15(11):2488. doi:10.1016/J.CELREP.2016.05.031

241. Howard SM, Yanez DA, Stark JM. DNA damage response factors from diverse pathways, including DNA crosslink repair, mediate alternative end joining. *PLoS Genet*. 2015;11(1). doi:10.1371/JOURNAL.PGEN.1004943

242. Ma J-L, Kim EM, Haber JE, Lee SE. Yeast Mre11 and Rad1 Proteins Define a Ku-Independent Mechanism To Repair Double-Strand Breaks Lacking Overlapping End Sequences. *Mol Cell Biol*. 2003;23(23):8820. doi:10.1128/MCB.23.23.8820-8828.2003

243. Xie A, Kwok A, Scully R. Role of mammalian Mre11 in classical and alternative nonhomologous end joining. *Nat Struct Mol Biol*. 2009;16(8):814-818. doi:10.1038/NSMB.1640

244. Truong LN, Li Y, Shi LZ, et al. Microhomology-mediated End Joining and Homologous Recombination share the initial end resection step to repair DNA double-strand breaks in mammalian cells. *Proc Natl Acad Sci U S A*.

2013;110(19):7720-7725. doi:10.1073/PNAS.1213431110/-/DCSUPPLEMENTAL/PNAS.201213431SI.PDF

245. Van Schendel R, Romeijn R, Buijs H, Tijsterman M. Preservation of lagging strand integrity at sites of stalled replication by Pol α-primase and 9-1-1 complex. *Sci Adv*. 2021;7(21). doi:10.1126/SCIADV.ABF2278/SUPPL_FILE/ABF2278_SM.PDF

246. Shukla V, Halabelian L, Balagere S, et al. HMCES Functions in the Alternative End-Joining Pathway of the DNA DSB Repair during Class Switch Recombination in B Cells. *Mol Cell*. 2020;77(2):384-394.e4. doi:10.1016/J.MOLCEL.2019.10.031

247. Carvajal-Garcia J, Cho JE, Carvajal-Garcia P, et al. Mechanistic basis for microhomology identification and genome scarring by polymerase theta. *Proc Natl Acad Sci U S A*. 2020;117(15):8476-8485. doi:10.1073/PNAS.1921791117

248. Zahn KE, Averill AM, Aller P, Wood RD, Doublié S. Human DNA polymerase θ grasps the primer terminus to mediate DNA repair. *Nat Struct Mol Biol*. 2015;22(4):304. doi:10.1038/NSMB.2993

249. Newman JA, Cooper CDO, Aitkenhead H, Gileadi O. Structure of the Helicase Domain of DNA Polymerase Theta Reveals a Possible Role in the Microhomology-Mediated End-Joining Pathway. *Structure*. 2015;23(12):2319-2330. doi:10.1016/J.STR.2015.10.014

250. Black SJ, Ozdemir AY, Kashkina E, et al. Molecular basis of microhomology-mediated end-joining by purified full-length Polθ. doi:10.1038/s41467-019-12272-9

251. He P, Yang W. Template and primer requirements for DNA Pol θ-mediated end joining. doi:10.1073/pnas.1807329115

252. Arana ME, Seki M, Wood RD, Rogozin IB, Kunkel TA. Low-fidelity DNA synthesis by human DNA polymerase theta. *Nucleic Acids Res*. 2008;36(11):3847-3856. doi:10.1093/NAR/GKN310

253. Meyer D, Xu B, Fu H, Heyer W-D. DNA polymerases δ and λ cooperate in

repairing double-strand breaks by microhomology-mediated end-joining in Saccharomyces cerevisiae. doi:10.1073/pnas.1507833112

254. Layer J V., Debaize L, van Scoyk A, et al. Polymerase δ promotes chromosomal rearrangements and imprecise double-strand break repair. *Proc Natl Acad Sci U S A*. 2020;117(44):27566-27577. doi:10.1073/PNAS.2014176117/-/DCSUPPLEMENTAL

255. Mengwasser KE, Adeyemi RO, Leng Y, et al. Genetic Screens Reveal FEN1 and APEX2 as BRCA2 Synthetic Lethal Targets. *Mol Cell*. 2019;73(5):885. doi:10.1016/J.MOLCEL.2018.12.008

256. Simsek D, Brunet E, Wong SYW, et al. DNA ligase III promotes alternative nonhomologous end-joining during chromosomal translocation formation. *PLoS Genet*. 2011;7(6). doi:10.1371/JOURNAL.PGEN.1002080

257. Masani S, Han L, Meek K, Yu K. Redundant function of DNA ligase 1 and 3 in alternative end-joining during immunoglobulin class switch recombination. *undefined*. 2016;113(5):1261-1266. doi:10.1073/PNAS.1521630113

258. Lin FL, Sperle K, Sternberg N. Model for homologous recombination during transfer of DNA into mouse L cells: role for DNA ends in the recombination process. *Mol Cell Biol*. 1984;4(6):1020-1034. doi:10.1128/MCB.4.6.1020-1034.1984

259. Bennardo N, Cheng A, Huang N, Stark JM. Alternative-NHEJ Is a Mechanistically Distinct Pathway of Mammalian Chromosome Break Repair. *PLOS Genet*. 2008;4(6):e1000110. doi:10.1371/JOURNAL.PGEN.1000110

260. Zhou Y, Caron P, Legube G, Paull TT. Quantitation of DNA double-strand break resection intermediates in human cells. *Nucleic Acids Res*. 2014;42(3). doi:10.1093/NAR/GKT1309

261. Xie A, Puget N, Shim I, et al. Control of Sister Chromatid Recombination by Histone H2AX. *Mol Cell*. 2005;16(6):1017. doi:10.1016/J.MOLCEL.2004.12.007

262. Escribano-Díaz C, Orthwein A, Fradet-Turcotte A, et al. A cell cycle-dependent regulatory circuit composed of 53BP1-RIF1 and BRCA1-CtIP controls DNA

repair pathway choice. *Mol Cell*. 2013;49(5):872-883. doi:10.1016/J.MOLCEL.2013.01.001

263. Helleday T, Petermann E, Lundin C, Hodgson B, Sharma RA. DNA repair pathways as targets for cancer therapy. *Nat Rev Cancer 2008 83*. 2008;8(3):193-204. doi:10.1038/nrc2342

264. Syed A, Tainer JA. The MRE11–RAD50–NBS1 Complex Conducts the Orchestration of Damage Signaling and Outcomes to Stress in DNA Replication and Repair. *Annu Rev Biochem*. 2018;87(1):263-294. doi:10.1146/annurev-biochem-062917-012415

265. Ajimura M, Leem SH, Ogawa H. Identification of new genes required for meiotic recombination in Saccharomyces cerevisiae. *Genetics*. 1993;133(1):51-66.

266. Ivanov EL, Korolev VG, Fabre F. Xrs2, a DNA Repair Gene of Saccharomyces Cerevisiae, Is Needed for Meiotic Recombination. *Genetics*. 1992;132(3):651.

267. Saeki T, Machida I, Nakai S. Genetic control of diploid recovery after γ-irradiation in the yeast Saccharomyces cerevisiae. *Mutat Res - Fundam Mol Mech Mutagen*. 1980;73(2):251-265. doi:10.1016/0027-5107(80)90192-X

268. De Jager M, Van Noort J, Van Gent DC, Dekker C, Kanaar R, Wyman C. Human Rad50/Mre11 is a flexible complex that can tether DNA ends. *Mol Cell*. 2001;8(5):1129-1135. doi:10.1016/S1097-2765(01)00381-1

269. D'Amours D, Jackson SP. The Mre11 complex: At the crossroads of DNA repair and checkpoint signalling. *Nat Rev Mol Cell Biol*. 2002;3(5):317-327. doi:10.1038/nrm805

270. Zha S, Boboila C, Alt FW. Mre11: roles in DNA repair beyond homologous recombination. *Nat Struct Mol Biol 2009 168*. 2009;16(8):798-800. doi:10.1038/nsmb0809-798

271. Takata H, Tanaka Y, Matsuura A. Late S phase-specific recruitment of Mre11 complex triggers hierarchical assembly of telomere replication proteins in Saccharomyces cerevisiae. *Mol Cell*. 2005;17(4):573-583. doi:10.1016/J.MOLCEL.2005.01.014

272. Goudsouzian LK, Tuzon CT, Zakian VA. S. cerevisiae Tel1p and Mre11p are required for normal levels of Est1p and Est2p telomere association. *Mol Cell*. 2006;24(4):603-610. doi:10.1016/J.MOLCEL.2006.10.005

273. Hopfner KP, Karcher A, Craig L, Woo TT, Carney JP, Tainer JA. Structural biochemistry and interaction architecture of the DNA double-strand break repair Mre11 nuclease and Rad50-ATPase. *Cell*. 2001;105(4):473-485. doi:10.1016/S0092-8674(01)00335-X

274. Bian L, Meng Y, Zhang M, Li D. MRE11-RAD50-NBS1 complex alterations and DNA damage response: Implications for cancer treatment. *Mol Cancer*. 2019;18(1). doi:10.1186/S12943-019-1100-5

275. Williams RS, Williams JS, Tainer JA. Mre11-Rad50-Nbs1 is a keystone complex connecting DNA repair machinery, double-strand break signaling, and the chromatin template. *Biochem Cell Biol*. 2007;85(4):509-520. doi:10.1139/O07-069

276. Tauchi H, Kobayashii J, Morishima KI, et al. The forkhead-associated domain of NBS1 is essential for nuclear foci formation after irradiation but not essential for hRAD50·hMRE11·-NBS1 complex DNA repair activity. *J Biol Chem*. 2001;276(1):12-15. doi:10.1074/jbc.C000578200

277. Van Der Linden E, Sanchez H, Kinoshita E, Kanaar R, Wyman C. RAD50 and NBS1 form a stable complex functional in DNA binding and tethering. *Nucleic Acids Res*. 2009;37(5):1580-1588. doi:10.1093/nar/gkn1072

278. Connelly JC, Leach DRF. Tethering on the brink: The evolutionarily conserved Mre11-Rad50 complex. *Trends Biochem Sci*. 2002;27(8):410-418. doi:10.1016/S0968-0004(02)02144-8

279. Moncalian G, Lengsfeld B, Bhaskara V, et al. The Rad50 Signature Motif: Essential to ATP Binding and Biological Function. *J Mol Biol*. 2004;335(4):937-951. doi:10.1016/j.jmb.2003.11.026

280. Hopfner KP, Karcher A, Shin DS, et al. Structural biology of Rad50 ATPase: ATP-driven conformational control in DNA double-strand break repair and the ABC-ATPase superfamily. *Cell*. 2000;101(7):789-800. doi:10.1016/S0092-

8674(00)80890-9

281. Cahill D, Carney JP. Dimerization of the Rad50 protein is independent of the conserved hook domain. *Mutagenesis*. 2007;22(4):269-274. doi:10.1093/mutage/gem011

282. Park YB, Hohl M, Padjasek M, et al. Eukaryotic Rad50 functions as a rod-shaped dimer. *Nat Struct Mol Biol*. 2017;24(3):248-257. doi:10.1038/nsmb.3369

283. Bai Y, Wang W, Li S, et al. C1QBP Promotes Homologous Recombination by Stabilizing MRE11 and Controlling the Assembly and Activation of MRE11/RAD50/NBS1 Complex. *Mol Cell*. 2019;75(6):1299-1314.e6. doi:10.1016/J.MOLCEL.2019.06.023

284. Symington LS. Mechanism and Regulation of DNA End Resection in Eukaryotes. *Crit Rev Biochem Mol Biol*. 2016;51(3):195. doi:10.3109/10409238.2016.1172552

285. Trujillo KM, Yuan SSF, Lee EYHP, Sung P. Nuclease activities in a complex of human recombination and DNA repair factors Rad50, Mre11, and p95. *J Biol Chem*. 1998;273(34):21447-21450. doi:10.1074/JBC.273.34.21447

286. Trujillo KM, Sung P. DNA Structure-specific Nuclease Activities in the Saccharomyces cerevisiae Rad50-Mre11 Complex. *J Biol Chem*. 2001;276(38):35458-35464. doi:10.1074/jbc.M105482200

287. Farah JA, Cromie GA, Smith GR. Ctp1 and Exonuclease 1, alternative nucleases regulated by the MRN complex, are required for efficient meiotic recombination. *Proc Natl Acad Sci U S A*. 2009;106(23):9356-9361. doi:10.1073/PNAS.0902793106

288. Desai-Mehta A, Cerosaletti KM, Concannon P. Distinct Functional Domains of Nibrin Mediate Mre11 Binding, Focus Formation, and Nuclear Localization. *Mol Cell Biol*. 2001;21(6):2184. doi:10.1128/MCB.21.6.2184-2191.2001

289. Johzuka K, Ogawa H. Interaction of Mre11 and Rad50: Two Proteins Required for DNA Repair and Meiosis-Specific Double-Strand Break Formation in Saccharomyces Cerevisiae. *Genetics*. 1995;139(4):1521.

doi:10.1093/GENETICS/139.4.1521

290. Stracker TH, Petrini JHJ. The MRE11 complex: Starting from the ends. *Nat Rev Mol Cell Biol*. 2011;12(2):90-103. doi:10.1038/nrm3047

291. Déry U, Coulombe Y, Rodrigue A, Stasiak A, Richard S, Masson J-Y. A Glycine-Arginine Domain in Control of the Human MRE11 DNA Repair Protein. *Mol Cell Biol*. 2008;28(9):3058-3069. doi:10.1128/mcb.02025-07

292. Li Z, Li J, Kong Y, Yan S, Ahmad N, Liu X. Plk1 Phosphorylation of Mre11 Antagonizes the DNA Damage Response. *Cancer Res*. 2017;77(12):3169. doi:10.1158/0008-5472.CAN-16-2787

293. Von Morgen P, Burdova K, Flower TG, et al. MRE11 stability is regulated by CK2-dependent interaction with R2TP complex. *Oncogene*. 2017;36:4943-4950. doi:10.1038/onc.2017.99

294. Goldberg M, Stucki M, Falck J, et al. MDC1 is required for the intra-S-phase DNA damage checkpoint. *Nat 2003 4216926*. 2003;421(6926):952-956. doi:10.1038/nature01445

295. Lukas C, Melander F, Stucki M, et al. Mdc1 couples DNA double-strand break recognition by Nbs1 with its H2AX-dependent chromatin retention. *EMBO J*. 2004;23(13):2674-2683. doi:10.1038/SJ.EMBOJ.7600269

296. Sartori AA, Lukas C, Coates J, et al. Human CtIP promotes DNA end resection. 2007;450. doi:10.1038/nature06337

297. Kobayashi J, Antoccia A, Tauchi H, Matsuura S, Komatsu K. NBS1 and its functional role in the DNA damage response. *DNA Repair (Amst)*. 2004;3(8-9):855-861. doi:10.1016/J.DNAREP.2004.03.023

298. Uziel T, Lerenthal Y, Moyal L, Andegeko Y, Mittelman L, Shiloh Y. Requirement of the MRN complex for ATM activation by DNA damage. *EMBO J*. 2003;22(20):5612. doi:10.1093/EMBOJ/CDG541

299. Girard PM, Riballo E, Begg AC, Waugh A, Jeggo PA. NBS1 promotes ATM dependent hosphorylation events including those required for G1/S arrest. *Oncogene*. 2002;21(27):4191-4199. doi:10.1038/sj.onc.1205596

300. Stewart GS, Maser RS, Stankovic T, et al. The DNA double-strand break repair gene hMRE11 is mutated in individuals with an ataxia-telangiectasia-like disorder. *Cell*. 1999;99(6):577-587. doi:10.1016/S0092-8674(00)81547-0

301. Staples CJ, Barone G, Myers KN, et al. MRNIP/C5orf45 Interacts with the MRN Complex and Contributes to the DNA Damage Response. *Cell Rep*. 2016;16(10):2565-2575. doi:10.1016/j.celrep.2016.07.087

302. Paull TT. Mechanisms of ATM Activation. *Annu Rev Biochem*. 2015;84(1):711-738. doi:10.1146/annurev-biochem-060614-034335

303. Tauchi H, Kobayashi J, Morishima KI, et al. Nbs1 is essential for DNA repair by homologous recombination in higher vertebrate cells. *Nature*. 2002;420(6911):93-98. doi:10.1038/nature01125

304. Nakamura K, Kato A, Kobayashi J, et al. Regulation of Homologous Recombination by RNF20-Dependent H2B Ubiquitination. *Mol Cell*. 2011;41(5):515-528. doi:10.1016/j.molcel.2011.02.002

305. Yanagihara H, Kobayashi J, Tateishi S, et al. NBS1 Recruits RAD18 via a RAD6-like Domain and Regulates Pol η-Dependent Translesion DNA Synthesis. *Mol Cell*. 2011;43(5):788-797. doi:10.1016/j.molcel.2011.07.026

306. Wu X, Ranganathant V, Weisman DS, et al. ATM phosphorylation of Nijmegen breakage syndrome protein is required in a DNA damage response. *Nature*. 2000;405(6785):477-482. doi:10.1038/35013089

307. Lim DS, Kim ST, Xu B, et al. ATM phosphorylates p95/nbs1 in an S-phase checkpoint pathway. *Nature*. 2000;404(6778):613-617. doi:10.1038/35007091

308. Yazdi PT, Wang Y, Zhao S, Patel N, Lee EYHP, Qin J. SMC1 is a downstream effector in the ATM/NBS1 branch of the human S-phase checkpoint. *Genes Dev*. 2002;16(5):571-582. doi:10.1101/GAD.970702

309. Gatei M, Jakob B, Chen P, et al. ATM protein-dependent phosphorylation of Rad50 protein Regulates DNA repair and cell cycle control. *J Biol Chem*. 2011;286(36):31542-31556. doi:10.1074/jbc.M111.258152

310. Kijas AW, Lim YC, Bolderson E, et al. ATM-dependent phosphorylation of MRE11 controls extent of resection during homology directed repair by

signalling through Exonuclease 1 . *Nucleic Acids Res*. 2015;43(17):8352-8367. doi:10.1093/nar/gkv754

311. Liu Y, Sung S, Kim Y, et al. ATP -dependent DNA binding, unwinding, and resection by the Mre11/Rad50 complex . *EMBO J*. 2016;35(7):743-758. doi:10.15252/embj.201592462

312. Bian L, Meng Y, Zhang M, Li D. MRE11-RAD50-NBS1 complex alterations and DNA damage response: implications for cancer treatment. *Mol Cancer 2019 181*. 2019;18(1):1-14. doi:10.1186/S12943-019-1100-5

313. Luo G, Yao MS, Bender CF, et al. Disruption of mRad50 causes embryonic stem cell lethality, abnormal embryonic development, and sensitivity to ionizing radiation. *Proc Natl Acad Sci U S A*. 1999;96(13):7376. doi:10.1073/PNAS.96.13.7376

314. Xiao Y, Weaver DT. *Conditional Gene Targeted Deletion by Cre Recombinase Demonstrates the Requirement for the Double-Strand Break Repair Mre11 Protein in Murine Embryonic Stem Cells*. Vol 25. Oxford University Press; 1997. https://academic.oup.com/nar/article/25/15/2985/2901947.

315. Zhu J, Petersen S, Tessarollo L, Nussenzweig A. Targeted disruption of the Nijmegen breakage syndrome gene NBS1 leads to early embryonic lethality in mice. *Curr Biol*. 2001;11(2):105-109. doi:10.1016/S0960-9822(01)00019-7

316. Yamaguchi-Iwai Y, Sonoda E, Sasaki MS, et al. Mre11 is essential for the maintenance of chromosomal DNA in vertebrate cells. *EMBO J*. 1999;18(23):6619-6629. doi:10.1093/EMBOJ/18.23.6619

317. Carney JP, Maser RS, Olivares H, et al. The hMre11/hRad50 protein complex and Nijmegen breakage syndrome: Linkage of double-strand break repair to the cellular DNA damage response. *Cell*. 1998;93(3):477-486. doi:10.1016/S0092-8674(00)81175-7

318. Waltes R, Kalb R, Gatei M, et al. Human RAD50 deficiency in a Nijmegen breakage syndrome-like disorder. *Am J Hum Genet*. 2009;84(5):605-616. doi:10.1016/j.ajhg.2009.04.010

319. Varon R, Vissinga C, Platzer M, et al. Nibrin, a novel DNA double-strand break

repair protein, is mutated in Nijmegen breakage syndrome. *Cell*. 1998;93(3):467-476. doi:10.1016/S0092-8674(00)81174-5

320. van den Bosch M, Bree RT, Lowndes NF. The MRN complex: Coordinating and mediating the response to broken chromosomes. *EMBO Rep*. 2003;4(9):844-849. doi:10.1038/sj.embor.embor925

321. Bartkova J, Tommiska J, Oplustilova L, et al. Aberrations of the MRE11-RAD50-NBS1 DNA damage sensor complex in human breast cancer: MRE11 as a candidate familial cancer-predisposing gene. *Mol Oncol*. 2008;2(4):296-316. doi:10.1016/j.molonc.2008.09.007

322. Kleibl Z, Kristensen VN. Women at high risk of breast cancer: Molecular characteristics, clinical presentation and management. *The Breast*. 2016;28:136-144. doi:10.1016/J.BREAST.2016.05.006

323. Brandt S, Samartzis EP, Zimmermann A-K, et al. Lack of MRE11-RAD50-NBS1 (MRN) complex detection occurs frequently in low-grade epithelial ovarian cancer. *BMC Cancer*. 2017;17(1):44. doi:10.1186/s12885-016-3026-2

324. Gravells P, Grant E, Smith KM, James DI, Bryant HE. Specific killing of DNA damage-response deficient cells with inhibitors of poly(ADP-ribose) glycohydrolase. *DNA Repair (Amst)*. 2017;52:81-91. doi:10.1016/j.dnarep.2017.02.010

325. Kim IK, Kiefer JR, Ho CMW, et al. Structure of mammalian poly(ADP-ribose) glycohydrolase reveals a flexible tyrosine clasp as a substrate-binding element. *Nat Struct Mol Biol*. 2012;19(6):653-656. doi:10.1038/nsmb.2305

326. Elvers I, Johansson F, Groth P, Erixon K, Helleday T. UV stalled replication forks restart by re-priming in human fibroblasts. *Nucleic Acids Res*. 2011;39(16):7049-7057. doi:10.1093/nar/gkr420

327. Thakar T, Moldovan GL. The emerging determinants of replication fork stability. *Nucleic Acids Res*. 2021;49(13):7224-7238. doi:10.1093/NAR/GKAB344

328. Liao H, Ji F, Helleday T, Ying S. Mechanisms for stalled replication fork stabilization: new targets for synthetic lethality strategies in cancer treatments.

EMBO Rep. 2018;19(9). doi:10.15252/EMBR.201846263

329. Neelsen KJ, Lopes M. Replication fork reversal in eukaryotes: From dead end to dynamic response. *Nat Rev Mol Cell Biol*. 2015;16(4):207-220. doi:10.1038/nrm3935

330. Higgins NP, Kato K, Strauss B. A model for replication repair in mammalian cells. *J Mol Biol*. 1976;101(3):417-425. doi:10.1016/0022-2836(76)90156-x

331. De Septenville AL, Duigou S, Boubakri H, Michel B. Replication Fork Reversal after Replication–Transcription Collision. Burkholder WF, ed. *PLoS Genet*. 2012;8(4):e1002622. doi:10.1371/journal.pgen.1002622

332. Manosas M, Perumal SK, Croquette V, Benkovic SJ. Direct observation of stalled fork restart via fork regression in the T4 replication system. *Science (80-)*. 2012;338(6111):1217-1220. doi:10.1126/science.1225437

333. Nelson SW, Benkovic SJ. Response of the Bacteriophage T4 Replisome to Noncoding Lesions and Regression of a Stalled Replication Fork. *J Mol Biol*. 2010;401(5):743-756. doi:10.1016/j.jmb.2010.06.027

334. Zellweger R, Dalcher D, Mutreja K, et al. Rad51-mediated replication fork reversal is a global response to genotoxic treatments in human cells. *J Cell Biol*. 2015;208(5):563-579. doi:10.1083/jcb.201406099

335. Ray Chaudhuri A, Hashimoto Y, Herrador R, et al. Topoisomerase i poisoning results in PARP-mediated replication fork reversal. *Nat Struct Mol Biol*. 2012;19(4):417-423. doi:10.1038/nsmb.2258

336. Zellweger R, Dalcher D, Mutreja K, et al. Rad51-mediated replication fork reversal is a global response to genotoxic treatments in human cells. *J Cell Biol*. 2015;208(5):563-579. doi:10.1083/jcb.201406099

337. Ciccia A, Bredemeyer AL, Sowa ME, et al. The SIOD disorder protein SMARCAL1 is an RPA-interacting protein involved in replication fork restart. *Genes Dev*. 2009;23(20):2415. doi:10.1101/GAD.1832309

338. Chen R, Wold MS. Replication Protein A: Single-stranded DNA's first responder : Dynamic DNA-interactions allow Replication Protein A to direct single-strand DNA intermediates into different pathways for synthesis or repair.

Bioessays. 2014;36(12):1156. doi:10.1002/BIES.201400107

339. Fan J, Pavletich NP. Structure and conformational change of a replication protein A heterotrimer bound to ssDNA. *Genes Dev*. 2012;26(20):2337. doi:10.1101/GAD.194787.112

340. Nam EA, Cortez D. ATR signaling: more than meeting at the fork. *Biochem J*. 2011;436(3):527. doi:10.1042/BJ20102162

341. Bass TE, Luzwick JW, Kavanaugh G, et al. ETAA1 acts at stalled replication forks to maintain genome integrity. *Nat Cell Biol*. 2016;18(11):1185. doi:10.1038/NCB3415

342. Vassin VM, Wold MS, Borowiec JA. Replication Protein A (RPA) Phosphorylation Prevents RPA Association with Replication Centers. *Mol Cell Biol*. 2004;24(5):1930. doi:10.1128/MCB.24.5.1930-1943.2004

343. Fanning E, Klimovich V, Nager AR. A dynamic model for replication protein A (RPA) function in DNA processing pathways. *Nucleic Acids Res*. 2006;34(15):4126. doi:10.1093/NAR/GKL550

344. Bétous R, Couch FB, Mason AC, Eichman BF, Manosas M, Cortez D. Substrate-Selective Repair and Restart of Replication Forks by DNA Translocases. *Cell Rep*. 2013;3(6):1958-1969. doi:10.1016/j.celrep.2013.05.002

345. Bansbach CE, Bétous R, Lovejoy CA, Glick GG, Cortez D. The annealing helicase SMARCAL1 maintains genome integrity at stalled replication forks. *Genes Dev*. 2009;23(20):2405-2414. doi:10.1101/gad.1839909

346. Ciccia A, Bredemeyer AL, Sowa ME, et al. The SIOD disorder protein SMARCAL1 is an RPA-interacting protein involved in replication fork restart. *Genes Dev*. 2009;23(20):2415-2425. doi:10.1101/gad.1832309

347. Couch FB, Bansbach CE, Driscoll R, et al. ATR phosphorylates SMARCAL1 to prevent replication fork collapse. *Genes Dev*. 2013;27(14):1610-1623. doi:10.1101/GAD.214080.113

348. Ciccia A, Nimonkar A V., Hu Y, et al. Polyubiquitinated PCNA Recruits the ZRANB3 Translocase to Maintain Genomic Integrity after Replication Stress.

Mol Cell. 2012;47(3):396-409. doi:10.1016/j.molcel.2012.05.024

349. Yuan J, Ghosal G, Chen J. The HARP-like Domain-Containing Protein AH2/ZRANB3 Binds to PCNA and Participates in Cellular Response to Replication Stress. *Mol Cell*. 2012;47(3):410-421. doi:10.1016/j.molcel.2012.05.025

350. Kile AC, Chavez DA, Bacal J, et al. HLTF's Ancient HIRAN Domain Binds 3' DNA Ends to Drive Replication Fork Reversal. *Mol Cell*. 2015;58(6):1090-1100. doi:10.1016/j.molcel.2015.05.013

351. Hishiki A, Hara K, Ikegaya Y, et al. Structure of a novel DNA-binding domain of Helicase-like Transcription Factor (HLTF) and its functional implication in DNA damage tolerance. *J Biol Chem*. 2015;290(21):13215-13223. doi:10.1074/jbc.M115.643643

352. Vujanovic M, Krietsch J, Raso MC, et al. Replication Fork Slowing and Reversal upon DNA Damage Require PCNA Polyubiquitination and ZRANB3 DNA Translocase Activity. *Mol Cell*. 2017;67(5):882-890.e5. doi:10.1016/j.molcel.2017.08.010

353. Taglialatela A, Alvarez S, Leuzzi G, et al. Restoration of Replication Fork Stability in BRCA1- and BRCA2-Deficient Cells by Inactivation of SNF2-Family Fork Remodelers. *Mol Cell*. 2017;68(2):414-430.e8. doi:10.1016/j.molcel.2017.09.036

354. Kolinjivadi AM, Sannino V, De Antoni A, et al. Smarcal1-Mediated Fork Reversal Triggers Mre11-Dependent Degradation of Nascent DNA in the Absence of Brca2 and Stable Rad51 Nucleofilaments. *Mol Cell*. 2017;67(5):867-881.e7. doi:10.1016/j.molcel.2017.07.001

355. Bugreev D V, Rossi MJ, Mazin A V. Cooperation of RAD51 and RAD54 in regression of a model replication fork. *Nucleic Acids Res*. 2011;39(6):2153-2164. doi:10.1093/nar/gkq1139

356. Gari K, Décaillet C, Delannoy M, Wu L, Constantinou A. Remodeling of DNA replication structures by the branch point translocase FANCM. *Proc Natl Acad Sci U S A*. 2008;105(42):16107-16112. doi:10.1073/pnas.0804777105

357. Mijic S, Zellweger R, Chappidi N, et al. Replication fork reversal triggers fork degradation in BRCA2-defective cells. *Nat Commun*. 2017;8(1):859. doi:10.1038/s41467-017-01164-5

358. Bhat KP, Cortez D. RPA and RAD51: Fork reversal, fork protection, and genome stability. *Nat Struct Mol Biol*. 2018;25(6):446-453. doi:10.1038/s41594-018-0075-z

359. Wang AT, Kim T, Wagner JE, et al. A Dominant Mutation in Human RAD51 Reveals Its Function in DNA Interstrand Crosslink Repair Independent of Homologous Recombination. *Mol Cell*. 2015;59(3):478-490. doi:10.1016/j.molcel.2015.07.009

360. Berti M, Chaudhuri AR, Thangavel S, et al. Human RECQ1 promotes restart of replication forks reversed by DNA topoisomerase I inhibition. *Nat Struct Mol Biol*. 2013;20(3):347. doi:10.1038/NSMB.2501

361. Rondinelli B, Gogola E, Yücel H, et al. EZH2 promotes degradation of stalled replication forks by recruiting MUS81 through histone H3 trimethylation. *Nat Cell Biol*. 2017;19(11):1371-1378. doi:10.1038/ncb3626

362. Lemaçon D, Jackson J, Quinet A, et al. MRE11 and EXO1 nucleases degrade reversed forks and elicit MUS81-dependent fork rescue in BRCA2-deficient cells. *Nat Commun*. 2017;8(1). doi:10.1038/S41467-017-01180-5

363. Thangavel S, Berti M, Levikova M, et al. DNA2 drives processing and restart of reversed replication forks in human cells. *J Cell Biol*. 2015;208(5):545-562. doi:10.1083/JCB.201406100

364. Schlacher K, Christ N, Siaud N, Egashira A, Wu H, Jasin M. Double-strand break repair-independent role for BRCA2 in blocking stalled replication fork degradation by MRE11. *Cell*. 2011;145(4):529-542. doi:10.1016/j.cell.2011.03.041

365. Ying S, Hamdy FC, Helleday T. Mre11-dependent degradation of stalled DNA replication forks is prevented by BRCA2 and PARP1. *Cancer Res*. 2012;72(11):2814-2821. doi:10.1158/0008-5472.CAN-11-3417

366. Schlacher K, Wu H, Jasin M. A distinct replication fork protection pathway

connects Fanconi anemia tumor suppressors to RAD51-BRCA1/2. *Cancer Cell*. 2012;22(1):106-116. doi:10.1016/j.ccr.2012.05.015

367. Higgs MR, Reynolds JJ, Winczura A, et al. BOD1L Is Required to Suppress Deleterious Resection of Stressed Replication Forks. *Mol Cell*. 2015;59(3):462-477. doi:10.1016/j.molcel.2015.06.007

368. Xu S, Wu X, Wu L, et al. Abro1 maintains genome stability and limits replication stress by protecting replication fork stability. *Genes Dev*. 2017;31(14):1469-1482. doi:10.1101/gad.299172.117

369. Liao H, Ji F, Helleday T, Ying S. Mechanisms for stalled replication fork stabilization: new targets for synthetic lethality strategies in cancer treatments. *EMBO Rep*. 2018;19(9):e46263. doi:10.15252/EMBR.201846263

370. Petermann E, Orta ML, Issaeva N, Schultz N, Helleday T. Hydroxyurea-Stalled Replication Forks Become Progressively Inactivated and Require Two Different RAD51-Mediated Pathways for Restart and Repair. *Mol Cell*. 2010;37(4):492-502. doi:10.1016/j.molcel.2010.01.021

371. Davies SL, North PS, Hickson ID. Role for BLM in replication-fork restart and suppression of origin firing after replicative stress. *Nat Struct Mol Biol*. 2007;14(7):677-679. doi:10.1038/nsmb1267

372. Xu Y, Ning S, Wei Z, et al. 53BP1 and BRCA1 control pathway choice for stalled replication restart. *Elife*. 2017;6. doi:10.7554/eLife.30523

373. Mukherjee C, Tripathi V, Manolika EM, et al. RIF1 promotes replication fork protection and efficient restart to maintain genome stability. *Nat Commun*. 2019;10(1):1-16. doi:10.1038/s41467-019-11246-1

374. Thangavel S, Berti M, Levikova M, et al. DNA2 drives processing and restart of reversed replication forks in human cells. *J Cell Biol*. 2015;208(5):545-562. doi:10.1083/jcb.201406100

375. Kawabe YI, Branzei D, Hayashi T, et al. A Novel Protein Interacts with the Werner's Syndrome Gene Product Physically and Functionally. *J Biol Chem*. 2001;276(23):20364-20369. doi:10.1074/jbc.C100035200

376. Leuzzi G, Marabitti V, Pichierri P, Franchitto A. WRNIP 1 protects stalled forks

from degradation and promotes fork restart after replication stress . *EMBO J*. 2016;35(13):1437-1451. doi:10.15252/embj.201593265

377. Sharma K, D'Souza RCJ, Tyanova S, et al. Ultradeep Human Phosphoproteome Reveals a Distinct Regulatory Nature of Tyr and Ser/Thr-Based Signaling. *Cell Rep*. 2014;8(5):1583-1594. doi:10.1016/j.celrep.2014.07.036

378. Mertins P, Mani DR, Ruggles K V, et al. Proteogenomics connects somatic mutations to signalling in breast cancer. *Nature*. 2016;534. doi:10.1038/nature18003

379. Wang Y-L, Zhao W-W, Bai S-M, et al. MRNIP condensates promote DNA double-strand break sensing and end resection. *Nat Commun 2022 131*. 2022;13(1):1-16. doi:10.1038/s41467-022-30303-w

380. Kilic S, Lezaja A, Gatti M, et al. Phase separation of 53BP1 determines liquid-like behavior of DNA repair compartments. *EMBO J*. 2019;38(16):e101379. doi:10.15252/EMBJ.2018101379

381. Pessina F, Giavazzi F, Yin Y, et al. Functional transcription promoters at DNA double-strand breaks mediate RNA-driven phase separation of damage response factors. *Nat Cell Biol*. 2019;21(10):1286. doi:10.1038/S41556-019-0392-4

382. Lin M, Lv J, Zhao D, et al. MRNIP is essential for meiotic progression and spermatogenesis in mice. *Biochem Biophys Res Commun*. 2021;550:127-133. doi:10.1016/J.BBRC.2021.02.143

383. Kazi S, Castañeda JM, Savolainen A, et al. MRNIP interacts with sex body chromatin to support meiotic progression, spermatogenesis, and male fertility in mice. *FASEB J*. 2022;36(9). doi:10.1096/FJ.202101168RR

384. Bennett LG, Wilkie AM, Antonopoulou E, et al. MRNIP is a replication fork protection factor. *Sci Adv*. 2020;6(28). doi:10.1126/sciadv.aba5974

385. O'Reilly EM, Lee JW, Zalupski M, et al. Randomized, Multicenter, Phase II Trial of Gemcitabine and Cisplatin With or Without Veliparib in Patients With Pancreas Adenocarcinoma and a Germline BRCA/PALB2 Mutation. *J Clin*

Oncol. 2020;38(13):1378. doi:10.1200/JCO.19.02931

386. Boeckemeier L, Kraehenbuehl R, Kraehenbuehl R, et al. Mre11 exonuclease activity removes the chain-terminating nucleoside analog gemcitabine from the nascent strand during DNA replication. *Sci Adv*. 2020;6(22). doi:10.1126/SCIADV.AAZ4126

387. Staples CJ, Barone G, Myers KN, et al. MRNIP/C5orf45 Interacts with the MRN Complex and Contributes to the DNA Damage Response. *Cell Rep*. 2016;16(10):2565. doi:10.1016/J.CELREP.2016.07.087

388. Neale MJ, Pan J, Keeney S. Endonucleolytic processing of covalent protein-linked DNA double-strand breaks. 2005. doi:10.1038/nature03872

389. Hartsuiker E, Neale MJ, Carr AM. Distinct Requirements for the Rad32Mre11 Nuclease and Ctp1CtIP in the Removal of Covalently Bound Topoisomerase I and II from DNA. *Mol Cell*. 2009;33(1):117-123. doi:10.1016/J.MOLCEL.2008.11.021

390. Cole F, Keeney S, Jasin M. Evolutionary conservation of meiotic DSB proteins: more than just Spo11. *Genes Dev*. 2010;24(12):1201. doi:10.1101/GAD.1944710

391. Ying S, Hamdy FC, Helleday T. Mre11-dependent degradation of stalled DNA replication forks is prevented by BRCA2 and PARP1. *Cancer Res*. 2012;72(11):2814-2821. doi:10.1158/0008-5472.CAN-11-3417/650068/AM/MRE11-DEPENDENT-DEGRADATION-OF-STALLED-DNA

392. Mohiuddin M, Rahman MM, Sale JE, Pearson CE. CtIP-BRCA1 complex and MRE11 maintain replication forks in the presence of chain terminating nucleoside analogs. *Nucleic Acids Res*. 2019;47(6):2966-2980. doi:10.1093/NAR/GKZ009

393. Koster DA, Croquette V, Dekker C, Shuman S, Dekker NH. Friction and torque govern the relaxation of DNA supercoils by eukaryotic topoisomerase IB. 2005. www.nature.com/nature. Accessed October 27, 2022.

394. Furuta T, Takemura H, Liao ZY, et al. Phosphorylation of Histone H2AX and Activation of Mre11, Rad50, and Nbs1 in Response to Replication-dependent

DNA Double-strand Breaks Induced by Mammalian DNA Topoisomerase I Cleavage Complexes. *J Biol Chem*. 2003;278(22):20303-20312. doi:10.1074/JBC.M300198200

395. Chanut P, Britton S, Coates J, Jackson SP, Calsou P. Coordinated nuclease activities counteract Ku at single-ended DNA double-strand breaks. *Nat Commun 2016 71*. 2016;7(1):1-12. doi:10.1038/ncomms12889

396. Ray Chaudhuri A, Callen E, Ding X, et al. Replication fork stability confers chemoresistance in BRCA-deficient cells. *Nature*. 2016;535(7612):382-387. doi:10.1038/nature18325

397. Somyajit K, Spies J, Coscia F, et al. Homology-directed repair protects the replicating genome from metabolic assaults. *Dev Cell*. 2021;56(4):461-477.e7. doi:10.1016/J.DEVCEL.2021.01.011

398. Sheetal Sharma A, Anand R, Zhang X, Rothenberg E, Cejka P. MRE11-RAD50-NBS1 Complex Is Sufficient to Promote Transcription by RNA Polymerase II at Double-Strand Breaks by Melting DNA Ends In Brief Sharma et al. show that in an in vitro reconstituted system, the DNA damage-sensing complex MRE11-RAD50-NBS1 (MRN) and RNA polymerase II are sufficient to synthesize RNA transcripts from broken DNA ends. MRN supports transcription by melting DNA ends and allowing RNA polymerase II to initiate RNA synthesis. doi:10.1016/j.celrep.2020.108565

399. Konstantinopoulos PA, Lheureux S, Moore KN. PARP Inhibitors for Ovarian Cancer: Current Indications, Future Combinations, and Novel Assets in Development to Target DNA Damage Repair. *Am Soc Clin Oncol Educ book Am Soc Clin Oncol Annu Meet*. 2020;40(40):1-16. doi:10.1200/EDBK_288015

400. Bhuripanyo K, Wang Y, Liu X, et al. Identifying the substrate proteins of U-box E3s E4B and CHIP by orthogonal ubiquitin transfer. *Sci Adv*. 2018;4(1). doi:10.1126/SCIADV.1701393

401. Tan C, Ginzberg MB, Webster R, et al. Cell size homeostasis is maintained by CDK4-dependent activation of p38 MAPK. *Dev Cell*. 2021;56(12):1756-1769.e7. doi:10.1016/J.DEVCEL.2021.04.030

402. Crozier L, Foy R, Mouery BL, et al. CDK4/6 inhibitors induce replication stress to cause long-term cell cycle withdrawal. *EMBO J*. 2022;41(6):e108599. doi:10.15252/EMBJ.2021108599

403. Simoneau A, Xiong R, Zou L. The trans cell cycle effects of PARP inhibitors underlie their selectivity toward BRCA1/2-deficient cells. *Genes Dev*. 2021;35(17-18):1271-1289. doi:10.1101/GAD.348479.121/-/DC1

404. Panzarino NJ, Krais JJ, Cong K, et al. Replication Gaps Underlie BRCA Deficiency and Therapy Response A C. doi:10.1158/0008-5472.CAN-20-1602

405. Kang Z, Fu P, Alcivar AL, et al. BRCA2 associates with MCM10 to suppress PRIMPOL-mediated repriming and single-stranded gap formation after DNA damage. *Nat Commun 2021 121*. 2021;12(1):1-12. doi:10.1038/s41467-021-26227-6

406. Quinet A, Tirman S, Jackson J, et al. PRIMPOL-Mediated Adaptive Response Suppresses Replication Fork Reversal in BRCA-Deficient Cells. *Mol Cell*. 2020;77(3):461. doi:10.1016/J.MOLCEL.2019.10.008

407. Ray Chaudhuri A, Hashimoto Y, Herrador R, et al. Topoisomerase I poisoning results in PARP-mediated replication fork reversal. *Nat Struct Mol Biol 2012 194*. 2012;19(4):417-423. doi:10.1038/nsmb.2258

408. Zhang X-H, Tee LY, Wang X-G, Huang Q-S, Yang S-H. Off-target Effects in CRISPR/Cas9-mediated Genome Engineering. 2015. doi:10.1038/mtna.2015.37

409. Naeem M, Majeed S, Hoque Z, Ahmad I. cells Latest Developed Strategies to Minimize the Off-Target Effects in CRISPR-Cas-Mediated Genome Editing. doi:10.3390/cells9071608

410. Modrzejewski D, Hartung F, Lehnert H, et al. Which Factors Affect the Occurrence of Off-Target Effects Caused by the Use of CRISPR/Cas: A Systematic Review in Plants. *Front Plant Sci*. 2020;11:1838. doi:10.3389/FPLS.2020.574959/BIBTEX

411. Garrood WT, Kranjc N, Petri K, et al. Analysis of off-target effects in CRISPR-based gene drives in the human malaria mosquito. *Proc Natl Acad Sci U S A*.

2021;118(22):e2004838117. doi:10.1073/PNAS.2004838117/SUPPL_FILE/PNAS.2004838117.SD06.XLSX

412. Sturme MHJ, Jan ⊥, Van Der Berg P, et al. Occurrence and Nature of Off-Target Modifications by CRISPR-Cas Genome Editing in Plants. *Cite This ACS Agric Sci Technol*. 2022. doi:10.1021/acsagscitech.1c00270

413. DNA repair mechanisms involved in gemcitabine cytotoxicity and in the interaction between gemcitabine and cisplatin. *Biochem Pharmacol*. 2003;65(2):275-282. doi:10.1016/S0006-2952(02)01508-3

414. Van Der Heijden MS, Brody JR, Dezentje DA, et al. In vivo Therapeutic Responses Contingent on Fanconi Anemia/BRCA2 Status of the Tumor. *Clin Cancer Res*. 2005;11(20):7508-7515. doi:10.1158/1078-0432.CCR-05-1048

415. Jones RM, Kotsantis P, Stewart GS, Groth P, Petermann E. BRCA2 and RAD51 promote double-strand break formation and cell death in response to gemcitabine. *Mol Cancer Ther*. 2014;13(10):2412-2421. doi:10.1158/1535-7163.MCT-13-0862/85897/AM/BRCA2-AND-RAD51-PROMOTE-DOUBLE-STRAND-BREAK

416. George JW, Bessho M, Bessho T. Inactivation of XPF Sensitizes Cancer Cells to Gemcitabine. 2019. doi:10.1155/2019/6357609

417. Tokarsky EJ, Wallenmeyer PC, Phi KK, Suo Z. Significant impact of divalent metal ions on the fidelity, sugar selectivity, and drug incorporation efficiency of human PrimPol. doi:10.1016/j.dnarep.2016.11.003

418. Guilliam TA, Doherty AJ. PrimPol—Prime Time to Reprime. *Genes (Basel)*. 2017;8(1). doi:10.3390/GENES8010020

419. Kobayashi K, Guilliam TA, Tsuda M, et al. Repriming by PrimPol is critical for DNA replication restart downstream of lesions and chain-terminating nucleosides. *Cell Cycle*. 2016;15(15):1997-2008. doi:10.1080/15384101.2016.1191711

420. Anand J, Chiou L, Sciandra C, et al. Roles of trans-lesion synthesis (TLS) DNA polymerases in tumorigenesis and cancer therapy. *NAR Cancer*. 2023;5(1). doi:10.1093/NARCAN/ZCAD005

421. etal J. Sequence dependent effect of paclitaxel on gemcitabine metabolism in relation to cell cycle and cytotoxicity in non-small-cell lung cancer cell lines. 2000. doi:10.1054/bjoc.2000.1399

422. Tsuda M, Terada K, Ooka M, et al. The dominant role of proofreading exonuclease activity of replicative polymerase ε in cellular tolerance to cytarabine (Ara-C). *Oncotarget*. 2017;8(20):33457-33474. doi:10.18632/ONCOTARGET.16508

423. Kamiya KI, Huang P, Plunkett W. Inhibition of the 3' --> 5' exonuclease of human DNA polymerase epsilon by fludarabine-terminated DNA. *J Biol Chem*. 1996;271(32):19428-19435. doi:10.1074/JBC.271.32.19428

424. Gandhi V, Plunkett W. Modulatory activity of 2',2'-difluorodeoxycytidine on the phosphorylation and cytotoxicity of arabinosyl nucleosides. *Cancer Res*. 1990.

425. Parker W, Shaddix S, Chang CH, et al. Effects of 2-chloro-9-(2-deoxy-2-fluoro-beta-D-arabinofuranosyl)adenine on K562 cellular metabolism and the inhibition of human ribonucleotide reductase and DNA polymerases by its 5'-triphosphate. *Cancer Res*. 1991.

426. Hashimoto Y, Chaudhuri AR, Lopes M, Costanzo V. Rad51 protects nascent DNA from Mre11-dependent degradation and promotes continuous DNA synthesis. *Nat Struct Mol Biol 2010 1711*. 2010;17(11):1305-1311. doi:10.1038/nsmb.1927

427. Örd M, Möll K, Agerova A, et al. Multisite phosphorylation code of CDK. doi:10.1038/s41594-019-0256-4

428. Chilkova O, Jonsson BH, Johansson E. The quaternary structure of DNA polymerase epsilon from Saccharomyces cerevisiae. *J Biol Chem*. 2003;278(16):14082-14086. doi:10.1074/JBC.M211818200

429. Plunkett W, Grindey GB, Plunkett W. Action of 2',2'-difluorodeoxycytidine on DNA synthesis. *Cancer Res*. 1991;51(22):6110-6117. https://europepmc.org/article/med/1718594. Accessed November 11, 2022.

430. Boeckemeier L, Kraehenbuehl R, Kraehenbuehl R, et al. Mre11 exonuclease activity removes the chain-terminating nucleoside analog gemcitabine from the

nascent strand during DNA replication. *Sci Adv*. 2020;6(22). doi:10.1126/SCIADV.AAZ4126/SUPPL_FILE/AAZ4126_SM.PDF

431. Valle L, Hernández-Illán E, Bellido F, et al. New insights into POLE and POLD1 germline mutations in familial colorectal cancer and polyposis. *Hum Mol Genet*. 2014;23(13):3506-3512. doi:10.1093/HMG/DDU058

432. Zou Y, Liu FY, Liu H, et al. Frequent POLE1 p.S297F mutation in Chinese patients with ovarian endometrioid carcinoma. *Mutat Res Mol Mech Mutagen*. 2014;761:49-52. doi:10.1016/J.MRFMMM.2014.01.003

433. Meng B, Hoang LN, McIntyre JB, et al. POLE exonuclease domain mutation predicts long progression-free survival in grade 3 endometrioid carcinoma of the endometrium. *Gynecol Oncol*. 2014;134(1):15-19. doi:10.1016/j.ygyno.2014.05.006

434. Di Virgilio M, Ying CY, Gautier J. PIKK-dependent phosphorylation of Mre11 induces MRN complex inactivation by disassembly from chromatin. *DNA Repair (Amst)*. 2009;8(11):1311-1320. doi:10.1016/J.DNAREP.2009.07.006

435. Mu JJ, Wang Y, Luo H, et al. A Proteomic Analysis of Ataxia Telangiectasia-mutated (ATM)/ATM-Rad3-related (ATR) Substrates Identifies the Ubiquitin-Proteasome System as a Regulator for DNA Damage Checkpoints. *J Biol Chem*. 2007;282(24):17330-17334. doi:10.1074/JBC.C700079200

436. Stokes MP, Rush J, MacNeill J, et al. Profiling of UV-induced ATM/ATR signaling pathways. *Proc Natl Acad Sci U S A*. 2007;104(50):19855-19860. doi:10.1073/PNAS.0707579104/SUPPL_FILE/07579FIG7.JPG

437. Costanzo V, Robertson K, Bibikova M, et al. Mre11 protein complex prevents double-strand break accumulation during chromosomal DNA replication. *Mol Cell*. 2001;8(1):137-147. doi:10.1016/S1097-2765(01)00294-5

438. Yuan SSF, Chang HL, Hou MF, et al. Neocarzinostatin induces Mre11 phosphorylation and focus formation through an ATM- and NBS1-dependent mechanism. *Toxicology*. 2002;177(2-3):123-130. doi:10.1016/S0300-483X(02)00220-2

439. Trenz K, Smith E, Smith S, Costanzo V. ATM and ATR promote Mre11

dependent restart of collapsed replication forks and prevent accumulation of DNA breaks. *EMBO J*. 2006;25(8):1764. doi:10.1038/SJ.EMBOJ.7601045

440. Chen C, Zhang L, Huang N-J, Huang B, Kornbluth S. Suppression of DNA-damage checkpoint signaling by Rsk-mediated phosphorylation of Mre11. doi:10.1073/pnas.1306328110

441. Khadka P, Reitman ZJ, Lu S, et al. PPM1D mutations are oncogenic drivers of de novo diffuse midline glioma formation. *Nat Commun 2022 131*. 2022;13(1):1-18. doi:10.1038/s41467-022-28198-8

442. Babur Ö, Luna A, Korkut A, et al. Causal interactions from proteomic profiles: Molecular data meet pathway knowledge. *Patterns*. 2021;2(6):100257. doi:10.1016/J.PATTER.2021.100257

443. Li W, Wang HY, Zhao X, et al. A methylation-phosphorylation switch determines Plk1 kinase activity and function in DNA damage repair. *Sci Adv*. 2019;5(3). doi:10.1126/SCIADV.AAU7566

444. Ström CE, Mortusewicz O, Finch D, et al. CK2 phosphorylation of XRCC1 facilitates dissociation from DNA and single-strand break formation during base excision repair. *DNA Repair (Amst)*. 2011;10(9):961-969. doi:10.1016/J.DNAREP.2011.07.004

445. Parsons JL, Dianova II, Finch D, et al. XRCC1 phosphorylation by CK2 is required for its stability and efficient DNA repair. *DNA Repair (Amst)*. 2010;9(7):835-841. doi:10.1016/J.DNAREP.2010.04.008

446. Spycher C, Miller ES, Townsend K, et al. Constitutive phosphorylation of MDC1 physically links the MRE11–RAD50–NBS1 complex to damaged chromatin. *J Cell Biol*. 2008;181(2):227. doi:10.1083/JCB.200709008

447. Becherel OJ, Jakob B, Cherry AL, et al. CK2 phosphorylation-dependent interaction between aprataxin and MDC1 in the DNA damage response. doi:10.1093/nar/gkp1149

448. Yata K, Lloyd J, Maslen S, et al. Plk1 and CK2 Act in Concert to Regulate Rad51 during DNA Double Strand Break Repair. *Mol Cell*. 2012;45(3):371. doi:10.1016/J.MOLCEL.2011.12.028

449. Herhaus L, Perez-Oliva AB, Cozza G, et al. Casein kinase 2 (CK2) phosphorylates the deubiquitylase OTUB1 at Ser16 to trigger its nuclear localization. *Sci Signal*. 2015;8(372):ra35. doi:10.1126/SCISIGNAL.AAA0441

450. Weßbecher IM, Hinrichsen I, Funke S, et al. DNA mismatch repair activity of MutLα is regulated by CK2-dependent phosphorylation of MLH1 (S477). *Mol Carcinog*. 2018;57(12):1723-1734. doi:10.1002/MC.22892

451. Dodson GE, Limbo O, Nieto D, Russell P. Phosphorylation-regulated binding of Ctp1 to Nbs1 is critical for repair of DNA double-strand breaks. *Cell Cycle*. 2010;9(8):1516. doi:10.4161/CC.9.8.11260

452. Guerra B, Doktor TK, Frederiksen SB, Somyajit · Kumar, Brage ·, Andresen S. Essential role of CK2α for the interaction and stability of replication fork factors during DNA synthesis and activation of the S-phase checkpoint. *Cell Mol Life Sci*. 2022;79:339. doi:10.1007/s00018-022-04374-3

453. Palma A, Pugliese GM, Murfuni I, et al. Phosphorylation by CK2 regulates MUS81/EME1 in mitosis and after replication stress. *Nucleic Acids Res*. 2018;46(10):5109-5124. doi:10.1093/nar/gky280

454. Bandyopadhyay K, Gjerset RA. Protein kinase CK2 is a central regulator of topoisomerase I hyperphosphorylation and camptothecin sensitivity in cancer cell lines. *Biochemistry*. 2011;50(5):704. doi:10.1021/BI101110E

455. Seki A, Coppinger JA, Jang C-Y, Yates Iii JR, Fang G. Bora and Aurora A Cooperatively Activate Plk1 and Control the Entry into Mitosis. doi:10.1126/science.1157425

456. Ciardo D, Haccard O, Narassimprakash H, Chiodelli V, Goldar A, Marheineke K. Polo-like kinase 1 (Plk1) is a positive regulator of DNA replication in the Xenopus in vitro system. *Cell Cycle*. 2020;19(14):1817. doi:10.1080/15384101.2020.1782589

457. Zuco V, De Cesare M, Zaffaroni N, Lanzi C, Cassinelli G. PLK1 is a critical determinant of tumor cell sensitivity to CPT11 and its inhibition enhances the drug antitumor efficacy in squamous cell carcinoma models sensitive and resistant to camptothecins. *Oncotarget*. 2015;6(11):8736.

doi:10.18632/ONCOTARGET.3538

458. He L, Fan X, Li Y, et al. Overexpression of zinc finger protein 384 (ZNF 384), a poor prognostic predictor, promotes cell growth by upregulating the expression of Cyclin D1 in Hepatocellular carcinoma. *Cell Death Dis 2019 106*. 2019;10(6):1-12. doi:10.1038/s41419-019-1681-3

459. Zhang T, Liu WD, Saunee NA, Breslin MB, Lan MS. Zinc Finger Transcription Factor INSM1 Interrupts Cyclin D1 and CDK4 Binding and Induces Cell Cycle Arrest. *J Biol Chem*. 2009;284(9):5574. doi:10.1074/JBC.M808843200

460. Echalier A, Endicott JA, Noble MEM. Recent developments in cyclin-dependent kinase biochemical and structural studies. *Biochim Biophys Acta*. 2010;1804(3):511-519. doi:10.1016/J.BBAPAP.2009.10.002

461. Orthwein A, Noordermeer SM, Wilson MD, et al. A mechanism for the suppression of homologous recombination in G1 cells. *Nature*. 2015;528(7582):422-426. doi:10.1038/NATURE16142

462. Wang H, Goode T, Iakova P, Albrecht JH, Timchenko NA. C/EBPα triggers proteasome-dependent degradation of cdk4 during growth arrest. *EMBO J*. 2002;21(5):930. doi:10.1093/EMBOJ/21.5.930

463. Chen H, Xu X, Wang G, et al. CDK4 protein is degraded by anaphase-promoting complex/cyclosome in mitosis and reaccumulates in early G1 phase to initiate a new cell cycle in HeLa cells. *J Biol Chem*. 2017;292(24):10131-10141. doi:10.1074/JBC.M116.773226

464. Esteller M. Epigenetics in Cancer. *https://doi.org/101056/NEJMra072067*. 2008;358(11):1148-1159. doi:10.1056/NEJMRA072067

465. Eastman A. Reevaluation of Interaction of cis-Dichloro(ethylenediamine)platinum(II) with DNA. *Biochemistry*. 1986;25(13):3912-3915. doi:10.1021/bi00361a026

466. Gargiulo D, Tomasz M, Musser SS, Yang L, Fukuyama T. Alkylation and Cross-Linking of DNA by the Unnatural Enantiomer of Mitomycin C: Mechanism of the DNA-Sequence Specificity of Mitomycins. *J Am Chem Soc*. 1995;117(37):9388-9398.

doi:10.1021/JA00142A002/ASSET/JA00142A002.FP.PNG_V03